Zinc in the Retinal Pigment Epithelium and Choriocapillaris Interface

A Thesis Submitted to University College London for the

degree of Doctor of Philosophy

Sabrina Cahyadi

BSc

Department of Ocular Biology and Therapeutics

Institute of Ophthalmology

University College London

2012

Declaration

I, Sabrina Cahyadi confirm that the work presented in the thesis titled "Zinc in the Retinal Pigment Epithelium and Choriocapillaris Interface" is my own work. Where information has been derived from other sources, I confirm that this has been indicated in the thesis.

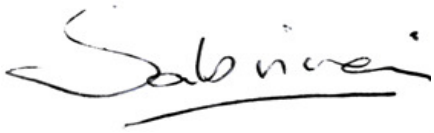

Sabrina Cahyadi

Date: 14 November 2011

Acknowledgements

"For wisdom will enter your heart and knowledge will be pleasant to your soul; discretion will guard you, understanding will watch over you."

First and foremost, I would like to thank my supervisors Professor Phil Luthert and Dr. Imre Lengyel for accepting me as their student, and the enormous support, help and guidance they have provided.

I would also like to thank the Dorothy Hodgkin Postgraduate Award, the Mercer Fund and Professor Alan Bird for their very generous studentship which enabled me to do this PhD. The funding I receive from the Special Trustees of Moorfields Eye Hospital allowed me to do my day-to-day lab works. I thank Peter Marshall who ensured that the funds reach me in time. I must also thank Dr. Peter Munro, Cynthia Langley, Alexandra Boss, and Dr. Virginia Calder for all the help and moral supports I have received.

I cannot believe how much have happened in the past three years. The people at the Institute of Ophthalmology have supported me through all the amazing, good, bad, ho-hum, and heartbreaking episodes of my PhD. My fellow lab members Neda Barzegar-Befroei and Ashraf Gango, who provided so much help and advice.The UCL students whom I have had the greatest privilege to work with, Bhavika Patel, Yemsrach Tadesse, Anishka Wilwaraachachii and Alexia Phedonos. Thank you for all of your help with the cell biology studies and supports throughout.

I thank members of the Ohnuma, Bhattacharya and Shima lab, Asma Aslam and Meihua Ju for showing the very clueless student that I was when I started how to manage and run a lab without glitches. I thank Margaret Dellett, Wanzhou Hu, Vasia Papadaki and Michelle Kim for constantly telling me to fight for my PhD and providing shoulders to cry on (literally speaking). I thank Amna Shah, Anna Rose, Sancy Low, Wendy Mustill, Liza Sharmini, and Giovanna Alfano for teaching me all the cloning aspects, for all the encouragement and for what seemed to be an infinite cake supply during my time in their office. To all my King's girls, Saleha Hassan, Rebecca Alade, Appitha Arulappu, Natasha Khalife, and Mehnaz Hossain, need I say more, you guys are truly the best.

Special thanks go to Prof. Christer Hogstrand from King's College London who took me as his student for my final year undergraduate project. It was also because of your recommendation that this PhD is possible. Tom Carroll, Josef Rasinger and Valentina Reffatto, former Hogstrand Lab PhD students who instilled the confidence in me that I am worthy enough of a PhD.I am grateful for my friends Vania Kusworo and Marco Japutra for all the 12 years that I have known you both.

I thank our collaborators Dr. Elod Kortvely, Matteo Gorza and Jennifer Behler from Helmholtz Zentrum Munchen for useful discussions, sheltering me for a month in your lab and pointing out a crucial error in my experimentation which would have otherwise been detrimental. I thank Professor Richard Thompson for taking some of his valuable time to read the drafts of the manuscript and for some very useful discussions about zinc stoichiometry.

I am indebted to the people closest to me, my parents who have been my ardent supporters for all 23 years of my life, my brother and my sisters for their emotional and financial support during my undergraduate and PhD degree. To my sister Janice, thank you for all the frozen Bolognese sauce tubs and banana cakes you made when cooking seemed to be the last thing on my mind. I also thank Winardi Suhali for five years of endless support, and encouragement. You have seen me at my best and at my worst, and thank you for sticking around for me.

Finally, I thank my examiners Prof. John Greenwood and Dr. Kathryn Taylor for their interest in my thesis and a valuable opportunity to discuss it with them.

List of Posters and Publications

Barzegar-Befroei, Neda, **Cahyadi, Sabrina**, Gango, Ashraf, Peto, Tunde, and Lengyel, Imre 2011. Zinc in Eye Diseases. *Zinc in Human Health*. Amsterdam: IOS Press.

Sabrina Cahyadi, Bhavika J. Patel, Meihua Ju, Alexia Phedonos, Anishka Wilwaraarachchi, and Imre Lengyel.
Effect of Zinc on Fenestrae Formation in Cultured Endothelial Cells.Poster presentation at the Association of Research in Vision and Ophthalmology (ARVO) annual meeting 2011.

Sabrina Cahyadi, Bhavika Patel, Meihua Ju and Imre Lengyel
Effect of zinc on fenestra formation in cultured endothelial cells. Poster presentation at the Young Researcher Vision Camp in Liebertingen June 25-27 2010.

Zinc in the RPE-Choroid Interface
Presentation at the Zinc-UK meeting 2010

Abbreviations

AE – Acrodermatitis Enteropathica

AD – Alzheimer's Disease

AKT – Serine Threonine Kinase

AMD – Age-Related Macular Degeneration

AMG - Autometallography

APS – Ammonium Persulfate

AREDS – Age-Related Eye Disease Study

BCA – Bichinconinic Assay

BSA – Bovine Serum Albumin

CDK4 – Cell division kinase 4

CRALBP - Cellular retinaldehyde binding protein

CFH – Complement Factor H

DNA – Deoxyribonucleic Acid

ERK - Extracellular-signal-Regulated Kinases

E-Cadherin – Epithelial Cadherin

FAM - 6-carboxyfluoroscein

FGF – Fibroblast Growth Factor

GABA - Gamma-Aminobutyric Acid

GAPDH - Glyceraldehyde 3-Phosphate Dehydrogenase

GDP – Guanosine Diphosphate

GFP – Green Fluorescent Protein

GPx – Glutathione Peroxidase

GTP – Guanosine Triphosphate

HMDS - Hexamethyldisilazone

HRP – Horseradish Peroxidase

HUVECs - Human umbilical vein endothelial cells

IL6 – Interleukin 6

IP3 - Inositol 1,4,5-Trisphosphate

kDa - Kilodalton

KDR - Kinase insert Domain Receptor

LA – Latrunculin A

LB- Luria-Bertani

N-Cadherin – Neural Cadherin

nM – Nano molar

MDCK – Madin-Darby Canine Kidney cell line

MMLV- Moloney Murine Leukemia Virus

MT – Metallothionein

MTF - Metal Responsive Element Binding Transcription Factor 1

NEAA – Non-Essential Amino Acid

NO – Nitric Oxide

NK – Natural Killer

PEDF – Pigment Epithelium Derived Factor

PDGF - Platelet- Derived Growth Factor

PCR – Polymerase Chain Reaction

PFA – Paraformaldehyde

PI3K - phosphoinositol-3-Kinase

PV-1 – Plasmalemma Vesicle Associated Protein

PVDF - Polyvinylidene Fluoride

QPCR- Quantitative Polymerase Chain Reaction

RNA – Ribonucleic Acid

RPE- Retinal Pigment Epithelium

RT-PCR – Reverse Transcription Polymerase Chain Reaction

SOC – Super Optimal Broth with glucose

SDS- Sodium Dodecyl Sulfate

TER – Transepithelial Resistance

TBS – Tris-Buffered Saline

TBST- Tris- Buffered Saline Tween

TPEN - N,N,N',N'-tetrakis (2 pyridylmethyl) ethylenediamine

TEMED - *N*,*N*,*N*′,*N*′-Tetramethylethylenediamine

TGF-b - Transforming Growth Factor – beta

UBC – Ubiquitin C protein

VEGF – Vascular Endothelial Growth Factor

YWHAZ - Tyrosine 3-monooxygenase/tryptophan 5-monooxygenase activation protein

ZIP – ZRT/IRT-like proteins

ZNT – also known as cation diffusion facilitator proteins

ZO-1 – Zona Occludin 1 protein

ZONAB – ZO-1 associated nucleic acid binding protein

Abstract

The highest concentration of zinc in human tissues is found in the retinal pigment epithelium (RPE)-choroid complex. Despite the association of zinc deficiency with age-related macular degeneration (AMD) and the widespread use of zinc supplementation to slow the progression ofAMD, very little is known about how zinc affects the RPE and the choroid. Molecular and cell biology techniques were used to uncover how changes in zinc levels could play a role in regulating the RPE-choroid complex.

First, QRT-PCR was used to assess the expressions of all 24 known zinc transporters in cadaveric human RPE, cultured RPE cells and cells isolated from other parts of the retina, ZIP12 was identified as a potentially important transporter to regulate zinc levels at the RPE-choroid interface. As there is very little published about ZIP12, bioinformatics and data mining were used to understand how this protein might function. Confirmation of these predictions was achieved through the cloning and expression of V5-tagged ZIP12 protein in different cell lines. Based on these experiments, we concluded that ZIP12 is a plasma membrane transporter that mediates zinc influx.

In parallel, we tested the hypothesis that extracellular zinc levels in Bruch's membrane might be involved in regulating both the RPE as well as the fenestrated choroidal capillaries using cultures of ARPE19 and bEND5 cells respectively. The presence of extracellular zinc in the growth media affected the characteristics of ARPE19 cells as well as fenestrae formation in bEND5 cells.

In summary, the range of zinc transporter at the RPE-choroid interface was defined and properties of one particular transporter, ZIP12 which may have a specific role at this site, were elucidated. Using cellular systems some of the effects of zinc on the RPE-choroid complex were investigated. Future studies are required to elucidate the role of zinc in the AMD pathogenesis.

Table of Contents

Declaration 2
Abstract 9
Acknowledgements 3
List of Posters and Publications 5
Abbreviations 6
List of Tables 14
List of Figures 15
1. General Introduction 17
1.1. Zinc Overview 17
1.1.1. Biological functions of Zinc 17
1.1.2. Zinc Homeostasis 19
1.2. Zinc Transporters 21
1.2.1. SLC30A Family of Transporters 21
1.2.2. SLC39A ZIP FAMILY OF TRANSPORTERS 22
1.3. Overview of the Structure of the Eye 25
1.4. Zinc in the Eye 27
1.4.1. Retina, RPE, Choroid 28
1.4.2. RPE Barrier Function 34
1.4.3. Zinc in Retinal Cellular Function 37
1.4.4. Bruch's Membrane 40
1.4.5. Cornea and Sclera 40
1.4.6. Lens and Iris 41
1.4.7. Vitreous and Optic Nerve 42
1.5. Consequences of Zinc Deficiency and Overload in the Body and Eye 43
1.5.1. Zinc Deficiency 43
1.5.2. Zinc Overload 44
1.6. Age-Related Macular Degeneration 45
1.6.1. Overview of Age-Related Macular Degeneration 45
1.6.2. AMD Pathogenesis 48
1.6.3. Use of Zinc in AMD 51
1.7. Aims of the Thesis 53
2. Materials and Methods 54
2.1. Reagents 54
2.2. Buffers, Solutions and Gel Preparations 54
2.3. Antibodies 59
2.4. Sample Preparation 59
2.4.1. Cadaveric tissue dissection 59

2.4.2. Tissue Preparation 59
2.4.3. Cadaveric Human RPE Preparation 59
2.4.4. Cell culture preparation 60
2.5. RNA Studies 60
2.5.1. RNA isolation 60
2.5.2. Quantification and integrity analysis 61
2.6. DNA Work 61
2.6.1. cDNA synthesis 61
2.6.2. Quantitative RT-PCR 62
2.6.3. DNA clean up 64
2.6.3.1. EtOH precipitation 64
2.6.3.2. Millipore Montage system 64
2.6.4. Agarose gels 64
2.6.5. DNA sequencing 65
2.7. Protein Studies 65
2.7.1. Western Blot 65
2.7.2. In Vitro Translation 66
2.7.3. Bichinconinic Assay 66
2.7.4. Transient Expression of protein in cells 66
2.8. Cell Culture 67
2.8.1. Cell lines 67
2.8.2. Propagation and Freezing 67
2.8.3. Cytotoxicity Assay 68
2.8.4. Cell Proliferation Assay 68
2.8.5. Wholemount TEM preparation 68
2.8.6. Transepithelial Resistance Measurement 69
2.9. Immunohistochemistry /Immunocytochemistry and Zinc Visualization 69
2.9.1. Fixation 69
2.9.2. Immunohistochemistry (Only BEND5) 70
2.9.3. Immunohistochemistry (All other cell lines) 70
2.9.4. Zinc probes 71
2.10. Cloning Strategies 71
2.10.1. Cloning Primer Designs 71
2.10.2. Cloning PCR 72
2.10.3. Expression vectors 72

2.10.4. Transformation of ccdB cells/ *E.Coli* 73
2.10.5. Purification of Proteins 73
2.10.6. Glycerol Stock 74
2.10.7. Restriction Digests 74
2.11. Statistical Analysis 74
3. Expression of Mammalian Zinc Transporters in the RPE and Choroid 75
3.1. Intracellular Zinc Transport 76
3.1.1. SLC30A Family of Transporters 76
3.1.2. SLC30A1 / ZnT1 76
3.1.3. SLC30A2/ ZnT2 77
3.1.4. SLC30A3/ ZNT3 78
3.1.5. SLC30A4/ ZnT4 79
3.1.6. SLC30A5/ ZnT5 79
3.1.7. SLC30A6/ ZnT6 80
3.1.8. SLC30A7/ ZnT7 80
3.1.9. SLC30A8/ZnT8 81
3.1.10. SLC30A9/ ZnT9, SLC30A10/ ZnT10 81
3.1.11. SLC39A ZIP FAMILY OF TRANSPORTERS 81
3.1.12. SLC39A1/ZIP1 81
3.1.13. SLC39A2 / ZIP2 82
3.1.14. SLC39A3/ ZIP3 82
3.1.15. SLC39A4/ ZIP4 83
3.1.16. SLC39A5/ ZIP5 83
3.1.17. SLC39A6/ ZIP6 84
3.1.18. SLC39A7/ ZIP7 84
3.1.19. SLC39A8/ ZIP8 84
3.1.20. SLC39A9/ ZIP9 85
3.1.21. SLC39A10/ ZIP10 85
3.1.22. SLC39A12/ ZIP12 85
3.1.23. SLC39A13/ ZIP13 85
3.1.24. SLC39A14/ ZIP14 85
3.2. Aims 88
3.3. Expression of SLC30A SLC39A Transporters in RPE Cells 88
3.4. Expression of SLC30A SLC39A Transporters in non RPE Cells 95
3.5. Confirmation of high SLC39A12 Expression in Cadaveric Tissue 98
3.6. Evidence of Cross-Contamination in Cadaveric Samples 99
3.7. Discussion 101

3.7.1. Zinc Transporters in Human Cadaveric and Cultured Retinal Pigment Epithelium Cells and non-RPE cell lines 101
3.7.2. Zinc transporters in the choroid and fenestrated endothelial cells 109
3.7.3. Zinc Transporters in the Retina 109
3.7.4. Eye Phenotype in Zinc Transporter Knockout Animals 110
3.8. Future Plans 110
Conclusion 111

4. Characterisation of ZIP12: Structure, Function and Localisation 112
4.1. SLC39A12 Isoforms 112
4.2. The ZIP12 protein 114
4.3. Specific Expression of SLC39A12 in Tissues 121
4.4. Aims 121
4.5. Cloning and expression of ZIP12 124
4.6. Generation and Characterisation of Antibodies for ZIP12 128
4.7. Localisation of ZIP12 138
4.8. Function of ZIP12 150
4.9. Discussion 152
4.10. Future Directions 155

5. Potential Role of Extracellular Zinc on RPE Cell Differentiation 158
5.1. Introduction 158
5.2. Aims and Hypothesis 160
5.3. Calculating the Zinc Concentration in DMEM/F12 160
5.4. Effect of Extracellular Zinc on TER of Cultured ARPE19 Cells 162
5.5. Effect of Extracellular Zinc on ZO-1 Distribution in ARPE19 Cells 164
5.6. Cell Proliferation Assay using alamarBlue 166
5.7. Zinc Induced Changes in ARPE19 Gene Expression 168
5.8. Discussion and Future Perspectives 171
5.9. Future Plans 174

6. Effect of Zinc on Fenestrae Formation: an in *Vitro* Study using bEND5 Cells. 175
6.1. General Introduction 176
6.1.1. The Endothelium 176
6.1.2. PV-1 Protein 177
6.1.3. Importance of Endothelium in RPE-choroid Interface 177
6.2. Aims and Hypothesis 178
6.3. Treatment with $ZnSO_4$ can Induce PV-1 Protein Rearrangement 182
6.4. Electron Microscopy Confirmation of Zinc Induced Fenestration 188
6.5. Cell Viability Assays 192
6.6. Treatment of bEND5 Cells with Other Divalent Metals 194
6.7. Possible Signalling Pathway(s) Involved in Zinc – Induced Fenestration . 199
6.8. Discussion 202
6.9. Further research 208
6.10. Conclusion 208

7. General Discussion 209

8. Appendices 214
8.1. Appendix 1 – Antibodies 214
8.2. Appendix 2: Cell Lines 216
8.3. Appendix 3 – Primer List 217
8.3.1. Cloning Primers 217
8.3.2. Sequencing Primers 217
8.4. QRT-PCR Primer Sequences (Primer Design, Southampton, UK) 218
8.4.1. Mouse Primers 218
8.5. Appendix 4: PCR and DNA Sequencing Conditions 219
8.5.1. Cloning PCR Cycling Conditions 219
8.5.2. DNA Sequencing Conditions 219
8.6. Appendix 5: Plasmids Used 220
9. References 223

List of Tables

Table 1-1- Total zinc concentration in tissues 27
Table 3-1- Expression of SLC30A1-10, SLC39A1-14 in RPE cells 91
Table 3-2 - Human primer sequences for SLC30A family and SLC39A family 93
Table 3-3 - Expression of SLC30A1-10, SLC39A1-14 in non- RPE cells 96
Table 3-4–Confirmation of SLC39A12 expression using TaqMan-style Probe 99
Table 3-5 – Cross contamination in human cadaveric samples 100
Table 3-6- Summary of zinc transporter expression in various RPE cels 103
Table 4-1- Five isoforms of SLC39A12 (ZIP12) 113
Table 4-2 - Details of Sequence Motif Found in ZIP12 Protein Sequence 120
Table 6-1 - Total fenestrae formed in $ZnSO_4$ and LA treated groups 191
Table 6-2 - Overlapping pathways between VEGFA, zinc and nicotine. 201

List of Figures

Figure 1-1 -Structure of SLC30 family and SLC39 family of zinc transporters. 23
Figure 1-2- Schematic diagram of the eye 26
Figure 1-3–Organisation of the retina/RPE/choroid complex 30
Figure 1-4- Transmission electron micrograph picture of a normal RPE.....33
Figure 1-5- The retinal cycle.....39
Figure 1-6- Fundus photograph and pathological features of AMD.....47
Figure 3-1- Distribution of zinc transporters in RPE-choroid complex.....87
Figure 3-2- Confirmation of QRT-PCR using 1% agarose gels 92
Figure 3-3 – Diagram representation of QRT-PCR data for RPE cells 94
Figure 3-4- Diagram representation of QRT-PCR data for non-RPE cells 97
Figure 3-5- Zinc transporters in RPE-Choroid. 108
Figure 4-1- Five isoforms of ZIP12 113
Figure 4-2 - Phylogenetic tree of SLC39 families. 115
Figure 4-3 – Multiple alignments of ZIP12 peptide sequences. 115
Figure 4-4 – Hydrophobic plot for ZIP12 protein.....116
Figure 4-5– Annotated sequence of ZIP12 protein 119
Figure 4-6– Expression Profile Analysis for SLC39A12 122
Figure 4-7–EST profile and for Slc39a12 and expression of Slc39a12 in brain 123
Figure 4-8– Gateway Recombination Cloning Technology 125
Figure 4-9– Polymorphism found in retinal cDNA for screening 125
Figure 4-10– ZIP12 transfection in HEK293 cells 127
Figure 4-11–Optimisation of ZIP12-5194 and ZIP12-5193 in Jurkat lysate 130
Figure 4-12 – Peptide incubation of ZIP12-5193 and ZIP12-5194 131
Figure 4-13–Cell-free production of ZIP12 protein.....133
Figure 4-14- Staining using V5 and ZIP12 antibodies 134
Figure 4-15–Sonication fails to remove protein aggregates 136
Figure 4-16– Aggregation of ZIP12.....137
Figure 4-17–Immunostaining of HEK293 and CHO cells.....139
Figure 4-18–ZIP12 protein is present on the plasma membrane of HEK293 cells. 142
Figure 4-19–ZIP12 protein is present on the plasma membrane of CHO cells. 143
Figure 4-20–Organelle localization of ZIP12 protein in HEK293 cells 144
Figure 4-21–ER localization of ZIP12 in CHO cells 145

Figure 4-22–Transfection of ZIP12 in ARPE19 cells.....147
Figure 4-23–ZIP12 is localized on the plasma membrane of ARPE19 cells.....148
Figure 4-24–Organelle localization of ZIP12 protein in ARPE19 cells.....149
Figure 4-25–Function of ZIP12.....151
Figure 5-1– Zinc measurement using ZnAF2 in DMEM/F12 growth medium.....161
Figure 5-2- TER measurement in ARPE19.....163
Figure 5-3–Immunostaining for ZO1 on ARPE19 cells.....165
Figure 5-4 – Percentage reduction of alamarBlue in ARPE19 cells.....167
Figure 5-5- QPCR data showing relative expression of RPE specific genes.....169
Figure 5-6 – Logarithmic relative expression of RPE specific genes.....170
Figure 6-1- Types of endothelia.....176
Figure 6-2- LA induces fenestrae formation.....181
Figure 6-3- Measurement of free intracellular zinc using $ZnAF_2$.....182
Figure 6-4 – 125 μM added ZnSO4 cause PV-1 protein rearrangement.....184
Figure 6-5 – Treatment of bEND5 cells with 100-200μM of added ZnSO4.....185
Figure 6-6 – Time course treatment with 125μM of added ZnSO4.....187
Figure 6-7 – TEM pictures showing fenestrae formation.....189
Figure 6-8 – Sizes of fenestrae were.....191
Figure 6-9–Calcein assay and propidium iodide staining in bEND5 cells.....193
Figure 6-10 – Effect of divalent metals on fenestrae formation.....196
Figure 6-11- Effect of divalent metals on fenestrae formation.....197
Figure 6-12–Effect of divalent metals on fenestrae formation (TEM).....197
Figure 6-13–Relationship between VEGF, nicotine and zinc.....200
Figure 6-14–Phosphorylation of ERK1/2 is not involved in fenestrae formation.....201
Figure 6-15–Bioavailable zinc in Bruch's membrane.....207
Figure 7-1–Schematic model of normal and diseased RPE.....213

1. General Introduction[1]

1.1. Zinc Overview

1.1.1. Biological functions of Zinc

Zinc is an indispensable and ubiquitous trace element present in many tissues in a wide range of organisms. The total amount of zinc found in human body is estimated to be 1.4-2.3 grams, with an average of approximately 20-30 µg/g zinc present in non-pathological human tissues (Karcioglu, 1982). The highest tissue concentrations of zinc in man are found in the retina and choroid complex, where, 464 and 472 µg/g of zinc is found respectively (Galin et al., 1962).

Zinc requirements for the body differ with gender and age. The National Institutes of Health established a recommended daily allowance (RDA) of 2-3 mg for infants, 9 mg for adult female, and 11 mg for adult male. For pregnant and lactating women, the RDA is raised to 12-13 mg (http://ods.od.nih.gov/factsheets/Zinc-HealthProfessional/). Within the body, zinc is predominantly obtained through dietary means. Food sources rich in zinc include oyster, red meat such as beef, as well as pulses and beans (http://ods.od.nih.gov/factsheets/Zinc-HealthProfessional/). Dietary zinc absorption occurs in the gastrointestinal tract; however, the level of absorption can be affected by the presence of as phytate. Phytate, an indigestible molecule present in majority of grains and legumes is able to form stable complexes with various metal cations such as zinc, copper, nickel, cobalt, manganese, iron and calcium (Rink, L (ed) 2011, *Zinc in Human Health*, Amsterdam). This results in poor absorption of these metals, causing a possibility of zinc and other metal deficiency if phytate is consumed in large quantities.

Zinc is able to bind into other proteins through interactions with other amino acids. It predominantly binds through the sulphur residue in cysteine, oxygen present in glutamate and aspartate, as well as nitrogen present in histidines (Rink, L (ed) 2011, *Zinc in Human Health*, Amsterdam). The affinity of zinc metal to the other atoms is

[1] Some elements of this chapter have been published in:

Barzegar-Befroei, N., Cahyadi, S., Gango, A., Peto, T., and Lengyel, I. 2011. Zinc in Eye Diseases. *Zinc in Human Health*. Amsterdam: IOS Press.

determined by the presence of hydrogen bonds in the structure. This has been shown in the case of carbonic anhydrase, one of the strongest binders of zinc metal. Carbonic anhydrase has 4 ligands for zinc, all of which are connected with hydrogen bonds with the side chains. This greatly increases the affinity of the binding site for zinc (Lesburg and Christianson, 1995). Zinc has been widely implicated as a structural component of metal-binding proteins such as metalloproteinases (Vallee and Falchuk, 1993). The zinc-binding metalloproteins such as protein kinase C (PKC) and superoxide dismutase (SOD) are involved in cellular proliferation, signalling, and structural functions. Furthermore, the binding of zinc to domains and motifs such as zinc finger, zinc cluster and zinc twist, enables specific gene regulatory processes to be activated (Vallee and Falchuk, 1993). Most strongly bound zinc form part of the structural component of proteins. If zinc affinity in the metal binding site is weak, the metal may participate in catalytic activities by acting as nucleophiles. For instance, alcohol dehydrogenases possess zinc binding site within the structure of the enzyme. The presence of zinc allows the transfer of negatively charged hydride ion from NADH to acetaldehyde (CH_3CHO), ultimately resulting in production of ethanol (CH_3CH_2OH). This is achieved through stabilisation of the oxygen residue in acetaldehyde, which in turn create a positive charge on the carbonyl residue of acetaldehyde where the hydride ion is transferred to (Kimura, Koike, and Shionoya, 1997).

Phagocytosing leukocytes such as natural killer (NK) cells, neutrophils and macrophages require zinc in order to function properly as a part of innate immunity. In adaptive immunity, CD4T+ T cell maturation is induced when intracellular zinc level is reduced (Murakami and Hirano, 2008). Furthermore, in mammals, SOD activity converts $O_2^{\bullet-}$ to H_2O_2, which reduces oxidative stress within the cell. Neuronal death following axonal injury was increased in Cu/ZnSOD-/-mice (Reaume et al., 1996).

Zinc has an anti-inflammatory effect on cells through negatively regulating NFκB. Nuclear factor kappa-light-chain-enhancer of activated B cells (NF-κB) is a transcription factor that mediate both pro- and anti-apoptotic genes (Uzzo, et al., 2006) in cells. Under normal condition, NF-κB protein complex is retained in the cytosol by IkB, a negative regulator of NF-κB. Under cellular stress, IkB

degradation occurs, subsequently translocating NF-κB into the nucleus, activating a series of transcription of transcription factor and genes (Uzzo et al., 2006). Zinc is able to interfere with the activation of NF-κB through reducing expression of the pro-inflammatory cytokine TNF-α (Prasad, 2008, Uzzo et al., 2006). Studies using pulmonary artery-derived endothelial cells showed that zinc deficiency aggravate production of IL-6, a pro-inflammatory cytokines triggered by exposure to TNF-α (Hennig 1999, activation zinc in porcine). Furthermore, zinc is able to interact with pro-apoptotic caspase 3 and reduce the activity of the enzyme (Clegg et al., 2005).

Previous reports have demonstrated the ability of zinc to act as a neurotransmitter as well as a second messenger. Synaptic vesicles have been shown to contain zinc. Glutamate and gamma-aminobutyric acid (GABA) receptors contain zinc binding sites which enable synaptic vesicles to store zinc and they also have zinc transporters that facilitate the release of zinc into the cytoplasm (Ueno et al., 2002, Hosie et al., 2003). Redenti and Chappell reported the presence of zinc transporter 3 (ZnT3) as specific for the brain synaptic vesicles (Redenti and Chappell, 2004b). Zinc binding to calcium activated potassium channels may cause oxidative stress and lead to brain toxicity (Sensi et al., 2000). Zinc may also have an intracellular signalling effect. In dendritic cells lipopolysaccharide binding to toll-like receptor induces dendritic cell maturation as well as activation of CD4+ T- cells through up-regulation of zinc exporters and downregulation of zinc importers (Kitamura et al., 2006).

1.1.2. Zinc Homeostasis

Intracellularly, the bioavailable zinc concentration is maintained at a nanomolar level through uptake, storage and secretion (Bozym et al., 2010). Studies have indicated that zinc transporters are likely to be the main mechanism of zinc movement in various mammalian cells, although diffusion of zinc ions may occur under physiological conditions (Reyes, 1996). In mammals, there are two zinc transporter families one composed of solute-linked carrier genes, ZRT or IRT-like proteins (also known as ZIP proteins) and the other of cation diffusion facilitators (CDFs, also known as ZnT proteins)(Kambe et al., 2004). So far, at least 14 ZIPs and 10 CDFs (Kambe et al., 2004) havebeen identified.

Metallothioneins are small metal-binding proteins that have the capability to bind zinc, and act as a buffer against oxidative stress. This allows metallothionein to become the first line of defense when the concentration of intracellular zinc rises. For instance, it has been shown that the expression of metallothionein mRNA is induced after cells from a human colonic epithelial cell line are exposed to zinc (Kindermann et al., 2005). Bobilya and colleagues constructed a blood-brain barrier model using porcine brain capillary endothelial cells and demonstrated that a 50 μm/L Zn^{2+} exposure increased the expression of metallothionein and protein level in 12 hours, suggesting that metallothionein is crucial to limit zinc concentration in the brain capillary endothelial cells (Bobilya et al., 2008).

The majority of zinc is bound with a high affinity to metalloproteins, and so is said to be non-bioavailable. Approximately 40% of putative zinc-binding proteins are transcription factors possessing zinc-binding domains such as zinc finger motifs. Other proteins are zinc transporters or enzymes. Many groups of enzymes require zinc binding to function properly. Hydrolases and phosphatases utilise zinc to induce a nucleophilic attack on substrate. Kinases use zinc mainly for structural support. Ligases, isomerases, and oxidoreductases also join the zinc-binding group. Furthermore, zinc is also needed for proteins involved in gene regulatory processes such as DNA repair, transcription, translation and signalling protein (Andreini et al., 2006).

In blood serum, approximately 19 μm of Zn^{2+} is found bound to zinc-binding albumin. Endothelial cells were reported to have zinc-bound albumin receptors. When Zn^{65} uptake was measured, endothelial cells specifically transported only albumin with zinc bound to it. After endocytosis, the albumin appears to be recycled to the cytosol (Rowe and Bobilya, 2000).

1.2. **Zinc Transporters**

Zinc transporters are likely to be the main method of maintaining the appropriate zinc concentrations within the cells. Alternatively, calcium channels (Reyes, 1996) and proton pumps can also transport zinc. They can also be transported by calcium channels or proton pumps (Sekler et al., 2007). There are two zinc transporter families belonging to solute-linked carrier genes, ZRT or IRT-like proteins (also known as ZIP proteins) and cation diffusion facilitators (CDFs, also known as ZNT proteins). So far, research has identified at least 14 ZIPs and 10 ZnTs (Kambe et al., 2004). In this thesis, we will refer to the protein under the name ZIP and ZnT, with its genes named SLC39A, and SLC30A respectively.

1.2.1. SLC30A Family of Transporters

The SLC30 gene codes for a family of zinc transporters (ZnTs) which are ubiquitously expressed in all organisms (Liuzzi and Cousins, 2004b). There are three subfamilies of which the ZnTs are assigned to, and the 10 members of the mammalian ZnT proteins belong in subfamily 2 and 3 whereby non-mammalian transporters are grouped in subfamily 1. The ZnT family of transporters specifically promotes the transport of zinc from the cytosol to extracellular environment or compartmentalise zinc into organelles within the cell thereby reducing the concentration of zinc within the cells. Most ZnTs, with the exception of ZnT5 possess six transmembrane domains with a variable region between domains III and IV, which contains many histidine residues able to bind zinc (See Figure 1.1). Loss of these histidine residues due to gene mutations or incorrect translation of mRNA has been reported to result in various pathological conditions, which may include embryonic lethality, incorrect absorption of zinc, reduced body fat and weight in mice (Huang et al., 2007) and lethal milk syndrome caused by a mutation in the SLC30A4 gene encoding the ZnT4 protein. In lethal milk syndrome, the milk produced by the dams were devoid of zinc, causing death of pups (Murgia et al., 2006). Mutations in ZnT8 has been associated with Type I diabetes (Wenzlau et al., 2007). The distribution of ZnTs is widespread; although some are cell-specific (Redenti and Chappell, 2004b, Palmiter and Huang, 2004).

1.2.2. SLC39A ZIP FAMILY OF TRANSPORTERS

The SLC39 genes encode a family of zinc transporters (ZIPs) that are ubiquitously expressed in all organisms. Structurally, ZIP proteins are composed of eight transmembrane domains with a cytoplasmic loop between domain III and IV composed of histidine residues. It is further divided into 4 subfamilies, with ZIP9 in subfamily I, ZIP1, ZIP2 and ZIP3 in subfamily II, ZIP11 in subfamily III (also known as gufA). The rest of the transporters belong in LIV-1 subfamily, with ZIP7 and ZIP13 further characterized as HKE4 family members (Taylor et al., 2004). Figure 1.1 shows a typical structure of the LIV-1 subfamily of ZIP transporters with 8 transmembrane domains. The HIS labeling is predicted to be histidine-rich regions, the ◆ symbol represents N-linked glycan sites. Transmembrane 4 and 5 contains histidine rich sequences (NH and HHE in the diagram) thought to be involved in transporting zinc (Taylor et al., 2004). ZIP family of zinc transporters promote the transport of zinc from the extracellular environment into the cytoplasm or from the cellular organelles to the cytoplasm (Liuzzi and Cousins, 2004b). Mutations in protein or genetic level of SLC39/ZIP family members may lead to the development of various pathological conditions such as acrodermatitis enteropathica (AE), an autosomal recessive metabolic disorder caused by mutations in ZIP4 (Dufner-Beattie et al., 2003). Overexpression of SLC39A2 (encoding ZIP2 protein) has been implicated in asthmatic infants (Xu et al., 2009). The overexpression of ZIP7 is upregulated in tamoxifen-resistant breast cancer cell line (Taylor et al., 2008) and a mutation in ZIP13 has been implicated in Ehlers-Danlos syndrome (Fukada et al., 2008).

Figure 1-1 -Structure of SLC30 family and SLC39 (LIV-1) family of zinc transporters.

(A) The typical structure of SLC30 (ZnT protein) family member shows the 6 transmembrane domain with a histidine rich region between transmembrane 4 and 5. (B) The typical figure of the LIV-1 subfamily of ZIP proteins shows the 8 transmembrane domains along with histidine rich regions (His) and ◆ N-linked gylcan sites. Transmembrane 4 and 5 contains histidine rich regions which have been predicted as zinc binding sites. Picture taken from (Eide, 2006, Taylor et al., 2004).

No studies have so far addressed the question as to why mammalians need 24 mammalian zinc transporters to regulate zinc homeostasis. Cousins and Lichten have suggested that this could be due to the vast requirement of zinc within the human body compared to other metals such as copper or iron. As it has been explained in section 1.1.1, zinc is involved in structural, enzymatic as well as becoming a part of the transcription factor which requires a tight homeostasis. Furthermore, studies have shown that zinc can co-transport other metals. ZIP8 has been shown to co-transport manganese (He et al., 2006), ZIP14 is able to transport iron, furthermore, studies using *Arabidopsis Thaliana* have suggested that zinc transporters belonging to this species can transport other metals such as iron or copper (Robinson, 2007, Lin et al., 2003).

1.3. **Overview of the Structure of the Eye**

The human eye is an organ that receives external light, converting it into signals, which are then transmitted along the optic nerve head towards the brain. The brain further processes the information and generates visual perception.

Human eyes are spherical and approximately 24 mm diameter. They are formed of three layers, (1) the external layer is comprised of the cornea at the front and the sclera posteriorly. The cornea is 8mm in diameter and its transparent structure allows light to enter the eye. The white fibrous sclera provides structural support for the rest of the eye. (2) The highly vascular 'uveal' layer lies internal to the sclera and is comprised of iris, ciliary body and choroid. The rich vasculature of this layer mainly provides oxygen and nutrients to the eye and clears waste products. (3) The neural layer is comprised of the retina. The retina contains photoreceptor cells and other neurons which are crucial in detecting light stimuli and converting them into visual signals (see next section).

Inside the eye globe, there are three chambers present (see Figure 1.2). The anterior chamber lies just behind the cornea. Directly behind the anterior chamber is the posterior chamber in which the lens is located. The largest chamber is the vitreous cavity, which contains vitreous humor, a clear gel material that is almost devoid of cells and composed mainly of collagen and hyaluronic acid. The vitreous functions to maintain ocular shape and contributes to the forces that hold the retina and choroid in place.

Figure 1-2- Schematic diagram of the eye

Schematic diagram of the eye (Image obtained from Remington, Lee Ann. Clinical Anatomy of the Visual System. Newton, Massachusetts: Butterworth-Heinemann, 1998.

1.4. **Zinc in the Eye**

The eye contains the highest concentration of zinc, compared to other tissues including bone, muscle, liver, pancreas and kidney. In 1962, Galin extensively reviewed the concentration of zinc in ocular tissues, concluding that the highest concentration of zinc is present in the retina and choroid (see Table 1.1), followed by the ciliary body and the optic nerve. The concentration of zinc in the cornea, iris and sclera are significantly lower compared to the other parts of the eye (Galin et al., 1962). While majority of zinc found within the eye is tightly bound to zinc-binding proteins, a substantial amount is termed exchangeable owing to its dynamic nature and involvement in various biological processes (Maret, 2008, Colvin et al., 2010).

Table 1-1- Total zinc concentration in tissues

Total zinc concentration in the ocular tissue, bone, muscle, liver, pancreas and kidney (Galin et al., 1962, McBean et al., 1972). Parts per million is equivalent to μg/g of dry mass.

	Parts Per Million (PPM)	Reference
Cornea	25-35	Galin 1962
Iris	17-26	Galin 1962
Ciliary Body	189-288	Galin 1962
Retina	**385-571**	Galin 1962
Choroid	**419-562**	Galin 1962
Optic Nerve	67-161	Galin 1962
Sclera	47-52	Galin 1962
Lens	17-29	Galin 1962
Bone	218	McBean 1972
Muscle	197	McBean 1972
Liver	179	McBean 1972
Pancreas	115	McBean 1972
Kidney	194	McBean 1972

1.4.1. Retina, RPE, Choroid

This thesis is concerned with zinc at the RPE-choroid interface and in this section a review of the currently available literature on zinc in the retina, RPE and choroid is presented with some coverage of zinc metabolism in other parts of the eye. The human neural retina is highly structured and may be considered to be formed of multiple layers: the inner limiting membrane (ILM), nerve fibre layer (NFL), ganglion cell layer (GCL), inner plexiform layer (IPL), inner nuclear layer (INL), outer plexiform layer (OPL), outer nuclear layer (ONL), external limiting membrane (ELM) and photoreceptor layer (See Figure 1.2). The retina rests on the RPE. The inner limiting membrane is at the interface between the vitreous humor and the retina. Here astrocytes as well as Muller cells (cells which span the length of the retina) can be found. Within the GCL, ganglion cells are present. These transmit visual information from the outer retina to the brain. The axonal projections of ganglion cells can be found in the NFL. In the IPL dendritic projections of the ganglion cells synapse with amacrine cells and bipolar cells, two other neuronal cells within the retina. The OPL contains synapses from photoreceptor cells to bipolar and horizontal cells. The ONL contains the cell bodies and the inner fibres of the two classes of photoreceptor cell, the rods and cones. The ELM is not a true membrane but is formed by junctions between the outer ends of the Muller cells and the photoreceptors. The photoreceptor outer segment contains visual pigment. The rods are much more abundant than cones and optimally detect light in the dark whereas cones mediate colour vision in daylight (Clinical Anatomy of The Visual System – Page 49-75). Cones are most abundant at the macula, a region within the retina, which processes the high-resolution central visual field. Atrophy of photoreceptor cells within the macula results in loss of vision in AMD.

The retina contains the second-highest concentration of total zinc after the choroid (Grahn et al., 2001, Galin et al., 1962) and Figure 1.3 annotates the localisation of total as well as bioavailable zinc within the retina. The effect of zinc on neuromodulation in the retina has been demonstrated by Rosenstein and Chappell, where activation of glutamate-dependent gamma-aminobutyric acid (GABA) receptors in bipolar cells of skate was successfully blocked by the addition of 1μM zinc (Rosenstein and Chappell, 2003). Furthermore, depolarisation of rat retinal cells was associated with increased exchangeable zinc concentration within the OPL and photoreceptor inner segments as measured using zinc-selective dye Newport Green (Redenti and Chappell, 2005). Within the OPL and IPL, bioavailable zinc was has been visualised using autometallography in various cells in the INL, Muller cells and the Golgi apparatus of the horizontal and amacrine cells (Akagi et al., 2001, Kaneda et al., 2005, Redenti and Chappell, 2004b). Bioavailable zinc labeling in the outer segment discs has been reported in several studies (Hirayama, 1990, Wang et al., 2006b). Here zinc is involved in stabilization of photoreceptor discs (Bettger, 1993).

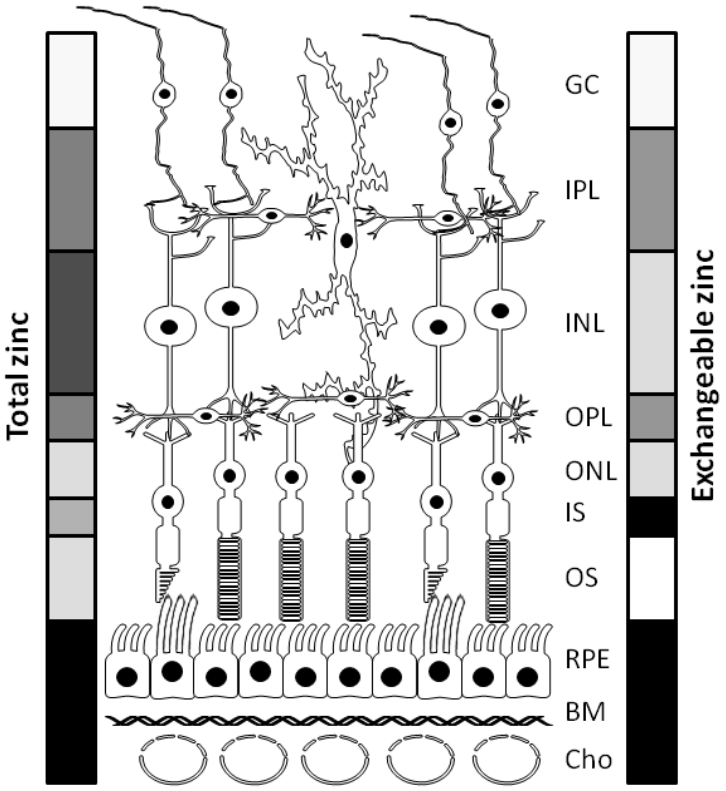

Figure 1-3–Organisation of the retina/RPE/choroid complex

A simplified diagram depicting the cellular organization of the retina/RPE/choroid complex: Cho, choroid; BM, Bruch's membrane; RPE, retinal pigment epithelium; OS, outer segment; IS, inner segment; ONL, outer nuclear layer; OPL, outer plexiform layer; INL, inner nuclear layer; IPL, inner plexiform layer and GC, ganglion cell layer. The shaded bar on the right represent exchangeable zinc levels in the different layers based on various studies (Akagi et al., 2001, Kaneda et al., 2005, Wang et al., 2006b, Ugarte and Osborne, 2001, Wu et al., 1993). The shaded bar on the left represents total zinc levels based on(Bowness et al., 1952, Galin et al., 1962, Tam et al., 1976, Eckhert, 1983, Koumantakis et al., 1983, Ulshafer et al., 1990, Fabe et al., 2000, Bentley and Grubb, 1991, Wills et al., 2008, Erie et al., 2009).

Picture taken from Barzegar-Befroei, N., Cahyadi, S., Gango, A., Peto, T., and Lengyel, I. 2011. Zinc in Eye Diseases. *Zinc in Human Health*. Amsterdam: IOS Press.

The RPE is a monolayer of hexagonal cells present underneath the photoreceptor outer segments (POS) of the retina (Figure 1.4). The main function of the RPE is to scavenge POS through its phagocytic capability. Much of the phagocytosed outer segment material is recycled but some accumulates in lysosomes to form lipofuscin and may ultimately be extruded into the sub-RPE space. From here, some material may gain access to the choroidal circulation (Strauss, 2005). Another function of the RPE cell is to mediate the retinal cycle (see section 1.4.3 on the retinal cycle). It also forms the outer blood-retina barrier. The majority of zinc within the RPE is tightly bound to zinc-binding proteins such as metallothionein, melanin, as well as enzymes responsible for the retinal cycle (Bok, 1993). Pigment granules have been associated with protection from oxidative stress as well as regulating phagolysosomal activity (Schraermeyer et al., 1999). Zinc is stored within melanin granules in the RPE cells, and hypopigmentation of the RPE has been linked to AMD. The RPE and choroid is rich in bioavailable zinc, significant amounts of which can be found within the Golgi apparatus (Huang et al., 2007), melanosomes and lysosomes (Ugarte and Osborne, 2001, Ulshafer, 1989). Zinc deficiency in the RPE predominantly compromises its anti-oxidative capacity, where cytotoxicity, reduced cellular proliferation and lowered metallothionein concentration have been observed (Tate et al., 1995, Tate et al., 1997). Furthermore, the failure in control of zinc homeostasis may contribute to aggregation of immunoproteins such as CFH found in sub-RPE deposits (Nan et al., 2008), ultimately leading to diseases like AMD.

The choriocapillaris is located directly underneath the RPE and Bruch's membrane. It is composed of a unique vascular network which provides nutrients and fluid for the RPE and the retina (Bernstein and Hollenberg, 1965). The abundance of fenestrations on the RPE aspect of the choriocapillaris endothelium makes this vascular bed much leakier than non-fenestrated vessels (Bernstein and Hollenberg, 1965). It is thought that the fenestration is maintained through VEGF secretion (Saint-Geniez et al., 2009b) from the RPE. A compromised interface can result in various abnormalities such as choroidal neovascularisation (CNV) and age-related macular degeneration (Lutty et al., 2010).

The choroid contains 416-572μg/g total zinc concentration, the highest within the eye (Galin et al., 1962, Wills et al., 2009). Discrepancies are present in studies attempting to measure the total zinc concentration in AMD or other non-AMD condition. A study by Wills et al reported an increase of total zinc concentration in human AMD eyes compared to control eyes (Wills et al., 2009). The result has been disputed by Erie, whose study reported reduced concentration of total zinc within the RPE and choroid in human AMD eyes. Unlike the retina, very little is known regarding the function of zinc within the choriocapillaris. However, both the RPE and choroid are heavily pigmented and pigmentation has been known to act as a mechanism for zinc storage (Kokkinou et al., 2004). The potential effect of zinc on a cellular model for fenestrated endothelium will be reported within this thesis (see Chapter 6).

Figure 1-4- Transmission electron micrograph picture of a normal RPE

A TEM picture showing normal RPEwhich is situated between the photoreceptor outer segments (POS) and the choriocapillaris (CH). On its apical side, the microvilli projection (V) aids the scavenging of POS by RPE. Within the intracellular region of the RPE, melanin granules (M), nucleus (N) and lysosomes (L) are present. On the basal side of the RPE, Bruch's membrane (B) separates the RPE from the CH. (Schraermeyer et al., 1999).

1.4.2. RPE Barrier Function

The retinal pigment epithelium (RPE) maintains the outer blood-retinal barrier function through expression of cell to cell junctions, secretion of growth factors and polarisation of its various receptor or proteins. An impairment of function in any of these functions can lead to RPE abnormalities.

Two main types of cell to cell junctions present in the RPE are tight and adherens junctions, each made up of complexes of transmembrane and non-transmembrane proteins. The functions of these junctions in the RPE include maintaining the integrity and polarity of epithelial cells and prevent leaking of fluid into the cells.

Located between the apical/ basolateral interface, tight junctions efficiently controls transportation of solutes, ions and immune cells between the cells (Hartsock, and Nelson, 2008). The two major transmembrane proteins forming tight junctions include claudin and occludin, as well as cytoskeletal connecting proteins such as zona occludens 1 (ZO-1) proteins. Tight junctions are important in maintaining cellular permeability which controls material diffusion in RPE cells. Occludins, a group of approximately 65kDa integral proteins were first reported by Furuse and colleagues (Furuse, et al., 1993). Occludins are indispensable in maintaining the characteristically high measurement of transepithelial resistance in epithelial cells. In MDCK cells, transfection with a mutant non-functioning occludin protein fails to form proper tight junctions as measured by the low transepithelial resistance. (Balda, et al., 1996). Occludins are known as the binding partner of various tight junction proteins, especially ZO-1 protein (Furuse, et al 1994). Peripheral membrane protein ZO-1 is important to maintain paracellular permeability as well as regulating cellular signalling through transcription factor ZO-1-associated nucleic-acid-binding protein (ZONAB) (Balda, and Matter, 2000). Claudins are a group of ubiquitous proteins of about 20-27 kDa in size with four transmembrane domains (Balkovetz, 2006). Claudins are also responsible in regulating permeability of the tight junction, whereby mice lacking claudin-1 failed to survive after birth due to dehydration caused by lack of epidermal barrier (Furuse, et al., 2002) meanwhile overexpression of claudin-2 protein in MDCK cells was found to increase permeability of the cells to cations (Amasheh, 2002).

Adherens junction mediates cell adhesion, intracellular signalling as well as regulating the actin cytoskeleton in epithelial cells. They are located underneath tight junctions and are composed of two groups of protein complexes, namely cadherin-catenin complex and nectin-afadin complex. Nectins and afadins bind to actin cytoskeleton meanwhile cadherins bind to a group of catenins, most commonly α and β-catenin. Through catenins, cadherins are able to mediate the intracellular signalling pathway, most notably through the Wnt signalling pathway which controls mouse RPE morphogenesis (Niessen, 2007, Westenkow, Piccolo and Fuhrmann, 2009). There are various types of cadherins, although the RPE predominantly expresses the neural cadherin (N-cadherin) and later during development the epithelial cadherin (E-cadherin) (Burke, et al., 1999). Despite it being a late onset, the expression of E-cadherin is crucial for differentiation of cultured primary cultures of human RPE and formation of adherens junction (Burke, et al., 1999).

Other than cellular junctions, the RPE is unique that it secretes a myriad of factors including vascular endothelial growth factor (VEGF), fibroblast growth factor (FGF), platelet derived growth factor (PDGF), epidermal growth factor (EGF) as well as pigment epithelium derived factor (PEDF). The main function of these factors is to mediate RPE metabolism, as well as the adjacent choriocapillaris. Arguably the most widely studied growth factor in RPE research, VEGF is secreted by the RPE to affect the choriocapillaris (Saint-Geniez 2009). The paracrine secretion of VEGF by the RPE has been shown to induce fenestration (Saint-Geniez 2009, Shimomura et al., 2009), and without RPE, choriocapillaris development fails to occur in mice (Marneros, et al., 2005). VEGF signalling is maintained through the polarised expression of VEGF receptors. In the RPE-choroid interface of human RPE primary cultures, expression of VEGF receptor can be found towards the RPE side (VEGFR 2 and 3), as well as within the choriocapillaris (VEGFR1) (Blaauwgeers, et al., 1999).

PEDF was first described in 1991 by Tombran-Tink and colleagues as an anti-angiogenic factor which promotes differentiation and neuroprotection in the retina (Tombran-Tink, Chader, and Johnson 1991, Barnstable and Tombran-Tink, 2004). PEDF counteracts the action of VEGF. Studies in rat shows that neovascularisation triggered by photocoagulation upregulates the expression of both PEDF and VEGF,

but expression of PEDF was maintained for three weeks in contrast to VEGF expression receded after a week, suggesting that PEDF protects against oxidative stress in the RPE (Ogata, et al., 2002). Polarisation of the RPE increased the level of expression and secretion of VEGF and PEDF significantly. PEDF is predominantly located apically in polarized cells meanwhile basolateral localization is preferred in non-polarised cells (Sonoda, et al., 2010). The research for PEDF receptor has not been as extensive as VEGFR research. However, the receptor for PEDF has been reported in neural retina (Aymerich et al., 2001).

Other than VEGF receptor, the expression of Na,K-ATPase is strictly confined to the apical RPE membrane. This receptor is responsible in providing energy for the purpose of transepithelial transport (Gundersen, 1991). Na,K-ATPase functions through transporting 3 sodium ions out and 2 potassium ions influx gradient which is mediated by ATP. This process ensures that the RPE has the energy to able to perform transport of solutes and molecules in and out of RPE cells (Preben-Morth et al., 2011). It has been suggested that Na,K-ATPase can interact with tight junction. Localisation of of Na, K-ATPase in the apical and basolateral membrane can be affected by Na, K-ATPase. Inhibition of Na, K-ATPase activity using ouabain was found to reduce transepithelial resistance value in cultured human RPE cells and associated with reduced permeability as there is no formation of tight junctions and another cellular junction desmosome (Rajasekaran, et al., 2001)

1.4.3. Zinc in Retinal Cellular Function

The retinal cycle is required for vision (Figure 1.5) and zinc is needed for the retinal cycle to function properly, as many of the retinal cycle enzymes are zinc-binding proteins. In the outer segment of the rod photoreceptor cells in the retina, 11-cis-retinal is tightly bound to opsin, producing a molecule called rhodopsin. The absorption of a photon of light induces the 11-cis retinal to undergo transisomerisation, which allows it to be transported into the RPE cell as all-trans-retinal. This occurs as the photoreceptors do not possess the cis-trans isomerase needed for the isomerisation of 11-cis-retinal to all-trans-retinol. The activated rhodopsin in turn activates transducin and the phototransduction cascade is initiated. Through phosphorylation of rhodopsin by rhodopsin receptor kinase and arrestin, all-trans-retinal is released, and transported through the disc membrane by the ATP binding cassette protein (ABCR). Using chaperones RPE65, CRBP, and LRAT the all-trans-retinal is converted to all-trans-retinyl ester. Isomerohydrolase converts the molecule to 11-cis-retinol and using NAD/NADP as substrate, through the action of retinol dehydrogenase 5 (RDH5), this gets converted to 11-cis-retinal to be transported back to photoreceptor outer segments (Strauss, 2005).

As majority of enzymes and other proteins involved in the retinal cycle require zinc to function properly, sub-RPE deposits found between the RPE cell and Bruch's membrane may indicate impaired activity of several zinc-related proteins. In summary, zinc is required for the proper functioning of proteins involved in the retinal cycle, and if proteins of the retinal cycle become disrupted, vision is disrupted.

Enzymes that aid phagocytosis of photoreceptor outer segments require zinc to be activated: A-mannosidase is a lytic enzyme found in RPE cell lysosomes which degrade photoreceptor outer segment. Wyszynski and colleagues reported that increasing the level of zinc induces the activity of α-mannosidase. The enzymatic activity of α-mannosidase, as determined by a decreased Vmax was also shown to decrease with older age. The Km value of the enzyme does not decrease. This suggested impairment in the degradation of photoreceptor outer segments in the retina with older age, which may lead to constant accumulation of debris in the

cells (Wyszynski et al., 1989, Tate et al., 1995). In addition, another report demonstrated that 0.25 μM of zinc was sufficient to induce a reduction in enzymes catalase and alkaline phosphatase and antioxidant metallothionein.

Neovascularisation is one of the hallmarks of late stage AMD. In order for blood vessels to breach Bruch's membrane, its remodelling must be disturbed with net, albeit focal, breakdown. The process of remodelling requires several protein-degrading enzymes namely matrix metalloproteinases (MMPs), suggesting that MMPs may have significant function in morphological changes of Bruch's membrane. MMPs are zinc-binding proteins. It has been reported that MMP3 inhibits angiogenesis in endothelial cell chemotaxis (Anand-Apte et al., 1997).

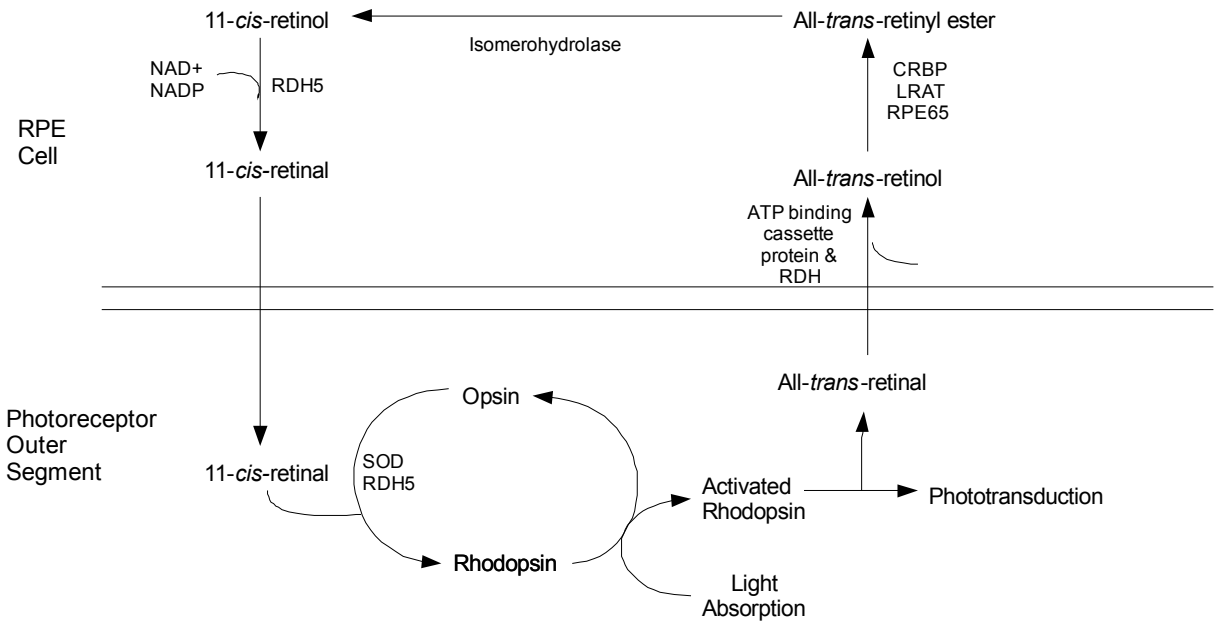

Figure 1-5- The retinal cycle

The retinal cycle (Diagram adapted from Olaf Strauss 2005).

1.4.4. Bruch's Membrane

Bruch's membrane is a connective matrix structure linking the RPE and the choriocapillaris as a part of the blood-ocular barriers. Bruch's membrane has 5 layers, formed of RPE basement membrane, inner collagen fibre layer, elastic fibre sheet, outer collagen fibre layer and basement membrane of the choriocapillaris (Sumita, 1961). It is heavily involved in controlling solutes and micronutrients passing between the two interfaces but restricts diffusion of large molecules (Cunha-Vaz, 1979). The thickening of Bruch's membrane, which can be followed by formation of protein aggregates (sub-RPE deposits) in aged-related diseases, could obstruct this material exchange. Very little is known about the presence of zinc in Bruch's membrane although the macula of normal BM contains 137ppm zinc, increasing to 254ppm in macula of AMD subjects (Lengyel et al., 2007). Information about zinc concentration in each respective layer is not available.

1.4.5. Cornea and Sclera

The cornea and sclera are interconnected and form the outer coat of the eye. The cornea is a clear and curved structure, which is involved in light transmission and light refraction. The cornea absorbs oxygen from the environment. Despite containing five layers within its structure, the cornea remains transparent; any opacity would compromise its function. The transparency of the cornea is maintained in part through the lack of blood vessels present within its structure. As a result of this, the cornea obtains its nutrition from the aqueous humor located in the anterior chamber as well as from vessels at the limbus (Clinical Anatomy of The Visual System – Page 19-25). As the concentration of zinc within the cornea is low (Karcioglu, 1982), studies have suggested that zinc delivery to the cornea is achieved through tears and systemically but not through the aqueous humor (Anderson et al., 1987). Zinc is required within the cornea to promote the process of wound healing. Neovascularisation has been observed in cornea of rats subjected to zinc deficiency (Leure-Dupree, 1986). Enzymes such as matrix-metalloproteinases are highly zinc-dependent (Takahashi et al., 2000) suggesting the involvement of zinc in corneal wound healing. Indeed, zinc deficiency in Wistar rats was found to lead to reduced microvilli on the corneal epithelium, an abnormality which was able to be reversed with zinc supplementation. Reduced

microvilli can promote tear film breakage which can compromise corneal immunity (Gong et al., 2004).

The sclera makes up the rest of the outermost layer of the eye. Formed of a layer of vascularised tissue and a robust fibrous layer of connective tissue, the sclera provides internal and structural support for the eye. The scleral fibers are composed of collagen fibrils arranged in an irregular way which contributes to its white colour and opacification (Clinical Anatomy of The Visual System – Page 24). Zinc may have a function in the connective tissue turnover in the sclera as zinc has been shown to affect collagen (Berman and Manabe, 1973) and matrix metalloproteinases in the anterior segment of the eye (Gaton et al., 1999).

1.4.6. Lens and Iris

Similar to the cornea, the lens is an avascular, transparent structure which functions to project light onto the retina. Approximately a third of the lens structure is protein, with water making up the rest. The cells within the lens continue to divide in one's lifetime; meanwhile the cells present are not removed but are instead compressed into thin layers. This results in increased lens weight and size throughout life, which can result in formation of cataract and impaired ocular optics (Clinical Anatomy of The Visual System – Page 79). The zinc content in the lens is lower than in the retina-choroid. However, studies have shown a possible correlation between zinc deficiency and formation of cataract in both animal models and man (Ketola, 1979, Richardson et al., 1985, Racz et al., 1979, Barash et al., 1982). Loss of zinc-copper superoxide dismutase activity has been associated with cataract (Behndig et al., 1998), suggestive of the loss of zinc mediated protection in cataract cases. However, zinc supplementation was not found to prevent progression of cataract (Seddon, 2007).

The iris is a pigmented structure which controls the amount of light that passes through the eye by altering the diameter of the pupil. Iris colour is determined by the amount of pigmentation present. Darker-coloured irides contain more melanocytes and melanosomes than those that are blue or lighter-coloured (Kokkinou et al., 2004). As melanin binds zinc, Newsome and colleagues have reported that the amount of melanin in the RPE can affect the uptake and

accumulation of zinc (Newsome et al., 1992). Melanin and zinc concentrations in the tissue are both reduced with age (Kokkinou et al., 2004).

1.4.7. Vitreous and Optic Nerve

The vitreous humor fills the large space in the posterior segment of the eye between the lens and retina. The gel-like substance contains 98.5-99.7% water, salt, soluble proteins and a network of fibers made up of type II collagen fibers and hyaluronic acid. The viscosity of the vitreous humor enables it to function as an effective shock absorber to prevent retinal damage. While few cells are found within the vitreous, hyalocytes and fibroblasts are thought to aid in the synthesis of glycoproteins and collagen (Clinical Anatomy of the Visual System page 95-99). The amount of zinc found within the vitreous humor can be affected by disease states such as cataract and diabetes (Nourmohammadi et al., 2006, Konerirajapuram et al., 2004). It has been suggested that zinc forms a part of the immune-defence mechanism through its anti-oxidative property (Bhooma et al., 1997).

Axons from the ganglion cells concentrate at the optic nerve head and signals are transmitted to the nervous system (Clinical Anatomy of the Visual System page 230-233). Rat models of zinc deficiency showed reduced myelinated axons and thinner myelin sheaths (Gong and Amemiya, 2001). The same observation was seen in monkeys treated with ethambutol, a tuberculosis drug which chelates zinc (Graham et al., 1998). The reduction in myelination was unable to be recovered with zinc supplementation, suggesting that zinc deficiency can lead to permanent loss of vision (Gong and Amemiya, 2001).

1.5. **Consequences of Zinc Deficiency and Overload in the Body and Eye**

1.5.1. Zinc Deficiency

Under normal conditions, cellular zinc concentration is very tightly controlled within a range of tolerable concentrations. Zinc homeostasis is achieved by regulating zinc-sequestering proteins such as metallothioneins, and albumin, or changing the expression of zinc transporter proteins which transports zinc in and out of the cell or intracellular compartments. It is also worth noting that the majority of zinc is bound with high affinity in the metal-binding domain of proteins.

Many diseases are associated with zinc deficiency caused by the failure of regulating proteins important for zinc homeostasis or dietary zinc deficiency. One of the most well-known zinc-associated disorders is acrodermatitis enteropathica, a condition caused by missense mutation in SLC39A4, the gene that encodes the ZIP4 importer protein, which is highly expressed in the apical part of jejunum and duodenum of small intestine. The onset of the disease often occurs during early childhood, often not long after weaning from breast milk (Cameron and McClain, 1986). The mutated ZIP4 protein does not possess the capability to bind zinc and hampers zinc absorption from the small intestine, leading to severe zinc deficiency (Muga and Grider, 1999). In addition to severe diarrhoea, skin lesions and growth retardation, there are ocular abnormalities associated with the disease. Decrease in thickness and polarity of the corneal epithelium, loss of Bowman's membrane, severe degeneration of the RPE, loss of optic nerve fibres and loss of ganglion cells have all been reported (Cameron and McClain, 1986). In 1963, Prasad reported the occurrence of growth stunting, and hypogonadism in Iranian patients with zinc deficiency (Prasad et al., 1963). Chronic alcohol consumption can lead to reduced serum zinc concentration which can cause impaired immunity, diarrhoea and depression. Ocular abnormalities associated with chronic alcohol consumption include impaired dark adaptation and night vision (McClain et al., 1986). Iron chelation therapy using desferoxamine in patients with thalassemia major has been associated with growth retardation, reduced hair and leukocyte zinc. Furthermore, increased urinary zinc was observed in patients treated with desferoxamine over the period of 1 month (De Virgillis, 1998). Many of the diseases are systemic and can

be improved by zinc supplementation (Grahn et al., 2001). However, supplements need to be prescribed with caution as excessive zinc can result in impaired copper absorption, leading to copper deficiency (Yolton, 1981).

Zinc deficiency results in various conditions in mammals. Animal studies using rats have shown that zinc deficiency leads to increased lipid peroxidation in the retinal pigment epithelium (RPE), as well as reduced metallothionein in the retina and RPE as visualised using electron microscopy (Miceli et al., 1999, Kindermann et al., 2005). Furthermore, developmental problems, increased cellular death and aberrant gestation have been seen (Jankowski et al., 1995). Rats subjected to marked zinc deficiency during gestation produced pups with severe eye disorders. Anopthalmia has also been reported in the pups (Rogers and Hurley, 1987, Grahn et al., 2001). Furthermore, in rat kidneys of animals subjected to a zinc deficient diet for 60 days, decreased number of glomeruli and increased nitric oxide synthase were observed. Increased nitric oxide synthase is a risk factor for vascular and renal diseases (Tomat et al., 2005).

1.5.2. Zinc Overload

Compared to the significant health problems associated with zinc deficiency, zinc overload does not generally cause health issues. *In vitro* experiments have documented the dual role of zinc in rabbit retinas. Isolated rabbit retinas treated with 500μM zinc released GABA and NMDA resulting in increased neurotoxicity in the eye. This condition could be reversed by adding equimolar concentration of the zinc chelator diethyldithiocarbamate (Ugarte and Osborne, 2001). Proteomics experiments showed that increasing the zinc concentration to cytotoxic level (10 ppm) results in reduced expression of eleven genes involved in the electron transport chain, and subsequently lower adenosine triphosphate (ATP) levels in cells (Kindermann et al., 2005).

The physiological effects of zinc overload are not very well documented. However, it was noted that increased zinc concentration may cause copper deficiency, which may result in anemia, neutropenia, arthritis, arterial disease and osteoporosis in humans (Danks, 1988). Cells respond to increased intracellular zinc concentration by upregulating the expression of zinc exporters and metallothioneins, in addition to down-regulating zinc importer expression (Miceli et al., 1999).

1.6. **Age-Related Macular Degeneration**

1.6.1. Overview of Age-Related Macular Degeneration

Age-related Macular Degeneration (AMD) is a multifactorial disease which is characterised by pathological changes such as pigment (RPE) remodelling, with hypertrophy and depigmentation associated with the formation of soft drusen, hard drusen and eventually in some cases geographical atrophy of RPE cells. The disease is presently the most common cause of blindness in the developed world, occurring in >35% in people over 75 years of age (Stone, 2007). Exudative choroidal neovascularisation occurs in approximately 10% of patients and cumulates in vision loss (Stone, 2007). Focal sub-RPE deposits, or drusen protein-rich aggregates of > 63μm - <124μm diameter and areeither diffuse,and covering a large area (soft drusen) or punctate, brighter and smaller (hard drusen). Figure 1.6 shows the four stages of AMD as viewed with fundus photography (top panel) or immunohistochemical staining (panel below), with early AMD (A) showing several small deposits but lacking atrophy of cells and generally causing no extensive vision problems. Intermediate AMD (panel B) showed a markedly increased number of deposits with some coalescing as well as areas of early geographic atrophy. Advanced AMD can result from widespread geographic atrophy, and/or choroidal neovascularisation (CNV). Widespread geographic atrophy that affects the fovea will result in the loss of cone photoreceptor cells required for producing high resolution and colour vision. What triggers the onset of CNV in 10-15% of AMD subjects is unknown, however around 80% of vision loss is associated with CNV (Jager et al., 2008).

There are several known predisposing factors for AMD. Genetic factors have included polymorphisms at AMD susceptibility loci on chromosome 1 and 10q26. High risk polymorphisms in Complement Factor H (CFH) (Klein et al., 2005), ARMS2 (Kanda et al., 2007), HTRA1 (Dewan et al., 2006), all located within these loci have been shown to predispose an individual to AMD (Stone, 2007, Francis and Klein, 2011). Other genetic associations have included polymorphisms in Apolipoprotein E (ApoE), ATP-binding cassette A4 (ABCA4), and Chemokine 3 Receptor 1 (CX3CR1) (Francis and Klein, 2011). Smoking strongly predisposes

one to AMD, and therefore has been considered an environmental risk factor (Stone, 2007, Francis and Klein, 2011).

Current treatment options are limited for AMD patients. In early and late stage AMD, zinc supplement containing zinc and antioxidants have been prescribed to patients (2001). Geographic atrophy at present is untreatable. CNV has been widely treated with laser ablation therapy as well as antibodies against vascular endothelial growth factor (VEGF) such as Lucentis and Avastin (Rattner and Nathans, 2006). Attempts have been made to transplant RPE cells into AMD patients to restore the dysfunctional RPE cells (Binder et al., 2007).

Figure 1-6- Fundus photograph and pathological features of AMD

The fundus photographs (top panels) and histopathological micrographs (lower panels) shows three stages of AMD, starting from early AMD (A), characterised by the presence few small-medium sized deposits. Intermediate AMD (B) with a few large deposits and a much increased number of small-medium sized deposits. The end stages of AMD showed either geographic atrophy (C), or neovascularisation (D). (Image from (Jager et al., 2008)

1.6.2. AMD Pathogenesis

The pathogenesis of age-related macular degeneration (AMD) is likely to be multifactorial, involving a complicated range of events. Prior studies have shown that the pathogenesis of AMD involves a combination of biological processes happening in the RPE, as well as other extrinsic factors. These events cumulatively result in damage to the RPE, choriocapillaris, as well as the thickening of Bruch's membrane. The changes in the RPE-choroid interface triggers inflammatory events in the interface, resulting in formation of large sub-RPE deposits, geographic atrophy and choroidal neovascularisation, the three hallmarks of advanced AMD.

The eye is highly susceptible to the presence of light-induced oxidative stress. The visual phototransduction occurring in the retina means that the region is regularly exposed to damaging blue light as well as oxygen, rendering it highly susceptible to light induced-oxidative stress (Beatty, et al., 1999). One of the functions of the RPE is to combat against oxidative stress by absorbing damaging blue/ultraviolet light through the presence of melanosomes in the RPE (Burke, 2011) and photoreceptor pigments such as such as lutein and zeaxanthin (Schupp, et al., 2004). The presence of lysosomes and phagosome in the RPE helps digests the photoreceptor outer segments (POS) to promote regular turnover. Under increased cellular stress, the failure to digest and remove the POS promotes the crosslinking of proteins. This crosslinking of proteins produces pigmented, insoluble aggregates termed lipofuscin (Jung, Bader, and Grune, 2007).

Lipofuscin is one of the two main cellular debris found in the RPE-choroid interface, the other being drusen (Nowak, 2006). One of the major effects of lipofuscin is its ability to reduce proteosomal activity of the RPE. One of the main substituent of lipofuscin is *N*-retinylidene-*N*-retinylethanolamine (A2E). The presence of A2E has been shown to interfere with the ability of the RPE cells to phagocytose photoreceptors, thereby increasing the presence of debris in the RPE. The disruption of RPE metabolism can potentially be implicated in the pathogenesis of AMD (Finnemann, 2002). In addition, A2E favours the formation of reactive oxygen species which promote more aggregate formation. *In vitro*, the presence of A2E in ARPE19 cells exacerbated the cellular damage and apoptosis caused by exposure to blue light (Sparrow et al., 2002). While lipofuscin is characteristic of AMD, whether it is a

secondary effect or a causative effect of AMD is unknown although there is an age-related increase in lipofuscin formation. (Swaroop, 2009). Recently, a publication indicated that rat subjected to zinc-deficient diet showed a much more prominent lipofuscin aggregation than those with zinc-replete diet although the mechanism is yet to be uncovered (Biesemeier, et al., 2011)

Apart from damages caused by oxidative stress, there are other factors which could influence and indirectly predispose an individual to AMD. These extrinsic factors include age, genetics, and personal habits such as smoking. AMD predominantly occurs in people of age > 65 years old, making it the most common cause of legal blindness in the aging population. Numerous studies have uncovered the susceptibility loci in Chromosome 10q26, where the presence of several genes including ARMS2, PLEKH1, and HTRA1 may predispose certain group of population to developing AMD (Jakobsdottir, et al., 2005). As of late 2008, studies have also named people with mutations in Complement Factor H (CFH) to be predisposed to AMD (Nan, et al 2008). Regular turnover of the extracellular matrix of Bruch's membrane by matrix metalloproteinases is crucial to maintain an optimal thickness of the matrix. Smoking is a strong contributor to the pathogenesis of AMD, with the AREDS study reporting smoking as the strongest extrinsic risk factor for AMD (AREDS, 2001).

Another hallmark of AMD is the formation of protein deposits between the RPE and Bruch's membrane termed drusen. Numerous publications have suggested that the source of drusen is inflammation occurring in the RPE. (Hageman et al., 2002, Anderson et al., 2002, Johnson et al., 2001) It is possible that the initiation of oxidative stress exacerbated immune reaction from the RPE/choroid which amplified the pathogenesis of AMD. Studies have reported of the upregulation of inflammatory cytokines and immune-related proteins in AMD patients such as IL1, IL6, and TNF-α. A recent study shows that the upregulation of IFN-γ caused by photooxidative stress of the ARPE19 also resulted in the upregulation of CFH. CFH is an inhibitor of the complement system which triggers pro-inflammatory complement cascade (Lau, et al., 2011). Positive immunostaining of coagulating-factor proteins such as thrombin, acute-phase proteins, immune-related proteins such as complement proteins, and amyloid-β has been seen in drusen (Hageman, et al 2001). In 2005, publications showed that a Tyr502His mutation in the CFH gene is related to increased risk of

developing AMD (Klein, et al., 2005, Edwards, et al., 2005). Furthermore it is possible that in aging population, the reduction of immune function results in lowered ability to combat oxidative stress, leaving the tissue more susceptible to AMD. The thickening of Bruch's membrane has been attributed to increase in tissue inhibitor of matrix metalloproteinases (TIMP-3). Activity of TIMP-3 is crucial to regulate extracellular matrix turnover. TIMP-3 level is increased with aging and in human AMD subjects (Kamei, and Hollyfield, 1999).

It is crucial that the RPE functions optimally to absorb damaging blue light as well as recycling photoreceptor outer segments. Failure to do so may result in increased formation of drusen and lipofuscin.The presence of drusen and lipofuscin resulted in morphological and cellular changes within the RPE, Bruch's membrane and choroid interface. These changes include, but are not limited to pigmentation changes in the RPE where hypo/hyperpigmentation can occur, and failure to phagocytose photoreceptor outer segment which affects RPE metabolism (McLeod et al 2009). The choriocapillaris experiences a reduction in lumen diameter as well as a loss of fenestration (McLeod et al 2009). Death of RPE cells can trigger a secondary loss of choriocapillaris (Mullins et al., 2011, McLeod et al 2009).

1.6.3. Use of Zinc in AMD

Zinc modulates many antioxidants which protect against oxidative stress that might be triggered in AMD. Antioxidants present in the Retinal Pigment Epithelium (RPE) include catalase, metallothionein (MT) and glutathione peroxidase (GPx). Low levels of zinc result in lowered antioxidants that leave the RPE vulnerable to oxidative injury which in turn may trigger AMD. Tate and colleagues reported that a reduced level of MT in cells results in less zinc being stored, and antioxidant levels were also found to be reduced. Similarly, pigmented mice fed with a low zinc diet were found to have increased lipid peroxidation as measured by the thiobarbituric acid reactive assay (TBARS). The group also found a reduced MT level in liver, RPE-choroid and retina (Miceli et al., 1999). Furthermore, lowered zinc may affect superoxide dismutase (SOD), a zinc protein that converts $O_2^{\bullet-}$ to H_2O_2 to prevent harmful oxidative damage to the cellular environment (Miceli et al., 1999). A 24% reduction in zinc concentration was found in the RPE-choroid complex of older patients, suggesting that zinc supplementation might have a beneficial effect in preventing AMD (Erie et al., 2009).

Clinical trials have reported mixed results regarding the use of zinc supplementation in AMD patients. The AREDS report number eight indicated that the consumption of 80 mg zinc oxide for 80 months in a late stage AMD clinical trial with 312 people resulted in improvement of vision and prevents night blindness. Furthermore, a follow-up study showed that lower oxidised cysteine or cystine was found in subjects who took zinc supplementation for AMD. This may indicate better protection against oxidative stress (Moriarty-Craige et al., 2007). Conversely, a similar study with 3654 patients with early stage AMD consuming zinc supplementation over a period of five years did not report a protective effect against AMD (Flood et al., 2002).

Excessive intracellular zinc can result in cytotoxicity, and therefore zinc concentration needs to be restrained within tolerable limits (Bozym et al., 2010). Wood and Osborne (2003) reported that in human RPE cell culture, zinc concentrationsof 25 μM are toxic if not chelated. Toxicity is likely to be caused by production of oxidative radicals. A concentration of 18 μM of zinc reduces cell

viability in human RPE cell culture to 50% which is reversed once supplemented with metabolic substrates and antioxidants (Wood and Osborne, 2003). Intriguingly, the concentration of zinc in the RPE-choroid complex is very high, but under normal conditions, the cells do not appear to undergo significant oxidative stress.

The varied results found in clinical trials indicate that further studies are required before zinc supplementation is introduced routinely as a preventative treatment of AMD. A recent study found that sub-RPE deposits contain a very high amount of bio-available zinc. Bruch's membrane was found to contain 254 ppm of zinc, meanwhile the macula contains 130 ppm and in the peripheral region of the choroid 123 ppm (Lengyel et al., 2007). However, presently there is a lack of knowledge regarding the source of zinc in these sub-RPE deposits. It was suggested that sub-RPE deposits may obtain its zinc from the choroid complex, and through Bruch's membrane. It was found that drusen form around choroidal intercapillary pillars in older patients (Lengyel et al., 2004). With the knowledge that the overall zinc level in the sub-RPE deposits is very high, it is interesting to speculate on the mechanism responsible for transport of zinc to the vicinity of sub-RPE deposits. Zinc transporter activity or expression might be improperly regulated in AMD patients.

1.7. **Aims of the Thesis**

The highest tissue concentration of zinc in man is found in the RPE/choroid complex (Grahn et al., 2001, Karcioglu, 1982). Here zinc is required for regulating a myriad of enzymes involved in the retinal cycle, in the phagocytic activity of the RPE as well as the oxidative processes that are so important at the RPE-choroid complex. We understand a great deal about the role zinc plays in enzymes and transcription factors, but how zinc levels are regulated intra- and extracellularly in the eye is largely unknown. As zinc deficiency had been associated with serious eye diseases like AMD (Grahn et al., 2001) it is perhaps not surprising that zinc supplementation is one of the most widely used preventive therapies for AMD, despite the mixed results of recent international clinical trials (Mitchell et al., 1995, 2001, Ho et al., 2011b). In 2004, work in our laboratory reported that sub-retinal RPE deposits, the hallmark of AMD, contained a surprising>500 ppm of zinc in the extracellular Bruch's membrane (Lengyel et al., 2007). How accumulation in drusen and decrease in Bruch's membrane and RPE cells contribute to AMD, however is largely unexplored.

The work described thesis aimed to elucidate potential mechanisms of zinc transport in the posterior eye and to explore the effects of altering extracellular zinc concentration on vascular endothelium and retinal pigment epithelium.

We embarked on a series of experiments that were designed to address how the RPE, the choroid and Bruch's membrane change their properties in an altered zinc environment. We used molecular and cell biology and bioinformatics as well as studies on human cadaveric tissues to gather information on how zinc might be involved in normal and pathological processes at the RPE/choroid interface.

1. First we aimed to identify the zinc transporter(s) at the RPE/choroid interface in cadaveric tissues and cultured cells.
2. Then we aimed to characterize how RPE/choroid specific transporter(s) contribute to altered zinc balance.
3. Finally, we aimed at investigating how cells respond to the modulation of extracellular zinc environment using cellular models for RPE as well as the fenestrated choroidal endothelium.

2. Materials and Methods

2.1. **Reagents**

Four percent paraformaldehyde (PFA) was freshly prepared using 32% PFA (Electronic Microscopy Sciences, Hatfield, USA) diluted in Phosphate Buffer Saline 1x concentration with neutral pH (Gibco Invitrogen, Paisley, UK). Ethanol (VWR International, Lutterworth, UK) used are molecular biology grade with 99.9% purity.

2.2. **Buffers, Solutions and Gel Preparations**

4% Paraformaldehyde

7 parts deionised water

1 part 32% Paraformaldehyde

Tris-Buffered Saline 10x

200mM Trizma (Sigma-Aldrich, Gillingham, UK)

1500mM NaCl (Sigma-Aldrich, Gillingham, UK)

Make up 600 ml solution with deionised water and adjust pH to 7.4. Top up volume with dH2O to 1000ml.

Tris-Buffered Saline Tween (TBST) 1x

900ml Deionised H2O

100ml TBS 10x

Tween20 0.1% (v/v)

SDS-Polyacrylamide Gels (10%)

For one gel, materials added in consequence:

Stacking Gel

2ml deionised water

1.65ml Acrylamide-Bis 30%

1.25ml Tris pH 6.8

50µl SDS10% (w/v)

25µl Ammonium Persulphate (APS) 10% (w/v)

10µl *N*,*N*,*N*′,*N*′-Tetramethylethylenediamine (TEMED)

Resolving Gel

2ml deionised water

1.65ml Acrylamide-Bis 30%

1.25ml Tris pH 8.8

50µl SDS10% (w/v)

25µl Ammonium Persulphate (APS) 10% (w/v)

10µl *N*,*N*,*N*′,*N*′-Tetramethylethylenediamine (TEMED)

Ammonium Persulfate (APS) 10%

10g APS (Sigma-Aldrich, Gillingham, UK)

100ml deionised H2O

Aliquot and frozen at -20^{o}C

Sodium-Dodecyl Sulfate (SDS) 10%

10g SDS (Sigma-Aldrich, Gillingham, UK)

100ml deionised H2O

Blotting Buffer 10x

1500mM Glycine (Sigma-Aldrich, Gillingham, UK)

20mM Trizma

Blotting Buffer 1x

For 500ml

350ml deionised water

100ml Methanol (20% v/v)

50ml Blotting buffer 10x

5ml 0.02% SDS

Western Blot Blocking Solution

5g Non-fat Dry Milk (Bio-Rad, Hemel Hampstead, UK)

100ml TBST 1x

Running Buffer 1x

192mM Glycine (Sigma-Aldrich, Gillingham, UK)

25mM Trizma

0.1% (w/v) SDS

Ponceau S Stain 10X

1g PonceauS (Sigma-Aldrich, Gillingham, UK)

50% Acetic Acid (Fisher-Scientific, Horsham, UK)

In order to use, dilute 1:10. Stain PVDF membrane for 5 minutes with gentle agitation before rinsing with H2O for 30 minutes on the shaker at room temperature.

Lysis Buffer for Western Blot

50 mM Tris pH 7.4

150 mM NaCl

0.5% NP40

10% Protease Inhibitor Cocktail (Sigma-Aldrich, Gillingham, UK)

5x Laemmli Buffer (Sample Buffer)

250mM Tris-Cl pH 6.8

5%(w/v) Sodium Dodecyl Sulfate (SDS)

50% (v/v) Glycerol

500 mM β-Mercaptoethanol

0.02% (w/v) Bromophenol Blue

Top up with deionised water to appropriate volume

Luria-Bertani Broth (LB Broth)

4g Tryptone (Merck, Feltham, UK)

2g Yeast extract (Merck, Feltham, UK)

4g NaCl

400ml deionised water and autoclave

Luria-Bertani Agar

2g Tryptone

1g Yeast extract

1.6g NaCl

3g Agar

200ml deionised water and autoclave

Whenever appropriate, antibiotics were used for agar and broth at concentrations:

Ampicillin 100µg/ml

Chloramphenicol 170µg/ml

Zeocin 30µg/ml

Glycerol Stock

20µl Glycerol

80µl unpelleted bacterial culture

Immunocytochemistry Blocking Solution for All Cell Lines Apart from BEND5 cells.

1.16g Bovine Serum Albumin (BSA) (Sigma-Aldrich, Gillingham, UK)

0.5g Glycine

200ml PBS 1x

Immunocytochemistry Permeabilisation Solution for All Cell Lines Apart from BEND5

0.3% BSA

0.3% TritonX-100

In PBS 1x

Immunocytochemistry Blocking Solution for BEND5 cells.

0.2% Fish skin gelatin (Sigma-Aldrich, Gillingham, UK)

5% Normal goat serum (Sigma-Aldrich, Gillingham, UK)

In PBS 1x

Immunocytochemistry Permeabilisation Solution for BEND5 cells

0.1% TritonX-100 in PBS 1x

2.3. **Antibodies**

Please see Appendix 1 for a list of all the antibodies used in this study.

2.4. **Sample Preparation**

2.4.1. Cadaveric tissue dissection

Human cadaveric eyes not exceeding 30 hours post-mortem were used. In instances where sclera was still attached to the back of eye, the whole eye was placed on a Petri dish under an inverted microscope. Following removal of the lens, the ora serrata was cut 3mm circumferentially and iris removed to facilitate the removal of the vitreous humor. Neurosensory retina (NS) attached to the vitreous humour was carefully isolated. Retinal pigment epithelium (RPE) cells were collected for RNA isolation using 600 µl of lysis buffer applied directly into the eye cup. Remaining choroid was rinsed with PBS and collected. For RNA work, RNAlater (Qiagen GmbH, Germany) was used to preserve the quality of RNA in choroid samples and deactivate RNAses. In order to preserve structure and morphology, tissues were treated with 4% PFA and stored in 4^{o}C temperature for future use.Remaining tissues were returned back to the Department of Pathology at Institute of Ophthalmology to be disposed of in accordance with best practise guidelines.

2.4.2. Tissue Preparation

Tissues were generally stored in RNAlater, which preserves RNA. A piece of tissue $\leq$ 30 mg in weight was dissected,and placed in a sterile blue homogenizing tube and using hand pestle or hand held rotor, ground well to produce homogenous lysate.

2.4.3. Cadaveric Human RPE Preparation

The retina, RPE and choroid were removed in subsequent order for RNA isolation. The anterior pole was removed from the posterior pole before removing the vitreous from the retina. The RPE and choroid was flatmounted. Using pipette, PBS was carefully applied onto the RPE layer to dissociate the cells. The RPE was placed on microcentrifuge tubes before spun at highest setting (14000rpm) for 10

minutes to pellet it. The choroid and retina was cut to ≤ 30mg sections for RNA isolation purpose. 600 µl of lysis buffer or alternatively RNAlater was applied to per 30mg tissue. The cell lysate was collected and transferred into sterile and RNAse free 2ml tube and mixed well either by pipetting or vortexing.

2.4.4. Cell culture preparation

Cell cultures were rinsed twice with PBS 1x to remove any traces of cell culture medium. 700 µl of lysis buffer containing protein denaturant guanidine thiocyanate (RLT) was added to the cell culture dish. A cell scraper (BD Biosciences, USA) was used to gather the lysate, which was then mixed by pipetting up and down in the cell culture dish. This was then followed by standard RNA isolation procedure as described in the manufacturer's protocol (See section 2.5.1).

2.5. **RNA Studies**

2.5.1. RNA isolation

Prior to starting the procedure, RNAseZap and DNAZap (Ambion Inc, USA) was always used to prevent contamination from genomic DNA and degradation of RNA. The addition of β-mercaptoethanol in the lysis buffer (RLT) further prevented RNAse activity. All RNA isolation was done using RNeasy Mini Kit (Qiagen GmbH, Germany) following the manufacturer's protocol. The cell or tissue lysate collected (700µl) was transferred onto a QIAshredder column (Qiagen GmbH, Germany), centrifuged for two minutes at 14000rpm and combined with 1x volume of 70% ethanol. The ethanol-lysate mixture was then transferred onto the spin column and centrifuged for 15 seconds at 10000rpm, washed once using wash buffer RW1, followed by 15 minutes of DNAse digestion step (Qiagen GmbH, Germany). The column was then washed again once with buffer RW1 and twice with buffer RPE. The RNA was eluted using DNAse/RNAse free water. The integrity of the RNA was tested using Bioanalyser (Bio-Rad, Germany) and only samples with RNA quality indicator (RQI) value of > 7 were used. Samples derived from cell culture regularly reach RQI value of 10, however due to potential post-mortem RNA degradation, RQI value from cadaveric tissues do not reach RQI of 10. In order to check for potential cross-contamination between the RPE, retina and choriocapillaris, qRT-PCR was performed with rhodopsin, RPE65 and Vascular

Endothelial Cadherin (VE-cadherin) for photoreceptor, RPE and endothelial specific genes respectively. The lower RQI number and evidence for cross-contamination (for data and explanation, refer to section 3.6) in cadaveric tissue indicated that our results need to be perceived carefully and that a false positive result for ZIP12 expression in RPE cannot be completely ruled out.

2.5.2. Quantification and integrity analysis

RNA concentration was measured using NanoDrop (ThermoScientific, Horsham, UK) and only RNA with 260/280nm ratio above 1.8 was used for all experiments. RNA integrity was assessed Bio-Rad Experion (Bio-Rad, Hemel Hampstead, UK).

2.6. **DNA Work**

2.6.1. cDNA synthesis

Precision Reverse Trancription Kit (PrimerDesign, Southampton UK) was used for cDNA synthesis according to the manufacturer's guide. For every cDNA synthesis reaction, 2.5 µg RNA template was used. A mixture of oligo-dT primers and random nonamer primers (2 µl), dNTP (1µl), RNA and water were added in a thin-walled 500 µl microcentrifuge tubes. Samples were heated with lids closed for 5 minutes at 65^{o}C, followed by immediate cooling on ice before 4 µl of MMLV 5x buffer, 5.2 µl of RNA-DNAse-free water, and 0.8 µl of MMLV enzyme were added. The reaction was placed on 42^{o}C hot block for 60 minutes and following that stored at -20^{o}C until used. See below for detailed protocol.

Annealing Step

RNA template, primer, dNTP and water mix was heated at 65^{o}C for five minutes before being rapidly cooled on a block of ice.

No		Amount
1	RNA template	2-5 µg
2	Reverse transcription primer (OligoDT and random nonamer)	1 µl
3	dNTP mix 10mM	1 µl
4	RNAse/DNAse free water	To 10µl

Extension Step

The mix containing RNA template, primers, dNTP and water (Annealing Step) was combined with MMLV buffer, enzyme and water before heated at 42^{o}C for 60 minutes. All cDNA samples were stored in -20^{o}C before used.

No		Amount
1	MMLV 5x buffer	4µl
2	RNAse/DNAse free water	5.2µl
3	MMLV reverse transcriptase enzyme	0.8µl
	Total	10µl

2.6.2. Quantitative RT-PCR

The primers were designed by PrimerDesign (Southampton, UK). The sequences for 24 murine and human zinc transporter primers and 3 housekeeping genes along with melting temperatures and cycling condition are shown in the Appendix 3 and 4. All qPCR reactions were done for 50 cycles with glyceraldehyde 3-phosphate dehydrogenase (GAPDH), tyrosine 3-monooxygenase/tryptophan 5-monooxygenase activation protein (YWHAZ) and ubiquitin C (UBC) as controls.

For every reaction, 50 ng of cDNA template, 10 µl of PrimerDesign 2x Precision^{TM} Mastermix, 4 µl of RNAse/DNAse free water and 1 µl of resuspended primer mix was included, giving a total reaction volume of 20µl. The mastermix contained 2x reaction buffer, 0.025 U/µl TAQ-Polymerase, 5 mM $MgCl_2$, 200 µm of each dNTP mix. Alongside this, the mastermix contained the fluorescence dye SYBR-green as well as calibrating dye ROX. SYBRgreen is a DNA-binding dye which increases the

level of fluorescence when encountering double stranded DNA. ROX was included as a baseline for the RT-PCR, normalising for pipetting error. Furthermore, for SLC39A12, a TaqMan style primer was designed to confirm observations from the SYBRgreen primer. The Applied Biosystems 7900 HT RT-PCR machine was used for all experiments. The cycling condition for the RT-PCR was done in four steps, comprising enzyme activation at 95^{o}C for 10 minutes, 50 cycles of enzyme denaturation for 15 seconds at 95^{o}C and data collection using the SYBRgreen dye for 60 seconds at 60^{o}C. This was followed by a melt curve analysis to check specificity. At least duplicates and a non-template control were performed for every single primer.

The data were analysed using the relative quantification method. The relative quantification method measures the fold difference in gene expression through ratio of crossing point (Ct) values normalized to ratio Ct values for the housekeeping genes. This method was chosen, as it does not require standards with known concentration as needed by the absolute quantification method, the accuracy of which is often disputed. The algorithm for the relative quantification is shown as follows:

$$Relative\ Expression = 2^{-(\Delta\Delta Cp)}$$

$$\Delta\Delta Cp = \Delta CpGene\ of\ Interest - \Delta CpCalibrator$$

$$\Delta CpGene\ of\ Interest = CpGene\ of\ Interest - Average\ Ct\ Housekeeping\ genes$$

$$\Delta CpCalibrator = Cp\ calibrator - Average\ Ct\ Housekeeping\ genes$$

Equation 1–The relative expression between two genes is calculated using the relative expression formula.

The relative expression for two genes was calculated by measuring the ΔCt for the calibrator and gene of interest separately. The calibrator can be any other genes in the set of genes. In general, we made a comparison with the same gene from different sample. We use three housekeeping genes as normalisers, GAPDH, UBC and YWHAZ. These three genes were chosen based on geNorm software analysis against 12 other reference genes performed by PrimerDesign (Southampton, UK) on retinal cDNA to represent eye samples. GAPDH, UBC and YWHAZ were the three most stable reference genes and were therefore chosen for this study. The raw cyclic data for the three genes were averaged using the GeoMean function in Microsoft Excel.

2.6.3. DNA clean up

2.6.3.1. EtOH precipitation

For every 10µl of the sequencing reaction, 40µl of 80% ethanol was added and the whole mixturevortexed. The mixture was left on ice for 10 minutes before centrifuging for 10 minutes at 4^{o}C. After aspirating the 80% ethanol, 180µl of 70% ethanol was added before 5 minutes of centrifugation at maximum speed at 4^{o}C. 25µl Millipore filtered water was used to resuspend the dried DNA pellet.

2.6.3.2. Millipore Montage system

This was used as per the company protocol. In brief, the DNA product to be purified was applied onto the Millipore blue plate, vacuumed to dryness before two washes of 25µl each with the washing buffer was carried out.

2.6.4. Agarose gels

DNA/ PCR samples were run on 1% (w/v) agarose gels dissolved in 1x TAE buffer at 100V with 1% Orange G in glycerol as a loading buffer. Ethidium Bromide was incorporated into the gel for visualisation under ultraviolet light. See below for agarose gel preparation.

3g Agarose (Sigma-Aldrich)

300ml deionised H2O

After boiling in a microwave oven the solution was left to cool slightly and ethidium bromide added at 0.5µg/ml

2.6.5. DNA sequencing

All sequencing was performed using Applied Biosystems 3730 DNA Analyzer. Each of the sequenced DNA sample contained 3µl of plasmid DNA, 2.5µl of sequencing buffer, 0.5µl of BigDye 3.1, 0.5µl of 100µM primer and deionised water to 20µl total volume. The reaction mix was then placed at 96^{o}C for 10 seconds, 50^{o}C for 5 minutes and 60^{o}C for 4 minutes for 25 cycles before purified either using ethanol precipitation or Millipore montage system. For detailed information on sequencing condition and materials, see Appendix 4.

2.7. **Protein Studies**

2.7.1. Western Blot

Most of the experiments were carried out on BioRad AnyKD precast gels or 10% SDS-Polyacrylamide gels (for gel preparation, please see section 2.2). Cells and tissues were lysed in lysis buffer (See section 2.2) on a rotator at 4^{o}C for one hour. Lysed tissues or cells were denatured with 5x Laemmli buffer and boiled for 5 minutes at 90^{o}C before being run on polyacrylamide gels. Twenty micrograms of sample were used unless stated and triplicates of experiments were performed unless stated. The self-casted gels were run at 70V for 30 minutes before the voltage was increased to 100V. The precasted gels were run at 120V until the smallest molecular weight marker reached the end of the gel. The gels were sandwiched with a PVDF membrane (Bio-Rad) between four sheets of Whatman filter paper (two on each side). Protein immobilisation was done on Bio-Rad Criterion system at 90-100V for 90 minutes each time at 4^{o}C. Following this, 1x Ponceau S solution was used to visualise and check protein transfer and rinsed before placing the membrane on blocking solution for at least 30 minutes. Depending on the antibody, antibody incubation was carried out at room temperature for two hours, or at 4^{o}C overnight with rotation. Secondary antibody incubation (anti-HRP) was done at room temperature for one hour. All incubation procedures were followed by three washing steps of ten minutes each with TBST 1x. The protein was visualised using ECL (Calbiochem) and films (Amersham).

2.7.2. In Vitro Translation

Each *in vitro* translation reaction contained:

20 µl TNT Quick Mastermix

0.5 µl Methionine 1mM

1 µl DNA template (1µg)

3.5µl Nuclease free H2O

Incubation was carried out at 30^{o}C for 90 minutes, and the reaction mixture stored in -20^{o}C prior to use.

In order to determine the molecular weight of the protein, TNT Quick Coupled Translation system was used. The pcDNA3.1 vector which was amplified, contained the T7 polymerase promoter required for the translation system. All materials were assembled in a microcentrifuge tube and left to incubate at 30^{o}C for 90 minutes. The resulting product was diluted 1:4 before being run on gel as per described in the Western blot protocol in Section 2.7.1.

2.7.3. Bichinconinic Assay

The Bichinconinic Assay (BCA) assay was used to determine protein concentration in tissue lysates for Western blot. The tissues were lysed as per normal, and BSA standards were serial-diluted in the lysis buffer ranging from 0-2000 µg/ml. The proprietary BCA working solution was mixed with $CuSO_4$ solution at 1:50 dilution. Equal amounts of sample/ standard were mixed with the working solution and incubated at 37^{o}C for 30 minutes. Two µl of samples and standards were measured on the Protein BCA program on the Nanodrop. None of the materials in the lysis buffer were found to interfere with the assay.

2.7.4. Transient Expression of protein in cells

The plasmid DNA generated was used to transfect various cell lines with different success rate. HEK293T and CHO cells were relatively easier to transfect than RPE cell lines. A day before transfection, cells were grown on 24 well plates with coverslips. BEND5 and ARPE19 cells were seeded at 30000 cells density. HEK293

cells were seeded at 60000 cells. All cells transfected were grown to a density of 80-90% in media supplemented with fetal calf serum but without antibiotics. Eight hundred ng of DNA was used with four µl of Lipofectamine2000 diluted in Opti-Mem reduced serum media. After incubation for four hours, the transfection media was topped up with twice as much media and left for 24-48 hours.

2.8. **Cell Culture**

2.8.1. Cell lines

All of the cell lines were cultured in 37^{o}C humidified chamber with 95% air and 5% CO2. For complete list of cells used in this study, and their growing conditions, see Appendix 2.

2.8.2. Propagation and Freezing

Frozen vials were rapidly warmed and warmed supplemented media added. The cells were left overnight to attach before changing to fresh media. Confluent cells were detached with 1x Trypsin-EDTA, neutralised with serum-supplemented DMEM and centrifuged at 800rpm for three minutes before being resuspended and seeded at appropriate density. The density of the cells was determined using a haemocytometer after dilution of 1:1 with trypan blue. In order to ensure there were enough nutrients for the cells, for every cm^2 in a confluent flask, 0.3 ml of complete medium was added.

On average, 3x10^6 cells were frozen in a vial. Following standard trypsin-EDTA detachment and centrifugation, the cell pellets were resuspended inmedium comprising of of 50% DMEM, 40% FCS, 10% DMSO filtered in 0.2 µm Millipore syringe. Following this the cells were transferred to a 1.8 ml cryovial (Fisher Scientific, Loughborough, UK) cell freezing container (Nalgene) and placed in -80^{o}C for a day before transferring to liquid nitrogen.

2.8.3. Cytotoxicity Assay

The calcein assay was used to determine cell death. A 1mM stock of calcein dye (Invitrogen, Paisley UK) was diluted 1:1100 with warm 1x PBS. Propidium iodide was added at 1:400. The solution was used to incubate cells for 15-20 minutes at 37C (standard cell culture condition) before visualised with a fluorescence microscope. Positive propidium iodide staining indicated non-viable cells as the dye is cell impermeant. The calcein dye shows viable cells.

2.8.4. Cell Proliferation Assay

AlamarBlue solution was purchased from ABDSerotec (Kidlington, UK). Cells were seeded at 5000 cells per well on a 96-well plate to match the cell density in the other experiments with 200µl growth media. After incubation for 1-6 days to identify with the other experimental conditions, 10% (volume of media to volume of Alamar Blue added) of undiluted AlamarBlue solution was added and left to incubate for 2 hours before its absorbance measured at 600nm and 450nm on a plate reader. Calculations for the absorbance were made according to the equation provided by the manufacturing company and presented as percentage reduction of AlamarBlue. As controls, cells without zinc treatment were used and as blanks, absorbance of growth media without zinc added was measured. It was pre-determined that the addition of zinc does not affect AlamarBlue absorbance.

2.8.5. Wholemount TEM preparation

Nickel grids 3.05mm (TAAB Microscopy, Aldermaston, UK) were rinsed in acetone to remove grease. The grids were then placed on top of 1% formvar film floating on a glass container before being covered with sterile coverslips; averaging three grids per coverslip. A non-coated glass slide was then used to sweep the film-grid-coverslip layer from the water. The resulting product was left to dry under a culture hood for 24 hours. The film-grid-coverslip layer was then carbon-coated before being sterilised for 30 minutes under the ultraviolet lamp. Following this, the sterilised coated grids were covered with 1% gelatine for 30 minutes under the cell culture hood before aspirated and rinsed with PBS 1x once. Twenty five thousand cells were seeded onto the grids overnight before media containing 125 µM $ZnSO_4$in growth media was applied onto the cells for a further 20 hours. As a

negative control, untreated samples were used, and as a positive control for fenestrae formation, cells were treated with 1.25μM Latrunculin A diluted in growth media for three hours. Post-treatment, the cells were immersed in Karnovsky's solution and left fixing overnight at 4^{o}C. The cells were then washed twice for five minutes each with PBS1x solution. Freshly diluted 1% osmium tetroxide (OsO_4) was used to post-fix the cells for 30 minutes. Care was taken to remove and discard the OsO_4 waste, and cells were washed in distilled water for three times five minutes each. Cells were then placed on serial ethanol dilution for five minutes each time, going from 30%, 50%, 70%, 80%, 90%, 95%, 100%, 100% and a final 100%. Cells were rinsed and incubated for three minutes in hexamethyldisilazone (HMDS) at room-temperature before any solutions were aspirated and the coverslips left to dry overnight.

2.8.6. Transepithelial Resistance Measurement

Transepithelial resistance measurements of ARPE19 cells were done using ECIS Zθ Disposable 8-Electrode Array (Applied Biophysics, USA). Prior to seeding with cells, each of the 8 wells in the array was incubated in a 10mM cell-culture grade cysteine solution (Sigma Aldrich, UK). Following cysteine treatment, the wells were washed once with sterile distilled water and incubated in media for 30 minutes at standard incubating condition before 20,000 cells were seeded on each well. The arrays were then attached to the ECIS Z$^{\theta}$ machine and placed in an incubator. The use of the ECIS Zθ machine prevented the arrays from being removed as this would introduce inconsistencies in the reading, therefore, the arrays were not taken off and media was not replaced for the period of 6 days of which measurements were taken.

2.9. **Immunohistochemistry /Immunocytochemistry and Zinc Visualization *in vitro***

2.9.1. Fixation

PFA/Triton

Cells were fixed with freshly diluted 4% PFA in 1x PBS at room temperature for 20 minutes. PFA solution was discarded, and 300μl of 1x PBS-Triton (See Section 2.2) was added per well in a 24 well plate. Following this, blocking buffer was

used to wash the cells twice, before incubating in the same buffer for at least 20 minutes.

Methanol

Ice cold methanol was added onto cells and immediately placed in a -20^{o}C freezer for five minutes. After methanol was aspirated, cells were rinsed once with PBS before beingreplaced with PBS for at least 5 minutes at room temperature. Blocking buffer (as described in section 2.2) was used to block the cells for at least 20 minutes.

2.9.2. Immunohistochemistry (Only BEND5)

The cells were seeded at 3.3x10^{4}cell density on glass coverslips in 24 well platewith 1% bovine gelatine as coating. Cells were left overnight to allow the cells to attach before being treated with either various $ZnSO_4$ concentrations or 1.25 μM Latrunculin A (LA) for 20 or 3 hours respectively and left to incubate at 37^{o}C. Freshly made 4% PFA was used to fix all the cells for 10 minutes followed by two PBS 1X washes and stored at 4^{o}C. Before staining, the cells were treated with 0.1% Triton X-100 in PBS1x to permeabilise cells for 15 minutes. The antibodies were diluted in blocking buffer (see section 2.2) and incubated for one hour with both primary and secondary layers before washing three times with washing buffer (see section 2.2) for two minutes each. The rinsed coverslips were placed cell side down on a glass microscopic slide with 10 μl of Vectashield mounting media containing DAPI stain (Vector Laboratories). All images were taken usingfluorescence or LSM700 confocal microscopy.

2.9.3. Immunohistochemistry (All other cell lines)

The cells were seeded at optimum density on glass coverslips in 24-well plate. Cells were left overnight to allow the cells to attach. Freshly made 4% PFA or ice cold methanol was used to fix the cells for 20 minutes at room temperature or 5 minutes at -20^{o}C, followed by two PBS 1X washes and stored at 4^{o}C. Before staining, the cells were treated with 0.3% Triton X-100 in PBS1x to permeabilise them for 5 minutes. The antibodies were diluted in blocking buffer (see section 2.2) and incubated for two hours (primary) and one hour (secondary) before washing three times with washing buffer (see section 2.2) for two minutes each. The rinsed

coverslips were placed cell side down on a glass microscopic slide with 10 µl of Vectashield mounting media containing DAPI staining (Vector Laboratories). All images were taken using fluorescence or confocal microscopy.

2.9.4. Zinc probes

Prior to treatment, cells were washed twice with pre-warmed PBS1x solution to remove traces of phenol red. A 5mM stock of zinc selective dye ZinPyr-1 was diluted to 1µM concentration in pre-warmed DMEM high glucose media without phenol red. The cells were incubated with the dye for 10 minutes at 37^{o}C standard incubating conditions. Following three washes in DMEM-high glucose media without phenol red, preparations was immediately visualised live using Olympus BX51 using 20 x magnifications. All images were using the same exposure. Image analysis was done using Image J.

2.10. **Cloning Strategies**

ZIP12 was cloned using Gateway Technology (Invitrogen, Carlsbad USA). SLC39A12 was cloned by PCR using retinal cDNA (gift from Dr. Amna Shah). The PCR was performed using specially designed AttB primers. Fifty fmol of the PCR product was purified using ethanol precipitation and incorporated into the entry and expression vectors using BP clonase and LR clonase enzymes respectively. The transformed bacteria were plated on LB agar containing the appropriate antibiotics selection. A single colony was picked and incubated in LB broth also with appropriate antibiotics before purification using miniprep and maxiprep kits. The clones were checked for mutations and correct insertions by using restriction enzymes and sequencing. Upon sequencing, it was discovered that the retinal cDNA had a known silent polymorphism, as this do not change the amino acid sequence, the resulting clones continued to be used.

2.10.1. Cloning Primer Designs

The PCR primers (for list see Appendix 3) were designed according to criteria from Invitrogen. The forward primers contained four guanine residues at the 5' to promote binding, a 25bp attB1 sequence and a TC base pair to maintain the reading frame. This was followed by a Kozak sequence (ACCATG), which aids the expression of eukaryotic proteins and the first 25bp of SLC39A12 sequence. A similar design

procedure was applied to the reverse primers, with also four guanine residues, 25 bp of attB2 sequence and an additional base pair to maintain the reading frame. For N-terminal fusion proteins, the stop codon remained a part of the 25bp SLC39A12 used, for the C-terminal fusion proteins, it is important to remove the stop codon to allow translation of the tag protein.

2.10.2. Cloning PCR

Each Cloning PCR reaction contained

2.5µl 2mM dNTPs
1.0µl 25mM MgSO4
2.5µl 10 x KOD-PCR buffer
0.75µl AttB-Forward primer 0.3µM final concentration
0.75µl AttB-Reverse primer 0.3µM final concentration
0.5 µl Enzyme – Kod Polymerase (1.0 U/µl)
1.0 µl CDNA/ Plasmid DNA template

PCR grade nuclease free water was used to make up to 25µl

A Veriti (Applied Biosystem, UK) thermal cycler was used. The PCR conditions comprised a two minute denaturation step at 95^{o}C and 35 cycles of 15 seconds at 95^{o}C, 30 seconds primer annealing step at 60^{o}C and 41 seconds elongation step at 72^{o}C.

2.10.3. Expression vectors

For figures of vectors, please refer to Appendix 6.

pDONR201/Zeo (Invitrogen) was used to create the entry clone for full-length ZIP12 protein.

pcDNA3.2/V5-DEST (Invitrogen) was used to create the full-length ZIP12 with C-terminal V5 tag fusion protein.

pcDNA-DEST47 (Invitrogen) was used to create the full-length ZIP12 with C-terminal GFP tag fusion protein.

2.10.4. Transformation of ccdB cells/ *E.Coli*

Transformation of competent cells with DNA was performed according to the manufacturer's protocol. One aliquot (200µl) of DH5α (Invitrogen, UK) was defrosted on ice and the completed BP/LR Clonase reaction added and incubated for 30 minutes. Following a 45 second heat shock step at 42^{o}C, super optimal broth (SOC) media was added and the sample placed at 37^{o}C shaking cabinet for one hour. The transformed cells were pelleted before being re-suspended and plated onto LB agar plates with antibiotic supplements.

2.10.5. Purification of Proteins

A single colony was picked using a plastic picker, and immediately transferred onto a 5ml LB broth with appropriate supplementation of antibiotics (See section 2.2 for concentrations) before incubated at 37^{o}C with 200rpm agitation for at least 16 hours. Following this, Wizard Plus SV Miniprep (Promega, UK) was used to purify the plasmid. Two ml of the overnight culture was centrifuged to produce a pellet, which was re-suspended, lysed and neutralised with the buffers provided by the kit. After centrifugation, the supernatant was collected and transferred to the miniprep column before endotoxin removal solution and multiple washes were performed to purify the protein. Proteins were eluted in nuclease free H_2O, and protein content measured with NanoDrop. Upon sequencing and restriction analysis to confirm the right orientation and sequence of clone, a maxiprep was done to produce enough plasmid for transfection. Fifty µl of glycerol stock was added to five ml of LB broth before placing in the 37^{o}C shaker for six hours and transferred onto 100ml LB broth and incubated for 16 hours. GenElute HP Endotoxin-Free Plasmid Maxiprep Kit (Sigma Aldrich, UK) was used to isolate DNA for maxipreps following the protocol provided. The culture was then pelleted and re-suspended before being lysed.The supernatant was purified through the syringes provided and washed to remove contaminants. Nuclease free water was used to elute the DNA. The resulting DNA was precipitated using ethanol precipitation and the concentration measured using NanoDrop. All plasmid constructs were aliquoted and stored at -80^{o}C.

2.10.6. Glycerol Stock

Glycerol was added to bacterial culture at a ratio of 1:4 before transferring into -80^{o}C freezer for storage.

2.10.7. Restriction Digests

All enzymes used were supplied by Promega (UK).
Each restriction digest contained:
1µl of plasmid construct (approximately 0.5µg)
0.5µl of restriction endonucleases
1.0µl Buffer (depends on endonuclease used)
Water to 10µl

DNA digests were run for one hour at 37^{o}C and resulting digest product was run on 1% agarose gel and visualised under UV light.

2.11. **Statistical Analysis**

Data presented in figure 4.25 is average fluorescence value ± standard deviation Statistical analysis for figure 4.25 was performed using Student's T-test, between sham and transfected group and P value (< 0.01) was observed.

3. Expression of Mammalian Zinc Transporters in the RPE and Choroid

There is little known about the presence and expression of zinc transporters in the eye. The work described in this chapter aimed to use quantitative RT-PCR to catalogue the presence and determine the relative expression levels of the 10 SLC30A (ZnT) and 14 SLC39A (ZIP) mammalian zinc transporters in the retinal pigment epithelium and choroid. For this, we used RNA isolated from ARPE19 (spontaneously immortalised human RPE cell line), SHEF-1 cells (a human embryonic stem cell-derived human RPE cell line), primary human RPE cells at passages (4 and 12), primary cultures of Muller cells, and human retina, RPE and choroid dissected from cadaveric eyes. The primers were designed and optimised by PrimerDesign Ltd and all data were normalised against three housekeeping genes, GAPDH, YWHAZ and UBC. After cataloguing the relative expression levels of the 24 zinc transporters, we found widespread expression of the majority of zinc transporters, although expression levels did vary between different cell types. Through this comparison, we identified one striking anomaly in expression levels that may have relevance for zinc homeostasis at the RPE-choroid interface. We found that the expression of SLC39A12 gene encoding zinc transporter ZIP12 is highly expressed in freshly isolated cadaveric RPE cells but absent in the cultured cells tested. Based on this observation, we specifically analysed this gene and its protein product in Chapter 4.[2]

[2]Several parts of this chapter (Section 3.6) have been published in Barzegar-Befroei, N., Cahyadi, S., Gango, A., Peto, T., and Lengyel, I. 2011. Zinc in Eye Diseases. Zinc in Human Health, Editor: Lothar Rink.IOS Press Amsterdam (see Appendix)

3.1. **Intracellular Zinc Transport**

3.1.1. SLC30A Family of Transporters

The SLC30 gene codes for a family of zinc transporters (ZnTs) which are ubiquitously expressed in all organisms (Liuzzi and Cousins, 2004b). The ZnT family of transporters specifically promotes the transport of zinc from the cytosol to extracellular environment or compartmentalise zinc into organelles within the cell. ZnTs possess six transmembrane domains with a variable region between domains III and IV, which contains many histidine residues able to bind zinc. Loss of zinc transporters due to gene mutations or incorrect translation of mRNA has been reported to result in various pathological conditions, which may include embryonic lethality, incorrect absorption of zinc, reduced body fat and weight in mice (Huang et al., 2007) and lethal milk syndrome caused by a mutation in the SLC30A4 gene encoding the ZnT4 protein (Murgia et al., 2006). The distribution of ZnTs is widespread; although some are cell-specific (Redenti and Chappell, 2004b, Palmiter and Huang, 2004).

3.1.2. SLC30A1 / ZnT1

The SLC30A1 gene codes for the ZnT1 protein, which is an ubiquitous zinc exporter protein that functions to reduce intracellular zinc concentration and that has been described as "conferring resistance to zinc" (Palmiter and Findley, 1995). Northern blot analysis showed that in rat, SLC30A1 mRNA was present in the kidney, small intestine, adipose tissue, liver, spleen and thymus tissues (Liuzzi et al., 2001b). The protein was found in placenta, kidney, small intestine, and moderately expressed in adipose tissue, liver, spleen and thymus. In the mouse gastrointestinal tract, ZnT1 was found to be differentially expressed within the small intestine, where it was found in the basolateral membrane of the epithelium of esophagus, duodenum of the small intestine and cecum of large intestine (Yu et al., 2007). Within the brain, ZnT1 is expressed in the choroid plexus of mice and rat (Wang et al., 2004b, Chowanadisai et al., 2005).

The evidence that ZnT1 is very widely expressed in almost all tissues on the plasma membrane suggests that ZnT1 protein acts as the main form of transporter involved in absorption or zinc transfer (Liuzzi et al., 2001b). The importance of ZnT1 was

shown by knock-out studies using Drosophila melanogaster where removal of ZnT1 caused failure of development, and death of larvae due to zinc deficiency (Wang et al., 2009b). ZnT1 expression is only activated under excessive zinc condition, where N,N,N',N'-tetrakis(2-pyridylmethyl) ethylenediamine (TPEN) treatment in HeLa cells was found to increase gene expression of other zinc transporters but not ZnT1 (Devergnas et al., 2004). Transcription of SLC30A1 is under the control of MTF1 (Kambe et al., 2004, Palmiter and Huang, 2004). The expression of SLC30A1 is sensitive to the concentration of extracellular zinc where animal studies have shown that cells treated with low concentration of zinc upregulated expression of SLC30A1. It is thought that the upregulation of intracellular zinc may be caused by zinc absorption or zinc export from intracellular organelles (Bury et al., 2008).

In disease states, expression of SLC30A1 was upregulated for 24 hours after ischemic shocks but decreased afterwards (Tsuda et al., 1997). Decreased immunolabeling of ZnT1 was observed in preclinical Alzheimer's disease in human brain samples which points to the involvement of zinc and dysregulation of zinc homeostasis in the development of AD (Lyubartseva et al., 2010). Huang and colleagues reported that there is a concentrated immunolabeling of many ZnT transporters including ZnT1 in Aβ plaques in the cortex of brains of Alzheimer's disease subjects. As these were more concentrated in the plaques, it was hypothesised that there is increased transport of zinc by the transporters (Zhang et al., 2008).

3.1.3. SLC30A2/ ZnT2

SLC30A2 gene codes for the ZnT2 zinc transporter protein. The mRNA expression of this gene was reported in the small intestine, kidney, placenta, prostate, mammary gland and liver using Northern blot analysis (Palmiter and Huang, 2004). ZnT2 protein is located on endosomal vesicles and functions to reduce the cytosolic zinc concentration (Liuzzi and Cousins, 2004b). In enterocytes, ZnT2 was shown to be located in the apical surface of microvilli, with vesicles nearby (Kambe et al., 2004). ZnT2 is located in the vesicles in M1 human fibroblast cells and functions to move zinc to lysosomes, replacing the role of M1 protein in cells (Falcon-Perez and Dell'Angelica, 2007). There are two isoforms of ZnT2 protein which codes for

proteins of 42 and 35 kDa respectively. The 42 kDa ZnT2 is localized to the endosomal compartment and is the major zinc transporter. The 35 kDa ZnT2 is located on the plasma membrane, and shows lower expression compared to the larger, 42 kDa isoform. Overexpression of these proteins lead to sequestration of zinc (Lopez and Kelleher, 2009).

ZnT2 mRNA expression is sensitive to changes in zinc concentration, and ZnT2 has been suggested to mainly function in protecting cells from sudden increases in intracellular zinc concentration (Liuzzi et al., 2001b). Zinc rich diet in rats led to 370% increase of ZnT2 mRNA in the small intestine and kidney although its expression was negligible under a zinc deficient diet. Exposure of porcine capillary endothelial cells to 50 μM/L zinc causes upregulation of ZnT2 which remains for 96 hours (Bobilya et al., 2008).

3.1.4. SLC30A3/ ZNT3

The SLC30A3 gene codes a 40 kDa ZnT3 protein. The mRNA has been detected in both the brain and testis of rodents, although so far, the protein has only been detected in the brain. ZnT3 mRNA has been found as early as three days before birth, and reaches its expression peak three weeks post-natally. ZnT3 localises to the synaptic vesicles, which indicated that they may aid in the process of neuromodulation, or zinc storage (Liuzzi and Cousins, 2004b). Lysosomal localisation of ZnT3 protein has been reported (Wang et al., 2004b). This lysosomal immunolabeling was found in fenestrated endothelial cells of the mouse choroid plexus. Furthermore, zinc-selenide metallography was able to detect bioavailable zinc in the apical membrane of mouse choroid plexus endothelial cells which suggests that ZnT3 aids in regulating zinc homeostasis in the choroid plexus of the brain (Wang et al., 2004b).

In the brain, zinc has been widely acknowledged as one of the key factors in the elongation of aggregated amyloid-β protein, which leads to the development of Alzheimer's disease. A ZnT3 knock out mouse model was found to be protected from the aggregation of amyloid-β protein (Kambe et al., 2004). In INS1-E rat pancreatic β-cell cultures, there is a positive correlation between glucose concentration in the media and expression of ZnT3 but not many other zinc

transporters. This implies that in a high glucose environment, ZnT3 plays an important role in zinc and glucose metabolism, which may be crucial in diabetes (Sondergaard et al., 2005).

3.1.5. SLC30A4/ ZnT4

The SLC30A4 gene is highly expressed in various epithelial cells especially those involved with absorption, such as the small and large intestine. Consistent but low expression was found in liver, kidney, spleen, thymus, muscle, adipose tissue and mammary glands (Liuzzi et al., 2001b). ZnT4 proteins are localised in the vesicles, golgi apparatus and endosome. Immunohistochemistry revealed ZnT4 expression in the large intestine in mice (Yu et al., 2007) and in the apical part of fenestrated choroid plexus epithelial cells (Wang et al., 2004b). ZnT4 has also been found in basal cell vesicles of mouse polarised Caco-2 intestinal cells. Studies in humans and rats have shown that SLC30A4 gene expression is not elevated in zinc sufficient or enriched conditions (Liuzzi and Cousins, 2004b). Based on this, it is suggested that ZnT4 aids absorption of zinc and sequestration into vesicles, until it is needed by the cell (Murgia et al., 2006).

A mutation in SLC30A4 gene has been associated with lethal milk syndrome in mice. The recessive single-point mutation in the termination codon results in the formation of defective protein (Murgia et al., 1999).

3.1.6. SLC30A5/ ZnT5

The SLC30A5 gene encodes zinc transporter ZnT5 protein, which is selectively expressed on the apical side of insulin containing pancreatic-β cells as opposed to insulin secreting acinar and α-cells (Palmiter and Huang, 2004). Two splice variants differ in their C and N terminal regions. Variant A has been expressed in the Golgi, meanwhile variant B ZnT5 protein can be seen in the cytosol as well as the plasma membrane (Thornton et al., 2011).

ZnT5 mRNA is found in the duodenum and in the parietal cells of the stomach, while the protein can be found in the gastric mucosa as well as the crypts of Lieberkuhn (Yu et al., 2007). ZnT5 is involved in the reabsorption of zinc in the gastrointestinal tract, as well as delivery of alkaline phosphatase in the secretory pathway (Yu et al., 2007). In a human intestinal cell line, CACO-2, ZnT5 isoform

B was found to be expressed in the cell's plasma membrane. The study showed that ZnT5 isoform B was able to decrease as well as increase intracellular zinc concentration (Thornton et al., 2011).

3.1.7. SLC30A6/ ZnT6

SLC30A6 mRNA has been shown to be expressed in the liver, kidney and brain, but the protein is only detected in the brain and lung (Palmiter and Huang, 2004). The function of ZnT6 protein is to transport zinc from the trans-Golgi network to cell periphery (Kambe et al., 2004). In mouse gastrointestinal tract, ZnT6 mRNA expression was found in the goblet cells of stomach, and columnar epithelial cells, where the protein is concentrated in the perinuclear and peripheral part of the crypts of the columnar epithelial cells (Yu et al., 2007). Immunochemistry showed that the ZnT6 protein is expressed in the epithelial cells of choroid plexus (Wang et al., 2004b). In preclinical Alzheimer's disease in human brain samples, it was shown using immunostaining for tau-protein marker, that ZnT6 was increased significantly (Lyubartseva et al., 2010) possibly indicating involvement of ZnT6 protein in AD.

3.1.8. SLC30A7/ ZnT7

SLC30A7 mRNA expression is found in various tissues, but the protein is only present in the small intestine and lung. In contrast to other ZnT family of transporters that are required for absorption process, ZnT7 is located in the perinuclear vesicles of the Golgi apparatus. In mouse choroid plexus, immunoreactivity of ZnT7 is strongest on the cis-side of the Golgi apparatus (Liuzzi and Cousins, 2004b). In the gastrointestinal tract of mice, immunochemistry showed that ZnT7 mRNA is expressed in all parts of the small and large intestine, Goblet cells in cecum, colon and rectum stain heavily for the ZnT7 protein, presumably reflecting a role in zinc reabsorption in the gastrointestinal tract (Liuzzi and Cousins, 2004b). ZnT7 is also required in mice for fat metabolism and zinc homeostasis. ZnT7 null mice were found to have lowered zinc concentration in the serum, liver, duodenum, brain, bone and low body weight and body fat for age (Huang et al., 2007).

3.1.9. SLC30A8/ZnT8

ZnT8 mRNA can be detected in brain and liver (Palmiter and Huang, 2004) and two SNPs are highly correlated with incidence of type 2 diabetes in Han Chinese. Chimienti et al reported the specific expression of ZnT8 in the pancreas as well as its localisation in pancreatic beta-cells which produce insulin (Chimienti et al., 2006, Chimienti et al., 2005).

3.1.10. SLC30A9/ ZnT9, SLC30A10/ ZnT10

Not much is known regarding the genes SLC30A9 and SLC30A10, which encode for proteins ZnT9 and ZnT10 respectively. In a phylogenetic tree constructed by Seve and colleagues (2005), ZnT10 was shown to have the closest phylogeny to ZnT1. It is the only zinc transporter so far which is embryonic-specific; at birth ZnT10 diminishes, and expression of ZnT1 starts, implying that the two may have similar functions and are homologous (Seve et al., 2004).

3.1.11. SLC39A ZIP FAMILY OF TRANSPORTERS

The SLC39 genes encode a family of zinc transporters (ZIPs) that are ubiquitously expressed in all organisms. Structurally, ZIP proteins are composed of eight transmembrane domains with a cytoplasmic loop between domain III and IV composed of histidine residues. The ZIP family of zinc transporters promote the transport of zinc from the extracellular environment into the cytoplasm or from the cellular organelles to the cytoplasm (Liuzzi and Cousins, 2004b). Loss of ZIPproteins may lead to the development of various pathological conditions such as acrodermatitis enteropathica (AE), an autosomal recessive metabolic disorder (Dufner-Beattie et al., 2003).

3.1.12. SLC39A1/ZIP1

SLC39A1 encodes for ZIP1 protein, whichis widely expressed (Liuzzi and Cousins, 2004b). Human ZIP1 protein is localised to the endoplasmic reticulum and plasma membrane. In K562 and PC3 cells, ZIP1 mainly localizes on the plasma membrane. In COS-7 and HepG2 cell lines, a perinuclear endoplasmic reticulum staining pattern was observed (Milon et al., 2001).

Animal studies have shown that ZIP1 expression was detected as early as day 14 of gestation, and that it is localised to the apical membrane of epithelial cell villi. Expression increases until day 20 of gestation and continues postnatally. Changing the level of zinc does not alter the level of ZIP1 mRNA in gestation or postnatal dam and pup intestine and expression of ZIP1 mRNA was unchanged after dietary zinc supplementation in human small intestine enterocytes (Cragg et al., 2005, Huang et al., 2006). In a blood-brain barrier model, exposure to 50 μm/L zinc in cell culture did not affect ZIP1 expression (Bobilya et al., 2008).

3.1.13. SLC39A2 / ZIP2

ZIP2 mRNA encoded by the SLC39A2 gene is expressed in mouse liver, spleen, small intestine and bone marrow, as well as human peripheral blood monocytes (Liuzzi and Cousins, 2004b). The protein localises to the plasma membrane. Under zinc deficient conditions, a marked upregulation of ZIP2 expression and downregulation of metallothionein was observed (Eide, 2004). A paediatric study showed that ZIP2 mRNA is the only transporter overexpressed in asthmatic infants compared to the rest of the transporters which were analysed, including ZnT1, ZnT3, ZnT4, and ZIP1 (Xu et al., 2009). In cultures of human THP-1 cells and human peripheral blood monocytes, ZIP2 gene expression was increased under zinc deficient conditions following treatment with TPEN (Cao et al., 2001).

3.1.14. SLC39A3/ ZIP3

The SLC39A3 gene is highly expressed in bone marrow, spleen and intestine (Liuzzi and Cousins, 2004b), liver (Liuzzi et al., 2005) and to a lesser extent in the fetal and neonatal intestine. A study by Kambe and colleagues (2003) showed that the ZIP3 protein is upregulated only under zinc deficient conditions. It was shown that ZIP1, ZIP2 and ZIP3 mouse knock-outs had 80% abnormality of the embryos under zinc deficient conditions, but did not cause major effects when zinc concentration was adequate. These effects highlighted how crucial the functions of zinc importers are during pregnancy, at least in animal models (Kambe et al., 2008). This effect was corroborated by a study by Wang and colleagues (2004), who found that mouse ZIP1 and ZIP3 protein is not endocytosed and degraded easily from the plasma membrane under zinc deficient conditions. Cells which were

treated with TPEN were found to retain a higher amount of zinc (Wang et al., 2004a).

3.1.15. SLC39A4/ ZIP4

The SLC39A4 gene expression is confined to the small intestine, colon, stomach and kidney, but not in the liver presumably reflecting a role in the absorption of zinc from dietary sources (Dufner-Beattie et al., 2003). ZIP4 protein is located in the apical membrane of enterocytes and endodermal cells (Liuzzi et al., 2005). Various studies have emphasised the importance of ZIP4 protein in gastrointestinal absorption of zinc. The expression of ZIP4 is required during gestation and lactation in mice; ZIP4 mRNA was expressed starting from day 18 and reached its peak at day 20 (Huang et al., 2006). In Acrodermatitis Enteropathica (AE), mutations yielding a premature termination codon that leads to failure of ZIP4 protein to transport zinc (Liuzzi et al., 2005).

Studies have demonstrated that zinc affects the stability of SLC39A4 mRNA. Zinc sufficiency caused ZIP4 to be engulfed in enterocytes and get degraded. Under zinc deficiency conditions, ZIP4 mRNA accumulates in the cytoplasm and ZIP4 protein gets transported to the apical membrane. This tightly controlled mechanism implies that ZIP4 is important for zinc absorption from diet (Weaver et al., 2007).

3.1.16. SLC39A5/ ZIP5

Previous research has indicated that the SLC39A5 gene is mainly expressed in the gastrointestinal tract of mice and from immunohistochemistry its protein is localised to basolateral membranes. During gestation, ZIP5 expression was first detected at day 16, and it remains expressed until birth. During lactation, expression of ZIP5 is very strong in intestines from both dams and pups, and remains unchanged even in response to a zinc deficient diet (Huang et al., 2006). ZIP5 functions to prevent excessive amount of intracellular zinc. Zinc deficiency increases ZIP5 mRNA expression and leads to shuttlling of the translated proteins to the lateral and basolateral membrane of enterocytes meanwhile zinc sufficient conditions prevent translation of ZIP5 and sends membrane to the degradation pathway (Weaver et al., 2007).

3.1.17. SLC39A6/ ZIP6

The SLC39A6 gene was found to be expressed in prostate, placenta and mammary gland cells. ZIP6, the protein coded by SLC39A6 gene is also called LIV-1 (Taylor et al., 2003). Immunohistochemistry has shown the protein's expression on the apical or plasma membrane of neuroblastoma cell line and CHO cells (Taylor et al., 2003, Chowanadisai et al., 2005). In mice subjected to zinc deficient diet, increased expression of ZIP6 was observed, indicative of its crucial function in regulating zinc homeostasis in the brain (Chowanadisai et al., 2005). ZIP6 may also have potential role in breast cancers (Taylor et al., 2007).

3.1.18. SLC39A7/ ZIP7

ZIP7 is currently the only ZIP family transporter found in the ER. The relationship betweenZIP7 expression and breast cancer has been explored by Taylor et al where ZIP7 expression was higher in tamoxifen resistant breast cancer cells compared to wild type cells. Up-regulation of ZIP7 causes increase of zinc influx into the cytosol with subsequent increase in phosphorylation of epidermal growth factor receptors due to inactivation of phosphatases and activation of downstream signaling cascades including MAPK and Erb pathways (Hogstrand et al., 2009, Taylor et al., 2008).

3.1.19. SLC39A8/ ZIP8

The SLC39A8 gene encodes ZIP8 protein found in lysosomes, endosomes and mitochondria (Besecker et al., 2008, Kambe et al., 2004). Studies have shown its involvement in the regulation of the immune system. Aydemir and colleagues (2008) reported that human T-cells are activated by 15 mg zinc per day supplementation for 4 days. SiRNA suppression ofZIP8 expression reduced IFN-y secretion by 66%. Furthermore, incubating T cells in increased zinc caused a reduction of calcineurin and an increase in CREB phosphorylation, ultimately resulting in increased IFN-y secretion (Aydemir et al., 2009). TNF-α exposure to lung epithelia can induce SLC39A8 expression. The increase of ZIP8 is thought to provide protection for the lung epithelium in inflammatory conditions (Besecker et al., 2008).

3.1.20. SLC39A9/ ZIP9

SLC39A9 localises in the trans-golgi network in HeLa cells. In the DT40 chicken cell line, knocking out ZIP9 did not cause apoptosis, and nor did it affect cytosolic zinc homeostasis as measured through zinquin staining. Secretory pathway function is often measured through alkaline phosphatase. ZIP9 overexpression was found to decrease ALP activity in wild type and ZIP9 -/- cells. (Matsuura et al., 2009).

3.1.21. SLC39A10/ ZIP10

SLC39A10 was found to encode a zinc transporter found in rat renal brush border membrane.The gene itself was found to be widely expressed, particularly in small intestine, pancreas, testis, brain, liver and kidney of rats. The protein was found to immunolocalise at the plasma membrane in LLC-PK1 cells (Kaler and Prasad, 2007).

3.1.22. SLC39A12/ ZIP12

Preliminary studies have implicatedSLC39A12 within schizophrenia possibly through serine to glycine mutations in residue 213 of the transporter protein (A213G → S36G)(Bly, 2006).

3.1.23. SLC39A13/ ZIP13

Fukada and colleagues reported that a mutation in SLC39A13 is linked to Ehler Danlos Syndrome, which results from defective collagen synthesis and improper connective tissue development. The protein localises to the perinuclear region (Golgi apparatus) of different connective tissue cells. Mouse knockouts of the SLC39A13 gene resulted in abnormal connective tissue development, poor bone mineral density including dentin, and curvature of the spine resulting in a hunchback appearance of SLC39A13 KO mice. A craniofacial abnormality was characterised by sunken eyes. Decreased collagen synthesis also results in poor skin development (Fukada et al., 2008).

3.1.24. SLC39A14/ ZIP14

ZIP14 protein expression has been found on the apical surface of the epithelium of transfected MDCK cells. Girijashanker and colleagues reported that ZIP14 and

ZIP8 have high homology which may explain both transporters' involvement in the acute-phase response. In mice, lipopolysaccharide and turpentine, major antigens for activation of the immune system, were found to increase the expression of ZIP14 in the mouse liver. Furthermore, it was noted that the increase in ZIP14 was triggered by inflammatory cytokine IL-6 and TNF-α. IL-6 null mice did not show any inflammation, which indicated that ZIP14 expression is required to trigger immune response in the liver (Liuzzi et al., 2005). Apart from zinc, the protein is also able to transport cadmium and manganese (Fujishiro et al., 2009).

Relatively little is known about the distribution of zinc transporters in the eye despite the fact that the RPE and choroid probably have the highest amount of zinc-per gram of tissue in the whole body. Also, it is well accepted that zinc plays a role in visual processing in the health and disease of the retina (Ugarte and Osborne, 2001). Currently available literature on expression of zinc transporters is summarised in Figure 3.1.

Figure 3-1- Distribution of zinc transporters in RPE-choroid complex

Distribution of zinc transporters in the RPE-choroid complex based on various publications. ER- Endoplasmic reticulum, MT - metallothionein (Leung et al., 2008a, Redenti and Chappell, 2003, Wang et al., 2006b)

3.2. **Aims**

The aim of this chapter was to provide extensive expression profiling of all SLC30A and SLC39A zinc transporters in various cultured RPE, and non RPE cell lines, as well as in human cadaveric retina, RPE and choroid using:

1. Quantitative real time PCR using SYBRGreen detection system for all the 24 zinc transporters

2. Quantitative real time PCR with TaqMan probes to clarify and confirm findings related to the expression of SLC39A12

3.3. **Expression of SLC30A SLC39A Transporters in RPE Cells**

Methods

In order to catalogue the expression levels in cells and tissues derived from the retina/ RPE/ choroid complex, RNA was isolated from ARPE19, SHEF-1 (Kind gift from Dr. Amanda Jayne Carr), primary human RPE cells, freshly isolated cadaveric human RPE and choroid. The expression levels of all 24 mammalian zinc transporters were measured using gene specific primers labeled with SYBRGreen (Table 3.1). Sequences are available in Table 3.2. The primers were designed, synthesised and optimised by PrimerDesign (Southampton, UK) (Sequences for these primers are available in Appendix 3). RNA quantification was done using NanoDrop (ThermoScientific, UK), and RNA integrity was assessed by BioRad Experion system. Relative gene expression levels were calculated based on the comparative Ct method (Schmittgen and Livak, 2008). This was achieved by normalising the cycle (Ct) values (the cross-over threshold value where the signal was first detected in a qPCR assay) of the gene of interest to the housekeeping genes, thereby giving a Δ Ct value (shown in Table 3.1). HigherΔCt values indicate lower expression. Genes were grouped according to three arbitrary thresholds: ΔCt values below 5 were considered to be high to medium (in red), ΔCt between 5-10 were low (in yellow), and ΔCt above 10, at which point the genes were probably not expressed as judged by the dissociation curves from each PCR product in grey. The results are the averages of at least 2 independent experiments carried out in duplicate. The low numbers of experiments are not enough to provide an accurate data as the variability of the qPCR data can be high. It is recommended that 3 independent experiments are carried out in the future.

As mentioned, the results were verified by closely examining the dissociation curves and running the PCR products on 1% agarose gels. Following electrophoretic separation, the ethidium bromide labeled PCR products were visualised under UV light (Figure 3.2). Non-template controls (amplification in the absence of cDNA) were run alongside the samples for the identification of primer dimers and non-specific products. While we included in Table 3.1 the ΔCt values for the genes from human cadaveric tissues, we could not apply similar threshold categories defined above as the housekeeping genes Ct values for the cadaveric tissues were unexpectedly high. This was probably due to variable post-mortem degradation of RNA. Nonetheless, comparing ΔCt values to each other allows the identification of potentially highly expressed genes. For ease of interpretation, the data is also presented in an additional format, with the same colour scheme as previously described (Figure 3.3).

Results

Following the q-RT-PCR experiments, most zinc transporters appear to be expressed in all cell lines. SLC30A3, SLC30A6, SLC30A7, SLC39A3, and SLC39A11 were expressed at a low level, while SLC30A9, SLC39A1, SLC39A7, and SLC39A13 were expressed at the medium to high levels in all cell lines. SLC30A8, SLC30A10 and SLC39A12 did not seem to be expressed in any of the RPE cell lines. There appeared to be some discernable differences in expression levels in the different cell lines: highest expression was observed for SLC39A4 in ARPE19, for SLC39A6 in SHEF1 and SLC30A1 in primary cultures, SLC30A2 expression was very low or absent in ARPE19, but present in SHEF1 and primary cultures. SLC39A2 was only expressed in SHEF1 cells, but not in ARPE19 and primary cultures. SLC39A5 was expressed in ARPE19 and SHEF1 cells but not in primary cultures. The absence of genes such as SLC30A8, SLC30A10 and SLC39A12 in these cell lines was confirmed by separating the PCR product on 1% agarose gels (Figure 3.2).

In cadaveric samples the presence of zinc transporter expression was visualised on 1% agarose gels. Those without a clear band or those where bandsco-migrated with the non-template controls, andgave similar fluorescence intensity bands to that of the non-template control (See Figure 3.2)were deemed to be non-expressed. Based

on this, SLC39A2 and SLC39A9 were not expressed in human cadaveric RPE and while probably present there was very low expression levels of SLC39A10 and SLC39A11. In contrast, we found that the expression of SLC39A12, whose expression was absent in all cell lines, appeared to be very high in human cadaveric RPE.

Table 3-1- Expression of SLC30A1-10, SLC39A1-14 in RPE cells

Expression of SLC30A1-10, SLC39A1-14 in ARPE19, human embryonic stem cell derived RPE cells (SHEF-1), primary cultures of human RPE, as well as cadaveric human RPE. Data was expressed in ΔCt format with mean standard deviation values. The results were derived from averaged values from 2-4 independent experiments carried out in duplicates. QPCR experiments were conducted on Applied Biosystem HT7900 system. The colours red indicated high expression (ΔCt < 5), yellow indicated medium expression (ΔCt 5-10), and grey (ΔCt >10) indicated low or no expression as assessed by ΔCt values and melt curve analysis.

	ARPE19		SHEF-1		Primary hRPE		Cad. HRPE	
	n		n		n		n	
SLC30A1/ ZnT1	4	7.7+1.7	4	7.8+1.8	2	5.0+0.5	4	1.3+1.9
SLC30A2/ZnT2	4	11.0+1.8	4	8.2+0.6	2	7.8+0.4	4	1.9+5.9
SLC30A3/ZnT3	3	9.2+0.7	3	8.6+1.0	2	8.2+0.3	4	0.9+3.2
SLC30A4/ZnT4	3	9.4+1.7	3	10.6+1.7	2	8.8+0.9	4	1.5+3.4
SLC30A5/ZnT5	2	5.2+0.2	2	4.0+0.0	2	5.0+0.4	4	1.1+3.4
SLC30A6/ZnT6	2	6.9+0.1	2	5.5+0.0	2	6.8+1.0	4	2.0+6.7
SLC30A7/ZnT7	2	6.8+0.1	2	5.9+0.5	2	6.4+0.5	4	0.9+6.0
SLC30A8/ZnT8	4	14.0+1.3	4	12.3+0.4	2	11.8+0.0	4	3.7+4.0
SLC30A9/ZnT9	2	3.9+0.2	2	3.1+0.2	2	3.6+0.2	4	0.9+5.4
SLC30A10/ZnT10	5	15.8+1.2	5	10.6+1.6	2	16.1+1.3	4	1.6+2.8
SLC39A1/ZIP1	2	2.4+1.1	2	2.0+1.3	2	3.4+0.6	4	1.2+3.1
SLC39A2/ZIP2	5	14.4+1.8	5	8.8+1.8	2	13.4+0.1	4	4.2+4.8
SLC39A3/ZIP3	3	7.3+2.2	3	6.3+1.9	2	5.8+0.0	4	0.9+5.8
SLC39A4/ZIP4	2	4.0+0.6	2	5.7+0.0	2	5.1+0.7	4	0.9+2.6
SLC39A5/ZIP5	3	7.9+1.6	3	5.7+0.6	2	10.2+0.4	4	3.2+3.2
SLC39A6/ZIP6	2	5.7+1.3	2	3.1+2.4	2	7.7+0.6	4	3.2+6.4
SLC39A7/ZIP7	2	3.3+1.2	2	2.0+1.3	2	5.1+0.9	4	1.9+5.6
SLC39A8/ZIP8	2	6.6+1.0	2	5.5+1.0	2	4.8+0.2	4	1.8+4.0
SLC39A9/ZIP9	2	5.5+1.5	2	4.9+1.6	2	10.2+0.0	4	2.8+3.7
SLC39A10/ZIP10	2	6.3+1.2	2	3.4+1.3	2	6.5+0.1	4	3.2+3.8
SLC39A11/ZIP11	2	7.4+1.1	2	5.6+1.1	2	6.4+0.1	4	4.0+0.9
SLC39A12/ZIP12	5	14.5+2.2	5	11.7+1.6	2	12.3+0.1	4	0.9+0.2
SLC39A13/ZIP13	2	3.5+1.3	2	4.1+0.9	2	3.9+1.2	4	2.1+3.0
SLC39A14/ZIP14	2	5.7+0.5	2	3.6+1.0	2	4.2+0.4	4	3.0+3.6

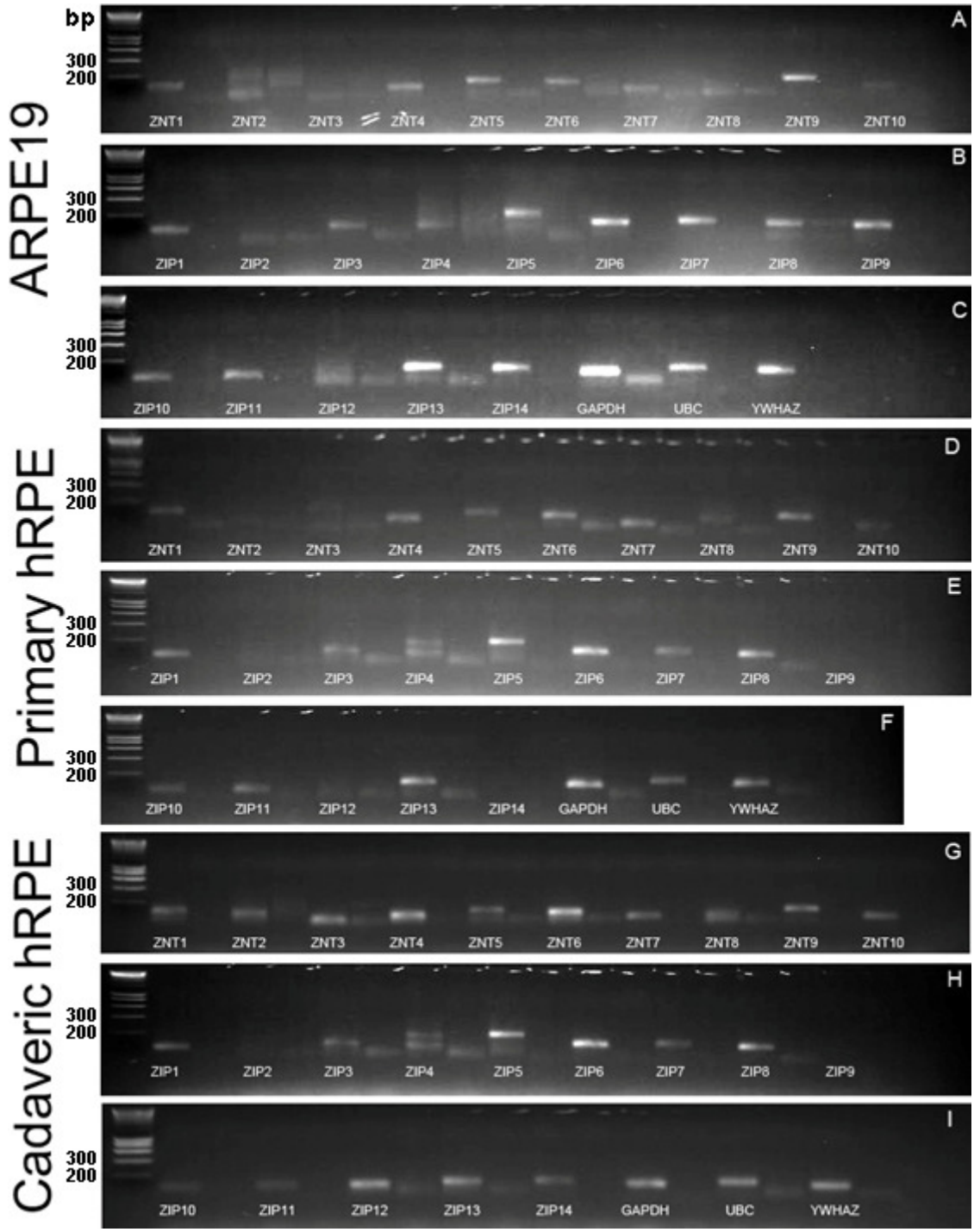

Figure 3-2- Confirmation of QRT-PCR using 1% agarose gels

The PCR products were run on 1% agarose gel and visualised using ethidium - bromide. The results for ARPE19 are shown in panels A,B,C, primary human RPE culture (passage 4) in D,E,F and cadaveric human RPE in G, H, I. The zinc transporters and the housekeeping genes for each sample are labeled, with the corresponding non-template controls on its right hand side. The 200 and 300 bp size markers are labeled on the pictures. For image purpose, the gene names have been replaced by protein names, for explanation refer to page 91.

Table 3-2 - Human primer sequences for SLC30A family and SLC39A family of zinc transporters

		Primer Sequences Homo sapiens		
Gene	**Accession Number**	**Forward**	**Reverse**	**BP**
SLC30A1	NM_021194	AAGACCCCAGCAGTTAGCA	AGGTTGTTTGTTTGGCATGTTT	129
SLC30A2	NM_001004434	GAGAAGTCGTTGGTGGGTAC	GAGGGAGAAGAGGCTGATGA	104
SLC30A3	NM_003459	CTTTGGCTGGCACCGTTCA	CTCGATGTGGTAGTCGCTGTG	124
SLC30A4	NM_013309	GCACATTTGGAGTCCCTTTTC	CATTGTTACCCTACTCTGATTCTTAG	96
SLC30A5	NM_022902	TTATAGAGCAGTTTGGATGGTTCA	TTCATATTCTGGTGGCAATCTCA	137
SLC30A6	NM_017964	CATTTGGGTTTGAAAGATTAGAAGTC	GTGTGTATCTCGGGCTGTTC	124
SLC30A7	NM_133496	TCCTGTGCCTGAACCTCTC	AGTCGGAAATCAAGCCTAAGC	81
SLC30A8	NM_173851	AGGGAGATTTTAAGGATTTTGAGATG	AGGGAAAGGGTAATGGGAGAG	104
SLC30A9	NM_006345	TCCATCCAGCCAGAACAAGT	TGTAACAACTCGCCCATCAAA	150
SLC30A10	NM_018713	ATATCAAGATGCCAGCACAAAAAT	GGGTTCCTTCAAGTCCACATT	97
SLC39A1	NM_014437	AGGAACAAGAGATGGTCAAGTC	GTATAGTGTCCAACCTCTGATTCT	96
SLC39A2	NM_014579	TTTGGAGTCGCTGGCATTG	TTTGAGGGTGAGGGTAAATGTC	126
SLC39A3	NM_144564	TTTGGAGGAGGGGTGTTTCT	GGGTAGTCGGTGCTGATGT	107
SLC39A4	NM_01167	GCTGCTGCTGTCCCTGTAC	GGTTTCTGGGCTGTAGGTTTG	107
SLC39A5	NM_173596	GGGGAGAATAGGAGCCAGAA	AAGACGACCCACACACAGAA	105
SLC39A6	NM_012319	ACTACCATCATATTCTCCATCATCA	CATCACCCATTATCACCATCCA	132
SLC39A7	NM_006979	GTTCTCCAAGGTCCAGTTTCC	CCCCAATCACTCCCAAATCAG	144
SLC39A8	NM_022154	CTCTCCTCGGATTGATTTTGACT	AATGCCTCTGGAATAAGTTGGAA	130
SLC39A9	NM_018375	AGTGGTTGTGGGTGAATAAAGG	GAAATTAACAGCCAAGGGAATGAT	120
SLC39A10	NM_001127257	TGGTGATGGTGACAATGAAGAA	GCAAATCCAAAGAGCAATCCTAA	84
SLC39A11	NM_139177	CTGAAATGTCCCTATAAAGAATGAGT	TTGCTACCCCTGTTGGAGAA	86
SLC39A12	NM_152725	CTTGCCTTCCCCAGACTACT	CCAGAGAGTGTTGAGGAGTTG	103
SLC39A13	NM_001128225	ATCGTGGTAATGGTGCTGTTC	CCCTCTCTGCCTCTCACATAT	126
SLC39A14	NM_015359	TTGCCGCTTCCATAAATCAAAG	AAACCCATCTGTAGCATAATCATTAG	127

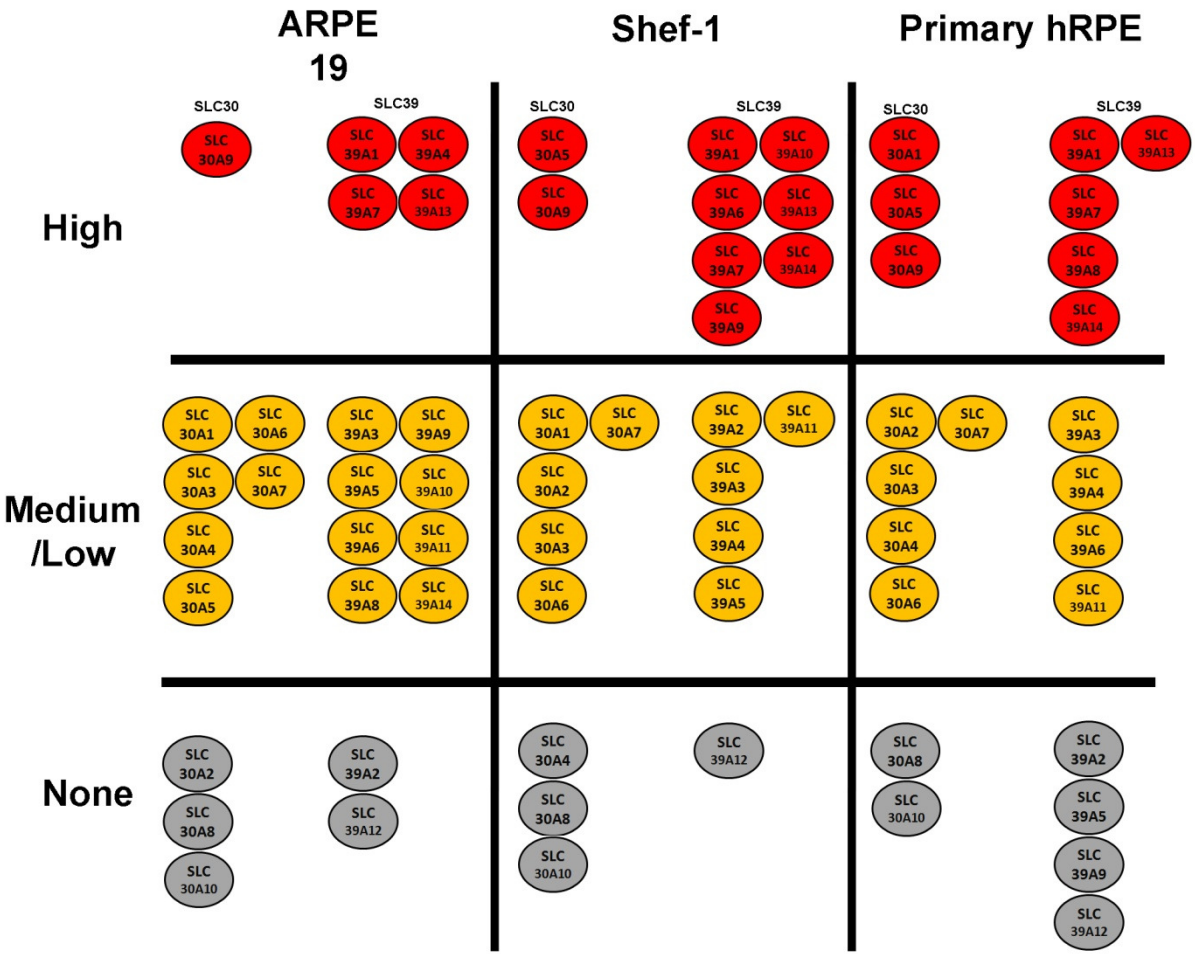

Figure 3-3 – Diagram representation of QRT-PCR data for RPE cells

Representation of QRT-PCR data for RPE cells in bullet format, separating the high (red), medium (yellow) and no expression (grey) for both SLC30 and SLC39 family of zinc transporter genes. From left to right, data for ARPE19, Shef-1 and primary hRPE are presented.

3.4. **Expression of SLC30A SLC39A Transporters in non RPE Cells**

We also assessed the expression of the 24 zinc transporters in other cells and tissues including those isolated from rat or human retina (see Table 3.3 and pictorial representation Figure 3.4) namely the murine endothelioma cell-line bEND5, primary rat retinal ganglion cells (kindly provided by Dr. Richard Foxton), human primary cultures of Muller cells (RNA kindly provided by Dr. Astrid Limb) and human cadaveric choroid. Similarly, threshold categories defined above as the housekeeping genes Ct values for the cadaveric tissues were unexpectedly high as described before. In addition human embryonic kidney HEK293 cells were also assayed (This cell line will be extensively used in the Chapter 4). In bEND5 cells out of the 24 transporters only SLC30A8, SLC30A10 and SLC39A12 were not expressed. In primary rat retinal ganglion cells (RGC) out of the 24 transporters only SLC30A7, SLC30A8, SLC39A2, and SLC39A12 were not expressed. In human primary cultures of Muller cells the genes which were not expressed were SLC30A8, SLC30A10, SLC39A5, and SLC39A12. In the HEK293 human embryonic kidney cell line it appeared that except SLC39A12 all other zinc transporters are detectable, although sometimes at very low levels of expression. The presence of SLC30A10 expression was one of the results which could only be confirmed after analysis of the dissociation curve. In human cadaveric choroid, based on dissociation curve analysis, SLC30A2, SLC30A8, and SLC39A2 genes are not expressed.

Table 3-3 - Expression of SLC30A1-10, SLC39A1-14 in non- RPE cells

Expression of SLC30A1-10, SLC39A1-14 in murine BEND5, rat retinal ganglion cells, HEK293 cells and human primary cultures of Muller cells. Data were expressed in ΔCt format with mean and standard deviation values. The results were derived from averaged values from 2/3 independent experiments carried out in duplicates. QPCR experiments were conducted on anApplied Biosystem HT7900 system. * Left blank due to presence of non-specific product in NTC, see confirmation performed using Taqman. The colours red indicated high expression (ΔCt < 5), yellow indicated medium expression (ΔCt 5-10), and grey (ΔCt >10) indicated low or no expression as assessed by ΔCt values and melt curve analysis.

	mBEND5		rRGC		HEK293		hMuller		Cad. hChoroid	
	n		n		n		n		n	
SLC30A1	3	4.6+1.8	2	7.0+0.4	2	6.7+0.5	2	7.2+0.1	4	2.9+2.8
SLC30A2	3	7.1+2.6	2	7.0+0.8	2	3.9+0.0	2	8.7+2.9	4	5.8+2.5
SLC30A3	3	8.1+2.8	2	7.0+0.5	2	5.0+0.1	2	6.9+0.3	4	2.1+4.8
SLC30A4	3	3.5+2.1	2	6.8+0.1	2	7.9+1.1	2	8.2+0.3	4	3.4+2.9
SLC30A5	3	4.8+0.8	2	6.7+0.1	2	2.9+0.6	2	4.5+0.2	4	3.0+1.4
SLC30A6	3	5.6+1.4	2	6.8+0.9	2	6.6+0.3	2	6.4+0.7	4	5.5+2.2
SLC30A7	3	5.2+0.3	2	10.9+2.6	2	9.6+0.3	2	6.4+0.1	4	4.8+2.3
SLC30A8	3	10.8+1.1	2	11.5+8.8	2	5.6+0.7	2	13.0+1.0	4	5.8+4.8
SLC30A9	3	3.9+0.9	2	5.9+0.6	2	3.6+0.2	2	4.4+0.7	4	4.5+1.0
SLC30A10	3	11.6+0.2	2	6.4+0.1	2	10.6+0.2	2	13.6+1.6	4	4.9+4.2
SLC39A1	3	2.7+0.5	2	6.5+1.5	2	4.0+0.2	2	3.8+0.1	4	1.9+2.1
SLC39A2	3	7.9+1.9	2	10.1+7.3	2	5.3+0.0	2	12.2+3.8	4	6.8+4.5
SLC39A3	3	6.3+1.0	2	6.5+0.0	2	3.4+0.1	2	6.1+0.8	4	3.4+2.2
SLC39A4	3	8.0+1.9	2	6.8+0.4	2	4.1+0.3	2	7.2+0.3	4	3.2+2.0
SLC39A5	3	8.8+2.6	2	8.3+0.2	2	4.7+1.2	2	10.0+2.8	4	5.9+4.1
SLC39A6	3	6.6+0.1	2	6.2+0.2	2	5.1+0.2	2	5.6+5.1	4	6.3+3.3
SLC39A7	3	3.4+0.7	2	7.1+0.4	2	4.6+0.1	2	2.8+0.4	4	3.5+0.9
SLC39A8	3	6.0+0.7	2	6.0+0.1	2	5.8+0.2	2	6.8+0.8	4	4.9+2.0
SLC39A9	3	7.5+1.4	2	6.9+0.3	2	9.3+0.0	2	6.8+1.2	4	4.4+2.9
SLC39A10	3	6.2+2.0	2	9.4+1.8	2	9.3+0.1	2	8.3+4.5	4	5.5+2.6
SLC39A11	3	4.6+0.4	2	6.1+0.3	2	6.4+0.1	2	6.8+0.2	4	4.6+2.8
SLC39A12	3	11.5+3.2	2	11.6+3.1	2	*4.7+2.0	2	14.2+1.1	4	2.1+2.9
SLC39A13	3	4.1+1.4	2	7.1+0.1	2	6.2+0.5	2	4.5+0.9	4	3.3+2.0
SLC39A14	3	9.3+0.8	2	5.9+0.1	2	4.9+0.0	2	3.2+0.8	4	3.9+2.4
TaqMan SLC39A12						15.3				

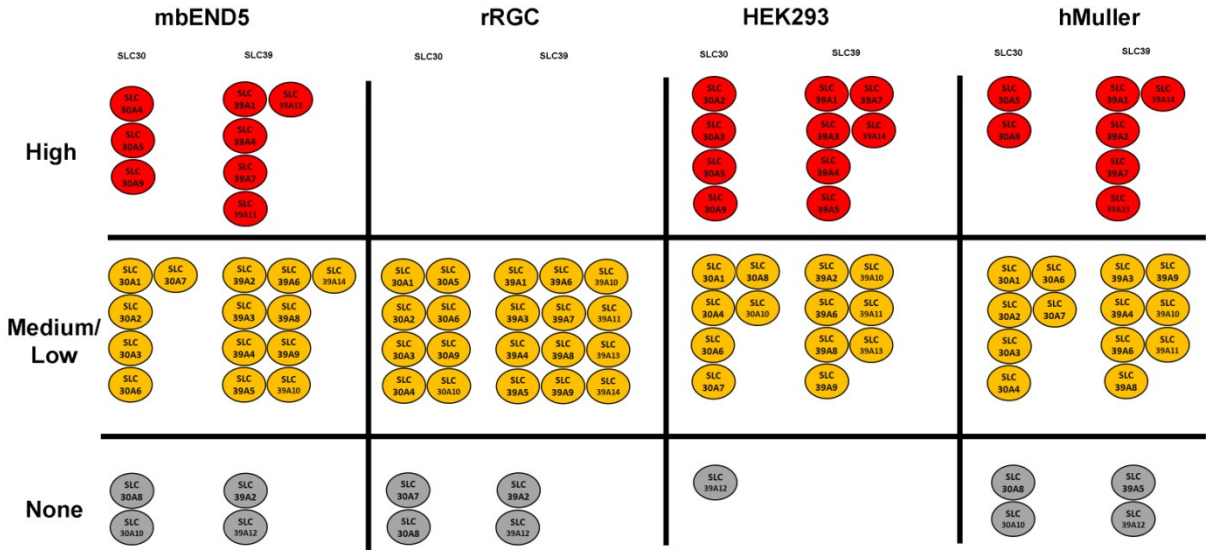

Figure 3-4- Diagram representation of QRT-PCR data for non-RPE cells

Representation of QRT-PCR data for non-RPE cells in bullet format, separating the high (red), medium (yellow) and no expression (grey) for both SLC30 and SLC39 family of zinc transporter genes. From left to right, data for mBend5, rRGC, HEK293 and hMuller are presented.

3.5. Confirmation of high SLC39A12 Expression in Cadaveric Tissue Using a TaqMan Style Probe

Methods

SYBR-Green dye-based detection is a highly efficient method to quantify the expression of the zinc transporters. This means that no specific probes are required, which reduces assay setup time and running costs. However, because SYBR Green dye binds to any double-stranded DNA, including nonspecific double-stranded DNA sequences, it has a potential to generate false positive signals and we showed that generation of signals from primer dimers does interfere with the detection of lowly expressed gene amplification products. This appeared to be the case for SLC39A12 in cultured cells. To overcome this problem, the TaqMan-based detection of gene amplification was employed. This method is based on specific hybridization between a probe and its target generating a gene amplification specific signal. The disadvantage of the TaqMan chemistry is that the synthesis of different probes is required for different sequences, making this method less cost effective. The probes were labelled with a fluorescent dye (in our case it was 6-carboxyfluoroscein (FAM) and a quencher that extinguishes fluorescence while both attached to the probe. During the polymerisation reaction the probe is cleaved and this releases the fluorescent dye from the quencher. As PCR product accumulates, fluorescence intensity increases, allowing quantitation of the generated PCR products. Table 3.4 shows the fold difference in expression compared to ARPE19 cells generated by first calculating the ΔCt values compared to the housekeeping genes (GAPDH, UBC, and YWHAZ) and then calculating the ΔΔCt values by comparing the ΔCt values for the gene of interest to ΔCt SLC39A12 in ARPE19 for normalisation.

Results

The values obtained by using SYBRGreen and TaqMan based detection systems were similar. The expression of SLC39A12 was 3-4 orders of magnitude higher in cadaveric samples and about 2 orders of magnitude higher in primary RPE cultures compared to expression in ARPE19. Currently we are confirming the results with further experimentations with the TaqMan-based probe for SLC39A12.

Table 3-4–Confirmation of SLC39A12 expression using TaqMan-style Probe
The level of expression of SLC39A12 measured by using SYBR-Green based detection or TaqMan -based detection. Cadaveric tissues and primary RPE cultures contain higher level of SLC39A12 expression than ARPE19 cells do.

	n	SYBRgreen	TaqMan
ARPE19	3	1.0	1.0
hRetina	3	2530.4	2014.9
hRPE	3	1708.7	1922.6
hChoroid	3	13378.5	12147.5
Primary RPE	3	375.0	355.3

3.6. Evidence of Cross-Contamination in Cadaveric Samples

Method:

QRT-PCR using RPE65 as RPE specific gene, VE-cadherin as endothelial specific gene and rhodopsin as retinal specific gene was used to validate for possible cross-contamination problem present in cadaveric human samples (Table 3.5). Primers for VE-cadherin was kindly provided by Dr. Jenny McKenzie, primers for RPE65 was kindly provided by Dr. Amanda Jayne Carr and primers for rhodopsin was purchased commercially from Applied Biosystem (Carlsbad, USA). The results presented here are the results from three or four separate experiments. Furthermore, in order to determine whether the expression of SLC39A12 increased with pigmentation, comparison was made between pigmented and non-pigmented ARPE19 cells. Three cDNA samples were kindly provided by Dr. Ahmed Ahmado and Dr. Amanda Jayne Carr. The data was presented as a delta Ct format as previously described. With low/ no expression having delta Ct >10 (grey), medium expression with delta Ct 5-10 (yellow) and high expression with delta Ct < 5 (red).

Results:

Table 3-5 – Cross contamination in human cadaveric samples

Cross-contamination present in human cadaveric samples and expression of ZIP12 in pigmented and non-pigmented ARPE19. Data is presented as the delta Ct value for each samples.

Choroid VE-cadherin	10.60
Choroid RPE65	1.91
Choroid Rhodopsin	10.02
RPE VE-cadherin	16.05
RPE RPE65	3.66
RPE Rhodopsin	8.80
Retina VE-cadherin	13.36
Retina RPE65	7.61
Retina Rhodopsin	2.14
ARPE19 pigmented SLC39A12	17.29
ARPE19 non-pigmented SLC39A12	21.46

In RPE samples, there is very little contamination from the choroid as assessed using endothelial specific VE-Cadherin primers, with a delta Ct of 16.05. There is moderate contamination (delta Ct 8.80) from the retina as assessed with retinal specific rhodopsin. The expression analysis for RPE65 is highest as expected in RPE samples with delta Ct of 3.66. In retina samples there is also minimal contamination from the choroid, (delta Ct 13.36), moderate contamination from RPE65 (delta Ct 7.61). The expression analysis for rhodopsin is highest in retinal samples with delta Ct of 2.14. The cross-contamination, particularly those present in choroid indicated that the results have to be taken with careful consideration. In pigmented ARPE19 cells, the expression of SLC39A12 is marginally increased (delta Ct of 17.29) compared to non pigmented (delta Ct of 21.46). However, as the changes are minimal and expression level remains very low, the results will have to be verified using other means.

3.7. **Discussion**

The ocular tissues contain exceptionally high concentrations of zinc (See Chapter 1 – Introduction) suggesting that zinc plays an important role in physiology and, potentially, pathology of the eye (Ugarte and Osborne, 2001). The primary mechanism(s) mediating zinc homeostasis in these cells is likely to involve at least some of the 10 ZnT exporters and the 14 ZIP importers encoded by the SLC30A and SLC39A solute-linked carrier families of transmembrane proteins (Liuzzi and Cousins, 2004a). While studies in other tissues have underlined the importance of these transporters in health and disease (Taylor et al., 2007, Zhang et al., 2008, Fukada et al., 2008, Dufner-Beattie et al., 2003), little is known about the distribution and function of these transporters in the eye. Here we examine the expression profile of all 24 zinc transporters in several cell lines, primary cell cultures and cadaveric samples from the retina/RPE/choroid complex to gain a better understanding of their distribution.

3.7.1. Zinc Transporters in Human Cadaveric and Cultured Retinal Pigment Epithelium Cells and non-RPE cell lines

The RPE is one of the most commonly studied cell type in ocular research. Previous studies have described the expression levels of zinc transporters in ARPE19 cells as well as primary RPE cell cultures from human adults and foetuses (Leung et al., 2008a, Rezaei et al., 2008a). ARPE19 is a spontaneously immortalised human RPE cell line. While it is widely used for RPE research, expression of RPE specific genes and several phenotypic characteristics of ARPE19 differ from those of RPE *in vivo* (Cai and Del Priore, 2006, Vugler et al., 2008). In their publication in 2008, Leung et al (Leung et al., 2008a) determined the expression of 23 zinc transporters (with exception to SLC30A10) in ARPE19 cells, as well as primary cultures derived from human foetuses and adults (summarized in Table 3.6). Another study (Rezaei et al., 2008a) analysed the expression of the 14 SLC39A genes (coding for ZIP importers). In our work we analysed the expression of all 24 zinc transporters in ARPE19, primary RPE cell cultures and RPE isolated from cadaveric eyes (data summarized in Figure 3.2). While the results obtained by Leung et al and Rezaei et al on cultured cells are not dissimilar, neither groups examined expression in cadaveric tissues. This is perhaps not surprising, considering the large variability in RNA samples we found in human cadaveric

RPE, which caused quantitative analysis impossible. This variability was probably due to post-mortem degradation of RPE and tissue handling. In recent experiments we were able to limit RNA degradation by doing a very thorough tissue disruption combining both hand held mortar and pestle tube as well as using Qiashredder tubes (Qiagen GmBH, Germany). Furthermore, retinal samples require complete removal of any vitreous humor attached before lysing.

However, analysing the dissociation curve from QRT-PCR experiments and separating of gene products on 1% agarose gels allowed us to draw some conclusion even on the difficult samples. In these SLC39A2, 9, 10 and 11 were either absent or had a very low level of expression while others appeared to be present with differing expression levels. Interestingly, in ARPE19 (and many other cultured cells, see later) the expression of SLC39A12 was absent while there is clear expression in cadaveric tissue derived RPE and primary RPE cells at passage 1 (Leung et al., 2008a) and low expression at passage 4 samples (our experiments). This raised the possibility that studying the role of ZIP12 protein might be possible by transfection of cultured RPE, which is discussed in details in the next chapter (Chapter 4).

Table 3-6- Summary of zinc transporter expression in various RPE cels

Summary of zinc transporter expression in various RPE cells based on the work of three different laboratories: a (Leung et al., 2008b); b (Rezaei et al., 2008b) and our own (Cahyadi, Berzegar-Befroei and Lengyel, unpublished). Black represents high, gray low and white no expression of a gene based on qRT-PCR experiments. Expression levels are compared to selected housekeeping genes. Abbreviations: RPE, retinal pigment epithelium; h, human; hf, human fetal; ha human adult; r, rat; m mouse; ND, not determined.

While information about the function of zinc transporters in the RPE is very limited, we combined our and the previously mentioned expression data with what is known about the location and function of zinc transporters in other cells, and have generated a speculative working model suggesting where zinc transporters might be. This is discussed below and depicted on Figure 3.5.

The discovery of ZnT1, the first zinc transporter identified (Palmiter and Findley, 1995) caused a major change in the understanding of zinc transport. It was discovered that overexpression of ZnT1 confers resistance to zinc pretreatment which was attributed to its plasma membrane localization. This allows the protein to constantly pump zinc to the extracellular space. ZnT1 is expected to be found on apical cell as well as basal membrane of RPE cells, although it has also been found around the perinuclear area of RPE cells (Kirschke and Huang, 2008, Wang et al., 2009a) (Leung et al., 2008b). The protein is unique compared to other plasma membrane transporters, as it is ubiquitously expressed compared to ZnT2 and ZnT5 which have a more limited expression and this led to the belief that it functions as the primary zinc exporter in cells. This was supported by the finding that the ZnT1 knockout mouse is embryonic lethal due to failure to remove excess zinc from cells (Langmade et al., 2000). Based on its pronounced expression in the RPE, ZnT1 is likely to be a plasma membrane exporter in RPE cells.

ZnT2 has been found in various tissues (Palmiter and Huang, 2004). Its localisation has been reported on endosomal vesicles, lysosomes, apical surface of microvilli and mitochondria (Kambe et al., 2004, Falcon-Perez and Dell'Angelica, 2007) (Kelleher and Lopez, 2008). The protein function is likely to be to reduce zinc concentration in the cytosol by transporting zinc into intracellular stores. Zinc treatment in various studies demonstrated an increase in ZnT2 at gene expression and protein levels (Falcon-Perez and Dell'Angelica, 2007, Bobilya et al., 2008). Within the RPE itself, it is possible that ZnT2 localisation in the vesicle/phagosome may indicate an involvement in phagocytosis of photoreceptor outer segments and degradation of opsins (Gleim et al., 2009). While we did not observe the expression of ZnT2 in our ARPE19 samples, gene expression of ZnT2 was reported by Leung and colleagues (Leung et al., 2008b, Liuzzi et al., 2001a).

ZnT3 protein is located on the apical membrane of the endothelial cells (Wang et al., 2004b). ZnT3 is usually associated with synaptic vesicles but has also been shown to be present in non-neuronal cells (Palmiter et al., 1996). In the human RPE cell lines, mRNA of ZnT3 was found to be expressed in ARPE-19 and human adult RPE, but not in human fetal RPE (Leung et al., 2008a), where our study reported no expression of ZnT3. If ZnT3 was present in RPE cells then it would be expected to be associated with vesicles around the apical plasma membrane. However, ZnT3 expression will need further verification as we were unable to confirm this observation.

In the eye, ZnT4 expression is found in all types of RPE cell cultures, ARPE-19, human fetal RPE, and human adult RPE (Leung et al., 2008a). It is expected that ZnT4 would be localised in the vesicles. In 2003, Henshall et al reported the localisation of ZnT4 in the vesicles and on the plasma membrane, indicative of its function to mediate efflux from the cells (Henshall 2003).

ZnT5 expression was absent in the study by Leung et al (Leung et al., 2008b) but present in the eye based on in silico data (Seve et al., 2004) and it was observed by us in all RPE cells analysed. This transporter is reported to be involved in vesicular zinc loading as well as associated with apical membranes, yet the direction of zinc transport through this transporter is not clear probably because of alternative splicing (Jackson et al., 2007, Valentine et al., 2007, Kambe et al., 2002). The expression of ZnT6,7 and 9 was observed both by us and Leung et al (Leung et al., 2008a). ZnT6 and 7 are involved in translocation of cytoplasmic zinc into the Golgi network (Kirschke and Huang, 2003), while ZnT9 is ubiquitously distributed in cells it was thought to be involved also in zinc transport into the nucleus (Sim and Chow, 1999, Sim et al., 2002). As intracellular immunoreactivity of ZnT7 in RPE is very high, transporting zinc into the Golgi might be important for appropriate RPE function.

The expression of ZnT7 in the retina of albino mice is localized to the axons and dendrites of ganglion cells,where reactivity was highest in the somata of ganglion cell layer, and moderate immunoreactivity was present in nerve fiber layer and inner nuclear layer. Weak staining was noted in the inner plexiform layer. Intracellularly, ZnT7 localizes to the perinuclear area, or Golgi apparatus (Kirschke

and Huang, 2003). In the RPE, expression of ZnT7 was reported by both our study and Leung (Leung et al., 2008a).

None of the RPE cells analysed in this study expressed ZnT8 mRNA. Previous studies have indicated the specific tissue localisation of ZnT8, where it is located in the pancreatic beta-cells. While we do not see the expression of ZnT8 in any of the tissues that we have analysed, Leung et al reported the expression of ZnT8 in human cultured fetal RPE, suggesting that this gene may have a developmental role. Studies from pancreatic beta-cells have shown vesicular localisation of ZnT8 (Chimienti et al., 2006), suggesting that if this protein is present in the RPE, it is likely to be localised in the same compartment.

Both Leung et al and our study observed a high expression of ZnT9 in RPE cells. While little functional data have been found for this protein, reports have associated the protein's localisation to the nucleus (Sim and Chow 1999, Sim et al., 2002). None of the studies reported the expression of ZnT10 although our data on 1% agarose gel seemed to indicate the presence of ZnT10 in human cadaveric samples. Seve has indicated that ZnT10 is embryonic specific, although no data are available on its function and localisation (Seve et al., 2004).

Relatively little is known about ZIP transporters. ZIP1-6, 8, 12 and 14 have been shown to be located on the plasma membrane and probably mediate zinc transport into RPE cells. ZIP7 is localized to the ER and Golgi, ZIP8 is present on vesicles and mitochondria and ZIP13 regulates zinc levels in the Golgi (Taylor et al., 2008, Aydemir et al., 2009, Fukada et al., 2008). In chapter 4, we will show the localization of ZIP12 protein on cultured cells.

ZIP1 protein is expressed in the ARPE19 cell line, as well as human fetal RPE and human adult cell lines (Leung et al., 2008a). Belloni-Olivi and colleagues have reported the dual localization of ZIP1 on the plasma membrane as well as intracellular vesicles under excessive zinc condition (Belloni-Olivi et al., 2009).

ZIP2 expression was observed in the ARPE-19 cell line and human fetal RPE, but not present in human adult RPE cells (Leung et al., 2008a). Increase in extracellular zinc levels in ARPE19 cells can increase the expression of ZIP2 and enzymes involved in glutathione synthesis to provide protection against oxidative stress in

RPE cells (Ha et al., 2006, Rezaei et al., 2008b). Expression of ZIP2 was also induced by various neurotrophic factors (Leung 2008). Studies by Rezaei and Leung both reported the expression of ZIP2 mRNA in ARPE19 cells, although we did not observe the expression in our studies. We postulate that this could be caused by differences in primers used. The expression of ZIP2 appears to be developmentally regulated and can be altered by neurotropic factors in RPE cells (Leung et al., 2008a) therefore it might be very important for normal and pathological processes in the eye.

ZIP3 expression has been found in both ARPE19 cell line and human cadaveric RPE in our studies. In addition to this, Leung et al and Rezaei et al have both reported expression of ZIP3 in ARPE19, human fetal and adult RPE cell cultures (Leung et al., 2008a).

ZIP12 is probably the least studied zinc transporter protein. Its gene expression is reported to be localized to the retina, kidney and brain according to the EST database (http://www.ncbi.nlm.nih.gov/nucest) (See section 4.7). Leung et al. (Leung et al., 2008a) reported that the expression of SLC39A12 was found in primary cultures of human fetal RPE, as well as human adult RPE but not in ARPE-19 cells. Rezaei et al (Rezaei et al., 2008a) and our work (Figure 3.2) confirms the absence of mRNA for ZIP12 in ARPE-19 cells. However, using TaqMan based detection we showed that its expression is 2-4 order higher in primary cultures and cadaveric RPE cells than in ARPE19, a finding that is strongly supported by the results of Booij et al (Booij et al., 2010b). They have shown that ZIP12 is not only expressed in RPE, but categorised it is one of the RPE specific genes. Given the important role for zinc in RPE cells, we have attempted to characterize this protein (see chapter 4) in order to understand the mechanism of zinc transport.

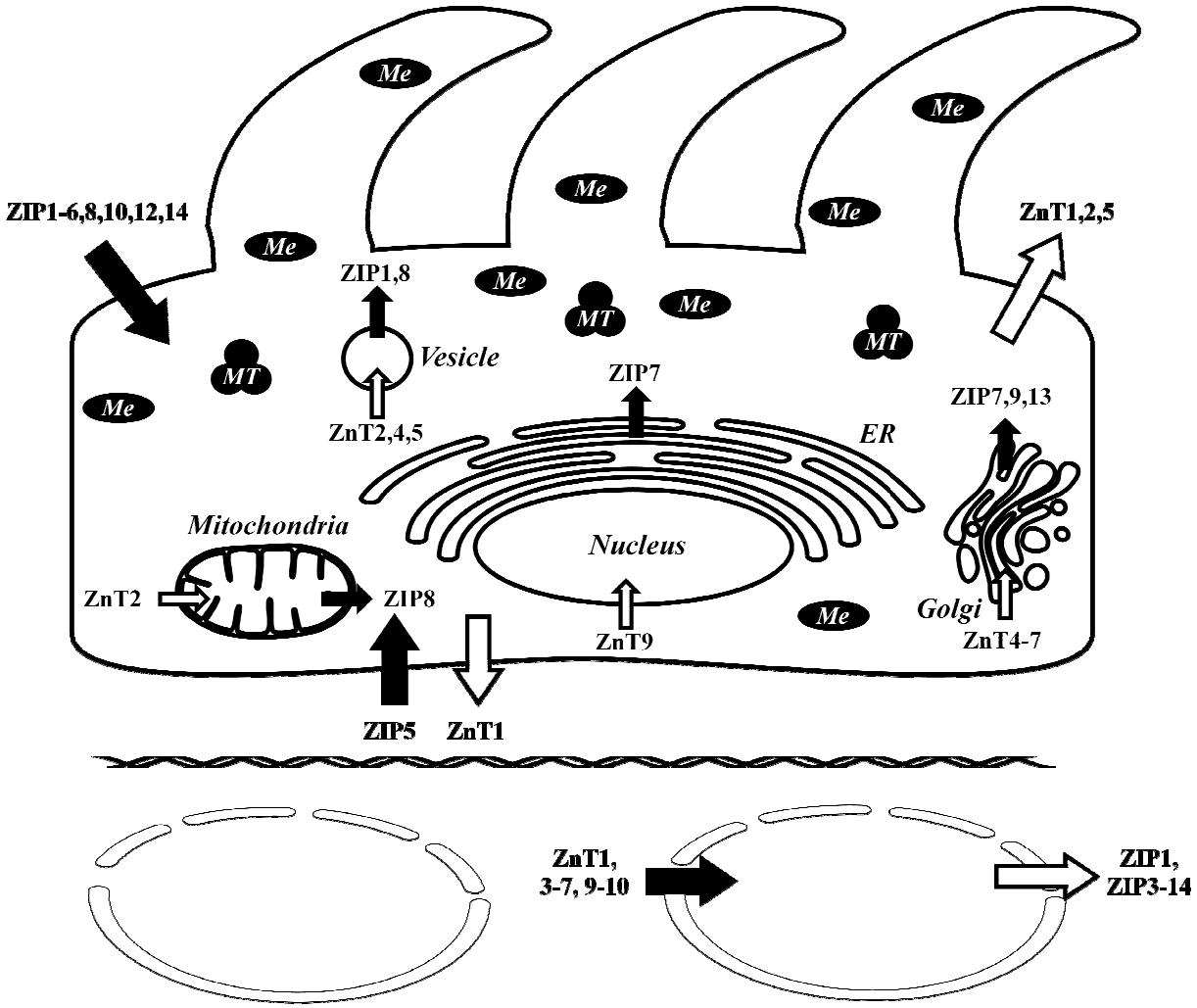

Figure 3-5- Zinc transporters in RPE-Choroid.

Based on the literature on other cell types and gene expression studies on RPE cells this figure summarizes our understanding of where zinc transporters may be located in RPE cells and includes potential zinc buffering or muffling compartments. For simplicity, on this figure endosomes, lysosomes, and secretory vesicles are labeled as "Vesicles" despite their vastly differing functions. Abbreviations: Me, melanosomes; MT metallothionein; ER, endoplasmic reticulum.

Picture taken from Barzegar-Befroei, N., Cahyadi, S., Gango, A., Peto, T., and Lengyel, I. 2011. Zinc in Eye Diseases. *Zinc in Human Health*. Amsterdam: IOS Press.

3.7.2. Zinc transporters in the choroid and fenestrated endothelial cells

Because of the difficulty of obtaining high quality RNA from cadaveric tissues, we could only generate information in relationship to the choroid through analysing zinc transporter expression in bEND5 cells. These cells are used to model fenestrae formation in endothelial and in Chapter 6 we will study the effects of zinc in this specialized system. While bEND5 cells are derived from rat they provide some indication about zinc transporter expression in fenestrated endothelial cells. The gene expression profile of bEND5 cells was very similar to that of ARPE19 cells. Many transporters appeared to be expressed in these cells although ZnT2, 3, 8, 10 and ZIP2 and 12 were not. Despite the lack of expression of SLC39A12 in bEND5 cells, the expression of this protein in cadaveric choroidal tissue is very high compared to the other tissues we examined. Given that Boiij et al found that ZIP12 is highly enriched in RPE cells compared to choroid in laser micro-dissected human cadaveric samples, the higher expression of SLC39A12 in choroid samples compared to the RPE in our experiments remains to be experimentally validated (Booij et al., 2010b).

3.7.3. Zinc Transporters in the Retina[3]

"Relatively little is known about zinc transporters in other parts of the eye. Our QRT-PCR data suggest that Muller cells express 8 out of the 10 ZnTs and 11 out of the 14 ZIPs, while primary retinal ganglion cells express 9 out of the 10 ZnTs and 13 out of the 14 ZIPs (see Figure 3.1). Redenti et al (Redenti and Chappell, 2004a) found ZnT3 protein in several layers of the retina, namely the inner segments and outer limiting membrane of photoreceptors, the inner nuclear layer and outer plexiform layer and the strongest labeling was present in both ganglion and Muller cells. This associates ZnT3 and therefore zinc with neuronal transmission (Palmiter et al., 1996). The only other transporter whose immunolabeling has been reported in the literature is ZnT7 (Wang et al., 2006a). Immunolabeling for ZnT7 is present in optic nerve fibers, ganglion cells, inner and outer plexiform layers, horizontal

[3] Barzegar-Befroei, N., Cahyadi, S., Gango, A., Peto, T., and Lengyel, I. 2011. Zinc in Eye Diseases. *Zinc in Human Health*. Amsterdam: IOS Press.

and amacrine cells and the photoreceptor outer segments (Wang et al., 2006a), suggesting that ZnT7 plays a wide ranging role in the retina."

3.7.4. Eye Phenotype in Zinc Transporter Knockout Animals[4]

"The role of zinc and zinc-dependent mechanisms in development (Prasad, 1998) indicated that appropriate zinc homeostasis might be important for normal eye development. In support of this, the examination of eye phenotypes of transgenic animals showed that an array of developmental abnormalities is associated with the lack of zinc transporter genes. For example, in ZIP4 knockout mice, exencephalia, severe growth retardation, and hydrocephaly, was accompanied by unilateral or bilateral anophthalmia. The manifestations of these could be exacerbated with zinc deficiency and ameliorated by zinc supplementation in heterozygous but not in homozygous embryos (Dufner-Beattie et al., 2007). Fukada et al reported that ZIP13 is crucial in connective tissue development. ZIP13 knockout caused sunken eyes which were also associated with down slanting palpebral fissures (Fukada et al., 2008). The abnormalities were attributed to a decrease in dermal collagen fibril sizes and thinning of corneal stroma. ZIP13 knockout effects also extended to improper osteogenesis and craniofacial tissue development."

3.8. **Future Plans**

One of the original goals of this thesis was to compare the expression of zinc transporters in AMD and control subjects to improve our understanding of how zinc homeostasis can be affected in diseased conditions. However, experiments on cadaveric tissues presented several problems, which we are just managing to resolve. Therefore, in the near future we will analyse zinc transporter expression in a selection of cadaveric samples. A comprehensive analysis of immunolocalisation of transporters would also be of interest. In a genetics study (in collaboration with Professor John Yates), we are examining the results from genome wide association studies to identify potential single nucleotide polymorphisms on the 24 zinc transporters. Based on preliminary data it appears that there are potential association between zinc transporter SNPs and AMD (data not shown) though

[4] Barzegar-Befroei, N., Cahyadi, S., Gango, A., Peto, T., and Lengyel, I. 2011. Zinc in Eye Diseases. *Zinc in Human Health*. Amsterdam: IOS Press.

further sampling and verification by PCR will be required before solid conclusions could be drawn (data not shown).

The results presented in this chapter needs to be taken with caution due to cross-contamination, lower quality RNA due to post-mortem tissue processing, particularly in the RPE and choroid samples. Future experiments will have to address cross-contamination issues, possibly through creation of very early passage primary cultures of human RPE. Furthermore, better dissection procedure need to be adopted for cadaveric RNA isolation, particularly in choroidal samples as QRT-PCR results indicated that there is heavy contamination from the RPE. Possible method to alleviate this problem may include laser microdissected samples from human cadaveric tissue.

Conclusion

Using SYBRGreen and TaqMan based detection assays we were able to start the cataloguing of zinc transporter expression in the retina/RPE/choroid complex. While this work is far from complete, it helped us and others to identify some potentially important zinc transporters for RPE cells. We became particularly interested in ZIP12 because of its unusually high expression in freshly isolated RPE cells and very low or non-existent expression in cultured cells although major caution needs to be exercised during interpretation of the result due to contamination from the corresponding tissue as well as low replication number of experiments.

4. Characterisation of ZIP12: Structure, Function and Localisation

As we showed in the previous chapter, several zinc transporters are expressed in the RPE-choroid interface. ZIP12 appears to be an exception. Its gene expression was either very low or absent in all cultured cells, including human primary RPE cultures, but was highly expressed in human cadaveric tissues. This finding was supported by recent findings on laser dissected human RPE cells, suggesting that SLC39A12 is one of the RPE specific genes (Booij et al., 2010b). We argue here that ZIP12 is a potentially important candidate gene for regulating zinc fluxes at the RPE-choroid interface and its lack of expression under culturing conditions might contribute to the phenotypic anomalies observed in *in vitro* experiments using ARPE19 cells. As ZIP12 is probably the least studied zinc transporter, we first examined how this transporter might function. Available information on ZIP12 was collected through data mining and bioinformatic tools to understand the protein structure before the cellular localisation of the protein was observed through transiently expressing it in various cell lines. Finally the possible relationship(s) between ZIP12 and RPE was explored.

There is very little published information on ZIP12 or its gene SLC39A12. Reports have linked ZIP12 to schizophrenia (Bly, 2006), Alzheimer's disease (Grupe et al., 2006) and cancer (Sotiriou et al., 2006). Despite the paucity of published peer reviewed information on ZIP12, we explored what can be found out about ZIP12 and its gene SLC39A12 in existing databases.

4.1. **SLC39A12 Isoforms**

SLC39A12 (UniProt accession Q504YO), is located on chromosome 10p12.33. There are 5 splice variants of SLC39A12 (www.ensembl.org) which is summarised in Table 4.1.

Table 4-1- Five isoforms of SLC39A12 (ZIP12). Data obtained from www.ensembl.org

Name	Amino Acid Length	Transcript Length
SLC39A12-001	690	2725 bps
SLC39A12-002	654	2639 bps
SLC39A12-201	691	2808 bps
SLC39A12-202	611	2483 bps
SLC39A12-203	557	1900 bps

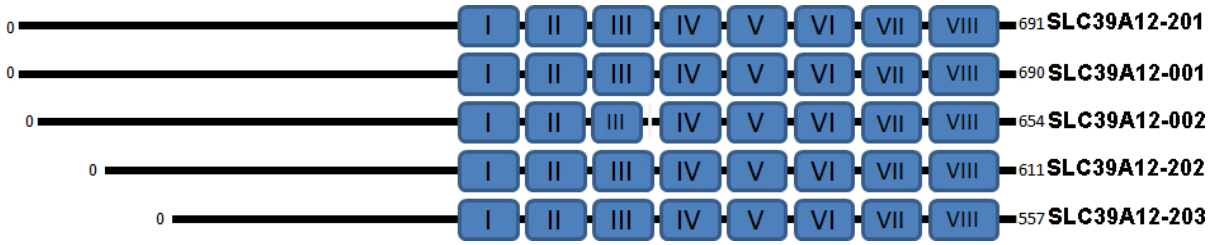

Figure 4-1- Five isoforms of ZIP12

Five isoforms of ZIP12 protein are shown, with the longest SLC39A12-201 isoform having 691 amino acid residues, SLC39A12-001 containing 690 amino acid residues with a deletion of residue K474. SLC39A12-002 contained a deletion between transmembrane III and IV, between residues 474-510 resulting in a protein with 654 amino acid residues. SLC39A12-202 has 611 amino acid residues, with truncation in the first 80 amino acids. SLC39A12-203 contains truncation in the first 134 amino acids.

4.2. **The ZIP12 protein**

Based on sequence homologies using ClustalW (http://www.ebi.ac.uk/Tools/msa/clustalw2/) the ZIP protein family was divided into four subfamilies where ZIP12 belongs to the LIV-1 subfamily (Figure 4.2). LIV-1 family members are thought to facilitate zinc uptake or influx (Taylor et al., 2007). There are three defining features of the LIV-1 subfamily:

-LIV-1 members are expected to have 8 transmembrane domains and are localised predominantly on the plasma membrane.

-All members should contain a histidine-rich motif, which has been suggested to be directly involved in zinc transport.

-All members should contain a highly conserved CPALLY domain at the N-terminal extracellular domain, whose function is currently unknown (Taylor et al., 2007).

Using Compute pI/Mw program from Expasy (http://web.expasy.org/compute_pi/), the molecular weight of the 691 amino acid long ZIP12 protein was predicted to be 76 kDa with an isoelectric point of 5.85. Based on prediction by DAScurve (http://mendel.imp.ac.at/sat/DAS/DAS.html), PSIPRED (http://bioinf.cs.ucl.ac.uk/psipred/) and TMPRED (http://www.ch.embnet.org/software/TMPRED_form.html) confirmed that ZIP12 is a protein with 8 transmembrane domains (Figure 4.4). However, Sosui (http://bp.nuap.nagoya-u.ac.jp/sosui/sosui_submit.html), that uses hydrophobicity features of the amino acid sequences to predict helical structures, returned with five transmembrane domains and TMHMM (http://www.cbs.dtu.dk/services/TMHMM/) returned seven transmembrane domains on ZIP12. All the transmembrane domains are located at the C-terminal half of the protein and the N-terminus is predicted to form a large part of the extracellular domain. There is a putative signal peptide sequence between residues 1-23 (http://www.cbs.dtu.dk/services/SignalP/) which could aid the insertion to the membrane. Overall the ZIP12 protein is expected to be a plasma membrane protein. As we will show later a C-terminal tagged form of ZIP12 is indeed localized to the plasma membrane (Figure 4.18).

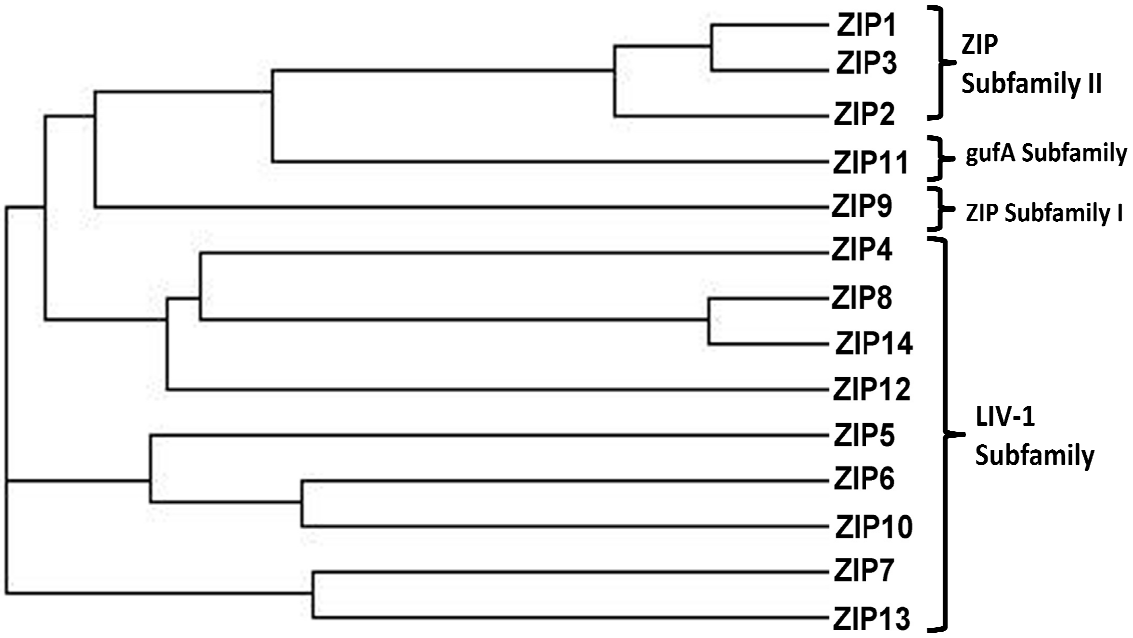

Figure 4-2 - Phylogenetic tree of SLC39 families.

SLC39 family of zinc transporters aredivided into 4 subfamilies. ZIP1, 2, and 3 belong to ZIP Subfamily II, ZIP 4 and 9 belong to Subfamily I, ZIP11 to gufA subfamily, ZIP4, 5, 6, 7, 8, 10, 12, 13 and 14 belong to the largest subfamily called LIV-1. ZIP7 and 13 is further grouped into HKE4 within the LIV-1 subfamily. Image was created using ClustalW and edited in Adobe Photoshop CS4.

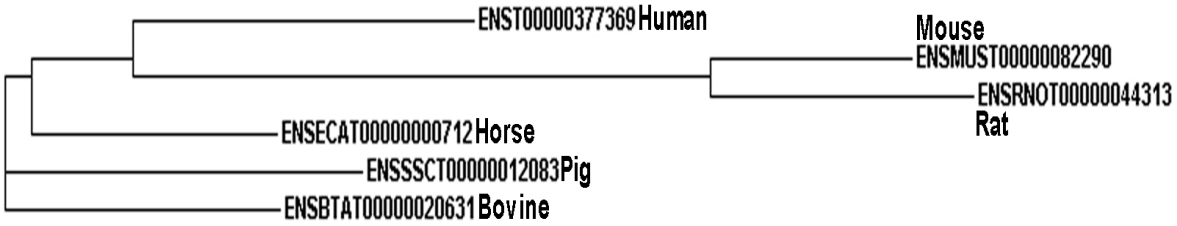

Figure 4-3 – Multiple alignments of ZIP12 peptide sequences among six common mammals human, mouse, rat, horse, pig and cow.

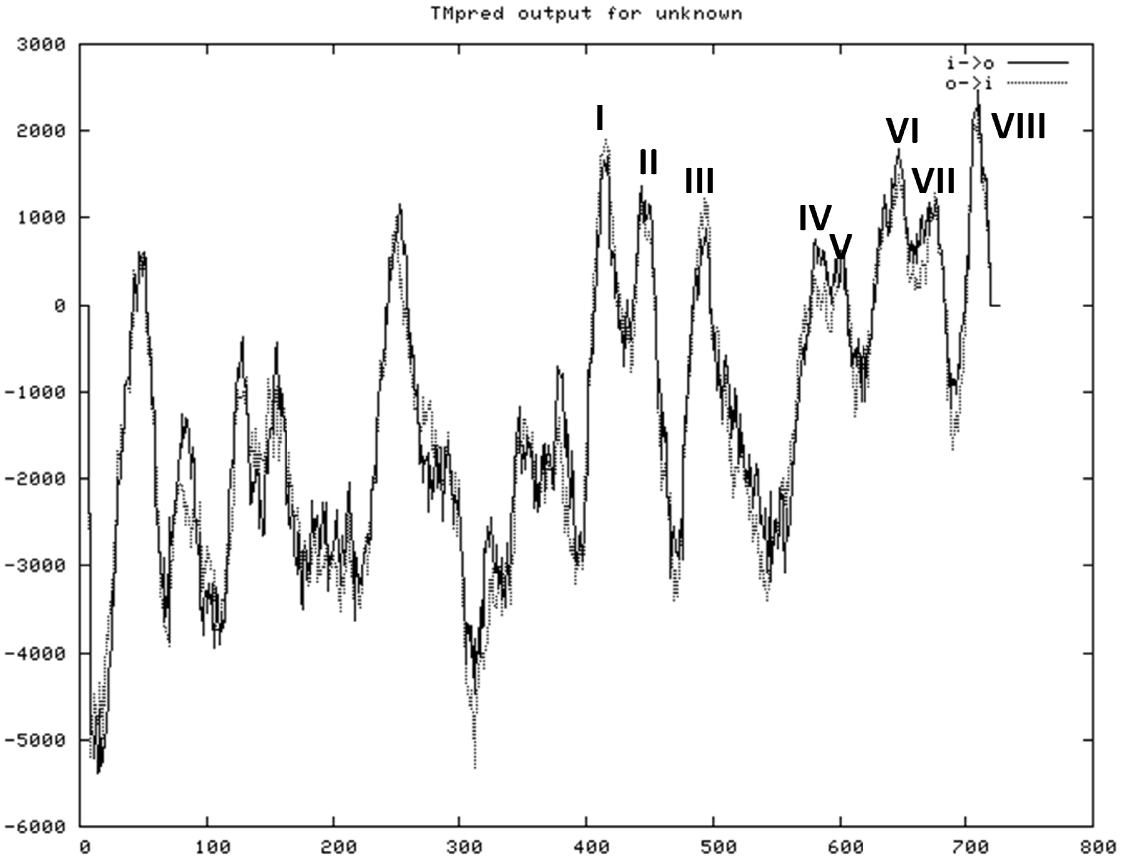

Figure 4-4 – Hydrophobic plot for ZIP12 protein

Hydrophobic plot created using TMpred program showed the presence of 10 peaks above the threshold. Combining the plot with results obtained from other transmembrane domains prediction programs indicated the potential presence of 8 transmembrane domains in ZIP12 protein (annotated on the graph). All the transmembrane domains are located in the second half of the protein structure from approximately residues 400-691. The annotation for transmembrane domains was made after comparing various secondary structure prediction programs (see section 4.2). TMPred returns with 2 additional transmembrane domains before transmembrane I, however, this was not shared by the other programs.

A histidine-rich HXXHXHH sequence can be found between transmembrane domains III and IV and a CPALLY-like domain is located adjacent to the TMI on the extracellular domain of ZIP12 (Figure 4.5). It is interesting to note that in isoform SLC39A12-002 a deletion of 35 amino acids between TMIII and IV eliminated the HXXHXHH residues, a histidine-rich sequence which has been suggested to bind zinc (Taylor, 2000). NetPhos3.8 program (http://www.cbs.dtu.dk/services/NetPhos/) predicted that there are 38 serine, 7 threonine and 6 tyrosine phosphorylation sites (data not annotated). One of these is Ser36, the amino acid residue that can be altered from serine into glycine, and this polymorphism has been associated with schizophrenia (Bly, 2006). This site is a consensus phosphorylation site for glycogen synthase kinase-3, suggesting that ZIP12 might be a target for GSK-3 signalling. Interestingly, GSK-3 signalling is thought to play a role in the pathogenesis of Alzheimer's disease (Takashima, 2006). This phosphorylation site is just downstream of a potential peptidase cleavage site located between residues 23 and 24 (http://www.cbs.dtu.dk). Annotated in pink are 6 potential glycosylation sites, all of which are found on the extracellular domain. In TMV, there is a conserved HEXXHEXGD metalloprotease-like domain, which is also present in other LIV-1 family members.

Table 4.2 highlights the sequence motifs or relevant sequences found in ZIP12 human protein sequence. Amino acids 1-20 show the sequence recognised by the Abcam (commercial) antibody which is used in this chapter. This sequence coincides with the signal peptide which would be cleaved in ZIP12 protein. We have used this antibody on cells and sections. Optimisation protocols using various fixation methods on ZIP12-transfected cells as well as various antigen-retrieval steps such as pressure cooker and microwaving sections did not produce any specific staining (data not shown). Upon enquiring with Abcam, it was determined that the antibody would not have worked as it coincides with the signal peptide. A potential cleavage site is located on residues 23-24 just after the signal peptide. A few of glycosylation sites (highlighted in pink) are present, all of which are located on the N-terminal of the protein. There is a potential GSK-3 beta phosphorylation site on residue 27-31 (red, underlined). In order to understand the function of ZIP12 further, we designed an antibody which recognises residues 294-305, which will subsequently be called ZIP12-5193 and ZIP12-5194 (red, highlighted). Soon after

the ZIP12 -5193/5194 sequence is a LIV-1 family-specific CPALLY motif (in green). Transmembrane I and II are located between residues 362-393 and 399-420. The histidine-rich region between residues 421-447 contains four histidine residues which is may have the capability to bind zinc. Transmembrane III is located between residues 448-469, and transmembrane IV from residues 540-563. Residues 474-510 contain a metal-binding motif HXXHXHH. The deletion of this residue in the truncated isoform of ZIP12 may have importance in function. Transmemrane V is located from residues 540-563. Within transmembrane V from 570-593 there is a metalloprotease domain HEIPHEMGD. The rest of the protein contains transmembranes VI, VII and VIII.

All five splice variants of ZIP12 protein share the same sequences, with no polymorphisms within conserved peptide sequences, with only deletions and truncations present. The longest variant has 691 amino acids (SLC39A12-201). The splice variant with the closest homology to SLC39A12-001 is SLC39A12-001 containing 690 amino acids with a deletion of a lysine residue at position 474 (www.ensembl.org). SLC39A12-002 contained a deletion between transmembrane III and IV, between residues 474-510 resulting in a protein with 654 amino acid residues where the histidine rich motif HXXHXHH is located. This result was also confirmed using GenBank. Histidine is an amino acid which has the capability to bind zinc through its imidazole ring. The loss of histidine-rich sequence in SLC39A12-002 creates an opportunity for functional analysis to see whether the truncation alters zinc transport capability as the sequence harbors a histidine rich motif HXXHXHH. Interestingly, sequence alignment using ClustalW2 shows that mouse does not have the human equivalent of sequence 474-510, meanwhile this sequence is preserved in other species such as pig, horse and rat.

SLC39A12-202 has 611 amino acid residues, with truncation in the first 80 amino acids. SLC39A12-203 is the shortest isoform of the five, with truncation in the first 134 amino acids. Alignments of SLC39A12 peptide sequences (Figure 4.3) in various species including human (Homo sapiens), mouse (Mus musculus), rat (Rattus norvegicus), pig (Sus scrofa), cow (Bos Taurus), and horse (Equus cabalus) showed similar protein sizes with often different but conserved amino acid residues (www.ensembl.org). There are three sub-branchings, with pig and bovine ZIP12 located on separate branches, the third sub-branch comprised of human, horse and

another smaller sub-branch containing rat and mouse ZIP12 sequences (see Figure 4.3)

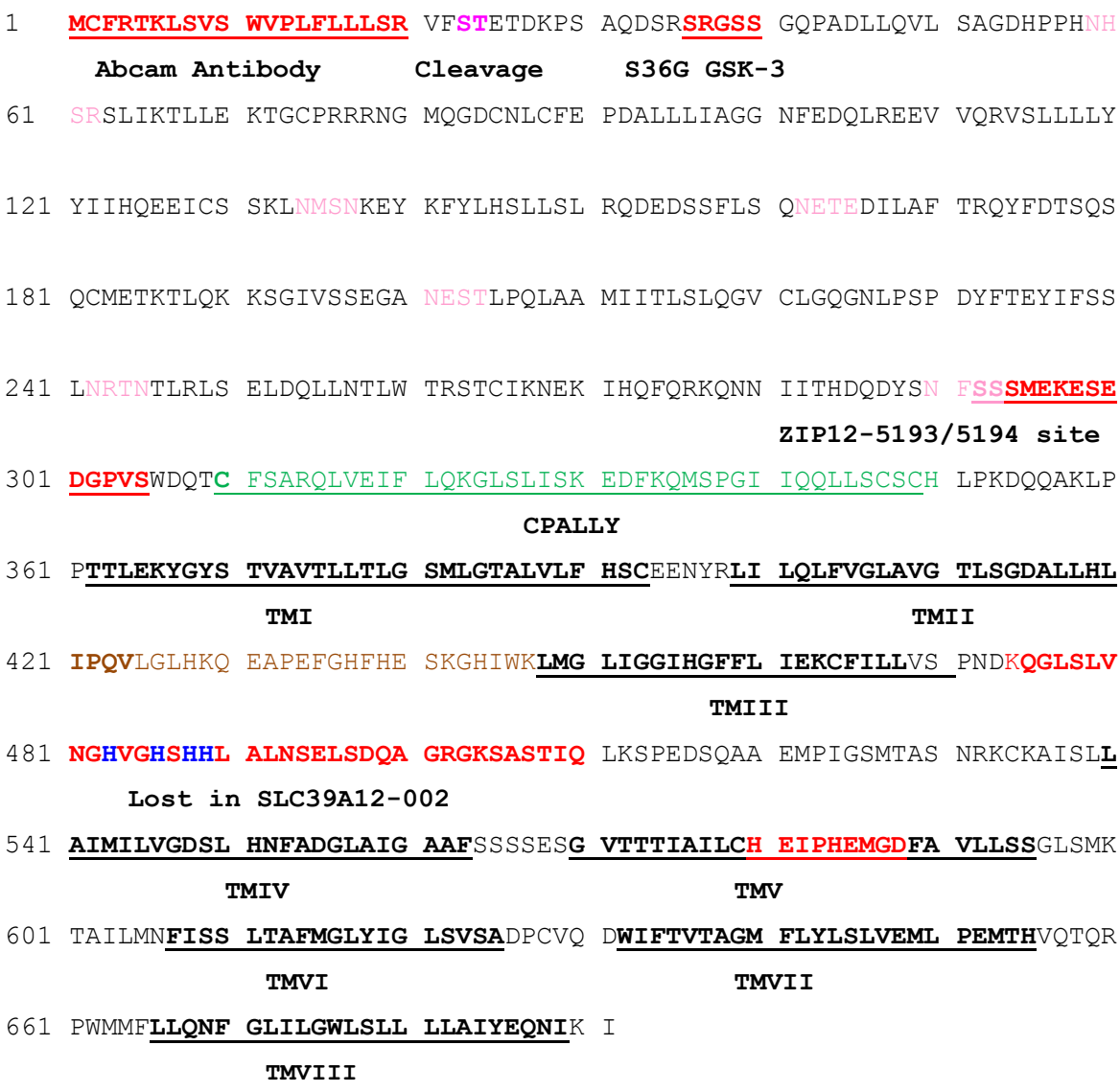

Figure 4-5– Annotated sequence of ZIP12 protein

The protein sequence for ZIP12 shows 8 potential transmembrane domains (underlined sequences labeled TMI-VIII), a classic CPALLY motif (labeled green), the HxxHxH zinc site (labeled blue) inside a a cleavage site between residue 23 and 24 (labeled with magenta), as well as potential phosphorylation site for Glycogen Synthase Kinase 3 (GSK-3) SRGSS (labeled red), between 421-447 (labeled brown) is the histidine-rich region (data obtained from various sources).

Table 4-2 - Details of Sequence Motif Found in ZIP12 Protein Sequence

Sequence Number	Sequence	Potential Motif/ Structure
1-20	MCFRTKLSVSWVPLFLLLSR	Abcam Antibody
1-17	MCFRTKLSVSWVPLFLL	Signal Peptide
23-24	ST	Potential cleavage site
59-62, 134-137, 162-165, 201-204, 242-245, 290-293	NHSR, NMSN, NETE, NEST, NRTN, NFSS	Glycosylation sites
27-31	SRGSS	GSK3-beta phosphorylation site
294-305	SMEKESEDGPVS	ZIP12-5193/4 Sequence
310-349	CLIPIIQC	CPALLY domain
362-393	PTTLEKYGYSTVAVTLLTLG SMLGTALVLF HSC	TMI
399-420	LI LQLFVGLAVG TLSGDALLHL	TM II
421-447	IPQVLGLHKQ EAPEFGHFHE SK GHIWK	Histidine Rich Region
448-469	LMG LIGGIHGFFL IEKCFILLVS	TM III
474-510	KQGLSLVNGHVGHSHHLALN SELSDQAGRGKSASTIQ	Deleted in truncated isoform with 654 amino acids
493-499	HVGHSHH	HXXHXHH
540-563	LAIMILVGDSL HNFADGLAIG AAF	TM IV
570-593	GVTTTIAILCH EIPHEMGDFA VLLSS	TM V
570-575	HEIPHEMGD	Metalloprotease domain
607-625	FISS LTAFMGLYIG LSVSA	TM VI
642-665	DWIFTVTAGM FLYLSLVEML PEMTH	TM VII
666-689	LLQNF GLILGWLSLL LLAIYEQNIK	TM VIII

4.3. **Specific Expression of SLC39A12 in Tissues**

Based on the EST database, SLC39A12 mRNA is expressed in brain, retina and kidney, throughout foetal, juvenile and adult life in human tissues (Figure 4.7) (http://ncbi.nlm.nih.gov/UniGene/ESTProfileViewer). Gene microarray data from mouse (http://biogps.gnf.org) showed that ZIP12 is expressed in the retinal pigment epithelium, the ciliary body, iris, and the eyecup (Figure 4.6). In situ hybridisation of mouse brain located ZIP12 to the brain ventricles (see figure 4.7 arrow). It has been known that ventricles harbor a high concentration of MTF-1 (Hao et al., 1994), which suggests that zinc can be released here and taken up by the brain probably through the involvement of zinc transporters.

4.4. **Aims**

In chapter 3, we showed the absence of ZIP12 expression in cultured cell lines and its high expression in cadaveric tissue. This chapter aims to study how ZIP12 is involved in regulating zinc using the following strategy:

1. Clone ZIP12 and generate tagged versions to express ZIP12 in different cell lines.
2. Raise and characterise antibodies against ZIP12.
3. Characterise commercially available ZIP12 antibodies.
4. Express ZIP12 protein in ARPE19 cells to understand how the expression affects the cells' phenotype.
5. Analyse available Genome-Wide Association studies or Microarray studies to develop further working hypotheses concerning the potential role of ZIP12 in the RPE.

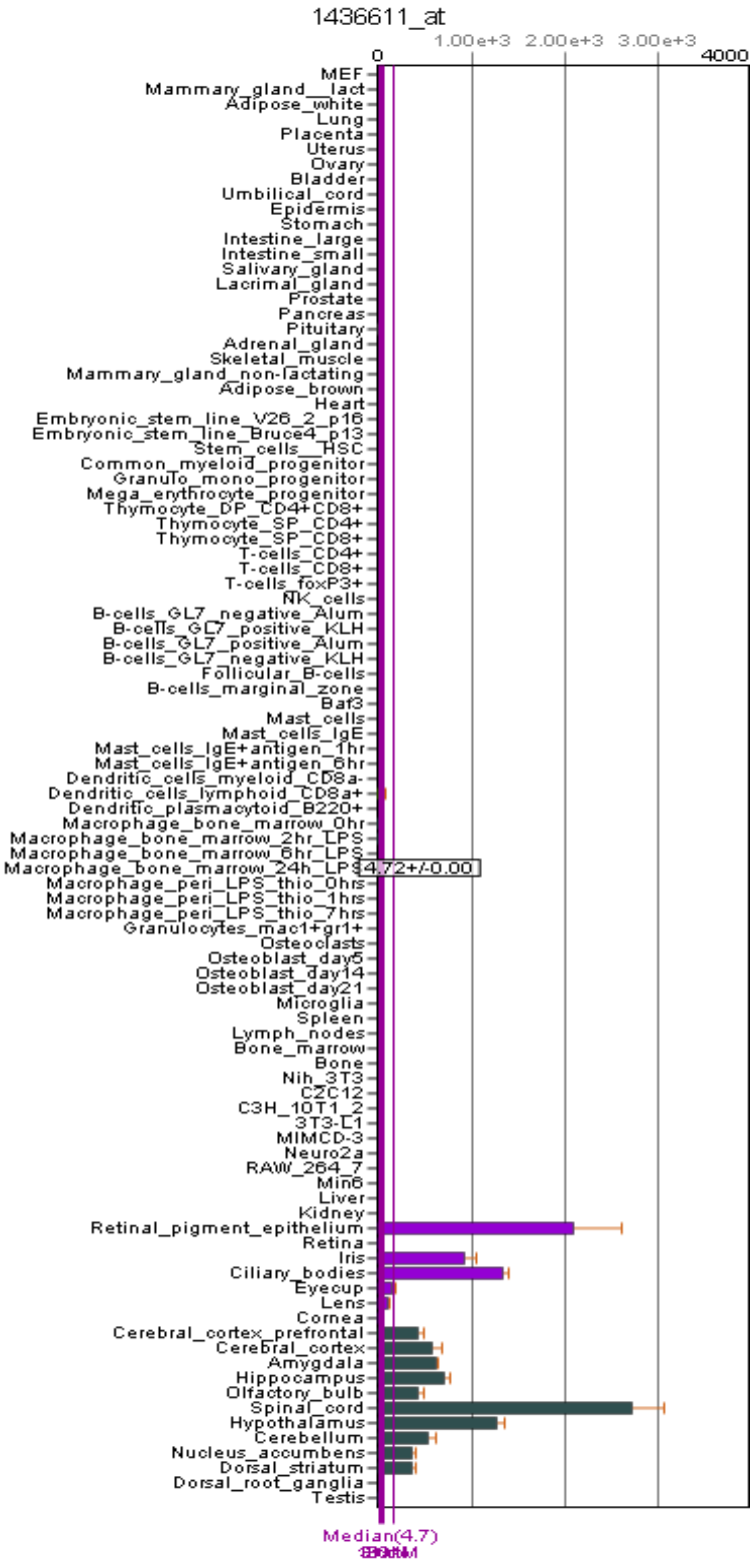

Figure 4-6– Expression Profile Analysis for SLC39A12

Expression profile analysis done on mouse microarray data and accessed from BioGPS (http://biogps.gnf.org) indicated that the expression of SLC39A12 is present in various areas of the brain and the spinal cord. Within the eye, expression of SLC39A12 is detected in the RPE, iris, ciliary body, eyecup and lens.

EST Profile

Slc39a12: Solute carrier family 39 (zinc transporter), member 12

brain	15		7/459991
embryonic tissue	27		18/664846
eye	21		4/184900

Breakdown by Developmental Stage

organogenesis	15		2/125372
juvenile	17		5/291299
adult	19		19/995094

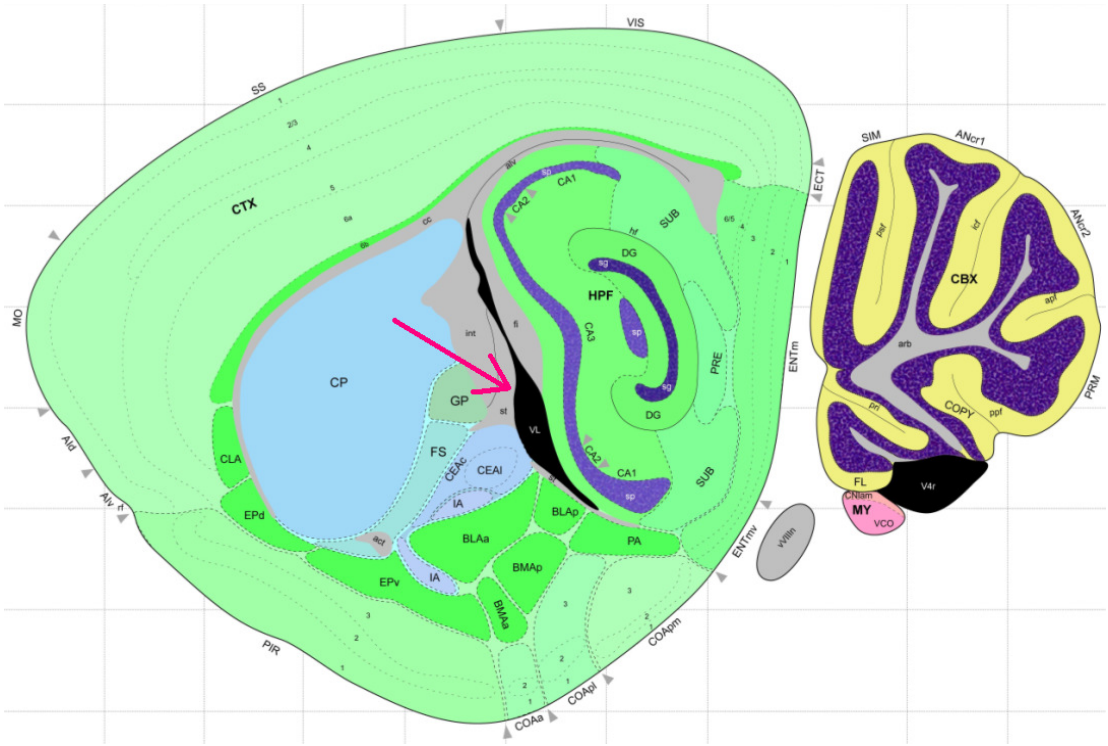

Figure 4-7–EST profile and for Slc39a12 and expression of Slc39a12 in brain

Expression of ZIP12 mRNA is highest in the brain ventricle of mouse (From Allen's brain atlas) http://mouse.brain-map.org/. Expression sequence tag (EST) profile analysis showed that the expression of SLC39A12 is limited to the brain, embryonic tissue and the eye, as well as being present during organogenesis as well as juvenile and adult state. EST profiles approximate gene expression levels from various cDNA library sources. The number on the right (125372, 291299, 995094, etc) refers to the total number of EST in pool, meanwhile on its left (2, 5, 19, etc) refers to the number of Slc39a12 transcript present in the EST pool. The leftmost number (15, 27, 21 etc) refers to the number of transcript per million EST, thereby allowing comparison to be made between samples.

4.5. **Cloning and expression of ZIP12**

The cloning of ZIP12 protein was done using Gateway® recombination cloning technology(Invitrogen, UK). The method differs from usual cloning using restriction enzymes in that preferred DNA fragments can immediately be inserted to expression vectors without the need of restriction endonucleases or DNA ligases. There are several advantages of using the Gateway Technology in contrast to standard way of cloning:

1. Improved accuracy and easier procedures as the use of restriction enzymes and ligases are not required. The design also prevents shifts in reading frames.

2. Once a donor clone has been generated, the donor clone can be used to produce other fusion proteins by immediate insertion to other expression vectors.

3. The insertion of attB-flanked PCR product to the donor vector or "entry clone" only takes 3-4 hours before the entry clone is ready to be plated on Zeocin agar plates and is therefore much faster than normal cloning strategies.

As none of our tested cell lines had ZIP12 expression, commercially purchased retinal cDNA (kind gift from Rebecca Kaye) was used as a template for cloning (Figure 4.8). The cDNA was used as a template for PCR using a specialised 25 base pair primer containing proprietary "attB" sequences and a Kozak sequence for the forward primer (for further details see materials and methods section as well as appendix). In the case where a C-terminal fusion protein was desired, the primer design did not incorporate the stop codon nucleotides to allow translation of the fusion proteins. The PCR template was inserted to a donor vector pDONR/Zeo through the use of proprietary BP clonase enzyme. The "entry clone" generated could then be used for insertion of a variety of expression vectors. Using LR-clonase, a similar recombination step was performed to insert the flanked ZIP12 to the expression vectors (see Appendix 5). ZIP12 proteins were created with the longest ZIP12 isoform containing 691 amino acids. The resulting expression vector containing ZIP12 was then amplified according to the protocol described in the materials and methods section before thoroughly screened for possible mutations using T7 promoter, and 5 primers, which screened overlapping sequences of the entire SLC39A12 gene

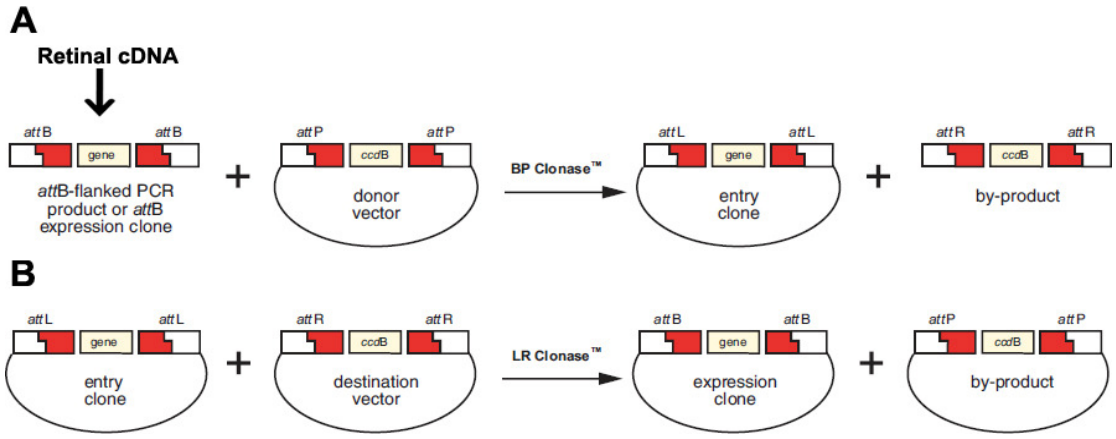

Figure 4-8– Gateway Recombination Cloning Technology

Gateway Technology is a two-step method to create a plasmid DNA containing the gene of interest. The process is started by using a DNA template (in our case, retinal cDNA) to create a PCR product flanked with proprietary attB cassette sequences. The use of BP clonase enzyme allows "swapping" between the attB and attP sites in the donor vector, inserting the attB flanked gene of interest into the donor vector and creating the attL sites inside the new entry clone (Panel A). This step also produced a by-product of attR flanked ccdB sensitivity gene cassette. The entry clone is a platform to generate plasmid DNAs that will generate fusion proteins. The recombination step of entry clone and destination vector involves the enzyme LR clonase, which generates the expression clone containing the gene of interest and the by-product of ccdB gene cassette inside what was originally the donor vector.

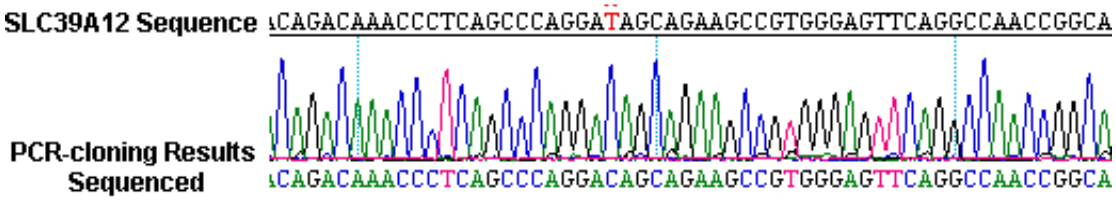

Figure 4-9– Polymorphism found in retinal cDNA for screening

The retinal cDNA used for creating the clones was found to have a silent mutation T33C which codes for the same amino acid residue aspartic acid. The mutation is a known SNP for SLC39A12 (rs691112).

Screening the human retinal cDNAresulted in the finding of a synonymous mutation (GAT → GAC) in amino acid residue 33 caused by a known SNP(rs691112) for SLC39A12 (Figure 4.9). As this did not change the amino acid sequence, the retinal cDNA was used in our experiments.

Two C-terminally tagged ZIP12 fusion proteins were generated (V5 affinity tag and GFP). Overexpression was only achieved with the C-terminally V5 tagged ZIP12 protein. The failure of expression of C-terminally tagged GFP-ZIP12 might possibly be caused by the interference of the large (27kD) GFP protein with folding and insertions into the membrane, a problem that had been previously reported for other GFP-fused membrane proteins (Pedelacq et al., 2006).

Transient expression of ZIP12-V5 fusion protein was first achieved through transfection of HEK293 cells. Transfection efficiency was assessed by using 200, 400, 800, 1000ng plasmid DNA and 2, 4, and 8µl of LipofectamineLTX (data not shown). Following this optimization step, HEK293 cells were routinely transfected with 800ng pcDNA3.1-ZIP12-V5 in the presence of 4µl of LipofectamineLTX (Invitrogen, UK) per 70,000 cells (Figure 4.10). The cells were incubated with the LipofectamineLTX-DNA complex for 30 hours at 37 °C before being fixed with ice cold MeOH for 5 minutes at -20 °C. As controls, sham transfections (where only LipofectamineLTX reagent was used) were performed following the same protocol except DNA was excluded. Transfection efficiency was checked by q-RT-PCR, which confirmed ZIP12 fusion protein overexpression with 800ng plasmid and by immunolabeling with a V5 and ZIP12 specific antibodies (Figure 4.10) (for antibody characterisation see later).

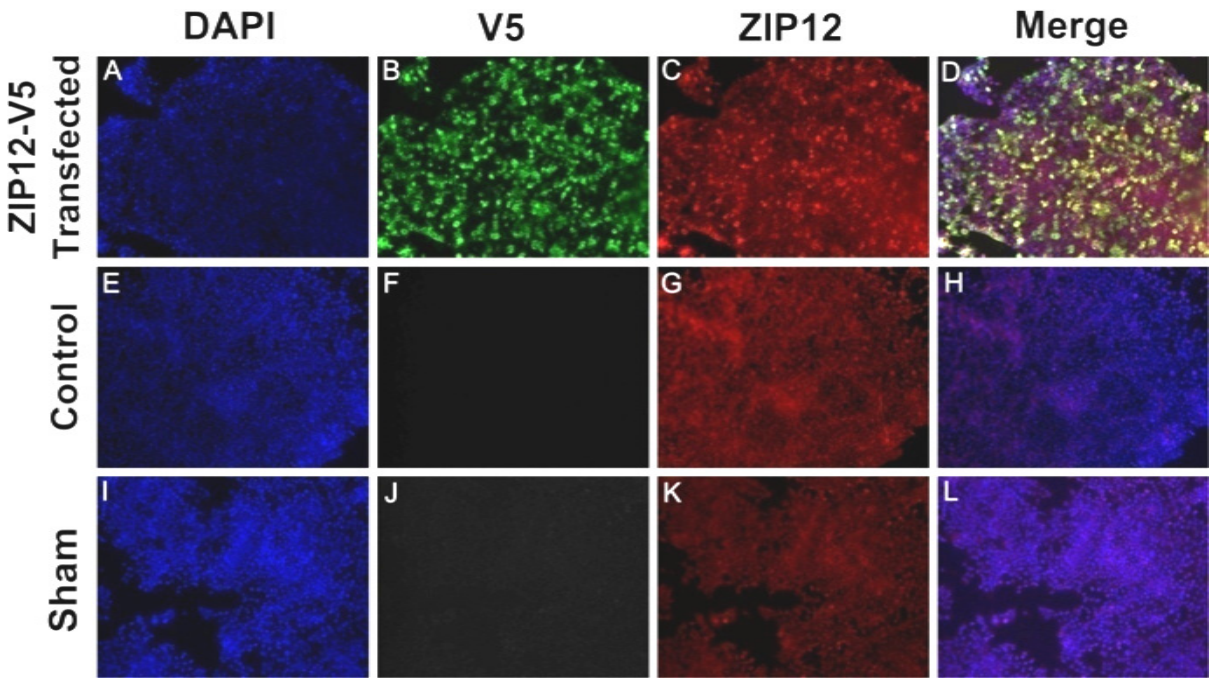

Figure 4-10– ZIP12 transfection in HEK293 cells

HEK293 cellswere either transfected with C-terminally tagged ZIP12-V5 protein or subjected to sham transfection with only the transfection reagent present. The cells were fixed with MeOH and stained with ZIP12-5194 (Panels C,G,K) and V5 (Panels B,F,J)(Invitrogen). ZIP12-5194 antibody was conjugated with Alexa-Fluor 594 meanwhile V5 antibody was conjugated with Alexa-Fluor 488. Transfected cells showed positive staining with V5 and ZIP12-5194, meanwhile sham transfected cells show no staining with V5 and background staining with ZIP12-5194. Quantitation of fluorescence was not performed. Nuclear staining was performed using DAPI. For higher magnification of HEK293 cells transfected with ZIP12-V5 protein labeled with V5 and ZIP12-5194, refer to figure 4.17 panels B and C. All images were viewed using LSM700 confocal microscopy with 20x magnification.

4.6. **Generation and Characterisation of Antibodies for ZIP12**

Methods

Antibodies were generated commercially by Biogenes GmBH (Germany). After exploring potential epitopes, considering the position of functional domains, and cleavage sites, antibodies were raised in two rabbits against residues 294-305 on ZIP12 protein which are located directly before the conserved, extracellular CPALLY domain on the N-terminal of the protein. The polyclonal antibodies generated in the two rabbits were termed ZIP12-5193 and ZIP12-5194. The antibodies were tested on Jurkat cell lysate, purchased from Abcam (Cambridge, UK) (Abcam, Cat No AB64463), ZIP12-V5 over-expressed in HEK293 cells and ZIP12-V5 over-expressed using a cell-free in vitro translational system. Simultaneously, immunocytochemistry was carried out on different cell lines using all three antibodies for ZIP12 (ZIP12-5193, ZIP12-5194 and Abcam) in transfected and fixed cells. The Jurkat lysate have been suggested to contain ZIP12 using a commercially available antibody against ZIP12 (Abcam, Cat No AB64463).

Results

Five µg protein of the Jurkat lysate was loaded onto precast AnyKD polyacrylamide gels from BioRad before being blotted onto PVDF (BioRad) membranes and probed with ZIP12-5193 and, ZIP12-5194. The antibodies (undiluted immunosera) were diluted between 1:7,000 and 1:30,000 (Figure 4.12). At 1:7,000 dilution we could identify two bands on SDS-PAGE with both antibodies one at ~80 kDa and the other at ~130 kDa. With dilution the band intensities decreased but to different degrees by the two antibodies. ZIP12-5194 labeled the 80 kDa band more strongly while the ZIP12-5193 labeled the 130 kDa band more strongly. No other bands were labeled in Jurkat cell lysate in this experiment (Figure 4.11). However, none of these antibodies labeled the 75kDa protein band identified by the commercial ZIP12 antibody (Figure 4.12)

In order to verify that the two bands observed on Figure 4.11 are both ZIP12, a peptide competition experiment was carried out using the synthetic peptide fragment we raised the antibodies against. For this, 1μg/1ml of peptide solution was used to deplete the 1:7000 dilutions of antibodies and blots containing five μg Jurkat lysate were probed with this peptide and antibody complex. Following visualization by electrochemiluminescence (ECL) the 80 kDa band was absent, but the 130kDa band remained strongly labeled using both of our antibodies. Incubating the PVDF membranes with the preimmune serum which demonstrates of any non-specificsignal showed no labeling (Figure 4.12). Interestingly, ZIP12-5193 this time labeled three bands, a ~ 130 kDa, a ~80 kDa and a ~60 kDa band. Peptide incubation of ZIP12-5193 did not block the labeling of the 60 kDa band.

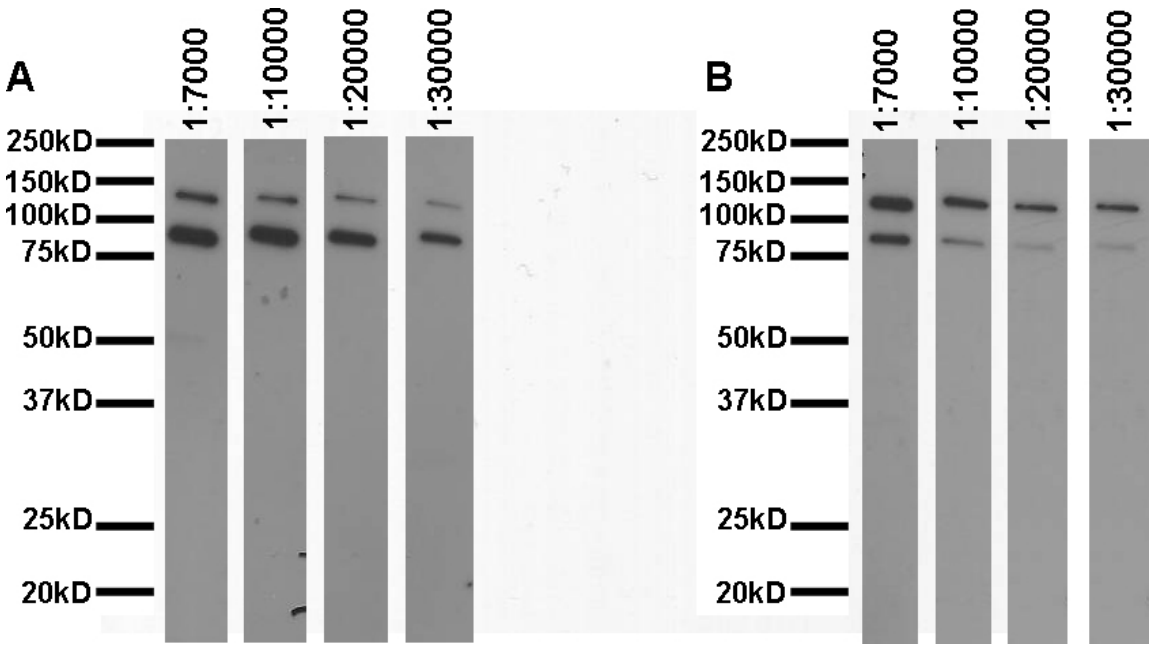

Figure 4-11–Optimisation of ZIP12-5194 and ZIP12-5193 in Jurkat lysate

Optimisation of ZIP12-5194 (Panel A) and ZIP12-5193 (Panel B) using diluted Jurkat lysate showed the presence of two bands just above 100kD and 75kD. 5µl of diluted lysate was used in every single lane. With dilution, the 100kD band was able to be seen. This is in contrast with Panel B, where incubation with antibody ZIP12-5193 showed that dilution of antibody removed the 75kDa band. Using peptide incubation, we had previously determined that the 75kDa band was able to be removed after incubation with peptide.

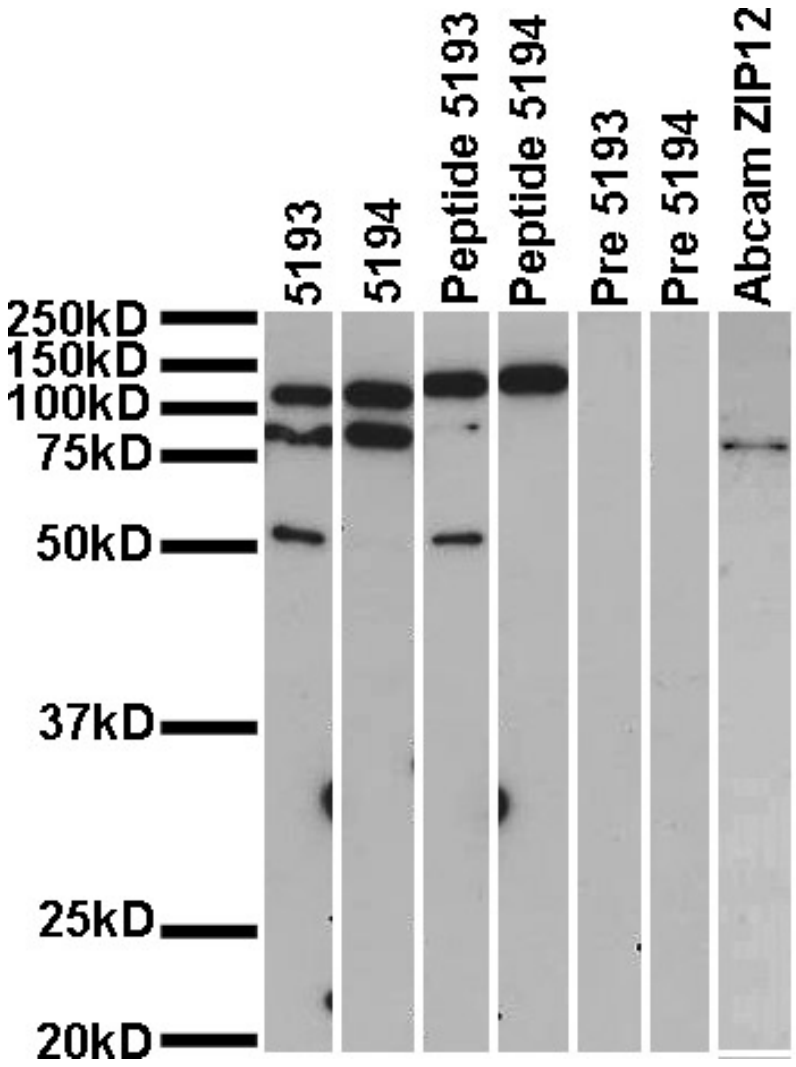

Figure 4-12 – Peptide incubation of ZIP12-5193 and ZIP12-5194

Incubation of ZIP12-5193 and ZIP12-5194 in Jurkat lysate at 1:7000 dilution show three bands and two bands at just above 100, 75 and 50 kD respectively. Peptide incubation for both ZIP12-5193 and ZIP12-5194 indicated that the band just above 100 kD was removed. This strongly indicated that the removed band is ZIP12 protein. Preimmune sera showed no bands. Antibody dilution used for both antibodies was 1:7000. ZIP12-Abcam shows a single band at 75kDa. Antibody dilution for ZIP12-Abcam was 1:1000.

To clarify further whether the different antibodies recognise ZIP12 protein the ZIP12-V5 plasmid was expressed using TnT® Quick Coupled Transcription/Translation System (Promega, UK).

Methods

This system uses a bacterial expression system to synthetically produce eukaryotic proteins from plasmid DNA sources without the need for cellular transfection. The protein products were run on SDS gels and blotted onto PVDF membrane as before, then labeled with a commercially available V5 antibody (Invitrogen, Paisley, UK) following the manufacturer's instructions.

Results

At higher concentrations of proteins we noticed two bands; a high molecular weight diffuse band at ~175 kDa and one at ~65kDa (Figure 4.13). Dilutions of the protein lysate with lysis buffer helped the dissolution of the high molecular weight band and above 1:64 dilutiononly the ~65 kDa band was apparent. In the negative control, which did not contain the ZIP12-V5 plasmid, no bands were detected (Figure 4.14). However, probing the ZIP12-V5 protein with ZIP12 Abcam or ZIP-5193 and ZIP12-5194 antibodies resulted in no specific immunoreactivity (Figure 4.14). While we have no clear explanation for this discrepancy, it is probable that the lack of cellular mechanisms required for appropriate folding and posttranslational modifications (phosphorylation, methylation, glycosylation) could have led to the unsuccessful immunolabeling with the ZIP12 antibodies. The apparent lower than expected molecular weight for ZIP12 in this cell free system appears to support this.

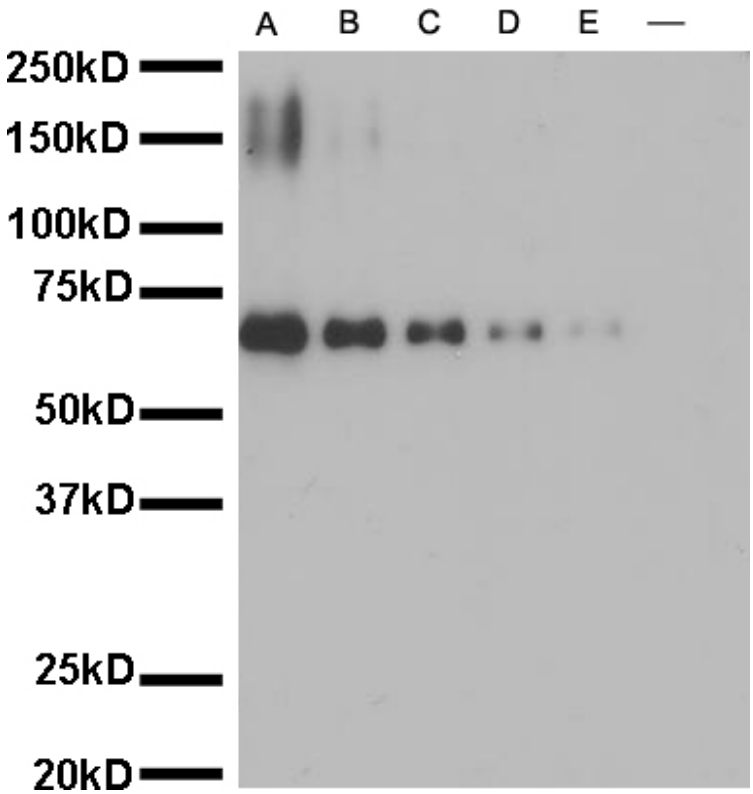

Figure 4-13–Cell-free production of ZIP12 protein

TnT® Quick Coupled Transcription/Translation System (Promega, UK) was used to synthetically produce eukaryotic proteins from plasmid DNA sources using a proprietary bacterial expression system. Protein products generated using C-terminally tagged ZIP12-V5 were diluted with lysis buffer and sample buffer to final dilution of 1:16 (Lane A), 1:32 (Lane B), 1:64 (Lane C), 1:128 (Lane D), 1:256 (Lane E) and negative control which does not contain plasmid DNA. Five µl of the products was loaded onto SDS-polyacrylamide gels, transferred onto PVDF membrane and immunoblotted using HRP antibody before visualising using ECL.

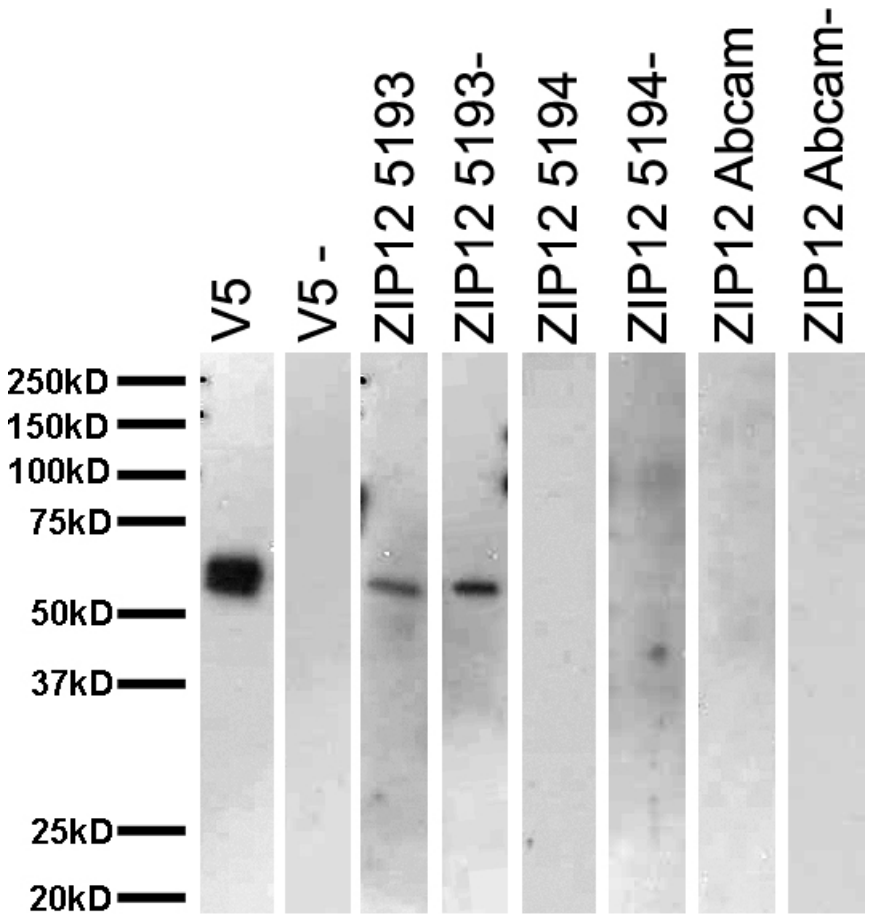

Figure 4-14- Staining using V5 and ZIP12 antibodies of TnT Quick coupled transcription Translation System

Staining using V5 and ZIP12 antibodies of TnT Quick coupled transcription Translation System produced proteins showing a single band at ~60kDa as seen using V5 antibody (Panel V5). The negative control shows no labeling of V5 antibody (Panel V5 -). Labeling with ZIP12-5194 and ZIP12 Abcam showed no labeling both with plasmid DNA included and without (Panels ZIP12 5194, ZIP12 5194 -, ZIP12 ABCAM, ZIP12 ABCAM-). ZIP12 5193 antibody detected a similar band at ~60kDa, however negative control for this antibody showed a positive signal of the same size. Dilution used in this experiment is 1:16 and 5µl of diluted lysate was used.

HEK293 cells over-expressing ZIP12-V5 fusion protein were used to overcome the lack of posttranslational modifications and folding of ZIP12 protein. Following lysis, 10 μg/lane cell lysates were run on SDS gels, blotted onto PVDF membranes and probed with the V5 and the ZIP12 antibodies and in some cases with an antibody against actin (Santa Cruz BT, UK). As expected actin migrated to 43kDa, corresponding to the size of the protein. V5 staining showed a diffuse band at about ~175kDa, a similar band to that seen in theTnT® Quick Coupled Transcription/Translation System, but no presence of a lower molecular weight band. This is unlikely to be caused by failure of all proteins to migrate, as clear labeling of appropriately migrated actin was observed. It is possible that the reason for this single high molecular weight band is protein aggregation of the overexpressed ZIP12-V5 protein with other proteins or itself. Therefore, we tried to disassemble this complex by sonication (Figure 4.15) or the use of different reducing agent and detergents (Figure 4.16) like beta-mercaptoethanol, Nonidet-P40 and TritonX-(100). However, none of these alleviated the presence of high-molecular weight protein aggregates (Figure 4.16B). Most importantly, while V5 antibody was able to detect the protein aggregates, none of the ZIP12 antibodies manage to label the protein complexes (Figure 4.16) though our antibodies detected the ~130 kDa and the ~80 kDa bands shown in Jurkat cell lysates even in those cells that had not been transfected, indicating that these bands are unlikely to be ZIP12.

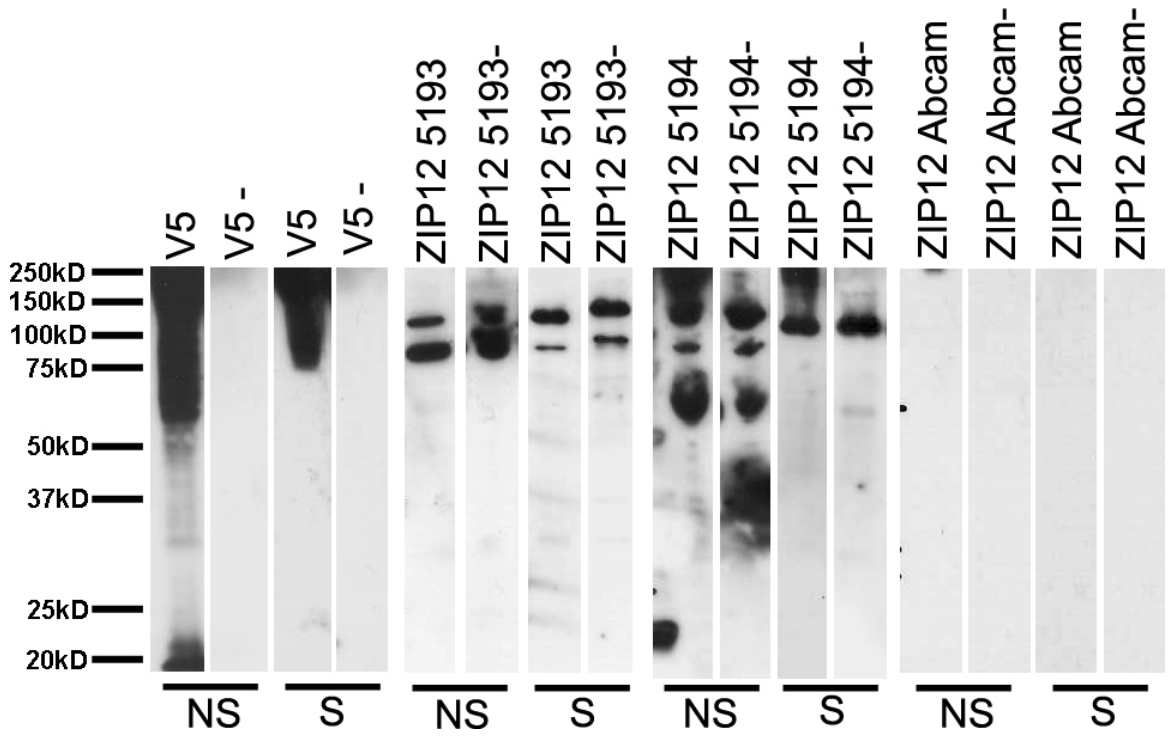

Figure 4-15–Sonication fails to remove protein aggregates

Twenty µg of transfected HEK293 lysate with C-terminal V5 ZIP12 protein was loaded on SDS-page gels before being either sonicated (S) or non-sonicated (NS). Membrane strips were blotted with V5 antibody, ZIP125193, ZIP12-5194 and ZIP12-Abcam with their respective negative controls (untransfected cells). V5 labeling produced a high molecular weight smear on both S and NS samples, ZIP12-5193 showed the presence of two bands similar to figure 4.11 in both conditions, although the same labeling was seen in the negative controls. ZIP12-5194 labeling showed three bands in NS samples, and only one band in S samples. Again, the same labeling was seen in the negative controls. ZIP12 Abcam showed no staining.

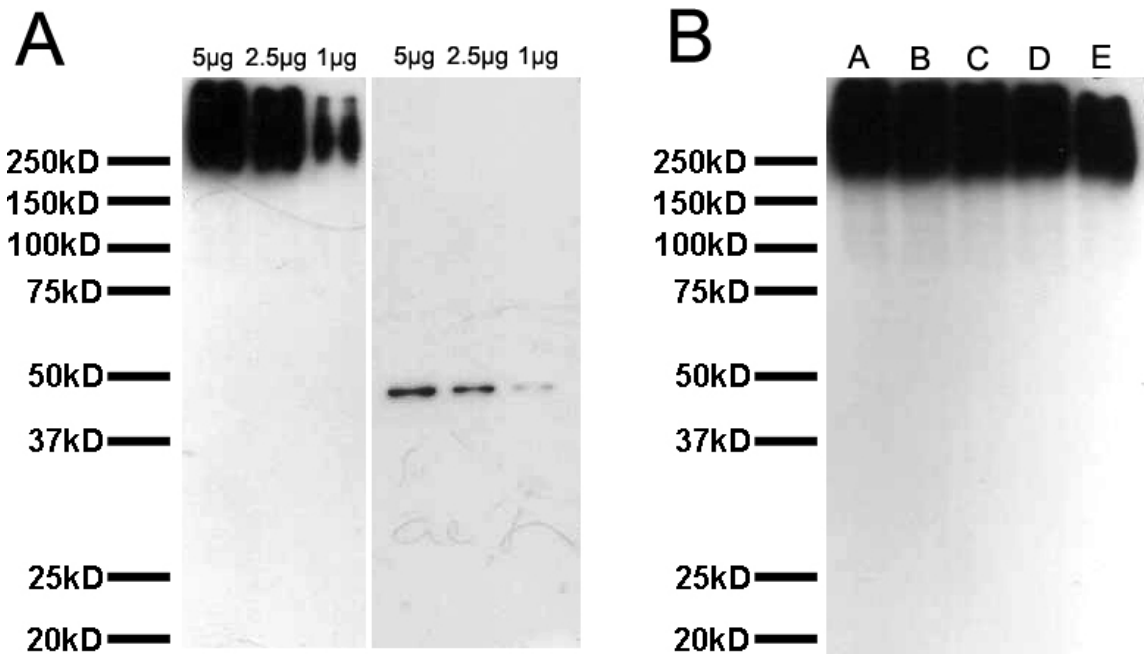

Figure 4-16–Aggregation remains after treatment with reducing agent and detergents,

Transfected HEK293 cells with ZIP12-V5 protein produced large aggregates which did not resolve on polyacrylamide gels. Panel A shows dilutions of 5, 2,5 and 1µg protein run and labeled with V5 (left) and beta-actin (right). Actin staining indicated that no abnormalities in protein running or transfer occurred. Dilution of 10µg samples 1:1 (total 5µg in each lane) with lysis buffers containing (A) 0.5% NP40 + 0.5M β-mercaptoethanol, (B) 0.5% NP40+1.0M β-mercaptoethanol, (C), 1% NP40, (D) 0.5% NP40 + 0.5% Igepal, (E) 0.5% NP40 + 0.5% TX-100.

4.7. **Localisation of ZIP12**

Methods

In parallel with experiments on cell lysates, the localization of ZIP12 was examined in ZIP12-V5 transfected cells. We used HEK293, CHO and ARPE-19 cells for these experiments. HEK293 and CHO cells were transfected as described previously, and immunostaining performed first on methanol fixed cells with V5 antibody (green) and ZIP12-5194 (red) or V5 antibody (green) and ZIP12-Abcam (red) (Figure 4.17).

Results

Labeling with the V5 antibody resulted in a plasma membrane, perinuclear and punctate cytosolic staining in HEK293 and CHO cells (Figure 4.17, B,F,J). Labeling with ZIP12-5194 resulted in similar staining to that of V5 (Figure 4.17, C,G). The use of ZIP12-5193 antibody did not result in immune-labeling (data not shown). The ZIP12-Abcam antibody failed to label HEK293 cells when fixed with MeOH (Figure 4.17, K) or 4% Paraformaldehyde (PFA) (data not shown).

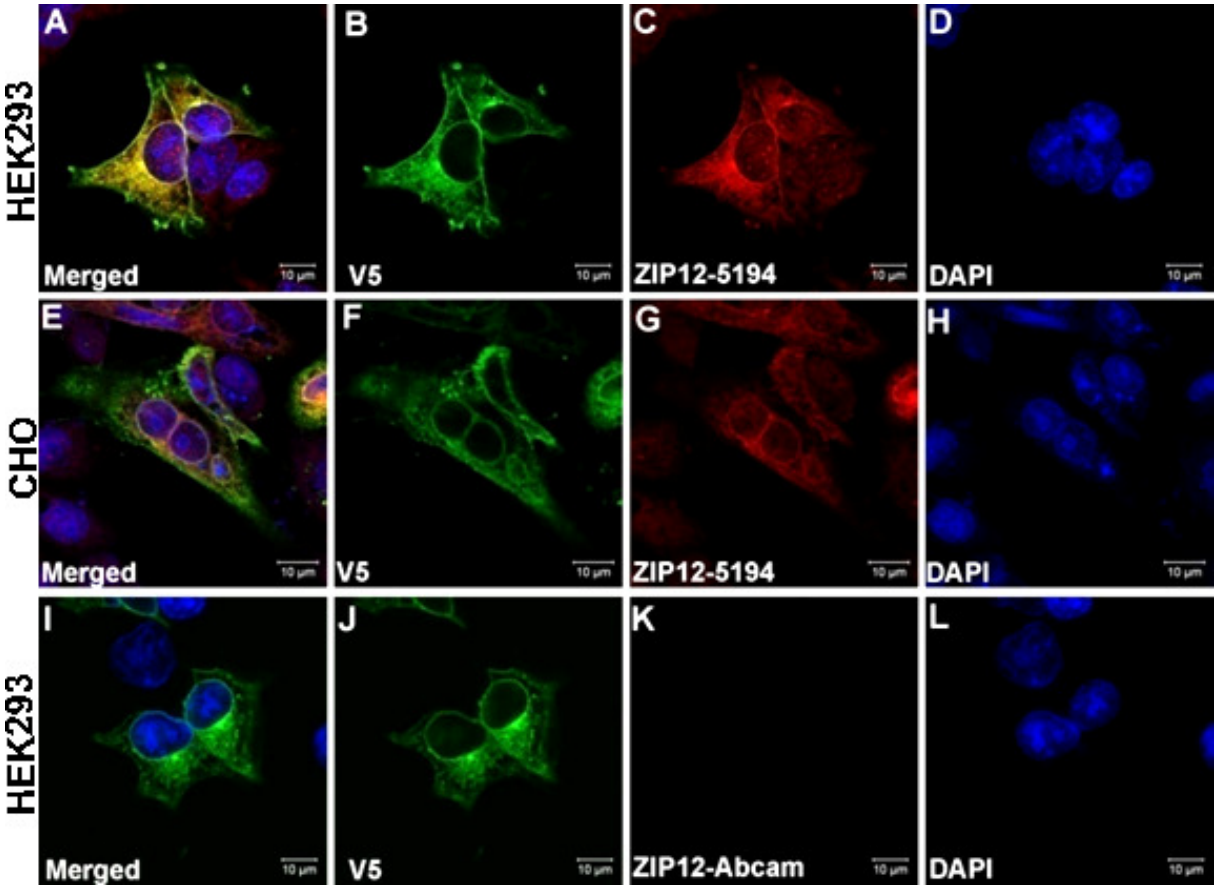

Figure 4-17–Immunostaining of HEK293 and CHO cells with ZIP12-5194, anti-V5 and ZIP12-Abcam antibody.

HEK293 (Panel A-D, I-L) and CHO (Panel E-H) cells transfected with C-terminally tagged ZIP12-V5 protein fixed and permeabilised with MeOH and stained with ZIP12-5194 (Panel G) as well as commercial ZIP12-Abcam (Panel K) labeled with Alexa 594. HEK293 (Panel A-D) and CHO (Panels E-H) cells showed strongly perinuclear staining using V5 antibody which colocalised with ZIP12-5194 and a membrane staining which has little colocalisation with ZIP12-5194. Staining with ZIP12-Abcam did not show labeling (Panel K, HEK293 cells). Nuclear staining was performed using DAPI (Panels D,H,L). All fixed cells were stained using V5 antibody from Invitrogen and imaged using LSM700 confocal microscopy at 63 x magnifications. Scale bar: 10µm. Cell labeling on left hand side added.

Methods

As ZIP12 appeared to be present on the plasma membrane on MeOH fixed samples, further confirmation for their membrane localization was done on 4% PFA fixed HEK293 and CHO cells. Cells were plated onto glass cover slips and transfected as described earlier. Four percent freshly prepared PFA was used to fix half of the cover slips and cells were rinsed before being treated with 0.1% Triton-X100 in PBS solution. The second half of the coverslips was treated with PBS only.

Results

Permeabilised HEK293 cells showed the previously described cytosolic labeling with both ZIP12-5194 (red) and V5 (green) antibodies (Figure 4.18, B,C). However, in non-permeabilised cells the labeling was restricted to the plasma membrane (Figure 4.18, F,G). Identical immunolabeling was observed on ZIP12-V5 transfected CHO cells (Figure 4.19 A-H).

In addition to localisation of the ZIP12 protein to the plasma membrane, the intracellular localisation of ZIP12 was examined. Transfected HEK293 cells were fixed with MeOH before being immunostained with V5 antibody, then conjugated with Alexa 488 and antibodies specific to endoplasmic reticulum (ER), Golgi or Lysosomes (Fig 4.20). Anti-Alpha-6-Isomerase antibody was used as an ER marker, anti-9.3Golgi antibody for Golgi marker and anti-CathepsinD as lysosomal marker (kindly provided by Professors Karl Matter and Claire Futter). Anti-V5 antibody labeling of fixed HEK293 cells shows perinuclear and plasma membrane staining, as observed earlier which showed colocalisation with the ER marker (Figure 4.20, A), but no co-localisation was observed with Golgi, (Figure 4.20, D) or the lysosome (Figure 4.20, G), although this could possibly be due to poor staining of both organelles which was caused by the small size of the cytosol of HEK293 cells. In order to confirm the ER colocalisation seen on HEK293 cells, ZIP12-V5 transfected CHO cells were also labelled with V5 and the ER marker alpha-6-isomerase antibody. There was a strong co-localisation in the perinuclear area (Fig 4.21, A). The densest staining is regularly observed between the dividing cells. The densest staining was observed between the cells, although this is not specific to the particular area. It needs to be determined whether the localisation to the ER is caused by overexpression artefact or whether endogenous ZIP12 is indeed

localised in the ER. However, this requires fully characterised ZIP12-specific antibody, which we currently do not have.

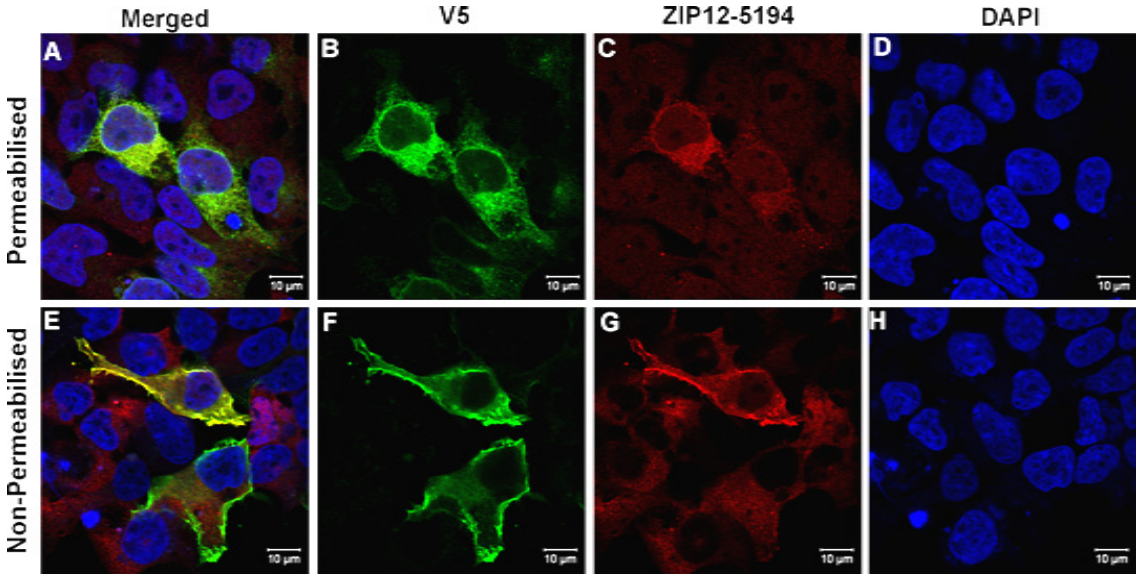

Figure 4-18–ZIP12 protein is present on the plasma membrane of HEK293 cells.

HEK293 cellswere transfected with C-terminally tagged ZIP12-V5 protein and fixed with 4% PFA before either being permeabilised with TX-100 in PBS (Panels A-D) or not treated (Panels E-H). All cells were stained with anti-V5 antibody and ZIP12-5194. Permeabilised cells (Panel A-D) showed perinuclear staining and cytosolic staining. Non-permeabilised samples (Panel E-F) showed plasma membrane staining. Colocalisation was both observed in permeabilised and non-permeabilised samples. All images were stained using anti-V5 antibody from Invitrogen and imaged using LSM700 confocal microscopy at 63 x. Scale bar: 10µm.

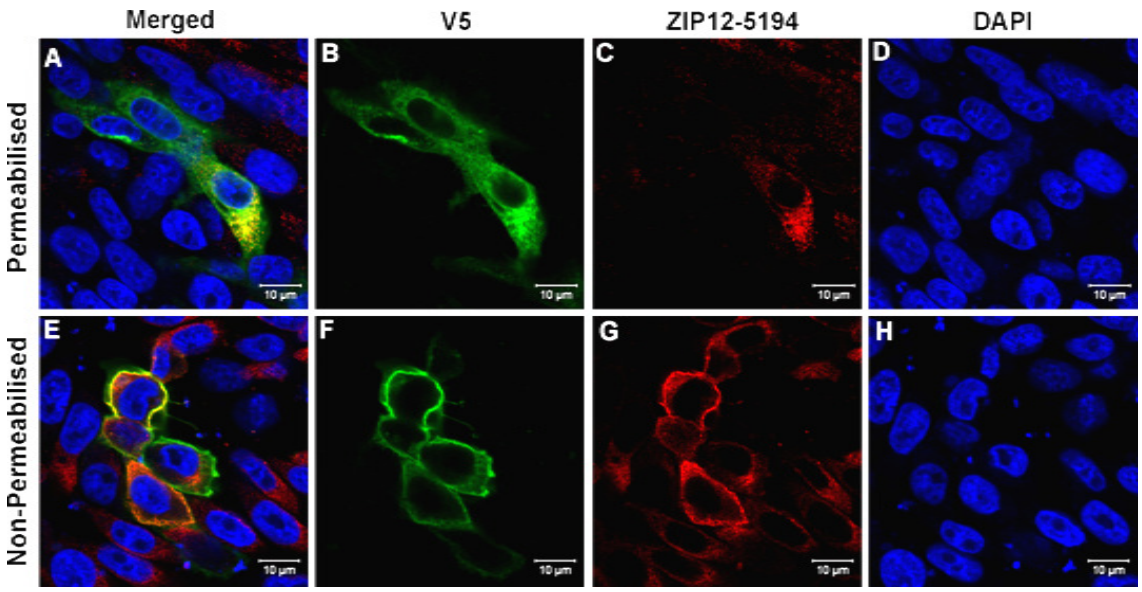

Figure 4-19–ZIP12 protein is present on the plasma membrane of CHO cells.

CHO cellswere transfected with C-terminally tagged ZIP12-V5 protein and fixed with 4% PFA before either being permeabilised with TX-100 in PBS (Panels A-D) or not treated (Panels E-H). All cells were stained with V5 antibody and ZIP12-5194. Permeabilised cells (Panel A-D) showed intracellular staining in the cytosol. Non-permeabilised samples (Panel E-H) showed plasma membrane staining. Colocalisation was both observed in permeabilised and non-permeabilised samples. All images were stained using V5 antibody from Invitrogen and imaged using LSM700 confocal microscopy at 63 x. Scale bar: 10µm.

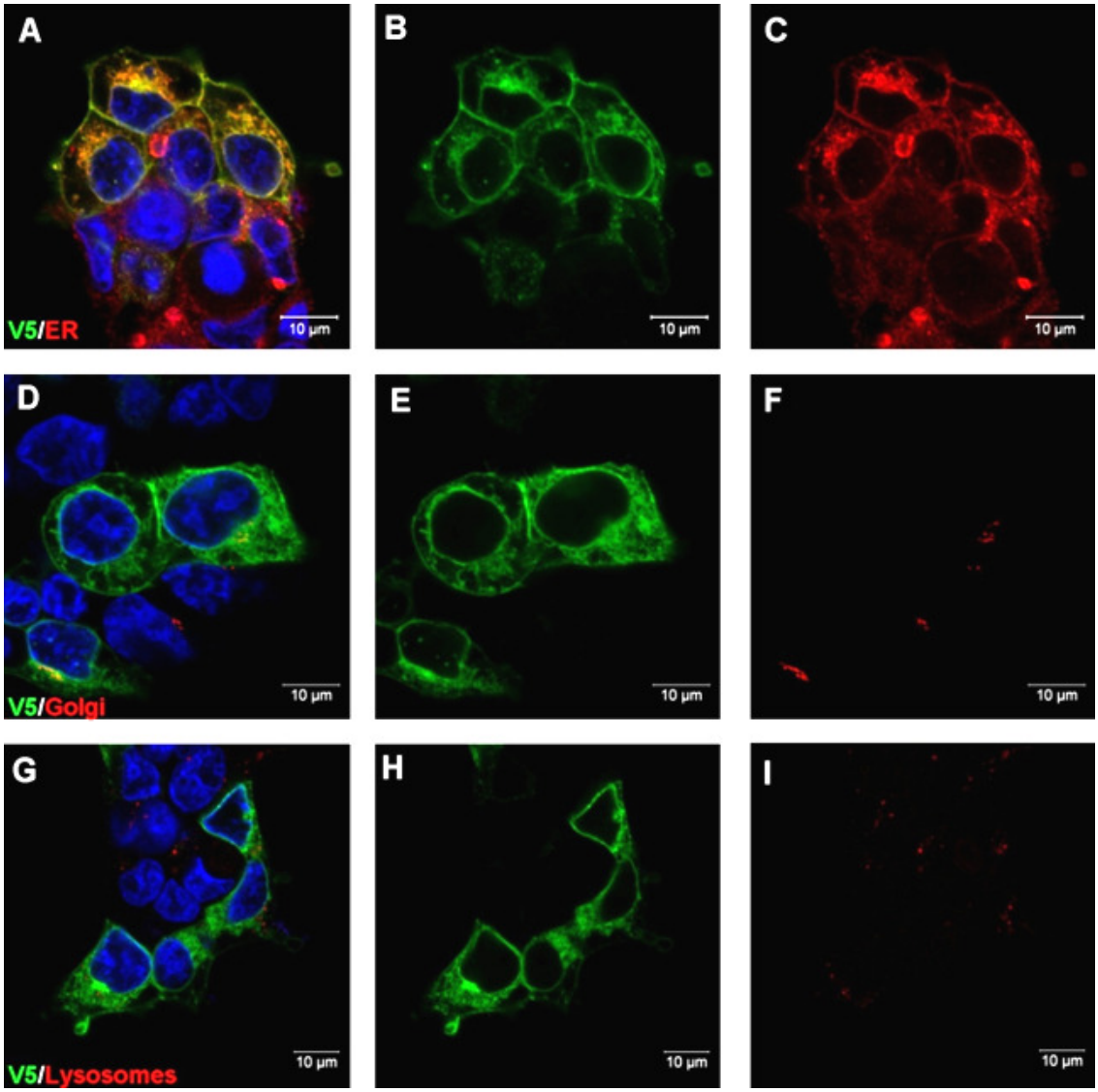

Figure 4-20–Organelle localization of ZIP12 protein in HEK293 cells

HEK293 cells were transfected with C-terminally tagged ZIP12-V5 protein and fixed with MeOH showed partial colocalisation with ER (panel A), and no colocalisation with either Golgi (panel D), or lysosomes (panel G). Staining for ER was performed using antibody against ER-specific Alpha-P 63 Isomerase. Staining for Golgi was performed using golgi-specific 9.3 Golgi. Staining for lysosomes was done using antibody against CathepsinD, a lysosome-specific organelle. Nuclear staining was performed using DAPI. Images A,B,D,E,G,H were stained using V5 antibody from Invitrogen and imaged using LSM700 confocal microscopy at 63 x magnification. Scale bar: 10µm.

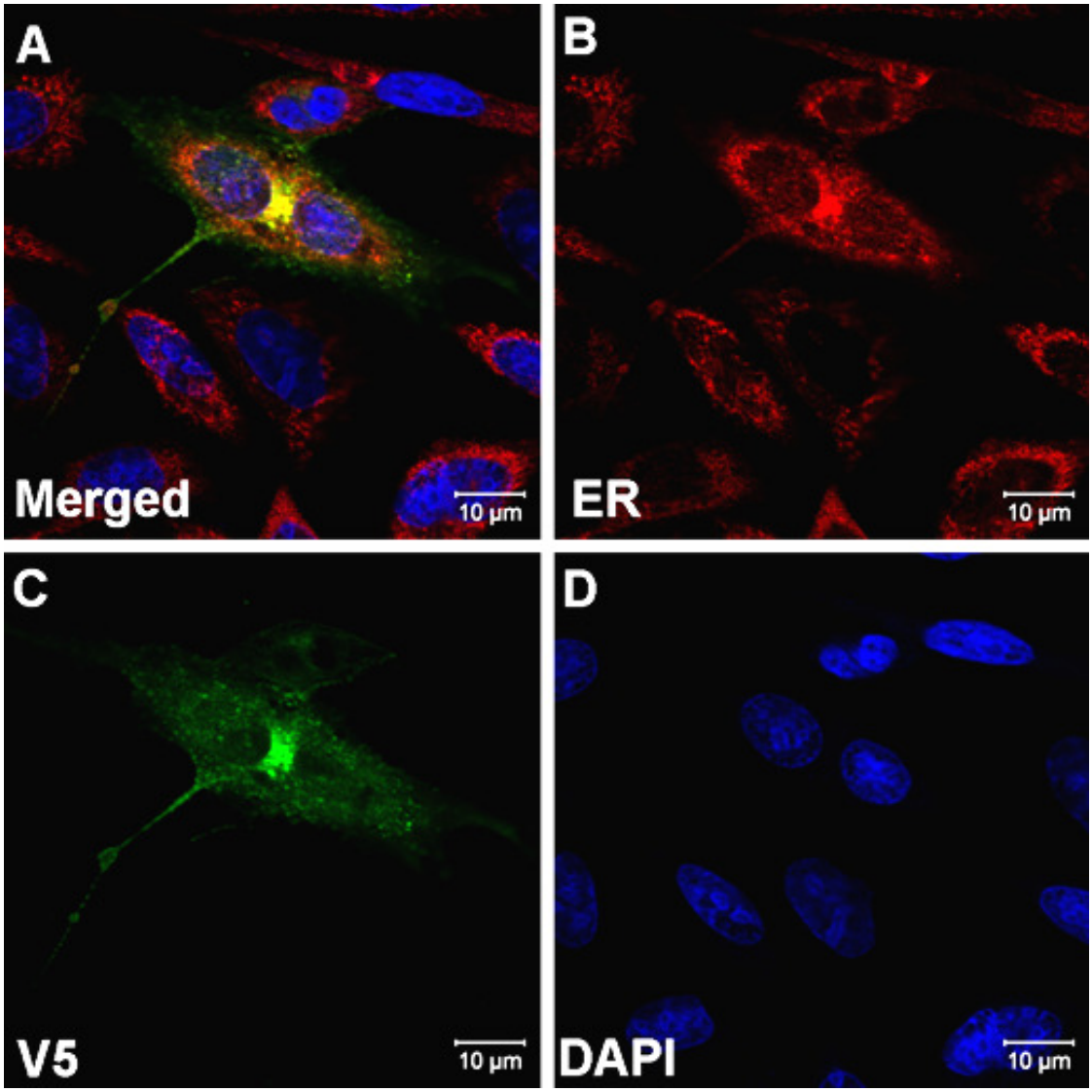

Figure 4-21–ER localization of ZIP12 in CHO cells

CHO cells transfected with ZIP12-V5, fixed with MeOH and stained with ER and V5 (Panels A-D) antibody showed partial colocalisation on the perinuclear area. The staining is not specific to the area between the cells, although it is an interesting observation that the densest staining was observed there. Image (C) was stained using anti-V5 antibody from Invitrogen and all picture was imaged using LSM700 confocal microscopy at 63 x magnification. Scale bar: 10µm.

Our ultimate aim is to understand the role ZIP12 plays in RPE cells. Transfection of ARPE19 cells with ZIP12-V5 fusion protein would allow the study of zinc transport as well as observing the phenotypical changes associated with the presence of ZIP12 protein on these RPE model cells. The high mRNA expression has been observed *in vivo* (See Chapter 3) and the absence of ZIP12 gene expression *in vitro* in ARPE19 cells provides the ideal system to study this. In order to achieve this, the SCL39A12 gene must be delivered efficiently and ZIP12 protein must be expressed with a good efficacy in ARPE19 cells. However, our attempts at transfecting ARPE19 with ZIP12-V5 did not result in a high-enough efficiency for functional assays. The transfection efficiency in ARPE-19 cells was < 20 cells per coverslip (100 mm diameter) but it allowed us to label the cells with the V5 antibody. As expected, ZIP12 protein was localised to the perinuclear and intracellular organelle(s) in MeOH fixed cells (Figure 4.22, B). Similar labeling was observed with our ZIP12-5194 antibody (Figure 4.22, C). Labeling of ARPE-19 cells following 4% PFA fixation, but without permeabilisation confirmed that ZIP12 is present on the plasma membrane in ARPE-19 cells (Figure 4.23, D,E).

After co-labeling with organelle specific antibodies, a modest co-localisation of ZIP12 with ER (Figure 4.24, A), good co-localisation with the Golgi apparatus (Figure 4.24, D) but no co-localisation with lysosomes (Figure 4.24, G) was apparent. While transfected HEK293 or CHO cells remainedviable, transfected ARPE-19 cells show nuclear blebbings and abnormally shaped nuclei suggesting that the present transfection protocol of ARPE19 will need to be refined.

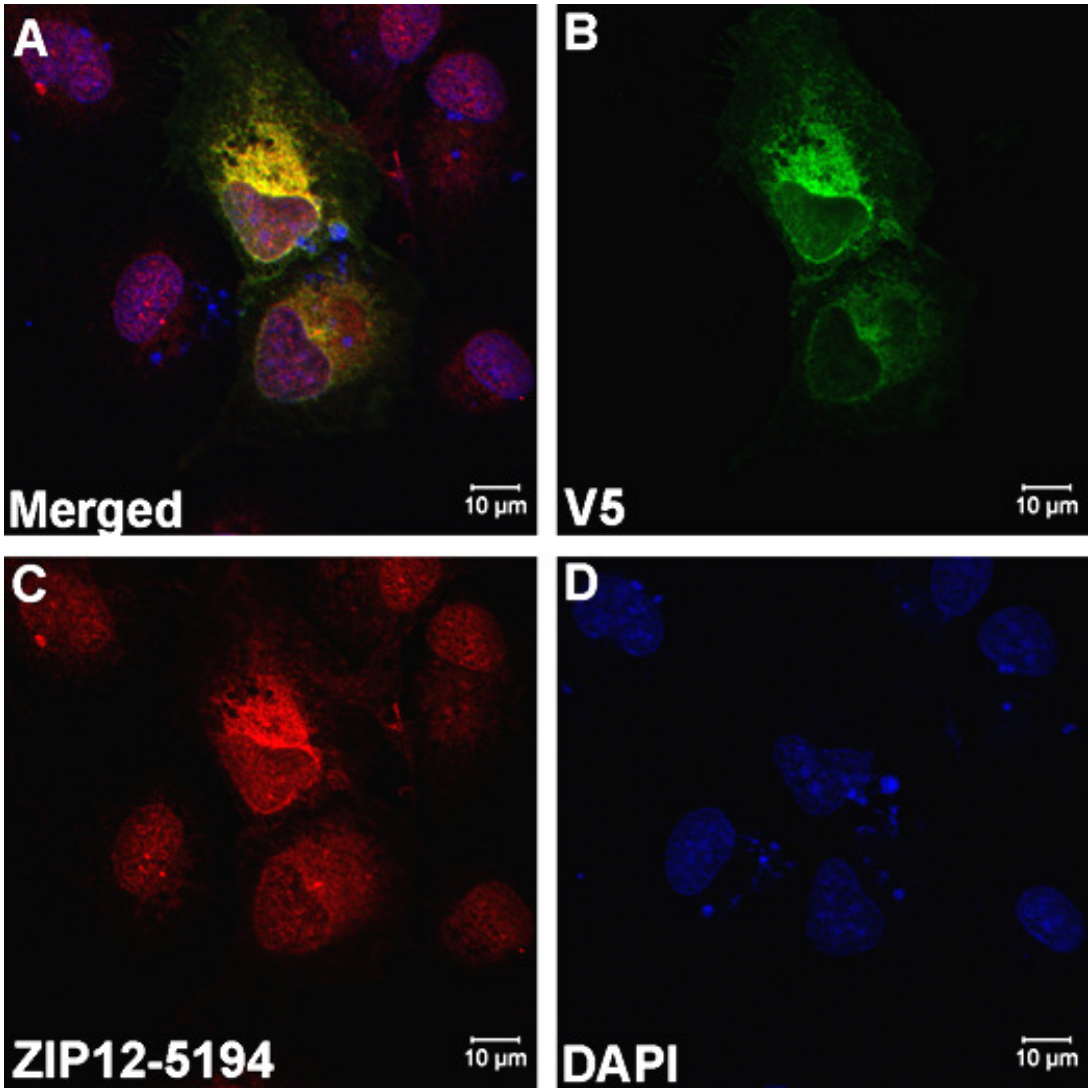

Figure 4-22–Transfection of ZIP12 in ARPE19 cells

ARPE19 transfected with C-terminally tagged ZIP12-V5 protein and fixed with MeOH showed perfect colocalisation between ZIP12-5194 antibody and V5 antibody. Nuclear staining performed using DAPI showed cellular debris as well as poor morphology of the nucleus indicating cytotoxicity. All images were of preparations stained using anti-V5 antibody from Invitrogen and imaged using LSM700 confocal microscopy at 63 x magnification. Scale bar: 10µm.

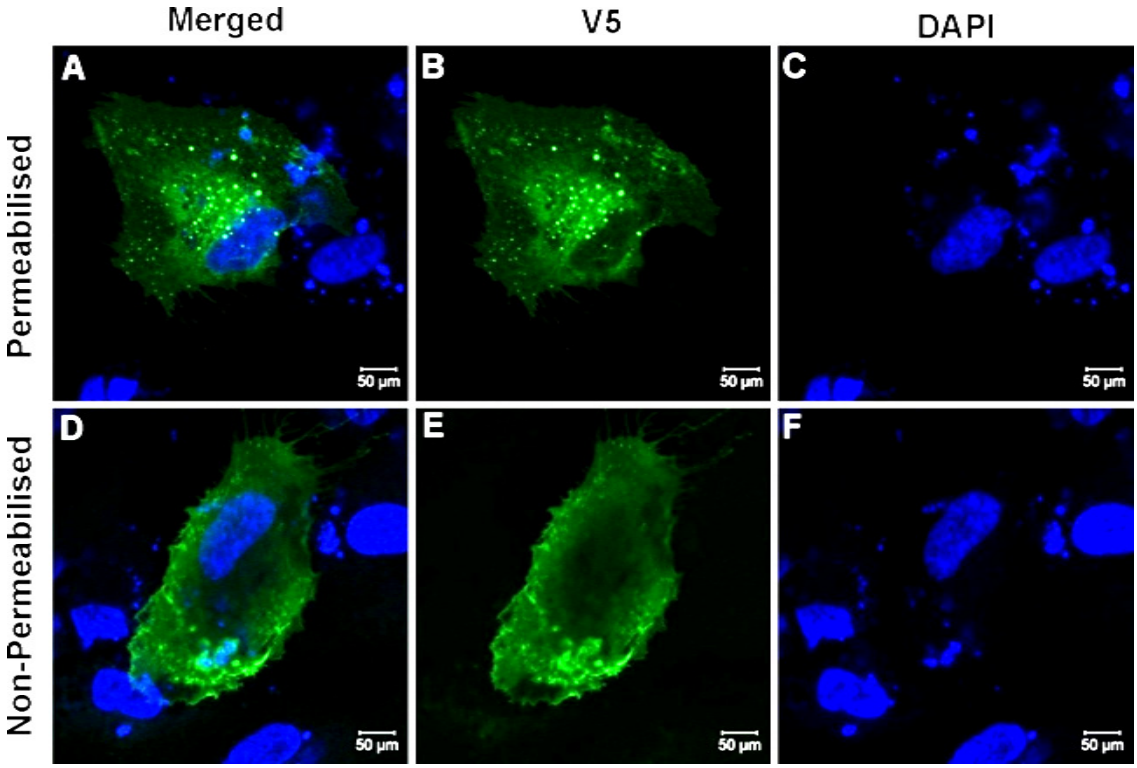

Figure 4-23–ZIP12 is localized on the plasma membrane of ARPE19 cells

ARPE19 transfected with C-terminally tagged ZIP12-V5 protein and fixed with 4% PFA before either not being permeabilised or being permeabilised with TX-100 in PBS. Permeabilised cell (Panel A-C) showed intracellular staining in the cytosol with punctate staining. Non-permeabilised samples (Panel D-F) showed plasma membrane staining. Nuclear staining performed using DAPI showed cellular debris as well as poor morphology of the nucleus indicating cytotoxicity. All images were stained using V5 antibody from Invitrogen and imaged using LSM700 confocal microscopy at 63 x magnifications. Scale bar: 10µm.

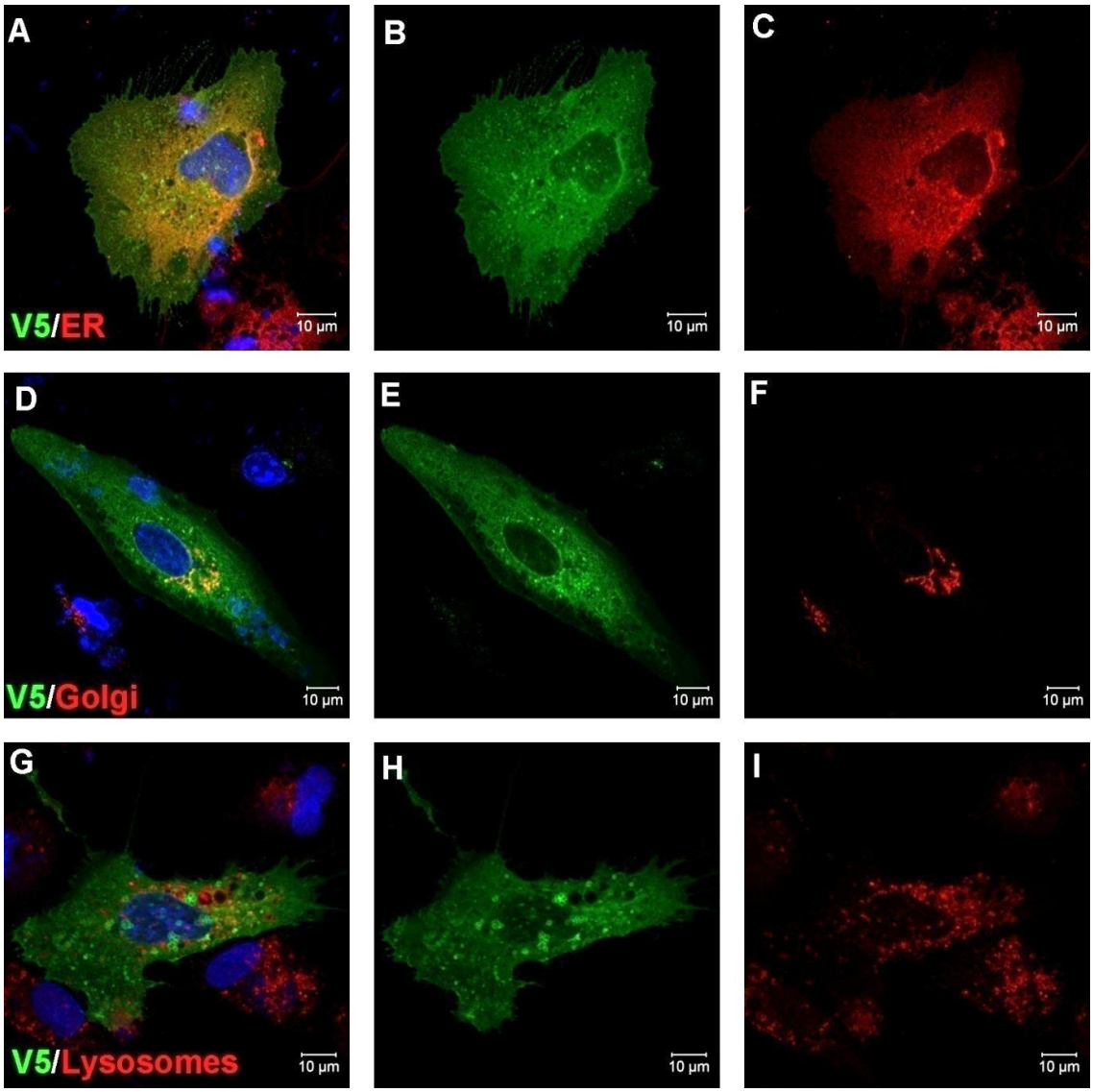

Figure 4-24–Organelle localization of ZIP12 protein in ARPE19 cells

ARPE19 transfected with C-terminally tagged ZIP12-V5 protein and fixed with MeOH showed colocalisation with ER (panel A), very partial colocalisation with golgi (panel D), and no colocalisation with lysosomes (panel G). Staining for ER was done using antibody against ER-specific Alpha-P 63 Isomerase. Staining for golgi was done using golgi-specific 9.3 Golgi. Staining for lysosomes was done using antibody against CathepsinD, a lysosome-specific organelle. Nuclear staining (in blue) was performed using DAPI. All images were stained using V5 antibody from Invitrogen and imaged using LSM700 confocal microscopy at 63 x magnification. Scale bar: 10µm.

4.8. **Function of ZIP12**

To date, no studies have shown the function of ZIP12 *in vivo* or *in vitro* although its localization to plasma membrane and the functional annotation based on the LIV-1 family where ZIP12 is assigned suggests that this protein is a potential zinc importer. Based on this, we expected that zinc content in transfected cells might be higher than without transfection. Therefore, cells were loaded with 5μM ZinPyr1, a zinc selective, high affinity fluorescent sensor, (Walkup et al., 2000) for 10 minutes under standard culturing conditions as described in the Materials and Methods section. After extensive washing with culture media the cells were imaged live using epifluorescence (excitation 488, emission 525 nm, Olympus) at 20x magnification. Fluorescence intensities of at least 10 images from triplicate experiments were analysed using ImageJ software (http://rsb.info.nih.gov/ij/). The fluorescence intensities of transfected cells were significantly higher than in non-transfected cells (5.65 ± 1.99 vs 14.30 ± 1.35, $p<0.01$, Student t-test) (Figure 4.25). Pretreatment with 10μM TPEN, a zinc selective cell permeable chelator for 10 minutes prior the application of ZinPyr1 resulted in a definite decrease of basal fluorescence (2.0 ± 0.1) and complete attenuation of the fluorescence in transfected cells (1.9 ± 0.1), suggesting that in cells expressing ZIP12, zinc influx is increased.

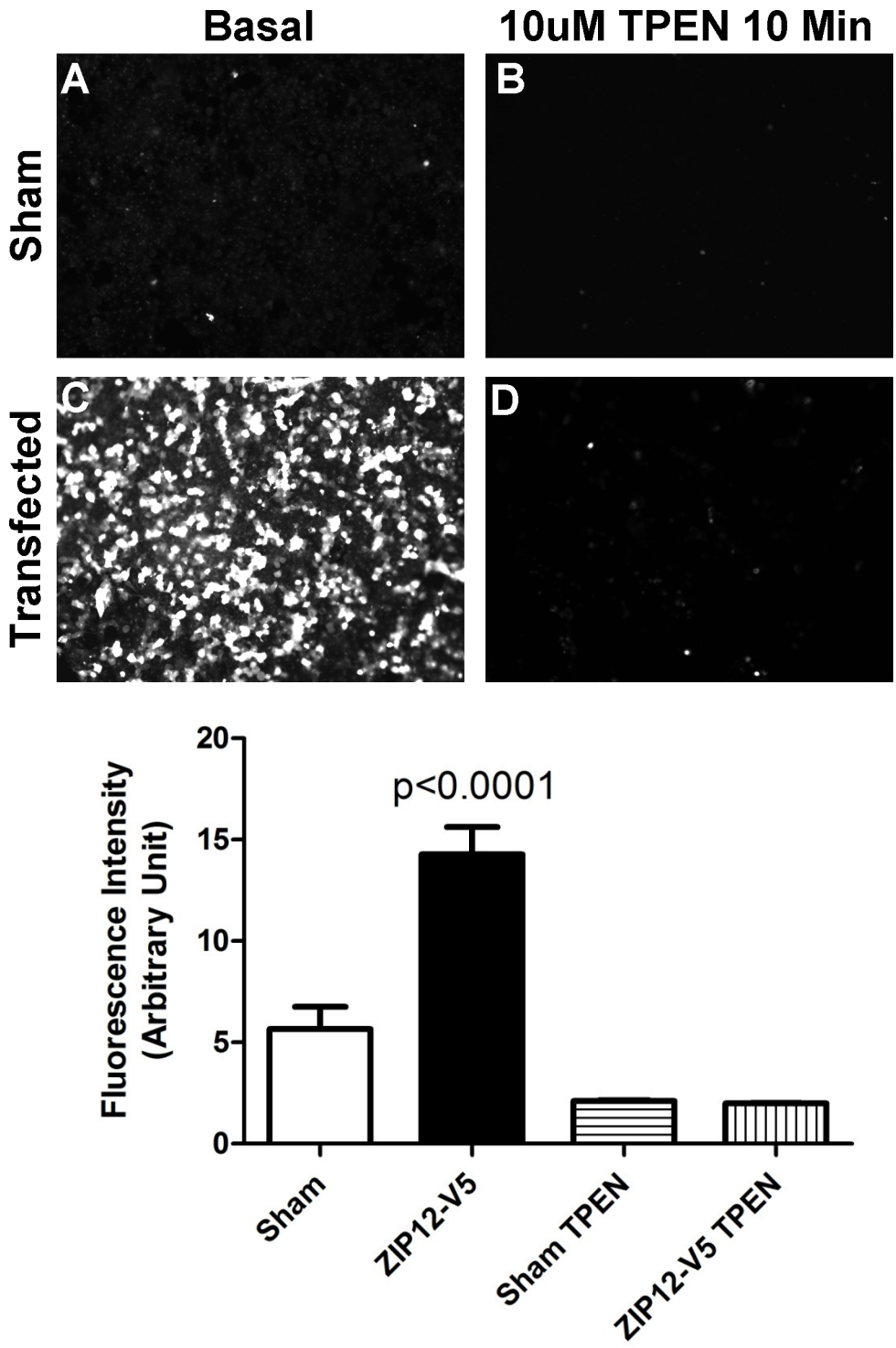

Figure 4-25–Function of ZIP12

Transfected HEK293 cells were probed with ZinPyr-1 which recognises bioavailable zinc. Under basal state, the transfected cells have higher signals of zinc within the cells, indicative of zinc influx (Panel C) occurring in the cells compared to basal state (Panel A). Treatment of 10μM TPEN for 10 minutes removed majority of the zinc signal in both sham and transfected group (Panels B,D). Data shown came from average ± standard deviation values of 12 pictures repeated three times. Student's T-test was performed between sham group and ZIP12-V5 transfected group ($p<0.0001$).

4.9. **Discussion**

ZIP12 is probably the least studied zinc transporter to date. It has been linked to schizophrenia (Bly, 2006), Alzheimer's disease (Grupe et al., 2006) and cancer (Sotiriou et al., 2006).

Previous studies have shown that the SLC39A12 gene is the most highly expressed zinc transporter gene in the retina (Nishimura and Naito, 2008). In addition, ZIP12 was found to be one of the most highly RPE specific genes amongst the 114 genes which have at least 2.5 fold higher expression in the RPE than the choroid or photoreceptors, placing the gene on par with more widely recognized RPE-specific genes such aslecithin retinol acyltransferase (LRAT) or retinaldehyde-binding protein 1 (RLBP1)(Booij et al., 2010b). The observation that a zinc transporter has the same high RPE expression level may indicate its potential importance in the RPE although we would still have to confirm this result through better RNA isolation process for the cadaveric RPE cells.

The bioinformatics predictions at the beginning of this chapter (Section 4.1) suggested that ZIP12 is an 8 transmembrane domain protein whose likely localisation is the plasma membrane. Its large N-terminal domain (52% of the protein) and its C-terminal short tail were predicted to be in the extracellular space. In order to confirm these we generated a C-terminal V5-tagged plasmid for expressing ZIP12 in cells that do not normally express it. In addition, we raised antibodies against an N-terminal extracellular domain next to transmembrane domain I. As expected, the V5 specific antibody labeled the plasma membrane of transfected, non-permeabilised cells, suggesting that not only our prediction that ZIP12 is, at least partly, a plasma membrane protein was correct but also confirmed that the C-terminal tail is pointing to the extracellular space. Labeling of permeabilised cells with the V5 antibody showed that ZIP12 protein might also be present on the membranes of ER and the Golgi. However, currently we cannot rule out that the ER localisation is an artefact caused by protein overexpression. The antibody we raised against the N-terminal domain of ZIP12 (5193 and 5194) provided mixed results. Experiments on cell lysates could not demonstrate that our polyclonal antibodies which were raised in rabbits can detect ZIP12 reliably although immunolabeling of transfected cells showed a very good correlation between ZIP12-5194 and V5 antibody labeling. For this reason further studies are

planned to purify and better characterize our ZIP12 antibodies for immunolabeling. Nevertheless, we could confirm that the C-terminus, where the V5 tag is positioned, is indeed in the extracellular space and if the protein is confirmed to be an 8 transmembrane domain structure then the N-terminal large domain is also in the extracellular space. The structure of LIV-1 subfamily transporters (See Figure 4.2) is highly conserved and usually have three features which define their homology: the histidine-rich loop between transmembrane domains III and IV, a histidine rich metalloproteinase-like sequence on transmebrane domain V (Loomans et al., 1998) and the so-called CPALLY domain just before transmembrane domain I. The histidine rich loop between transmembrane III and IV is not strictly limited to the LIV-1 subfamily, but is also present in other SLC39 family members (Guerinot, 2000). Following our results that show ZIP12 on the plasma membrane we believe that this loop is located in the cytosol and, together with the metalloprotease-like sequence in transmembrane V (Taylor and Nicholson, 2003) facilitates zinc import into cells. The exact function of the CPALLY domain is still not known. It might be involved in the localisation of ZIP12 to the plasma membrane since ZIP7 and ZIP13, both of which lack this motif, are localised to intracellular membranes but not the plasma membrane (Taylor et al., 2007, Fukada et al., 2008). It is possible to speculate that cleavage of the large N-terminal domain might cause the migration of ZIP12 to intracellular membranes although future experiments using truncated ZIP12 expression will be required to test this idea. The V5 tagged ZIP12 can certainly be detected on intracellular membranes, but whether this is the result of regulated protein processing cannot be determined from these experiments. The localisation of ZIP12 protein to the ER can certainly be the result of the overexpression of the protein in our experiments.

Following expression of V5 tagged ZIP12 protein in an artificial translational system (TnT Quick Coupled Translation System) and in cells we found that ZIP12 may form aggregates with either itself or some other proteins. This can be the caused by overexpression but may also indicate that ZIP12 forms homo or hetero dimers with other proteins. Proteomic characterisation of these large aggregates (Figure 4.16) is being planned together with co-immunoprecipitation assays using anti-V5 agarose affinity gels (Sigma-Aldrich A7345) to identify ZIP12 interacting proteins.Interestingly, the protein derived from the Quick Coupled Translation

System migrated to ~60 kDa while ZIP12 protein expressed in HEK293 cells has an apparent molecular weight of ~80 kDa. This suggests that appropriate folding and/or posttranslational modification is important for the ZIP12 protein. As there are many potential posttranslational modification sites on ZIP12 (see Section 4.2 earlier) further experiments will need to clarify which potential sites may play a role in the function of ZIP12. One of the candidates for functional modification is at S36, a potential glycogen synthase kinase 3 phosphorylation site, that had been associated with schizophrenia through a S36G mutation (Bly, 2006), suggesting that phosphorylation at this site might be important for ZIP12 function.

The histidine-rich regions between transmembrane III and IV, which is involved in transporting zinc into the cells, appear to be highly conserved in LIV-1 family transporters (Taylor and Nicholson, 2003, Taylor et al., 2007). Therefore, the plasma membrane location and the orientations of the transmembrane domains suggested that ZIP12 will transport zinc into cells. To test this hypothesis we over expressed ZIP12-V5 in HEK293 cells and measured basal zinc accumulation by the high affinity zinc selective fluorescence probe, ZinPyr1 (Walkup et al., 2000). The specificity of an increase in fluorescence intensity to zinc was assessed by treatment with TPEN, a cell permeable zinc selective chelator (Figure 4.25). The source for zinc influx into the HEK293 cell is the culturing medium. DMEM complete medium contains ~1.5 uM added zinc (manufacturer's data sheet) that is further enhanced by the zinc contained in fetal calf serum (Bozym et al., 2010). While this total zinc level translates to nanomolar levels of bioavailable zinc in the medium (Bozym et al., 2010) this level is far higher than the picomolar intracellular free zinc (Bozym et al., 2006) reported in cells. Nanomolar levels of extracellular zinc had been shown to elevate intracellular levels after transfection of cells with zinc transporters (Gaither and Eide, 2001, Leung et al., 2008a, Liuzzi et al., 2005), and we expected this to be the same for ZIP12 transfected HEK293 cells. While HEK293 cells do not express ZIP12 in their native state, they express several other zinc transporters on their plasma membrane. Therefore it is not surprising that there is a basal level of TPEN chelatable zinc in these cells (Figure 4.25). However, when cells were transfected with ZIP12 the intracellular level of ZinPyr1 fluorescence increased significantly. As this increase could be completely abolished

by pretreatment with TPEN, we concluded that this fluorescence signal represented zinc influx.

In summary, we were able to provide evidence that ZIP12 is indeed a zinc importer that is, at least partly, located on the plasma membrane as an 8 transmembrane domain protein. Its importance for RPE however, could not be investigated due to difficulties with transfection of ARE19 cells and problems with commercial antibodies and antibodies raised ourselves. Further experiments are being planned to clarify the role ZIP12 plays in cells in general and specifically in RPE.

4.10. **Future Directions**

ARPE19 cells were transfected with the ZIP12-V5 plasmid to assess where the protein is expressed and how this expression might affect the phenotype of the cells. While we were able to transfect some cells with low efficiency, a transfection method with better efficacy and less toxicity to ARPE19 cells will have to be implemented. Recently a non-viral transfection method using a combination of cationic lipid, plasmid DNA and magnetic nanoparticles was reported for ARPE-19 cells (Fujii et al., 2010) and we are in the process of implementing this in our laboratory. Furthermore, a study recently reported the use of the Nucleofection (Amaxa AG, Koln Germany) method, which resulted in 78% transfection of ARPE19 cells in contrast to 5% observed with LipofectamineLTX, which we used in our studies. Creating a stably transfected cell line would be highly beneficial in order to understand the function of ZIP12 protein; however ARPE19 is an unlikely candidate for this. The Nucleofection method is non-viral and therefore does not create constitutively expressed gene, however, expression was observed at least 7 days post transfection, which might be sufficient for functional assays like measurement of trans epithelial resistance, gene expression and monitoring pigmentation. The transfected ARPE19 cells would be useful in measuring the zinc influx from different extracellular zinc compartments on polarised cells cultured on transwell membranes.

We will also attempt to disaggregate the high molecular weight aggregates correlated with overexpression of ZIP12 in cells through optimisation of buffers and reagents. Furthermore, proteomics characterisation of the large aggregates shown in Figure 4.16 would identify the interacting proteins involved in the

formation of aggregates. Optimisation and characterisation of the antibodies which were generated and purchased should help us to uncover the localisation and possible involvement of ZIP12 with cellular processes and disease states. For this we will try to further optimize our immunolabeling and purify our ZIP12 antibodies. In addition, efforts will be made to isolate RPE RNA free from contamination from neighboring tissue compartments. Potential method for this include very early passage of human RPE cultures.

There are over 100 potential polymorphisms of the SLC39A12 gene (www.ensembl.org). Whether any of these are associated with AMD is now under scrutiny in collaboration with Professor John Yates and Dr Valentina Cipriani at the UCL Insitute of Ophthalmology using Genome Wide Association Studies data on AMD patients. Our preliminary analysis indicated that some polymorphisms are associated with AMD but this requires further statistical analysis to confirm the results. Further analysis of existing microarray data using data mining tools have identified potential protein networks ZIP12 protein is involved in. Together with the planned proteomics studies, this will highlight the molecular interactions between ZIP12 and other proteins.

It will be important to measure zinc influx by modifying extracellular zinc levels and controlled expression of ZIP12. Initial experiments suggested that addition of 100μM $ZnSO_4$ which elevated the extracellular zinc levels in the media to >100 nM is toxic to the transfected cells we tried. At these concentrations, we observed reduced cellular density and the appearance of cellular debris in the culturing medium in HEK293 cells that were transfected with ZIP12-V5 (data not shown). It is expected that most cells are unable to cope with hundreds of nanomolar bioavailable zinc (Bozym et al., 2006, Bozym et al., 2010) so these preliminary data are probably not surprising. Interestingly, as we will show in the next two chapters, similarly high extracellular levels of zinc are well tolerated by ARPE19 cells or bEND5 cells used as a model for fenestrae formation.

Apart from being bound to proteins like metallothioneins, zinc is likely to be stored in intracellular stores. It is believed that metallothionein will bind zinc almost immediately after it enters the cell and shuffle zinc into intracellular stores a

process termed muffling (Colvin et al., 2010). The muffling process is transient, and therefore zinc can be released should there be a need for zinc within the cells. Various zinc-binding proteins or cellular organelles such as lysosomes, mitochondria, endoplasmic reticulum or Golgi may serve as intracellular stores (Colvin et al., 2010). It will be important to examine in detail where and how zinc regulation occurs in these cells and how transfection with ZIP12 will affect these shuttling mechanisms.

5. Potential Role of Extracellular Zinc on RPE Cell Differentiation In Vitro: A Preliminary Study

The experimental part of this study was conducted under my supervision by Ms. Yemsrach Tadesse as a part of her MSc. I was responsible for experimental design; and data analysis was performed jointly.

In vitro studies of cultured RPE cells have generated much valuable information. However, the culture media used to grow cells often contains fetal calf serum (FCS), which contains high-affinity metal binding proteins such as albumin (Maret and Li, 2009), which in turn may render the cells zinc deficient. Since RPE cells are located adjacent to a large and potentially mobile pool of zinc, we hypothesise that the addition of zinc to the medium of cultured RPE cells will alter RPE behavior including transepithelial resistance (TER), ZO-1 protein staining and the expression of RPE-associated genes. Majority of the data presented here came are intended to be observational and most came from a single experiment and therefore drawing any major conclusion from these data would not be warranted before sufficient replication of data.

5.1. Introduction

The RPE is a monolayer of highly uniform cells located between the photoreceptor outer segments of the retina and Bruch's membrane. General characteristics of the RPE cells have previously been described in section 1.3.1. Cultured RPE cells have served as a valuable model for RPE cell behaviour and there are various immortalised cell lines commonly used in ocular research in addition to primary RPE cultures. Some of the more commonly used cell lines include hARPE19 (Dunn et al., 1996), hTERT-RPE1 (Bodnar et al., 1998), hD407 (Davis et al., 1995), mBR-RPE07 (Chen et al., 2008) and rRPE-J (Nabi et al., 1993). These cells are either spontaneously arising (hARPE19, hD407, mBR-RPE07), or transformed (hTERT-RPE1, rRPE-J) cell lines. Since its introduction in 1996 by Dunn *et al* (Dunn et al., 1996), ARPE19 has been the most widely used in ophthalmic research as an *in vitro* model of the RPE.

Dunn et al, demonstrated that ARPE19 cells form polarised epithelial monolayers and express the RPE-specific genes CRALBP, and RPE65. Transepithelial resistance of the ARPE19 cells reached about 50-100Ωcm^2 after 4 weeks in culture (Dunn et al., 1996, Dunn et al., 1998). However, despite the extensive use of ARPE19 cells, there are discrepancies between these cells and native RPE. RPE65 protein was not found in cultured ARPE19 cells despite its mRNA being present (Vugler et al., 2008), although pigmentation and expression of RPE65 has can be induced (Ahmado et al., 2011). While the original study (Dunn et al., 1996) reported pigmentation in ARPE19 cells after 4 weeks in culture, various studies struggled to demonstrate pigmentation even after prolonged periods of culture (Amemiya et al., 2004, Biesemeier et al., 2010, Sonoda et al., 2009). Furthermore, studies comparing primary cultures of human RPE and ARPE19 cells have demonstrated that TER values are consistently higher in primary cultures of human RPE cells >500 Ω cm^2 vs 50-100 ohms cm^2 (Sonoda et al., 2009, Geisen et al., 2006).

Several groups have sought to enhance the differentiation of ARPE19 cells by placing them in an environment that better mimics the *in vivo* condition. The use of porcine lens capsule as a way to create extracellular matrix akin to Bruch's membrane improved the distribution of tight junction proteins ZO-1 and occludin, and increased the TER values and the phagocytic capability of ARPE19 cells (Turowski et al., 2004). Co-cultures of ARPE19 cells with choroidal endothelial cells (Geisen et al., 2006), retinal neurons (German et al., 2008) and glial cells (Constable and Lawrenson, 2009) have also been shown to improve ARPE19 cells differentiation.

ARPE19 cells are usually cultured in the presence of 10% fetal calf serum (FCS) as first described by Dunn *et al* (1986). Serum contains many different proteins, including albumin, transferring, antibodies and complement factors (Adkins et al., 2002). Serum albumin is known to bind zinc with a kD of ~45nM (Maret and Li, 2009) as do several other FCS proteins (Harris and Stenback, 1988). Therefore, we speculated that the addition of 10% FCS to the culture media might create a zinc deficient environment which may affect the phenotype of the ARPE19 cells.

5.2. **Aims and Hypothesis**

Hypothesis:

In this chapter, we hypothesise that elevation of extracellular zinc in the growth media will affect the phenotype of ARPE19 cells.

Methods:

To test this hypothesis, ARPE19 cells were cultured in the presence of $ZnSO_4$ enriched growth media and the phenotypic changes induced by the inclusion of zinc were assessed by measuring TER, ZO-1 immunoreactivity and RPE specific gene expression.

5.3. **Calculating the Zinc Concentration in DMEM/F12**

Methods

As discussed, zinc binds to proteins in tissue culture media (Maret and Li, 2009, Harris and Stenback, 1988). ZnAF2 (Neurobiotex, Galveston, TX, USA), a zinc-selective fluorescent probe was used to measure the zinc buffering capacity of the DMEM/F12 with 10% FCS (complete media) added. A standard curve was generated by dissolving increasing concentrations (1-1000 nM) of $ZnSO_4$ in deionised water before 5 μM ZnAF2 was added. Fluorescence intensities were measured in a specifically designed fluorometer (Neurobiotex, Galveston, TX, USA) (Excitation: 460-490nm, emission: 515-525nm). Then, 0, 50, 100, 250 and 500μM of $ZnSO_4$ were added to the complete media and fluorescence changes used to calculate free zinc concentration using the standard curve. Background autofluorescence was measured before the addition of ZnAF2, a high affinity Zn^{2+}probe (K_d 2.7 nM) and subtracted from test readings.

Results

The resulting bioavailable zinc concentrations in the growth media were approximately ~10 nM, 100nM, 255nM, 755nM and 1550nM respectively (Figure 5.1). Therefore, in subsequent experiments ARPE19 cells were cultured in the presence of 0, 50, 100, 150 and 175μM added $ZnSO_4$. At higher concentrations altered morphology and cellular detachment was evident (data not shown), indicating toxicity.

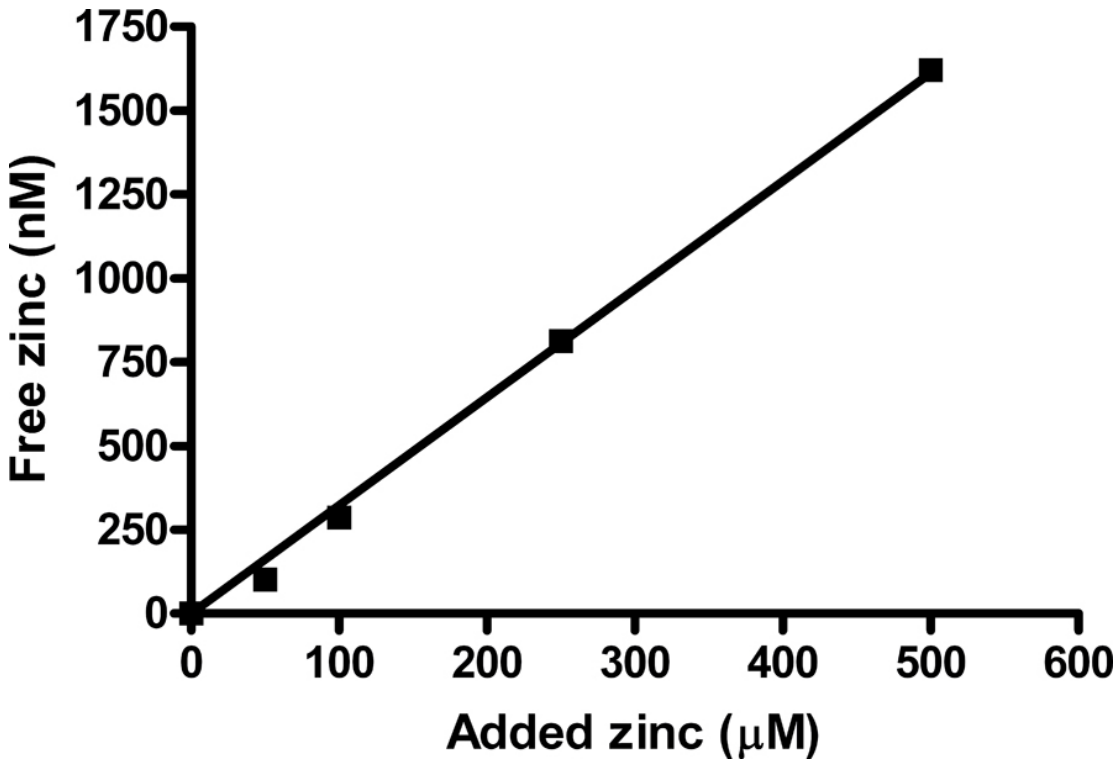

Figure 5-1– Zinc measurement using ZnAF2 in DMEM/F12 growth medium

Zinc measurements were performed in 1μM ZnAF2 diluted in solution containing ZnSO4 in DMEM/F12 phenol-red free media supplemented with 10%FCS.

5.4. **Effect of Extracellular Zinc on TER of Cultured ARPE19 Cells**

Methods:

Measurements of transepithelial resistance (TER) were conducted on ECIS real time cell growth monitoring system (Applied Biophysics, Troy, NY, USA) placed into an incubator over a six day period. Care was exercised to not remove the electrode array chips from the TER measuring device in order to prevent inconsistency and artefacts in TER impedance measurement. During this period, growth media was not replaced and enough media was placed on the cells to ensure cellular viability was not compromised. The data collected were normalised to the TER values measured at time 0 (i.e. time when the electrode array was placed in impedance measurement device) and data measured the end of the 6 days period. The results (Figure 5.2) are the averages of at least 2 independent measurements.

Results:

Over the 6 day period, adding increased concentrations of zinc delayed the development of TER (Figure 5-2). Without zinc,TER reached a half maximal value by 68 hours in culture then a plateau after 96 hours. In the presence of zinc the half maximal values were reached after 74 hours in the presence of 50µM, 90 hours in the presence of 100µM, 120 hours with 150µM and 130 hours in the presence of 175µM $ZnSO_4$. Despite the initial delays, TER reached a similar maximum as the controls within 6 days.

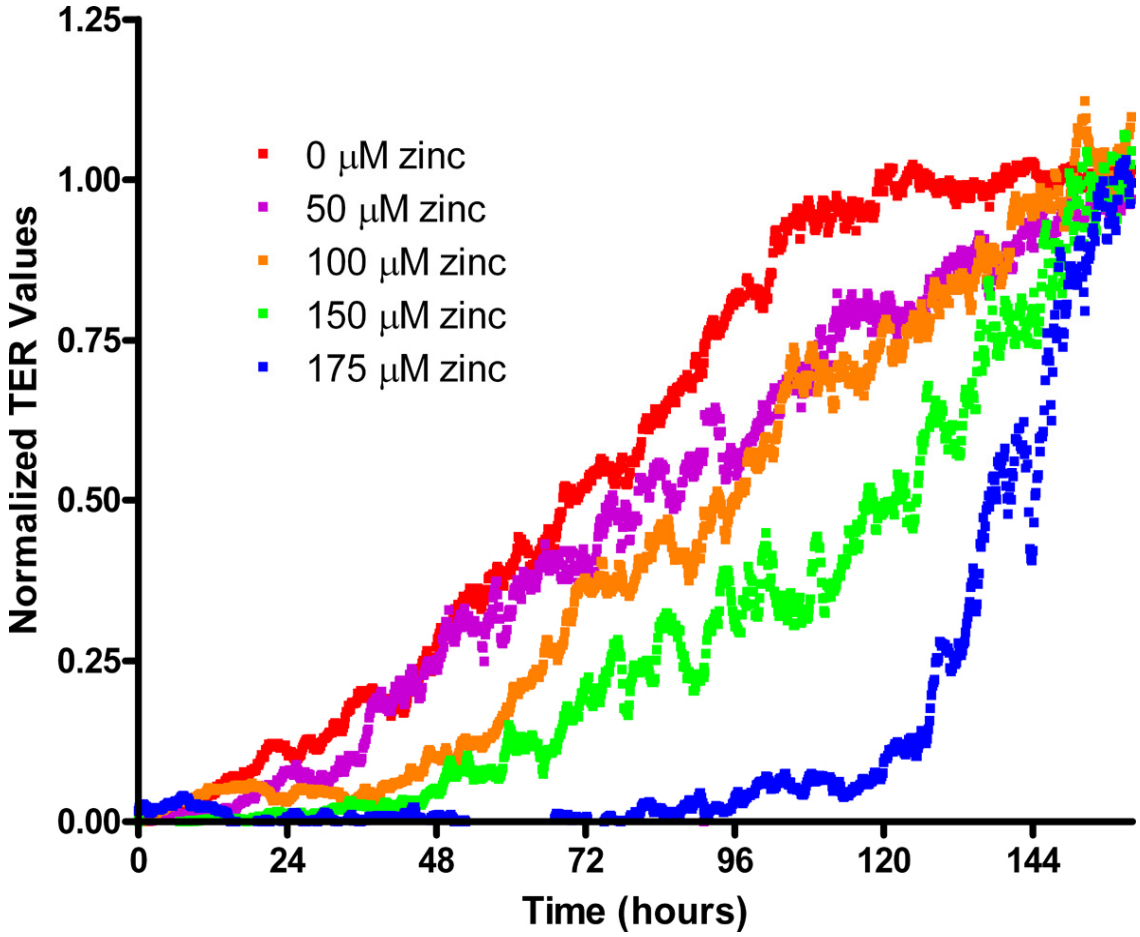

Figure 5-2- TER measurement in ARPE19

TER measurement was done on 8-electrode array chips (Wolf Labs, UK) over 6 days without changing the media. The addition of zinc into the growth media seemed to delay the attachment and growth phase, resulting in lowered transepithelial resistance, although the TER value reached plateau after 6 days in all of the samples. The experiment was repeated 3 times and results averaged.Data are normalized against TER for control culture at 6 days.

5.5. **Effect of Extracellular Zinc on ZO-1 Distribution in ARPE19 Cells**

Methods:

The TER measurements indicated that the development of tight junctions might be affected by extracellular zinc. Therefore, immunocytochemistry using an antibody against tight junction protein was performed on cultured ARPE19 cells receiving the same treatment as section 5.4. There are several tight junction proteins including ZO-1, claudin and occludin (Balda and Matter, 2008). In this study, we have chosen to use an antibody against ZO-1, a widely used marker for tight junctions (Sonoda et al., 2009).ARPE19 cells were fixed with 4% PFA after 1 and 3 weeks in culture and labeled with ZO-1 antibody (BD Biosciences, UK) and fluorescent-labelled with FITC secondary antibody.

Results:

After 1 week of culture, the cells had reached confluency independent of zinc concentration, as indicated by cobblestone-like appearance of the cells (Figure 5.3). A continuous ZO-1 band of immunoreactivity can be seen in control samples, which contain no added zinc. However, in the presence of increasing concentrations of zinc the ZO-1 staining became more and more discontinuous after 1 week treatment (Figure 5.3). At 3 weeks in culture the ZO-1 stain had a continuous appearance in the controls, but in the presence of added zinc at all concentrations the ZO-1 labeling was discontinuous (Figure 5.3).

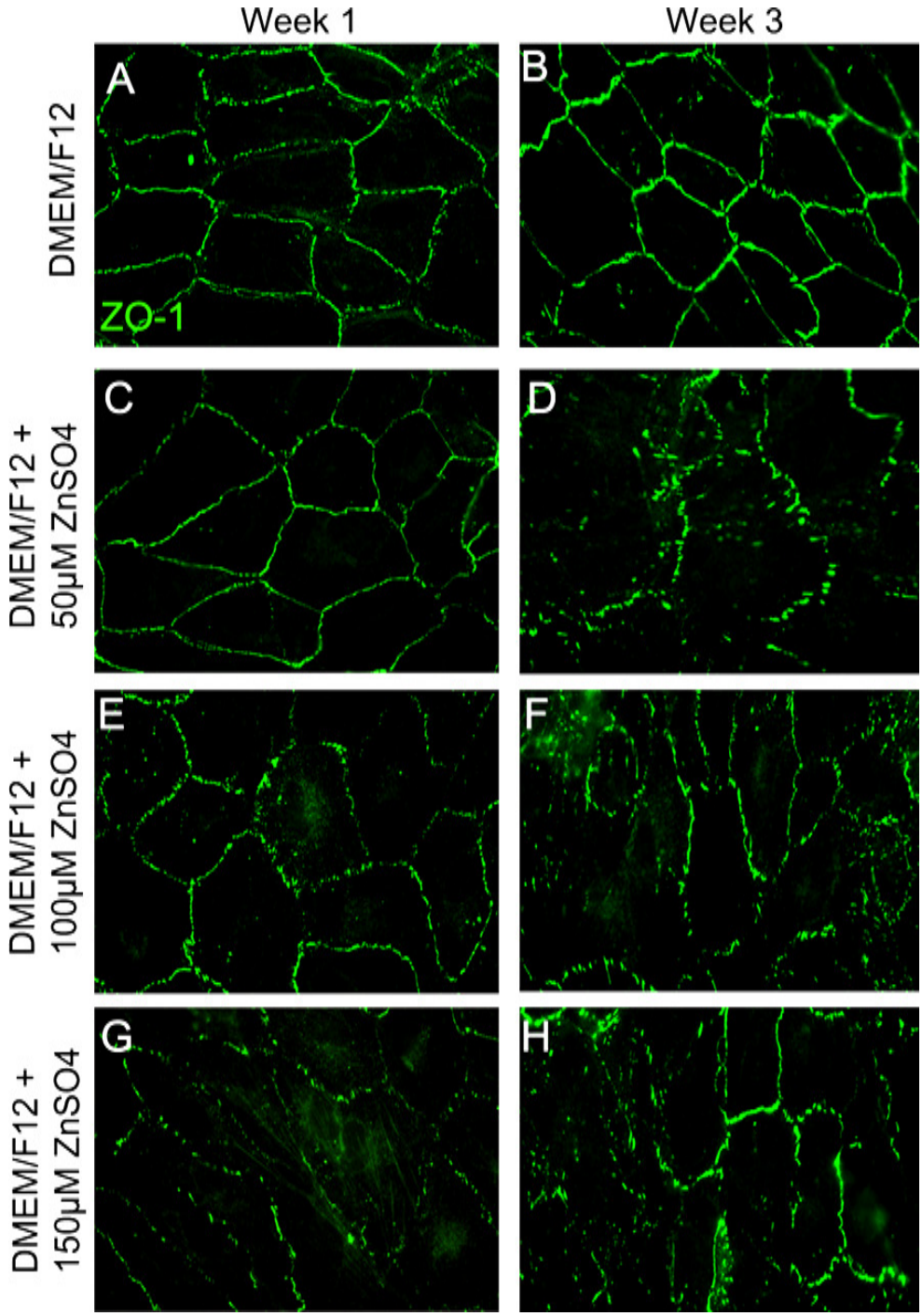

Figure 5-3–Immunostaining for ZO1 on ARPE19 cells

Immunostaining for ZO1 on ARPE19 shows clear formation of tight-junctions 1 week after culturing (Panel A) which persists after 3 weeks of culturing (Panel B) in DMEM/F12. The addition of zinc at 50µM (Panel C) did not show any difference compared to non-zinc treated cells in Week 1. Although after 3 weeks (Panel D), discontinuous ZO-1 staining was observed in cells grown with higher concentration of zinc for 1 week (Panel E, G) and 3 weeks (Panel F, H). Immunostaining was conducted using ZO-1 antibody (BD Biosciences) at 1:400 dilution and fluorescent stained with FITC (BD Biosciences) at 1:300. Images were taken using epifluorescence microscope BX51 (Olympus) at 63x magnification.

5.6. **Cell Proliferation Assay using alamarBlue**

Methods:

As the TER measurements and ZO-1 staining was done in sub-confluent cells to observe effect of zinc immediately after seeding, a cell proliferation assay was performed to confirm that immunostaining results are not caused by effect of zinc on cellular proliferation. AlamarBlue solution was purchased from ABDSerotec (Kidlington, UK). ARPE19 cells were seeded at 5000 cells per well on a 96-well plate with 200µl growth media to match the experimental conditions in the previous sections. After incubation for 1-6 days, 10% of alamarBlue solution was added and left to incubate for 2 hours before its absorbance measured at 600nm and 450nm. Calculations for the absorbance were made according to the equation provided by the manufacturing company and presented as percentage reduction of alamarBlue. As controls, cells without zinc treatment was used and as blanks, growth media without zinc added was used. It was pre-determined that the addition of zinc does not affect AlamarBlue absorbance.

Results:

After 1-3 days (Figure 5.4), percentage reduction of alamarBlue is reduced as the concentration of zinc added increased. Cell viability was very low after addition of 150µM zinc on day 1, although the level slowly increased as the growth time increase. However, towards the end of 6 days, the reduction levels of alamarBlue reached approximately the same level with exception of ARPE19 cells grown in the presence of 150µM $ZnSO_4$ which shows reduction in cell viability after 6 days. Treatment with 200 and 250µM of $ZnSO_4$ resulted total loss of cellular viability (data not shown). The result suggests that zinc delays cellular proliferation, which may possibly affect the ZO-1 staining pattern seen.

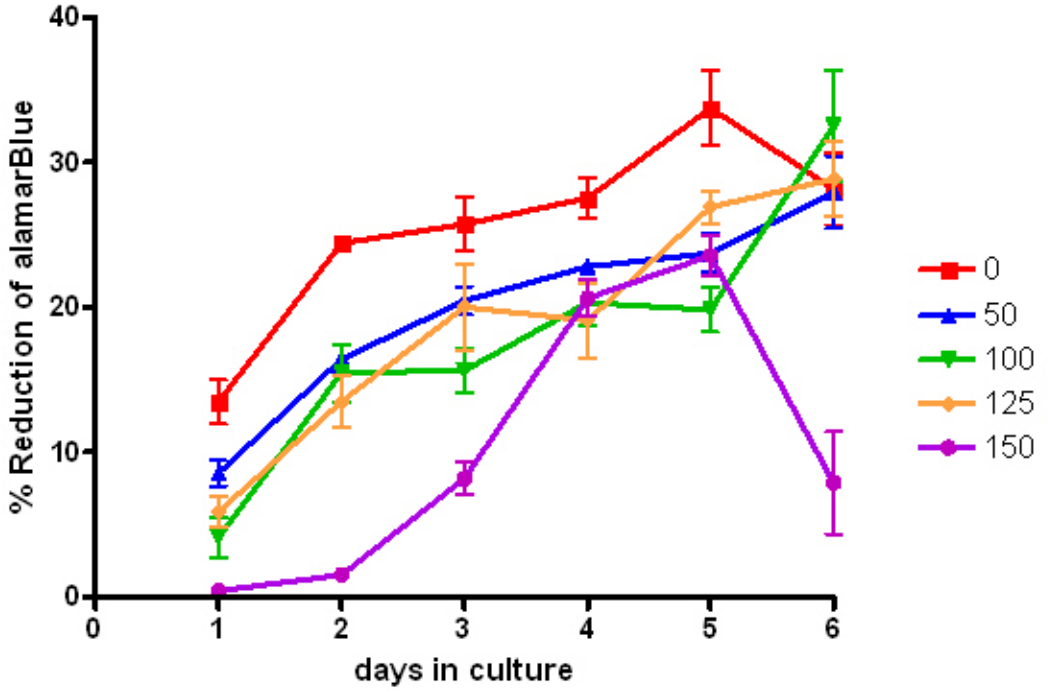

Figure 5-4 – Percentage reduction of alamarBlue in ARPE19 cells

Percentage reduction of alamarBlue in ARPE19 cells cultured in DMEM/F12 supplemented with increasing concentration of $ZnSO_4$ (0-150µM). In the first 3 days there is a lower reduction of alamarBlue with increasing zinc concentration, after 3 days, the changes become less pronounced, eventually level of cellular viability reaches the same level after 6 days with the exception of cells with 150µM added zinc which had less alamarBlue reduced.

5.7. **Zinc Induced Changes in ARPE19 Gene Expression**

Methods:

The effect of extracellular zinc addition to DMEM/F12 complete media on gene expression of RPE marker genes was assessed. Quantitative RT-PCR was carried out to monitor changes in RPE65, RLBP1, SILV, BEST1 and TJP1 expression. RPE65 is a protein involved in the visual cycle where it aids the conversion of all-trans-retinol to 11-cis-retinol (Strauss, 2005). RLBP1 is a gene encoding for a retinaldehyde binding protein 1, which binds 11-cis-retinal in the visual cycle. SILV encodes the protein PMEL17, which is expressed in the RPE and is present in melanosome precursors. BEST1 encodes for bestrophin1 protein, which forms basolateral, calcium activated chloride ion channels (Kunzelmann et al., 2007). The TJP1 gene is not RPE-specific but codes for a tight junction protein and is a marker for differentiated RPE cells.

ARPE19 cells were plated at a density of 12000 cells/cm^2. RNA samples were isolated weekly for 6 weeks using the RNEasy Kit (Qiagen, Crawley, UK), assayed for RNA quality and stored at -80C until being analysed by Q-RT-PCR. The culture medium was prepared as explained above by adding 50µM, 100µM and150µM $ZnSO_4$. Similar to the methods used in Chapter 3, gene expression changes were evaluated by the comparative delta CT method (Schmittgen and Livak, 2008). Expression was compared to 3 housekeeping genes: GAPDH, YWHAZ and UBC and fold expression was calculated by expression= 2^-ΔΔCt. It is important to highlight here that this experiment provided only a single point for every measurement; therefore statistical evaluation be carried out.

Results:

It appears that addition of zinc has a marked, concentration dependent effect on RPE65 gene expression at week 1 and 2 (Figures 5.5 and 5.6). RPE65 gene expression (red) was stimulated by up to one order of magnitude by 150 uM zinc. At week 2, BEST1 expression was up-regulated by almost one order of magnitude and at week 6, TJP1 expression was up-regulated by 1.5 orders of magnitude, although this was not apparent at week 3, 4, and 5 (Figure 5.5, 5.6). While there appears to be a down-regulation of some of the other genes at week one and two (Figure 5.6), the decreases were small and possibly not of significance.

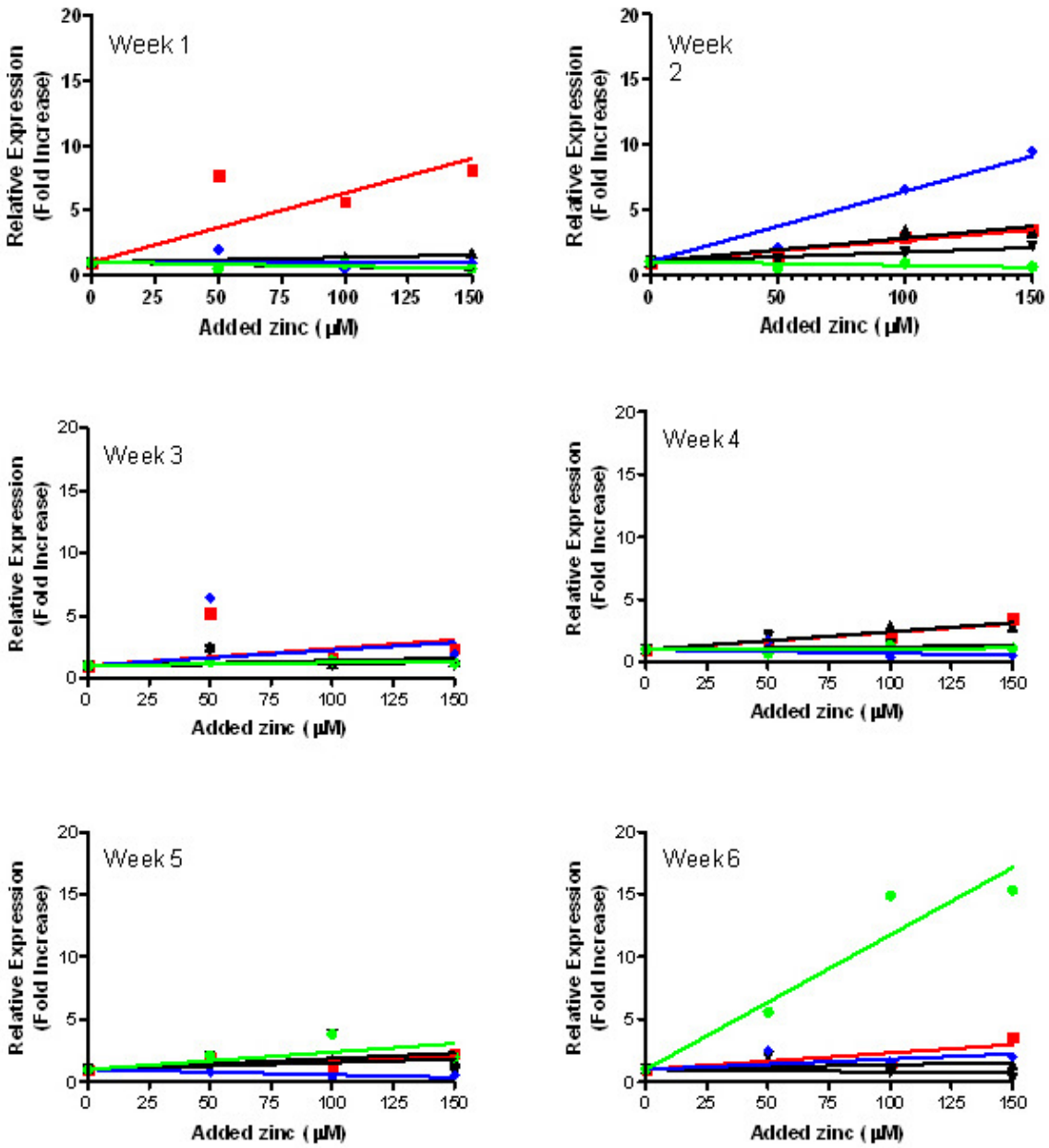

Figure 5-5- QPCR data showing relative expression of RPE65, TJP1, SILV, BEST and CRLBP1 in ARPE19 cells

QPCR data showing relative expression of RPE65, TJP1, SILV, BEST and CRLBP1 in ARPE19 cells cultured over the period of 6 weeks after addition of 100 and 150µM ZnSO4 in the growth media. The results were normalised against values obtained for untreated ARPE19 cells (relative expression = 1). After 1 week of culture, only expression of RPE65 was 7.5x higher compared to untreated cells, a trend which continues in week 2. However, results were markedly more variable at weeks 3-6. The experiment was repeated once. Red: RPE65, Blue: BEST1, TJP1: Green, RLBP1: Black, SILV: Black.

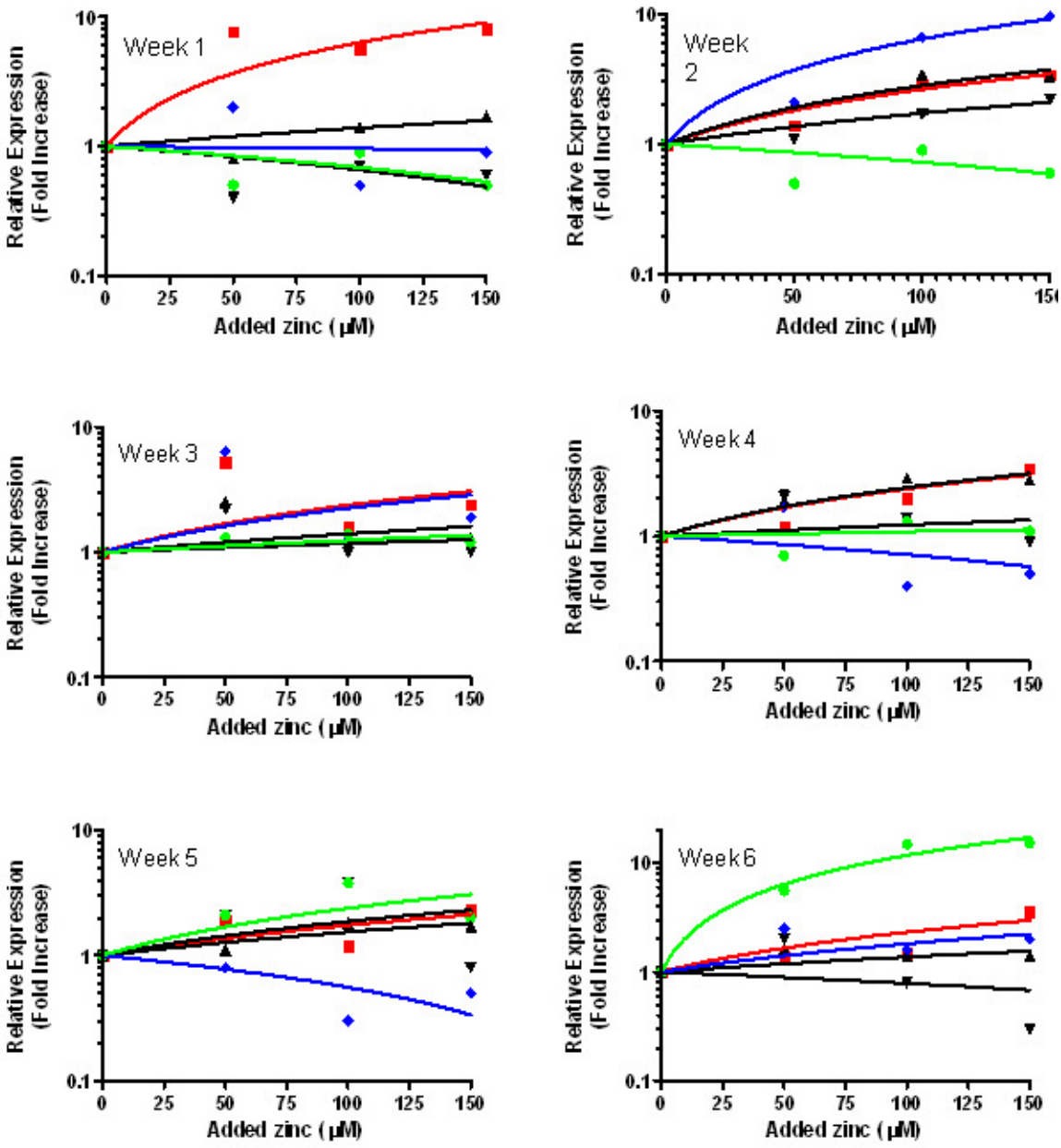

Figure 5-6 – Logarithmic relative expression of RPE65, TJP1, SILV, BEST and CRLBP1 in ARPE19 cells

Logarithmic relative expression of RPE65, TJP1, SILV, BEST and CRLBP1 in ARPE19 cells cultured over the period of 6 weeks after addition of 100 and 150µM ZnSO4 in the growth media. The results were normalised against values obtained for untreated ARPE19 cells (relative expression = 1). After 1 week of culture, only expression of RPE65 was 7.5x higher compared to untreated cells, a trend which continues in week 2. However, results were markedly more variable at weeks 3-6. The experiment was repeated once. Red: RPE65, Blue: BEST1, TJP1: Green, RLBP1: Black, SILV: Black.

5.8. **Discussion and Future Perspectives**

We hypothesized that culturing ARPE19 cells in a culture medium that contains 10% FCS potentially places the cells into an environment that is deficient in biologically available zinc. As zinc has been shown to be important for the appropriate function of cultured RPE cells (Tate et al., 1995), we set out to explore whether or not elevated extracellular zinc altered the morphology or cause gene expression changes to these cells. In order to show this, we assessed the effect of zinc on TER, distribution of ZO-1 immunoreactivity and the expression of RPE65, RLBP1, TJP1, BEST1 and SILV genes in pilot experiments.

The RPE depends on a fine regulation of material diffusion through expression of cellular junctions. The expression of tight junctions results in the formation of high transepithelial resistance. These are characterized by formation of specific tight junction proteins ZO-1, occludin and claudins (Geisen, et al., 2006). The localization of tight junctions on the apical-basolateral membrane of RPE cells ensures control of material diffusion. ZO-1 protein is crucial for the formation of tight junction, where it binds to other proteins such as those belonging to the occludin family and forms a support structure for tight junction (Sonoda, et al., 2009). The function of ZO-1 protein is not only limited to its structural capacity, ZO-1 has been shown to maintain cellular signaling by controlling ZO-1 associated nucleic acid binding protein (ZONAB), a transcription factor which controls proliferation of epithelial cells through interaction with cell division kinase 4 (CDK4) (Balda, Garrett, and Matter, 2003). Based on the importance of ZO-1 in epithelial functions, we have used ZO-1 as a marker for tight junction formation for our studies.

Our results show that after 1 week of culture, all ARPE19 cells cultured in the presence of zinc had reached confluency. However, with increasing zinc concentration, the staining of ZO-1 was more discontinuous. The same results were repeated after 3 weeks of culture but the staining of ZO-1 was becoming increasingly discontinuous. This indicated that addition of zinc at 50-150μM concentration is associated with lowered permeability of RPE. The failure for tight junctions to mature in those cultured in the presence of zinc may pose several problems for the RPE to function appropriately.

The failure of tight junctions to form properly can result in the loss of polarity to RPE cells. The loss of polarity in the RPE can affect the paracellular signaling between the RPE/choroid interface. As discussed in section 1.4.2, RPE barrier function requires optimal balance between secretion of pro-angiogenic factor VEGF as well as anti-angiogenic factor PEDF. Non-polarized cells show markedly lower expression and secretion of VEGF and PEDF (Sonoda, et al., 2010). The secretion of VEGF is required to mediate the fenestration in the adjacent choriocapillaris (St. Geniez, et al., 2009). The lowered of VEGF secretion will reduce material diffusion presumably mediated by the fenestrated choriocapillaris. Furthermore, there is a synergy between the formation of tight junction protein and localization of Na, K-ATPase channel, which is responsible to generate ATP for RPE metabolism. In human RPE primary cultures, the reduced function of Na, K-ATPase channel caused by potassium deficiency resulted in lowered transepithelial resistance (Rajasekaran, et al., 2003).

The increase in cellular permeability has been related to increase in the metastatic potential in cancer (Martin and Jiang 2008). The increase in permeability has been attributed to reduced expression levels of tight junction proteins (Liu, et al., 2008) In RPE cells, it is possible that the loss of polarity and increased permeability may lead to migration of RPE cells. It is known that disruption of tight junction can result in RPE cells adopting the characteristic epithelial-mesenchymal transition commonly encountered in cancer. Intra retinal RPE migration cases have been reported in AMD patients (Ho, et al., 2010).

It is still uncertain why zinc seems to reduce the staining of ZO-1 protein after 3 weeks in culture. The preliminary data presented in this chapter does not seem to support the use of zinc in culturing ARPE19 cells as zinc addition correlates with poor tight junction maturation and thus affecting RPE permeability. Furthermore, our data with alamarBlue assay indicated that RPE proliferation seems to be delayed by the presence of zinc in the first 6 days of culture. If the results presented here are indicative of what happened *in vivo*, keeping in mind the highly preliminary nature of the data, it may possibly mean that further research need to be carried out in order to determine how oral zinc supplementation (Newsome, 1988) affects the RPE/choroid interface in early AMD subjects where disruptions to the RPE are still minimal. Zinc supplementations are thought to improve immune

function that is deficient in aging subjects, yet minimal studies have been done on the effect of zinc on cellular junctions of RPE cells. The study presented here would greatly benefit from having further optimization of the amount of zinc added to ARPE19 cells. It is possible that the ~200-500nM free zinc available in cultured ARPE19 with 125μM $ZnSO_4$ added is already providing too much stress for the cultured cells. Furthermore, this study was done on non-differentiated ARPE19 cells and thus it would be feasible to repeat the study using differentiated ARPE19 cells, optimized zinc concentration, and correlating the study with measurements of transepithelial resistance of ARPE19 cells.

Hu and Bok have reported that reducing concentration of FCS used in culturing media to 1% is essential for human fetal RPE cell culture differentiation. The culturing condition was maintained for one month in which the cells finally reached maturation (Hu and Bok, 2001). As previously discussed, the presence of strong zinc binding proteins in serum can potentially create a zinc deficient environment for cellular growth. The DMEM/F12 media contained 1.5μM of ZnSO4, meanwhile the protocol used by Hu and Bok contained 5μM of ZnSO4. This suggests that the reduction of FCS may increase free zinc concentration due to lowered buffering capacity which pushes cells towards in vivo phenotype. However, as serum contains a lot of of other components, this is fairly speculative. Therefore, in order to confirm the effect of zinc on RPE cells, it is recommended that a culture media supplemented with appropriate substitutions for FCS are used to confirm the effect of zinc addition to growth media.

In parallel with TER measurement and the ZO-1 immunostaining, the expression of some RPE specific gene was monitored. The qPCR measurements showed that at least in the case of the RPE65 gene, zinc has a concentration-dependent enhancing effect on expression. RPE65 protein is a highly important enzyme, which converts all-trans-retinyl ester into 11-cis retinol (Moiseyev et al., 2006) without which the visual cycle cannot be completed. Mutations in RPE65 have been associated with blindness (Thompson et al., 2000) and RPE65 deficiency has been associated with severe loss of photoreceptors (Rohrer et al., 2003). Based on this, zinc is potentially important in maintaining visual function through modulation of RPE65.

5.9. **Future Plans**

A recent publication by Ahmado et al (Ahmado et al., 2011a) has exhaustively sought the most optimal conditions under which to culture RPE cells. They reported that DMEM high glucose with the addition of pyruvate generated better differentiated ARPE19 cells when compared to DMEM/F12 or DMEM high glucose without pyruvate. Furthermore, phagocytic function, pigmentation and expression of RLBP1, RPE65 and PMEL17 proteins were most prominent in ARPE19 cells grown in DMEM high glucose. It would be interesting to examine the TER measurements, ZO-1 staining and RPE-associated gene expression caused by adding zinc to DMEM high glucose with pyruvate. It is warranted that experiments be carried out on confluent cells in order to eliminate the false positive result caused by the effect of zinc on cell proliferation. It would also be of interest to explore the effects of growing cells in Matrigel (BD Biosciences, Oxford) and reducing the concentration of FCS to 1% as described by Ahmado and colleagues (Ahmado et al., 2011b). The decrease of FCS content would be expected to increase the concentration of freely available zinc.

In the future, it will be important to check whether coating of culturing surfaces and the use of serum deprivation are necessary to differentiate ARPE19 cells into a more *in vivo*-like phenotype. It will also be important to assess whether there is a need for the presence of extracellular zinc when plating the cells or whether addition of zinc would achieve a better phenotype when added after the cells reached confluence. A further question is whether addition of zinc to polarised cells (cells cultured to confluence on Transwell membranes) will affect cell differentiation depending on whether zinc is added apically or basally. Once appropriate conditions are found experiments using externally elevated zinc need to return to the basic characterisation of the cells in which TER, gene expression changes and pigmentation changes are monitored for an extended period of time to see the long term effect of zinc supplementation on RPE cells. Despite the many questions raised by this pilot experiment we propose that an appropriate zinc environment might be important for the development of appropriate RPE phenotype.

6. Effect of Zinc on Fenestrae Formation: an in *Vitro* Study using bEND5 Cells

The fenestrated choriocapillaris plays a crucial role in the clearance of unwanted material from the retina and the RPE. In pathologic conditions such as AMD fenestration of the capillaries is compromised but the mechanism behind this is not fully understood. In this chapter we explore the effect of zinc ($ZnSO_4$) on the formation of fenestrae in bEND5 cells, a murine cellular endothelial model system for fenestrae formation. Fenestrae formation was assessed through immunofluorescence staining for PV-1 protein, a glycoprotein found in the diaphragm of fenestrae (Stan et al., 1999). Actin immunoreactivity was used to monitor changes in the cytoskeleton. We found that treatment of bEND5 cells with~400nM bio-available zinc for 20 hours induced PV-1 rearrangement into the so called "sieve plates", an indicator of fenestrae formation. Fenestrae formation itself was confirmed by whole mount electron microscopy. The sizes of zinc-induced fenestrae were found to be ~60nm which corresponded to their size *in vivo* and when chemically induced (Latrunculin A) *in vitro*. To assess the specificity of zinc treatment bEND5 cells were exposed to equimolar levels of various divalent metals. Treatment with calcium, nickel and iron was able to induce fenestration but the extent of this fenestration was marginal when compared to that following treatment with zinc. Magnesium sulphate did not induce fenestrae formation and copper and cadmium were highly toxic to bEND5 cells. Bioavailable zinc is present at high concentration in Bruch's membrane adjacent to the choriocapillaris, therefore it could affect the endothelial cells and modulate the formation of fenestrae *in vivo*. The discovery that zinc can induce fenestrae suggests that maintaining an optimum level of bio-available zinc within Bruch's membrane might be crucial for the optimal function of the choriocapillaris and that entrapment of zinc in sub-RPE deposits in AMD might be involved in the defenestration seen in this disease.

6.1. **General Introduction**

6.1.1. The Endothelium

Endothelium is classified according to whether or not fenestrations are present. In the fenestrated capillaries, discontinuous and fenestrated endothelia are found. (Aird, 2007). Two types of fenestrae may be present; one with and one without thin 3-5 nm diaphragms (See Figure 6.1) (Braet and Wisse, 2002). Continuous capillaries are found in the myocardial vasculature (Predescu et al., 1994), central nervous system as a part of the blood-brain-barrier (Hofman et al., 2001), lung and skeletal muscle (Schnitzer, 1992). Discontinuous fenestrations are found in the liver sinusoids (Braet and Wisse, 2002), spleen and bone marrow (Satchell and Braet, 2009). Continuous fenestrated capillaries are present in the kidney glomeruli, digestive system (Satchell and Braet, 2009) and the choriocapillaris (Mancini et al., 1986). There is a marked difference in fenestrae diameter and density, especially in man (diameters ranging from 50-300 nm in diameter and density from 15-25 fenestrations per μm^2 (Braet and Wisse, 2002). This is in contrast to other animals such as rat, mouse and chicken, all of which have fenestrations with a tight range of diameters from around 80-100 nm (Braet and Wisse, 2002).

Figure 6-1- Types of endothelia

Types of endothelia: continous (a, b, c, d), fenestrated (e), and discontinuous (f). Picture accessed from http://www.cvphysiology.com/Microcirculation/M016.htm date:20 06 11

6.1.2. PV-1 Protein

PV-1, a protein coded by Plasmalemmal Vesicle Associated Protein (PLVAP*)* gene is a specific protein present in the stomatal diaphrams of fenestrated endothelia (Stan, 2004, Stan, 2007). In its monomeric form, the molecular weight of PV-1 protein is 50-60kD, although the protein usually forms dimers (Stan, 2004, Stan, 2007). Northern blot analysis of human tissues suggested that the expression of PV1 is ubiquitous, with expression highest in the thyroid gland and small intestines (Stan et al., 2001). EST data from NCBI has indicated that tissue expression for PLVAP gene was found in all states of development and its expression is highest in the mammary gland, nerve, spleen and thyroid. Furthermore, the expression is also associated with various tumors. The protein PV-1 is present as a dimer in the fenestrae diaphragms (Stan, 2004). Formation of fenestrae is highly dependent on PV1 expression. Treatment of endothelial cells in culture with Phorbol Myristate Acetate (PMA) was found to upregulate both the protein levels as well as its expression. Activation of ERK1/2 kinase pathway is crucial for the formation of fenestrae as inhibiting ERK1/2 prevented PV-1 upregulation (Stan, 2004). It is also known that PLVAP expression is dependent on kinases p38, PI3K but not MEK1 (Strickland et al., 2005). Expression of PV-1 has been associated with pathological states. Immunohistochemical staining of ischaemic human brain showed that PV-1 expression peaked 7 days post ischemia (Shue et al., 2008). In another study, the expression of PLVAP was found in various malignant neoplastic tissues, including kidney, colon, pancreatic carcinoma and non-small cell lung carcinoma (Strickland et al., 2005). PV-1 is a highly valuable marker for fenestrae formation as its homogenous distribution within cells changes into the so-called “sieve plates” once fenestration starts.

6.1.3. Importance of Endothelium in RPE-choroid Interface

The choriocapillaris is outside of the tight blood-retinal barriers at the vessels of the neural retina and the retinal pigment epithelium (Cunha-Vaz, 1979). The choriocapillaris has fenestrations mainly on the side facing Bruch’s Membrane and the RPE. The main function of the choriocapillaris is presumed to be to mediate transport of solutes and nutrients to the outer retinal layers through the RPE (Bernstein and Hollenberg, 1965) and clear the debris generated through the

processing of photoreceptor outer segments (Bok, 1993). The transport between the RPE and choroid is highly dependent on signalling by the RPE. Esser et al showed that epithelial cells associated with fenestrated endothelium continuously express VEGF as a way to control angiogenesis and fenestration (Esser et al., 1998). Interestingly, a mutant mouse which expresses solely VEGF188 but not the VEGF164 and VEGF120 present in the RPE was devoid of choroidal fenestration and had a thickened endothelium at 12 months of age (Saint-Geniez et al., 2009a), highlighting the specificity of VEGF isoforms in fenestration. Apart from pro-angiogenic factors, the RPE also mediates the prevention of neovascularisation, possibly by releasing and maintaining level of pigment-epithelium derived factor (PEDF) (Ida et al., 2003, Mori et al., 2001, Park et al., 2011).

Maintaining proper interaction between the choroidal endothelium and the RPE is likely to be crucial to the maintaintenance of normal function(s) at this interface. Several studies have indicated that ageing compromises the integrity of the RPE-choriocapillaris interface. Animal studies haveshown that vasculature density and fenestrations decrease with age (Burns and Hartz, 1992).

Structural changes in AMD affect the morphology of the RPE and the. McLeod et al (McLeod, et al 2009 IOVS) concluded that significant loss of the RPE and vasculature occurred in human AMD eyes with geographic atrophy compared to aged non-AMD eyes. They also showed that no fenestrations could be observed in the region of RPE loss (McLeod et al., 2009). The presence of sub-retinal RPE deposits is thought to contribute to these changes as they interrupt the communication between RPE and the choroidal capillaries. Various environmental and non-environmental factors like diet and lifestyle factors (Wright et al., 1983), alcohol (Wang et al., 2005), smoking and nicotine (Espinosa-Heidmann et al., 2006, Yang et al., 2010) can interfere with fenestrae formation. Here we present evidence that zinc is important for fenestrae formation as well.

6.2. **Aims and Hypothesis**

Fenestration of the choroidal capillaries is maintained through the release of VEGF, and probably other biomolecules, by the RPE(Roberts and Palade, 1995). The thickening of Bruch's membrane and the development of sub-RPE deposits is thought to interfere with the diffusion of these intermediaries (Booij et al., 2010a)

causing the defenestration and eventually the atrophy of the choriocapillaris. Impaired nutrient exchange and product removal then leads to the degeneration of the RPE. As zinc, both bound and bio-available, is present in Bruch's membrane in high concentrations (Lengyel et al., 2007), we hypothesised that zinc is one of the biomolecules involved in fenestrae formation. Totest this hypothesis we:

1. Used a cellular model system for fenestrae formation.

2. Exposed cells to extracellular zinc, and monitored fenestrae formation using immunocytochemistry and TEM.

3. Determined the specificity of zinc-induced fenestration by treating bEND5 cells with equimolar concentrations of other divalent metals.

4. Identified the signalling pathway(s) involved in zinc induced fenestrae formation using bioinformatic tools

Latrunculin A treatment of bEND5 cells as a Model for Fenestration

Methods:

In this study, we followed the protocol of Ioannidou et al (2006) who used cultured bEnd5 cells and Lantrunculun A (LA) treatment to induce fenestrae formation (Ioannidou et al., 2006). Latrunculin A is a toxin isolated from *Latrunculia magnifica,*or red sea sponge (Coue et al., 1987). Latrunculin A (1.25uM)has been shown to bind to actin leading to the disruption of the cytoskeleton (Ioannidou et al., 2006). As a consequence LA induces a widespread relocation of PV-1 proteins and, fenestrae formation (Ioannidou et al., 2006).

Results:

Figure 6.2 summarizes the results of 1.25 μM LA on bEND5 cells. PV-1 immunoreactivity (panel B) highlights typical "sieve plates", an indication that PV-1 protein was redistributed. A counterstain with Rhodamine Phalloidin shows that the cytoskeleton was disrupted. Actin staining shows bands of immunoreactivity in the control samples, which were replaced by punctate, dotty linear staining. Using whole-mount transmission electron microscopy (TEM), we were able to reproduce Ioannidou's results and show that not only PV-1 redistributed into "sieve plates"

but that it also led to formation of fenestrae. Figure 6.2 shows uniform fenestration resulting from Latrunculin A treatment. The average diameter of the fenestrae was 74±19nm, similar to the 60-80nm reported by Ioannidou et al (see Figure 6.8). At higher magnification, the cores of each fenestration become apparent (Figure 6.2 Panel F). The structure holds the size of the fenestration and is present in every single fenestra. In this chapter, we will highlight the effect of zinc and various other metals in inducing fenestrae formation, and Latrunculin A treatment will be used as a control for each of the reactions.

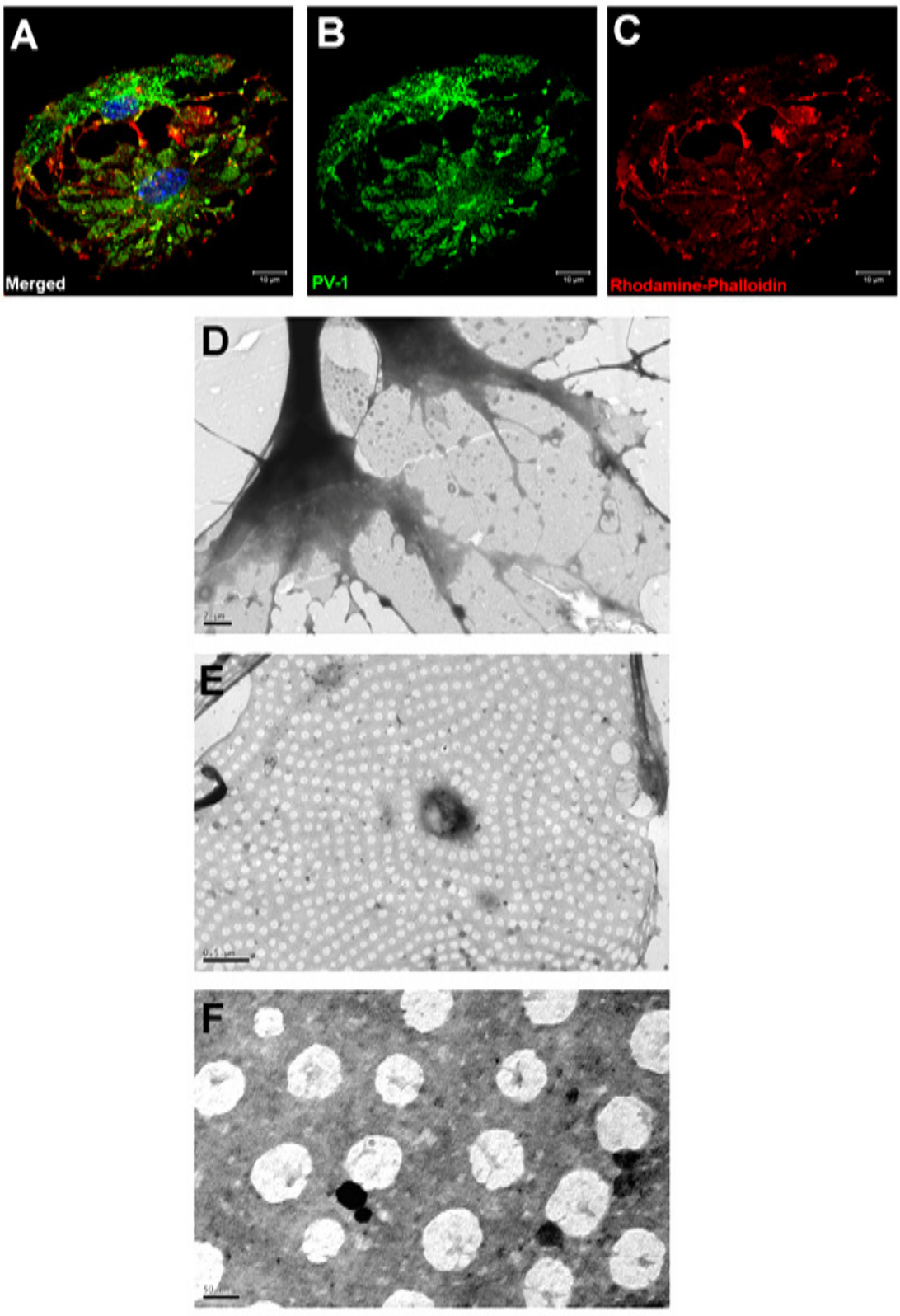

Figure 6-2- LA induces fenestrae formation

Treatment of bEND5 cells with 1.25µM of Latrunculin A resulted in rearrangement of PV-1 protein (Panel B) and actin (Panel C). Panel A, B,C were taken using LSM700 confocal microscope with 63x magnification, scale bar 10µM. TEM analysis showed typical actin rearrangement forming thin uniform layers full of fenestration (Panel D, 800x magnification, scale bar: 1µM, Panel E, 5000x magnification, scale bar: 0.5µM). High magnification shows the presence of typical fenestrae diaphragms (Panel F, 12000x magnification, scale bar: 200 nm)

6.3. **Treatment with $ZnSO_4$ can Induce PV-1 Protein Rearrangement**

Methods:

The bEND5 cells were cultured in DMEM with added glutamine and pyruvate supplemented with 10% FCS, 1% penicillin streptomycin, 1x NEAA, and 50µl of 50mM β-mercaptoethanol. Zinc, in the form of $ZnSO_4$, was added to this media. As some of the constituents of this media can bind added zinc we calculated the buffering capacity (with the help of Prof. Richard Thompson, University of Maryland, USA) and measured bioavailable extracellular zinc concentration using $ZnAF_2$ (see Chapter 5) and found that bioavailable zinc levels detected were below 1µM, with up to 250 µM added $ZnSO_4$ (Figure 6.3). At 100, 150, 175, 200 and 250µM added $ZnSO_4$, the concentration of free zinc detected was 447±68, 600±73, 629±33, 698±50, and 926±214 nM respectively. Based on the calculation, the total amount of zinc present in growth media of bEND5 cells at 125µM is 516 nM.

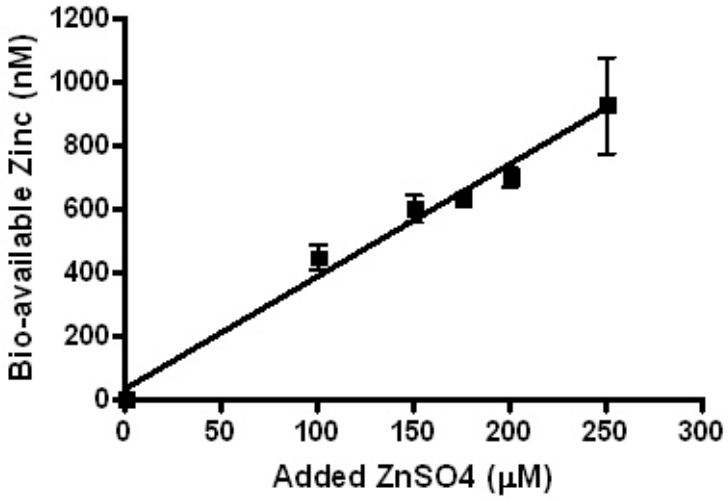

Figure 6-3- Measurement of free intracellular zinc using $ZnAF_2$.
The presence of zinc buffering constituents in the growth media of cells buffered zinc. Addition of 100, 150, 175, 200 and 250µM $ZnSO_4$ resulted in 447±68, 600±73, 629±33, 698±50, and 926±214 nM respectively. R^2= 0.97.

Results:

In untreated (control) samples (Figure 6.4, panel C), the cytoskeleton appears normal and PV-1 is distributed homogenously, apart from dense perinuclear staining. When cells were exposed to 125μM $ZnSO_4$, (a concentration chosen based on the experiments in Chapter 5 on RPE cells), corresponding to ~370-500 nM bioavailable zinc, for 20 hours, rearrangement of PV-1 became apparent (Figure 6.4, panel E,F). However, no rearrangement of actin was apparent. Compared to LA treatment, which produced widespread "sieve plates" formation and a substantial rearrangement of actin, zinc treatment induced the formation of smaller clusters of sieve plates without apparent actin rearrangement (Figure 6.4, panel E,F).

Next we explored how different concentrations of zinc affect "sieve plate" formation. Cells were treated with 50, 100, 125, 150, 175 and 200μM of added $ZnSO_4$ for 20 hours at 37^{o}C with 5% CO2. PV-1 rearrangements were only seen starting at 100μM (50μM data not shown), in the form of very fine PV-1 rearrangements inside the cells close to the plasma membrane of the cells (Figure 6.5 Panels E-H). At 125μM, more defined clusters of sieve plates were produced (Figure 6.4 Panels E-F). At 150μM and 175μM, sieve plates did not increase compared to 125μM (Figure 6.5 Panels I-P). At 200μM added zinc evidence of cells losing membrane integrity was apparent (Figure 6.5 Q-T). In pilot studies 250μM $ZnSO_4$ treatment resulted in clear indications of toxicity with cells shrinking, as well as nuclear condensation and blebbing (Data not shown). This confirms the notion that there is a narrow range of "bioavailable" zinc that can be tolerated by cells.

In order to minimise the possibility of zinc toxicity, it was decided that the lowest concentration that could induce PV-1 rearrangement, namely 125μM, would be used for subsequent experiments.

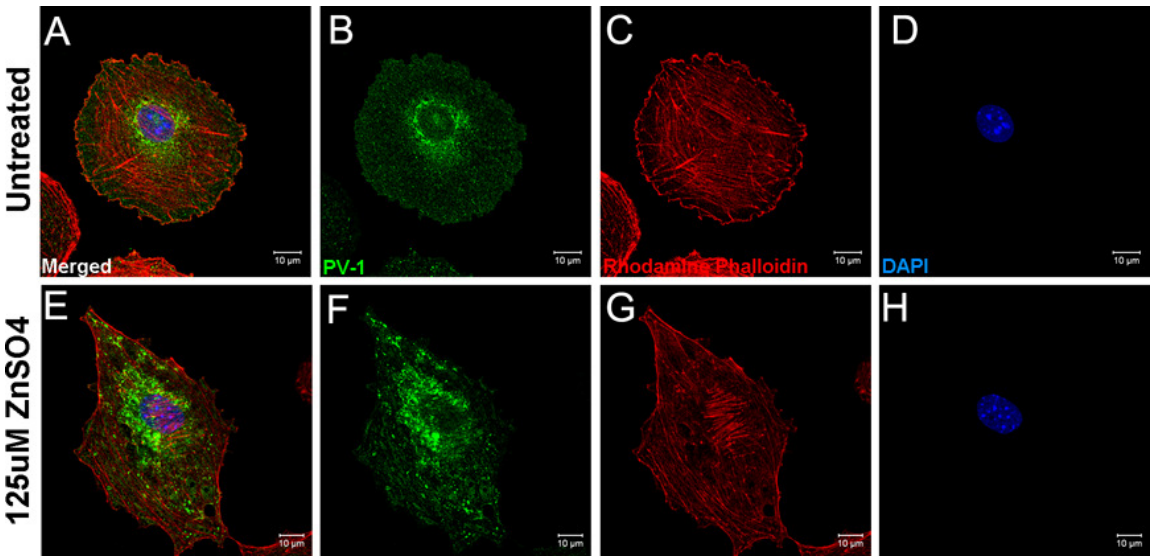

Figure 6-4 – 125 µM added ZnSO4 cause PV-1 protein rearrangement

Treatment of bEND5 cells with 125µM of added $ZnSO_4$ for 20 hours caused PV-1 protein rearrangement and formation of sieve plates (Panels E-L) compared to untreated cell (Panel A-D). Actin staining using Rhodamine Phalloidin indicated the lack of cytoskeletal changes (Panels C, G, K). Panels E-H showed a more extensive PV-1 rearrangement compared to Panels I-L. Pictures were taken using LSM700 confocal microscope at 60x magnification. All scale bars = 10µm.

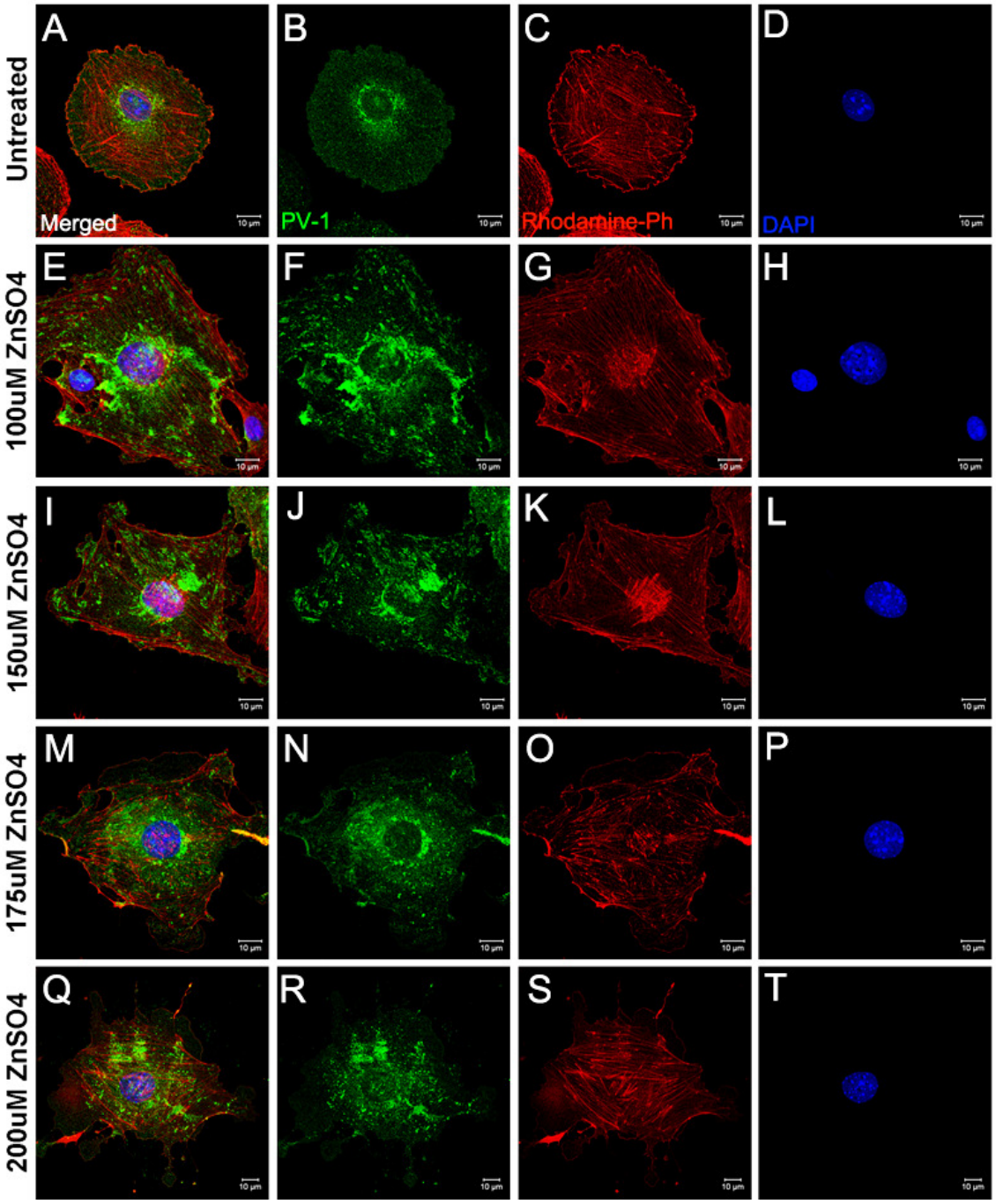

Figure 6-5 – Treatment of bEND5 cells with 100-200µM of added ZnSO4

Treatment of bEND5 cells with 100-200µM of added ZnSO4 caused varying levels of PV-1 protein rearrangement and formation of sieve plates (Panels E-T) compared to untreated cell (Panel A-D). Actin staining using Rhodamine Phalloidin (Panels C, G, K, O, S) indicated the lack of cytoskeletal changes. Pictures were taken using LSM700 confocal microscope at 60x magnification. All scale bars = 10µm.

Next the time-course of fenestrae formation was investigated. The cells were exposed to 125 uM added zinc for 3, 6, 9, and 20 hours. While fenestration could be seen as early as 3 hours, 9 hours of zinc treatment was required for consistent fenestrae formation. Untreated samples again showed diffuse and homogenous staining of PV-1 protein across the cytoplasm with normal staining of actin and DAPI. At three hours of treatment, minor changes in PV-1 staining could be observed. After six hours, there was rearrangement of PV-1 where diffuse PV-1 staining could be seen around the cells (Figure 6.6 Panels I-L). At 9 hours and 20 hours, several clusters of sieve plates could be seen (Figure 6.6 Panels M-T).

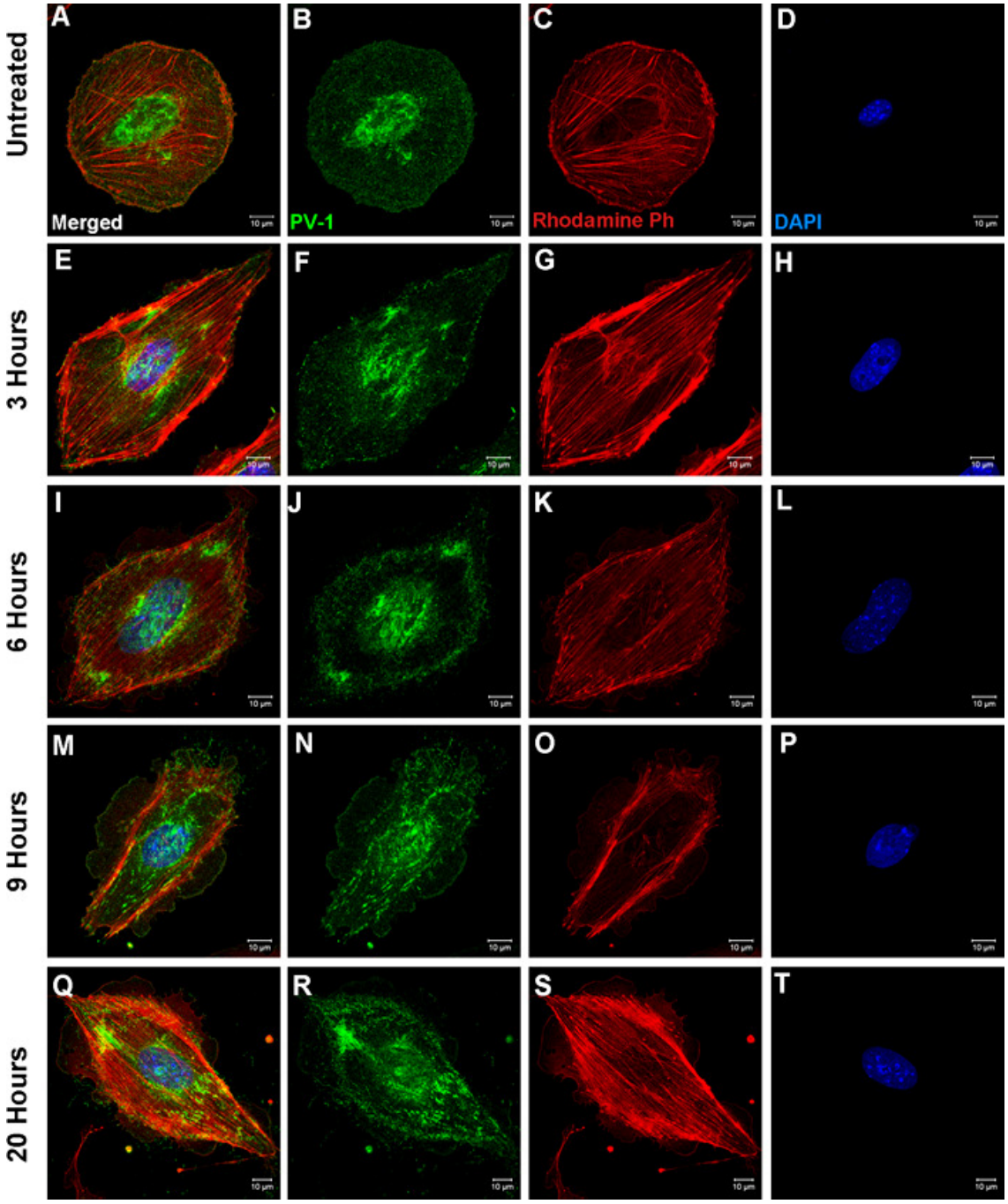

Figure 6-6 – Time course treatment with 125µM of added ZnSO4

Treatment of bEND5 cells with 125µM of added $ZnSO_4$ for 3-20 hours showed rearrangement of PV-1 protein from 3 hours (Panel E-H), however, sieve plates formation were only apparent in cells treated with zinc for 9 and 20 hours (Panels M-P and Q-T). Actin staining (Panels C, G, K, O, S) was conducted using Rhodamine Phalloidin Dye. PV-1 staining was done using anti-PV1 antibody and Alexa 488 secondary antibody. Pictures were taken using LSM700 confocal microscope at 60x magnification. All scale bars = 10µm.

6.4. **Electron Microscopy Confirmation of Zinc Induced Fenestration**

PV-1 immunoreactivity is a reliable indicator of PV-1 protein translocation but by light microscopy we cannot confirm that this has led to fenestrae formation. Therefore fenestrae formation was monitored by whole mount transmission electron microscopy.

Methods:

bEND5 cells were grown overnight on formvar coated nickel TEM grids in the presence of standard culture media supplemented with 10% FCS and 1% penicillin-streptomycin. The cells were then treated either with LA for three hours or 125µM $ZnSO_4$ for 20 hours or were left untreated as controls. The timing of the LA treatment was synchronized with the 20 hours zinc treatment, meaning that LA treatment commenced 3 hour before the zinc treatment finished. Therefore, all reactions were stopped at the same time by fixing the cells. Following fixation, the cells were treated with osmium tetroxide and were viewed using a JEOL10TEM microscope.

Results:

Cells treated with LA showed the expected rearrangement of actin and formation of fenestrae. The endothelial cells have multiple sieve plates arranged around cytoskeletal actin bundles which radiated from the nucleus (Figure 6.7 Panel A). At 5000x and 12000x magnification (Figure 6.7 Panel B and C), the fenestration formed by LA treatment showed uniform pattern. These fenestrae formed by $ZnSO_4$ and LA all possessed central diaphragms (Figure 6.7, Panel C and I). Limited spontaneous fenestrae formation was apparent in untreated control cells but they were very small (Figure 6.7, Panel E). Cells treated with 125µM $ZnSO_4$ for 20 hours were consistently fenestrated (Figure 6.7, Panel G-I) and sieve plates were present (Figure 6.7, Panel G). These sieve plates covered smaller areas than in LA-treated cells. This confirms our findings with PV-1 antibody labeling.

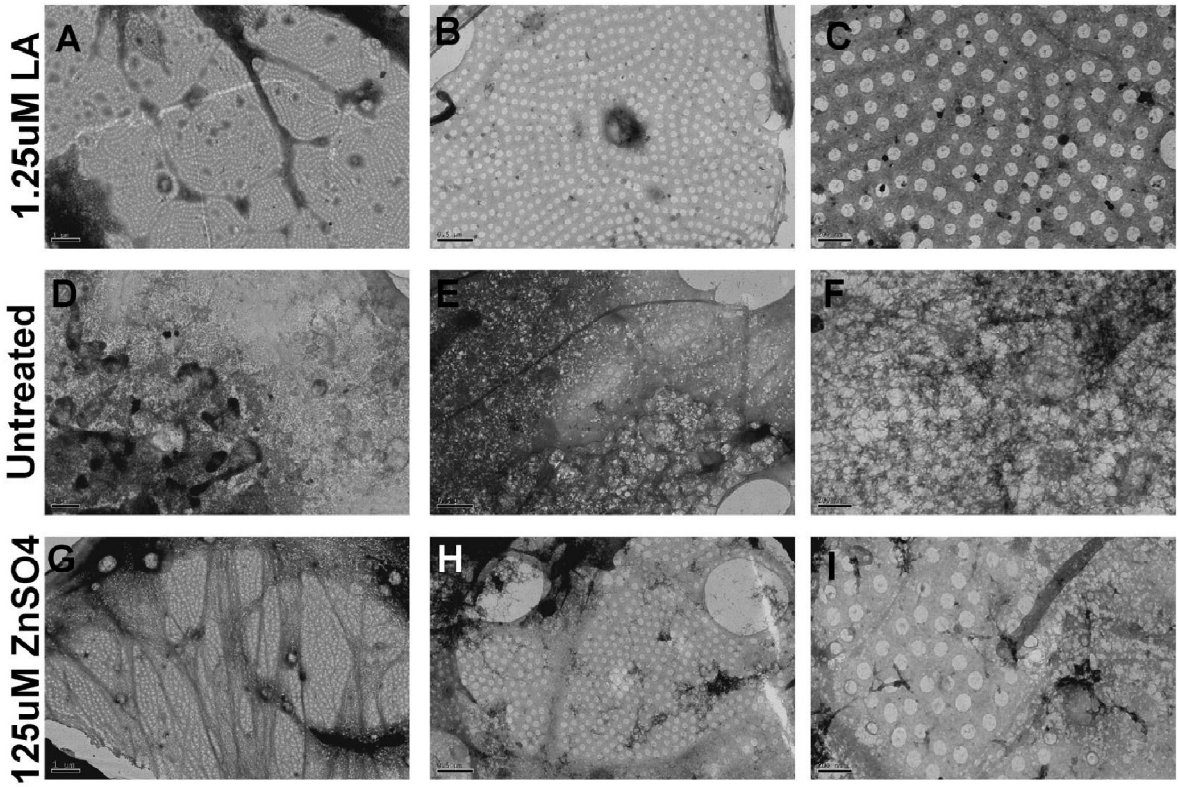

Figure 6-7 – TEM pictures showing fenestrae formation

Transmission electron microscopy showed fenestrae formation after treatment with 1.25µM Latrunculin A (LA) (Panels A,-C) and 125µM added ZnSO4 (Panels G-I). Fenestration was not observed in untreated cells (Panels D-F). Panels A-G showed formation of fenestrae at 800x magnification, where extensive changes in cellular cytoskeleton was observed in cells treated with LA (Panel A), zinc treatment forms smaller areas of fenestration without extensive cytoskeletal arrangements (Panel G). At higher magnifications, LA treatment forms highly uniform fenestration pores (Panel B 5000x, scale bar 1µm. Panel C 12000x, scale bar 0.5µm) and zinc treatment forms smaller areas of fenestration, also with uniform size (Panel H 5000x, Panel I 12000x, scale bar 200nm). Images taken with JEOL10TEM.

Furthermore, we would like to compare the size of fenestrae formed $ZnSO_4$ treatment compared to those formed by LA.

Methods:

Six pictures and four pictures of 12000x magnification were randomly taken from LA and zinc sulphate treated bEND5 cells from three different experiments respectively. Areas with fenestrae were imported into ImageJ software. After removal of speckles and outliers, the area and diameter of individual fenestrae were determined. Objects less than 40nm in diameter were rejected as it had been determined from manual observations that the smallest of the fenestrae assessed was 46nm in diameter.

Results:

The size of 393 fenestrae from $ZnSO_4$ treated samples, and 775 fenestrae from LA treated samples were estimated. Fenestrae of LA-treated cells were 74 ± 19 nm in diameter and those from $ZnSO_4$ treated cells were 67 ± 14 nm.

The size distributions for zinc and LA-treated cells are as follows. In zinc treated samples, 20.9% of the fenestrations formed were of 45-64nm in size, compared to 9.7% in LA treated group. 22.4% were of 55-65nm size in ZnSO4 treated samples compared to 23.0% in LA treated group. Most fenestrations formed were 65-74nm diameter, with 31% of ZnSO4 treated group and 24.8% of LA treated group falling into this category. 13.0% of ZnSO4 treated group formed fenestrations 75-84nm in size compared to 24% in LA treated group. The data indicate that the sizes of fenestrae formed are variable in both treated groups. Zinc induced fenestration formed more fenestrae in the 45-54nm group compared to LA which have more fenestrae in the 75-84nm range (Table 6.1, Figure 6.8).

Table 6-1 - Total fenestrae formed in $ZnSO_4$ and LA treated groups. Four and 6 pictures were analysed for ZnSO4 and LA- treated groups respectively.

	% of Total Fenestrae Formed	
	125 uM ZnSO4	1.25 uM LA
45-54	20.9	9.7
55-64	22.4	23.0
65-74	31.0	24.8
75-84	13.0	24.0
85-94	8.7	8.1
95-104	2.0	4.4
105-114	0.5	1.9
115-124	0.5	1.7
125-134	0.3	0.9
135-144	0.0	0.4
145-154	0.0	0.1
155-164	0.0	0.3
165-174	0.0	0.4
>175	0.8	0.4
Fenestrae analysed	393	775
Pictures analysed	4	6

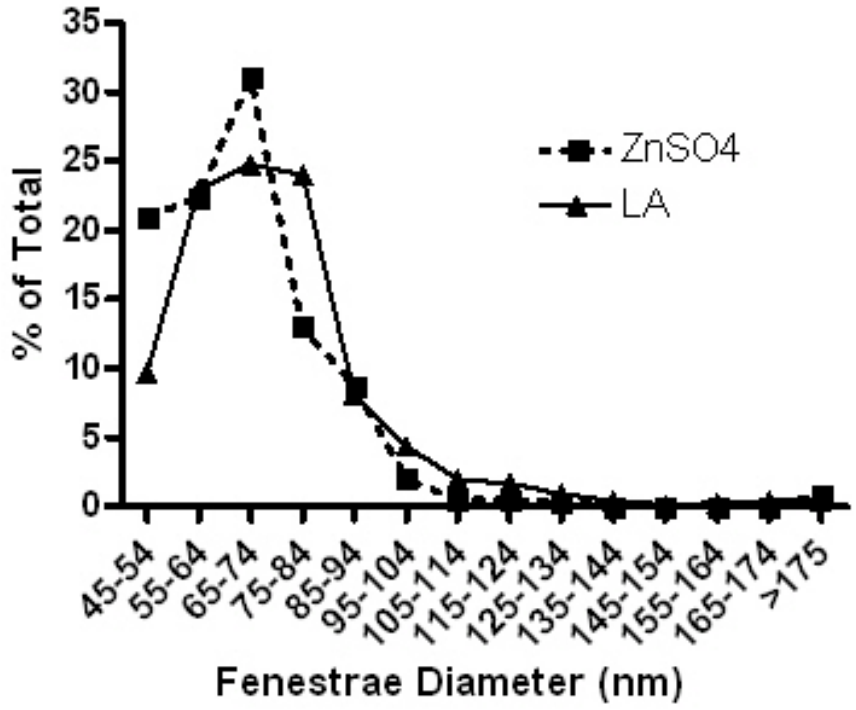

Figure 6-8 – Sizes of fenestrae were measured in $ZnSO_4$ and LA treated bEND5 cells. Treatment with ZnSO4 and LA resulted in formation of fenestrae of various sizes. Data are expressed as percentage of total fenestrations formed against the diameter in nm and summarised in Table 6.1

6.5. **Cell Viability Assays**

$ZnSO_4$ treatment to up to 150μM was not found to be overtly toxic. Based on MINEQL (Environmental Research Software, Hallowell, USA) calculation, the bio-available zinc concentration present in DMEM high glucose used for bEND5 cells is <1.0μM zinc (Professor Richard Thompson, personal communication). We have shown here that using $ZnAF_2$ measurement, addition of 125μM added $ZnSO_4$ the bioavailable zinc concentration is ~370-500 nM. However above, 200 μM of added $ZnSO_4$ abnormal nucleus shape signalled cell toxicity.

Methods:

To gain a better understanding of cellular viability, calcein AM and propidium iodide staining were used to measure the extent of cell death in our assays. Propidium iodide is a DNA intercalating agent, which stains the nucleus of necrotic or apoptotic cells. In contrast to the cell-impermeant nature of propidium iodide, Calcein AM is a highly cell-permeant fluorescent dye, which fluoresces strongly selectively in live cells.

Results:

Figure 6.8 shows that bEND5 cells untreated, treated with 1.25 μM LA or125μM $ZnSO_4$ for three hours or treated with 125μM $ZnSO_4$ for 20 hours showed no sign of cell death. In all four groups, the green Calcein AM staining could be seen clearly highlighting the shape of the cells.The two main phenotypes of the cells, a smaller more elongated shape and larger more rounded cells were present in all four tested groups. In LA treated groups, the rearrangement of cytoskeletal network could be seen through the calcein dye.

Qualitative assessment of the cells does not indicate a difference in the cell numbers as assessed through calcein staining, while the lack of propidium iodide staining showed no evidences of cell death. No floating cells were observed in any of the experiments.

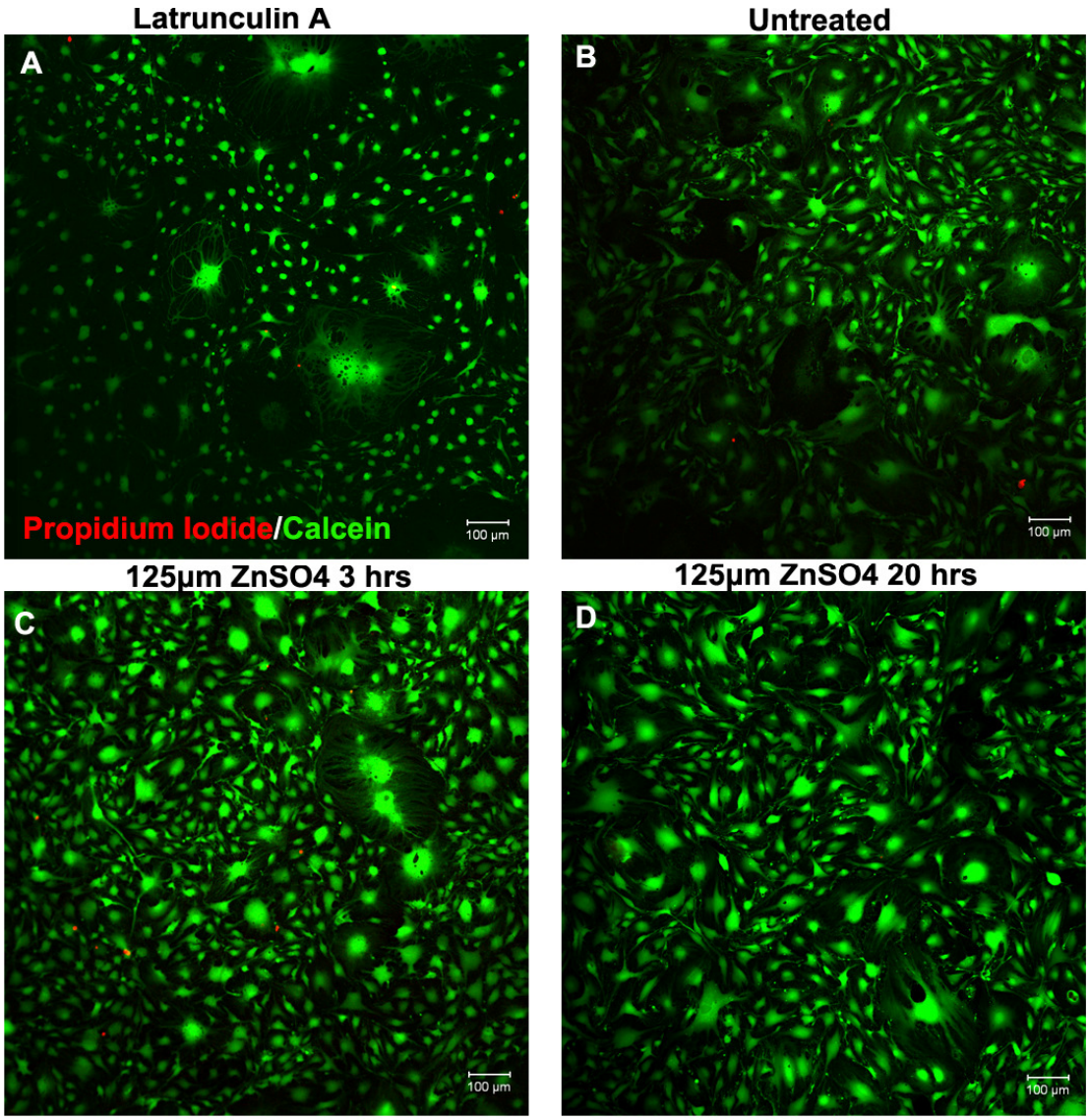

Figure 6-9–Calcein assay and propidium iodide staining in bEND5 cells

The use of propidium iodide and calcein AM allows the differentiation between dead and live cells. Panel A shows bEND5 cells treated with 1.25µM LA, Panel B shows untreated cells. Panel C and D shows cells treated with 125µM $ZnSO_4$ for 3 and 20 hours respectively. The calcein staining (green) shows that cell viability was preserved after zinc treatment (Panel C and D), and there is a lack of propidium iodide staining in all treated and untreated groups. Representative images taken from 3 independent experiments. Scale bar 100µm.

6.6. **Treatment of bEND5 Cells with Other Divalent Metals**

In order to explore the specificity of zinc, the effects of various divalent metals on fenestrae formation was examined. The selection of metals was based on results obtained on synchrotron X-ray fluorescent studies on Bruch's membrane and sub-RPE deposits which showed that apart from zinc, there is an accumulation of copper, iron, nickel, calcium, magnesium and cadmium (Lengyel unpublished data) (Wills et al., 2009).

Methods:

Equimolar (125 uM) concentration of $CaSO_4$, $FeSO_4$, $CuSO_4$, $NiSO_4$, $MgSO_4$ and $CdSO_4$ were used to treat bEND5 cells for 20 hours. Treatment of cells with 125µM $CuSO_4$ and 30uM $CdSO_4$ severely compromised cell viability. Cadmium sulphate treatment caused all the cells to die (data not shown), while $CuSO_4$ treated samples had visible nuclear blebbing, shrinking cells and compromised actin structure (Figure 6.11 M-P). Therefore these metals were not examined further in any detail. To assess the effectiveness of divalent metals in inducing fenestrae formation we followed the characterisation steps described for zinc. Namely we visualized changes in PV-1 and actin distribution followed by whole mount TEM to determine whether fenestrae were formed. Results were compared to untreated, 125 µM ZnSO4 treated and 1.25 uM LA treated cells.

Results:

Treatment of bEND5 cells with $CaSO_4$ (Figure 6.10 Panel I-L) showed PV-1 rearrangement but only at the edges of the cells.TEM results confirmed the presence of fenestration here (Figure 6.12 Panel E-F), but these fenestrae were much sparser, though similarly sized,to those formed in the presence of zinc (~65nm diameter). Following treatment with $FeSO_4$, PV-1 formed large clumps rather than sieve plates (Figure 6.11 Panel E-H) although fenestrae formation is clearly visible on TEM (Figure 6.12 Panel G-H). These fenestrae, however, were sparsely distributed, just like in the case of $CaSO_4$, and there were several areas with only misshapen but very large fenestrae. Nickel sulphate treatment produced sieve plate formation only rarely (approximately 10 cells per cover slips) (Figure

6.10 Panels M-P). However, in these cells sieve plates looked similar to those seen with zinc. Despite the similarity in sieve plate formation in $NiSO_4$ treated cells we could not see fenestrae by TEM (Figure 6.12 Panels I-J). Magnesium sulphate (Figure 6.11 I-L) did not lead to sieve plate or fenestrae formation. Visible change in actin staining could be observed in some of the metal treated cells, most visibly in $CuSO_4$, $CaSO_4$ and $MgSO_4$ treated samples. In $CuSO_4$ treated samples, changes in actin staning could be seen in the cytoskeletal changes related to the cell death. In $CaSO_4$ and $MgSO_4$ treated cells, there is visible activation of stress fibers as seen through rhodamine phalloidin staining of the actin cytoskeleton.

We also showed that confluent cell layers behave similarly to disperse invididual cells. Treatment of bEND5 cells with equimolar concentrations of with $ZnSO_4$, $CaSO_4$ and $NiSO_4$ (125μM) shows the same observation as before (Data not shown). Treatments with these metals but not LA produced cells with normal actin structures and normal nuclear staining. Treatment with 125μM $FeSO_4$ and 125μM $MgSO_4$ did not provoke fenestration (Data not shown).

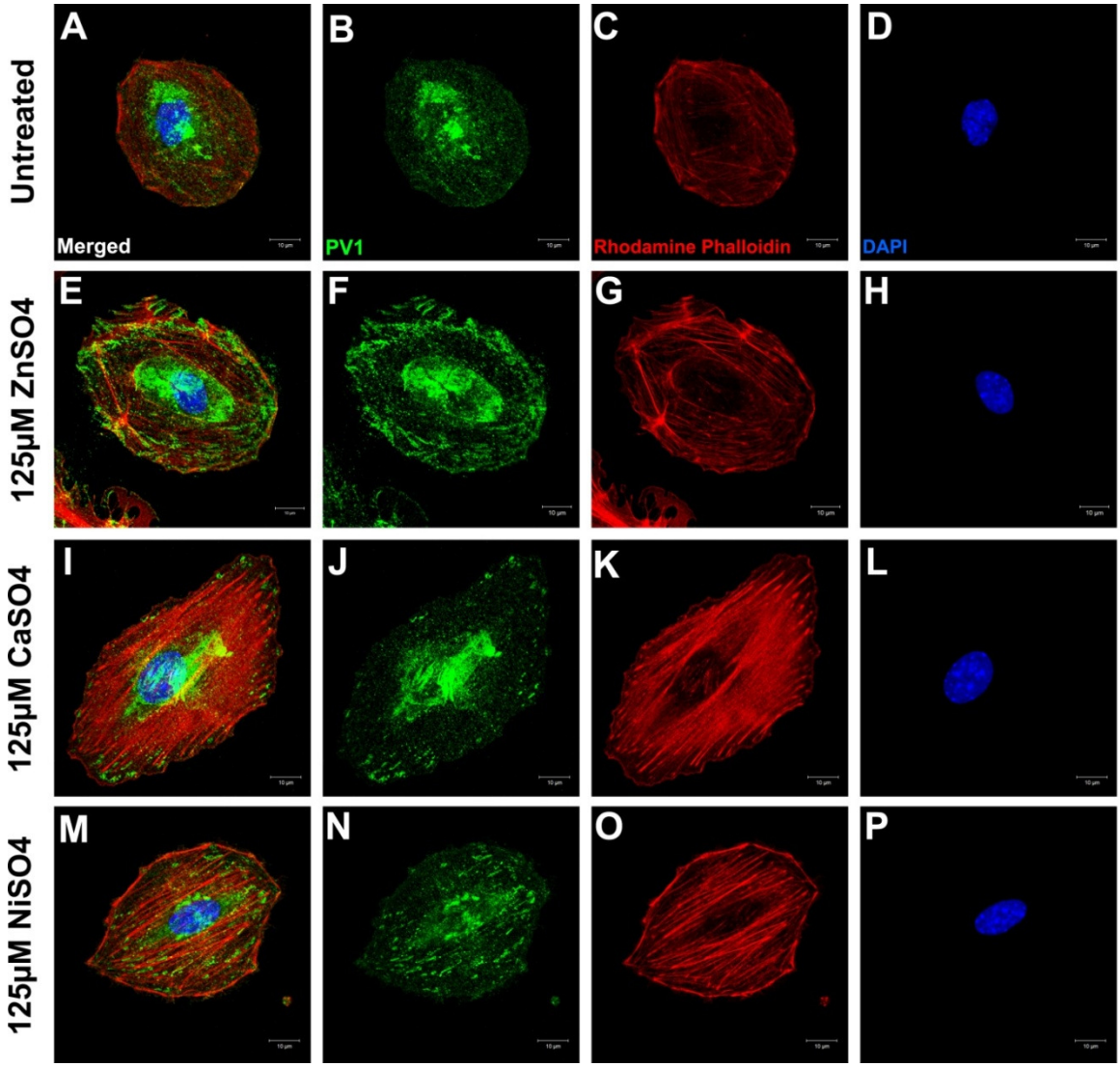

Figure 6-10 – Effect of divalent metals on fenestrae formation

Treatment of bEND5 cells with equimolar concentrations of 125µM added ZnSO4(Panels E-H), CaSO4(Panels I-L), and NiSO4 (Panels M-P) for 20 hours showed rearrangement of PV-1 protein which is not seen in the untreated cells (Panels A-D). Actin staining conducted using Rhodamine Phalloidin does not show cytoskeletal rearrangements (Panels C,G,O) with the exception of calcium (Panel K), which shows activation of stress fibers. with exception of CaSO. Pictures were taken using LSM700 confocal microscope at 60x magnification. All scale bars = 10µM.

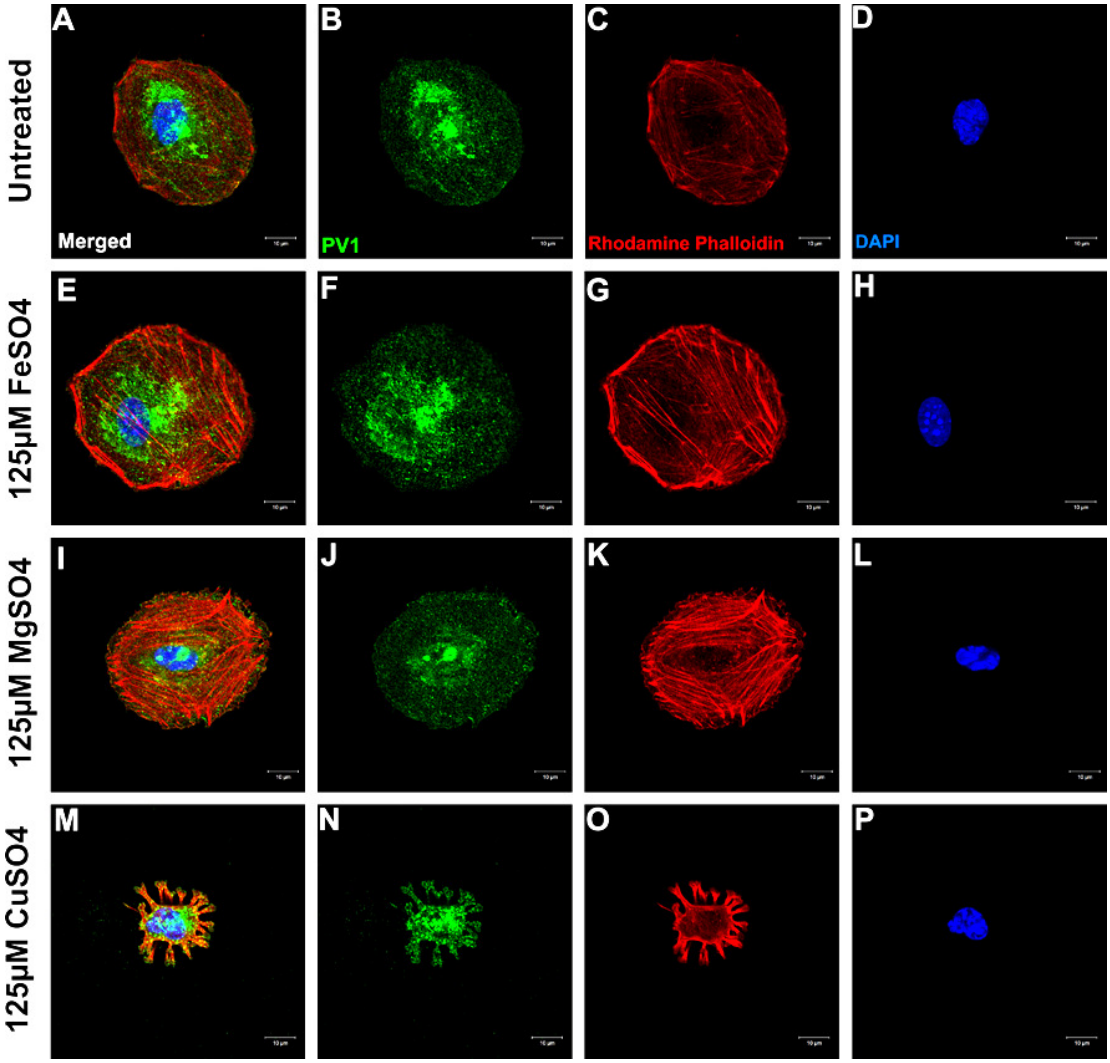

Figure 6-11- Effect of divalent metals on fenestrae formation

Treatment of bEND5 cells with equimolar concentrations of 125µM added $FeSO_4$(Panels E-H), $MgSO_4$(Panels I-L), and $CuSO_4$ (Panels M-P) for 20 hours showed no rearrangement of PV-1 protein compared to untreated cells (PanelsA-D). PV-1 staining was done using anti-PV1 antibody and Alexa 488 secondary antibody. Actin staining does not show cytoskeletal rearrangements (Panels C,G,O) with the exception of magnesium (Panel K), which shows activation of stress fibers. conducted using Rhodamine Phalloidin does not show significant cytoskeletal rearrangements apart from $CuSO_4$-treated group (Panel O). Pictures were taken using LSM700 confocal microscope at 60x magnification. All scale bars = 10µM

Figure 6-12–Effect of divalent metals on fenestrae formation (TEM)

Transmission electron microscopy showed fenestrae formation after treatment with equimolar (125µM), $ZnSO_4$ (Panels C-D), $CaSO_4$(Panels E-F), $FeSO_4$(Panels G-H) and $NiSO_4$ (Panels I-J). Fenestration was not observed in untreated cells (Panels A-B). $ZnSO_4$ treatment produces fenestrate with varied sizes. Fenestrae formed after $CaSO_4$ treatment is limited to the periphery. $FeSO_4$treatment produced patch of fenestration within the cells. $NiSO_4$treatment failed to produce fenestration. Panels A,C,E,G,I at 5000x magnification and panels B,D,F,H,J at 12000x magnification. Scale bars = 5000x, 0.5µm, 12000x 200nm.

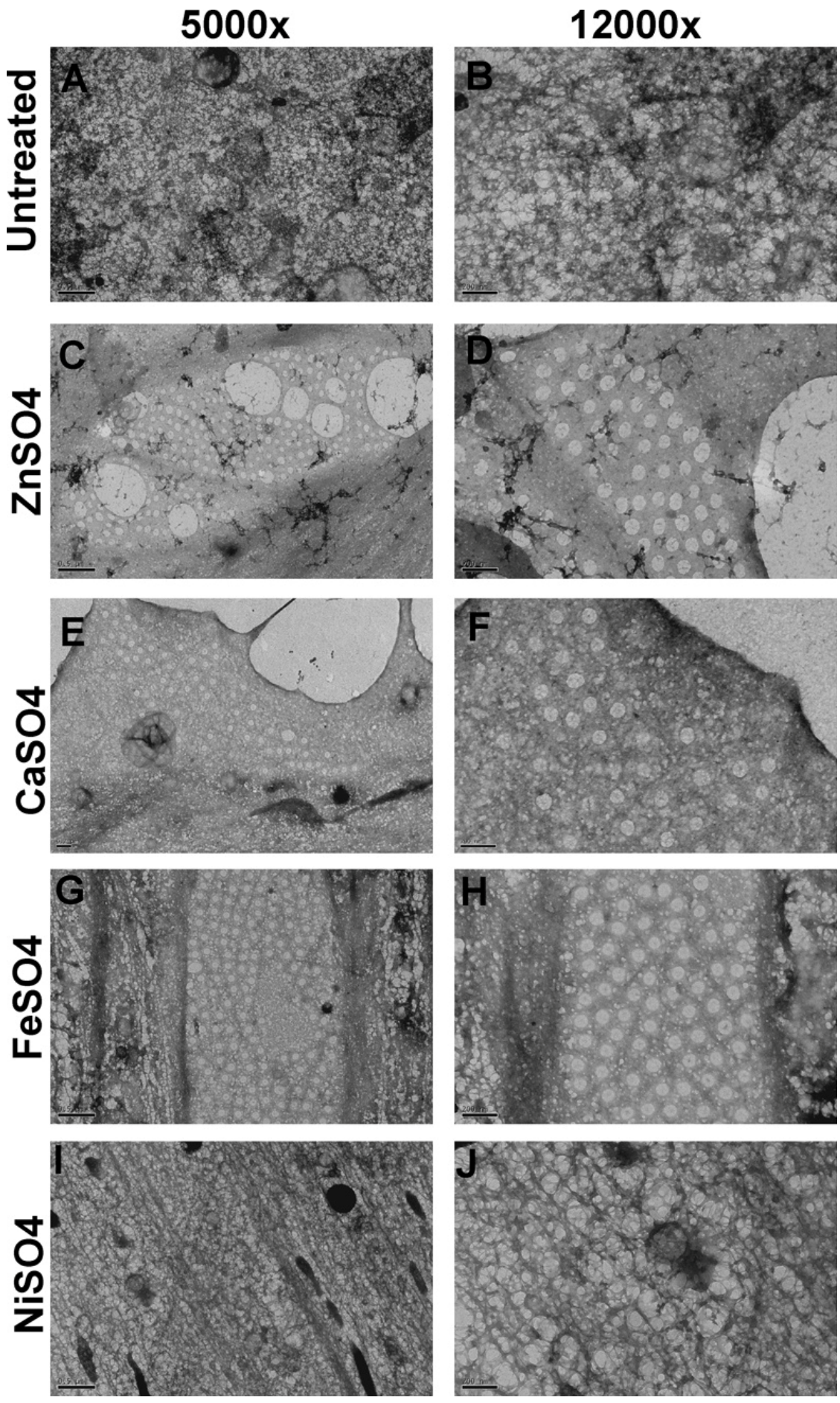
5000x
12000x
Untreated
ZnSO4
CaSO4
FeSO4
NiSO4
A
B
C
D
E
F
G
H
I
J

6.7. **Possible Signalling Pathway(s) Involved in Zinc – Induced Fenestration**

Activation of extracellular-signal-regulated kinases (ERK1/2) kinase pathway is crucial for formation of fenestrae as inhibiting ERK1/2 prevented PV-1 up-regulation (Stan, et al 2004). It is also known that expression of PLVAP, the gene for PV-1, is dependent on kinases such as p38 and phosphatidylinositol 3-kinases (PI3K) (Strickland et al Pathology 2005). In fact, these proteins are part of the signalling cascade for VEGF, that stimulates fenestrae formation, as well as nicotine that inhibits it. In addition these molecules are affected by zinc itself. In this section we aim to understand whether phosphorylation of ERK is involved in zinc induced fenestration.

Methods:

To identify the molecules involved in zinc-induced fenestrae formation we explored information available in Ingenuity Pathway Analysis (IPA, Ingenuity Systems, Inc., California, USA). Using the "grow" and then the "connect" functions in pathway builder in IPA the molecules shared by VEGF, nicotine and zinc signalling pathways were explored (Figure 6.13). Amongst the several overlapping molecules there were ERK1/2, IP3 and NFkB that were shared by all three molecules. Akt is shared between VEGFand nicotine while Src is shared between VEGFA and zinc. Interestingly, p38 is only connected to zinc. Naturally, IPA may not contain all possible relevant data, but nevertheless indicated that molecules that have been suggested to be involved in PV-1 regulation and fenestrae formation are shared by these signalling molecules.

The way some of these molecules are involved in signalling is through phosphorylation. Therefore, we treated bEND5 cells with 125 uM zinc for 20 hours then lysed the cells and proteins were separated on SDS-PAGE, blotted to Nitrocellulose and probed for phospho-specific antibodies and antibodies that detect both the phospho- and non-phospho- forms of ERK1/2, PI3K,, P38, and AKT.

Results:

Our results indicated that phosphorylation of ERK1/2 or pERK1/2 at all time points (Figure 6.14) does not seem to be involved in zinc-induced fenestration suggesting that other kinases would be responsible. However, beta-actin expression seems to gradually increase up to one hour and returns back to normal at 20 hours. The pictures are representative diagrams from three independent experiments.

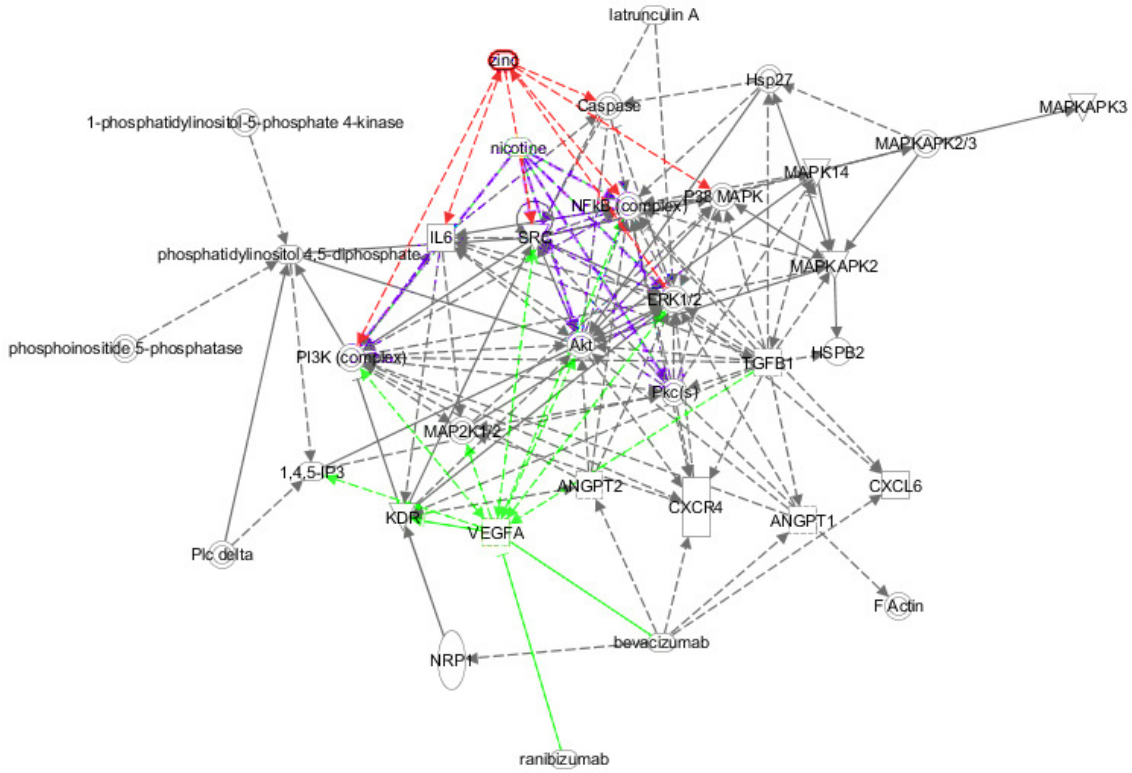

Figure 6-13–Relationship between VEGF, nicotine and zinc

Ingenuity Pathway (IPA) software showed relationship of VEGF, nicotine and zinc, the three molecules which have been shown to be involved in AMD. Using the "grow" and "connect" functions, various signalling pathways were explored. VEGFA affected KDR, 1,4,5-IP4, PI3K, ANGPT2, AKT, SRC, ERK1/2, bevacizumab and ranibizumab. Zinc affects PI3K, IL6, SRC, ERK1/2, P38, NFκB, and caspase. Nicotine affects SRC, PI3K, Akt, Pkc, ERK1/2 and NFκB. Shared and overlapping pathways have been summarised in table 6.2.

Table 6-2 - Overlapping pathways between VEGFA, zinc and nicotine.

No	VEGFA	Zinc	Nicotine
1	PI3K	PI3K	PI3K
2	ERK1/2	ERK1/2	ERK1/2
3		NFkB	NFkB
4	AKT		AKT
5	SRC	SRC	
6		PKC*	PKC
7		P38	

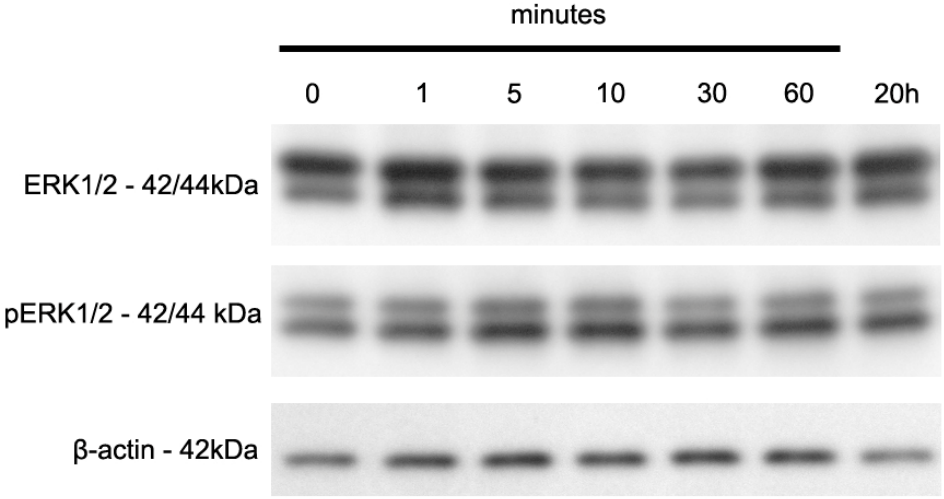

Figure 6-14–Phosphorylation of ERK1/2 is not involved in fenestrae formation

Probing of 10µg untreated (first lane) and 125µM $ZnSO_4$ treated for 1, 5, 10, 30, 60 minutes and 20 hours revealed that there is no increase in ERK1/2 phosphorylation, nor of its phosphorylated form pERK1/2. Beta-actin expression seems to increase after 1 minute and sustained up to 1 hour before decreasing again at 20 hour time point. Picture is representative from three independent experiments.

6.8. **Discussion**

The hypothesis to be tested in this chapter was that zinc was involved in fenestrae formation in endothelial cells. Data presented support this in that zinc can induce fenestration. Furthermore, elements of the signal transduction cascade that is involved in the zinc induced signalling leading to fenestration have been identified. To our knowledge this is the first demonstration of zinc-dependent fenestrae formation.

Zinc and VEGF

The choroidal vasculature differs from the retinal vasculature in that it is fenestrated (Bernstein and Hollenberg, 1965). In 1986, Mancini *et al* published that the fenestrations found in the choriocapillaris were not randomly distributed, but they were found predominantly in the endothelium closest to the RPE (Mancini et al., 1986)(Mancini et al 1986). The endothelium thickens further away from the RPE and it was speculated that there might be a signal from the RPE that "polarizes" the endothelium and induces the fenestration formation (Mancini et al., 1986). Fenestrae initially increase with age but in advanced age the number of fenestrae decreases (Burns and Hartz, 1992). This is further affected by age related pathologies like AMD (McLeod et al., 2009). At present the major signal that controls fenestration is believed to be Vascular Endothelium Growth Factor (VEGF). Esser et al described VEGF basally secreted by RPE as a regulator of angiogenesis and vascular permeability (Esser et al., 1998). When adrenal cortex capillary endothelial cells were co-cultured with epithelial cells transfected with VEGF 164 and VEGF120 many fenestrae were induced on the endothelium (Esser et al., 1998). Furthermore, treatment of adrenal cortex endothelial cells with VEGF165 or fibroblast growth factor (FGF) showed that fenestrations could be induced by VEGF but not FGF (Saint-Geniez et al., 2009b). There are three VEGF isoforms but only VEGF120 and VEGF164 can induce fenestration VEGF188 cannot (Saint-Geniez et al., 2009b , Saint-Geniez 2009 PNAS). Loss of fenestration in the VEGF188 expressing animal model led to formation of sub-RPE deposits providing evidence that supports the notion of a link between fenestrationin AMD (Saint-Geniez et al., 2009b). There is an inverse correlation between zinc levels and VEGF production. Treatment of PC-3 and DU-145 prostate cancer cell lines with

TPEN, a zinc selective chelator, at 2-8μM for 2 hours suppressed VEGF levels (Golovine et al., 2008). Zinc chelation in HT-29, another prostate cancer cell line, also reduced the level of VEGF (Gurusamy et al., 2011). Overexpression of hZIP1 protein, a plasma membrane zinc transporter that imports zinc into cells, also inhibited VEGF production (Golovine et al., 2008). The mechanism behind the effect of zinc on lowering VEGF levels is thought to be through the inhibition of transcription of hypoxia inducible factor (HIF-1) a pro-angiogenic factor often associated with the aggressiveness of tumours (Nardinocchi et al., 2010).

Zinc and PV-1

In our experiments a surrogate marker for fenestrae formation was the redistribution of Plasmalemmal Vesicle Associated Protein-1 (PV-1) into the so called sieve plates. PLVAP (the gene encoding PV-1) encodes a TypeII transmembrane glycoprotein that is associated with the caveolae of fenestrated microvascular endothelial cells. It is normally expressed in the lung, liver, kidney, immature brain and in the eye (Stan, 2007). This protein is only associated with fenestraethat have diaphragms, these being formed by PV-1 dimers (Stan, 2007). RNA silencing of PLVAP expression led to large variability in fenestrae diameter providing support that this protein does controls the size of fenestrae (Ioannidou et al., 2006). The fact that the diameter of zinc-induced fenestrae was similar to those requiring PV-1 *in vivo* or following LA treatment suggested zinc-induced fenestration does involve PV-1. It is not known whether zinc or any metals could directly affect PV-1 or PLVAP. Our search did not locate any metal response element transcription factor up to 1000bp upstream of the 5' un-translated region of PLVAP gene therefore it is not very likely that altered zinc balance would lead to regulation of gene expression and recent zinc supplementation experiments in our laboratories did not demonstrate changes in PLVAP expression of this gene (Barzegar-Befroei and Lengyel, personal communication). It seems probable, therefore, that sieve plate formation and formation of fenestrae does not involve direct PV-1/zinc interaction.

It is believed that the formation of fenestrae requires the reorganization of the cytoskeleton. It had been reported that zinc, and several other divalent metals, can affect polymerisation of actin, although only at very high (>300 uM) concentrations

(Strzelecka-Golaszewska et al., 1978). At the levels of bio-available zinc in our experiments (~200 nM) we did not see discernable evidence for actin remodelling, although we cannot rule out local changes in the cytoskeleton around the zinc-induced sieve plates. Therefore we assume that fenestrae formation in our experiments is unlikely to be due to a direct zinc/cytoskeleton interaction.

Zinc can be toxic to cells (Bozym et al., 2010). However, treatment of bEND5 cells with up to 150 µM externally added $ZnSO_4$ did not appear to be toxic to these cells, as shown by a calcein/propidium iodide assay. Similar concentrations of extracellular zinc have been widely used in other studies with success. Richard *et al* added 150µM of zinc chloride to cultured human skin fibroblasts and noted that these concentrations,in the presence of FCS, lowered the concentration of thiobarbituric acid reactants as a marker of lipid peroxidation (Richard et al., 1993). In Chinese Hamster Ovary (CHO) cells, addition of up to 100µM zinc chloride to media supplemented with FCS increased metallothionein levels within the cells without inducing toxicity (Wallace et al., 1995). It is particularly important to emphasize that the high concentration of externally added zinc does not translate to equal amount of bio-available zinc. We and others (Bozym et al., 2006, Bozym et al., 2010) found that growth media with FCS very strongly buffered zinc levels, keeping bio-available zinc < 1 uM. It is interesting to note that in the absence of added zinc, but in the presence of FCS, cells are potentially in a zinc deficient environment (Bozym et al., 2010, Bozym et al., 2006). This might need to be taken into account when results on cultured cells are interpreted. Overall, it appears unlikely that the zinc-induced fenestration of bEND5 cells would, per se be associated with toxicity.

We have also examined the specificity of zinc-induced fenestrae formation by treating bEND5 cells with $CaSO_4$, $FeSO_4$, $NiSO_4$, $MgSO_4$, $CdSO_4$ and $CuSO_4$. While $CdSO_4$ and $CuSO_4$ were toxic to cells, other divalent metals except Mg SO4 were able to induce either PV-1 rearrangement, fenestrae formation or both. However, these effects were marginal compared to the reliable sieve plate and fenestrae formation seen in the presence of zinc. Interestingly NiSO4 was able to induce sieve plate formation in a few cells, but this was not accompanied by fenestrae formation. This suggests that PV-1 reorganization is not sufficient to

induce fenestration. Based on the results with divalent metals it is concluded that fenestrae formation was not specific to zinc but is most prominent in zinc-treated cells.

The formation of stress fibers observed in $CaSO_4$, and $MgSO_4$ treated cells may be mediated through activation of Rho GTPases. The activation of Rho GTPases is particularly important in cellular movement, particularly in cellular migration through extension of lamellipodium, and cell contraction (Manneville and Hall, 2002). The cellular movement and contraction is achieved through changes in stress fibers, a structure formed of myosin II, and actin filaments (Nobes and Hall, 1995). Studies have reported the role of calcium and magnesium in regulating Rho GTPases in various cells. Katoh and colleagues reported that isolated stress fibres in vitro can be activated using calcium and ATP through phosphorylation of myosin light chain (Katoh et al., 1998). Calcium has also been shown in regulating Rho GTPases in adrenal chromaffin cells (Gasman et al., 1999), and plant pollen tubes (Yan, Xu, and Yang, 2009). It is known that Rho-GTPases induce endothelial cell permeability (Wójciak-Stothard et al., 2001) and magnesium is essential for activity of Rho-GTPase activating proteins (Zhang et al., 2000). As we did not observe fenestration in either magnesium or calcium, it is possible that these two metals have effect on proliferation of or activate other mechanism in bEND5 cells. Such effect has been seen in human umbilical vein endothelial cells (HUVECs) treated with physiologically viable millimolar concentrations of magnesium. Increased proliferation was observed, as well as increased nitric oxide level, suggesting that magnesium treatment may have vasodilatative effect on endothelial cells (Maier, et al., 2004). It would be interesting to do functional assay on Rho-GTPase activation on magnesium or calcium treated bEND5 cells to observe how these metals affect the cell line.

Twenty hours treatment of bEND5 cells with >30µM $CdSO_4$ results in nuclear blebbing, major cell contraction and cytoskeletal rearrangement. This is probably not surprising, considering various other studies have reported on the toxicity of cadmium on endothelial cells. Loss of stress fibers and cytoskeletal rearrangement have been reported in MDCK cells treated with very high (500µM) concentration of cadmium (Hernandez et al., 1989). Using egg yolk angiogenesis assay, it was

shown that treatments with as low as 1μM cadmium chloride reduces angiogenesis and wound healing, an effect possibly mediated by lowered production of nitric oxide (Kolluru, et al., 2006). It needs to be stressed that unlike the zinc concentration, we did not optimize the concentration of cadmium. It is likely that >30μM of cadmium exceeds the buffering capacity of bEND5 cells which activated the pro-apoptotic mechanisms

The fenestration induced by zinc appears to be a relatively slow process as we did not observe sieve plate formation by light microscopy until 9 hours after the start of the treatment. However, formation of some fenestrae can be seen as early as 3 hours of zinc treatment by TEM. The process appears to be concentration dependent requiring the increase in bio-available zinc to ~200 nM for a reliable and repeatable effect. This corresponds to 125 μM added zinc. The environment the choroidal capillaries are nested in is high in zinc including bio-available zinc (Lengyel et al., 2007). Indeed, bio-available zinc can be readily detected adjacent to the fenestrated choroidal capillaries in ex *vivo* human eyes (Figure 6.15, courtesy of Gango and Lengyel, Unpublished) by autometallography, providing evidence that zinc is present around the choriocapillaris and potentially able to initiate a cascade of events leading to fenestration. Based on literature data on fenestrae formation and signalling by VEGF (inducing fenestration), nicotine (inhibiting fenestration) and zinc we developed a model using IPA to explore whether phosphorylation is involved in zinc-induced fenestrae formation. We identify here that ERK1/2 is not involved in regulating zinc-induced fenestration in bEND5 cells, suggesting that fenestration is mediated by other kinases or cellular processes.

Taken together, it is feasible to speculate that both zinc and VEGF are involved in regulating fenestration of the choroidal endothelium and individually or synergistically regulate fenestration at places like the RPE/choroid interface where there is high enough concentration of zinc to exert an effect. The potential for a dual regulation of fenestrae formation had not been previously described. This would allow both zinc and VEGF to participate in the health, and in fact pathology, of the outer retina-blood barrier.

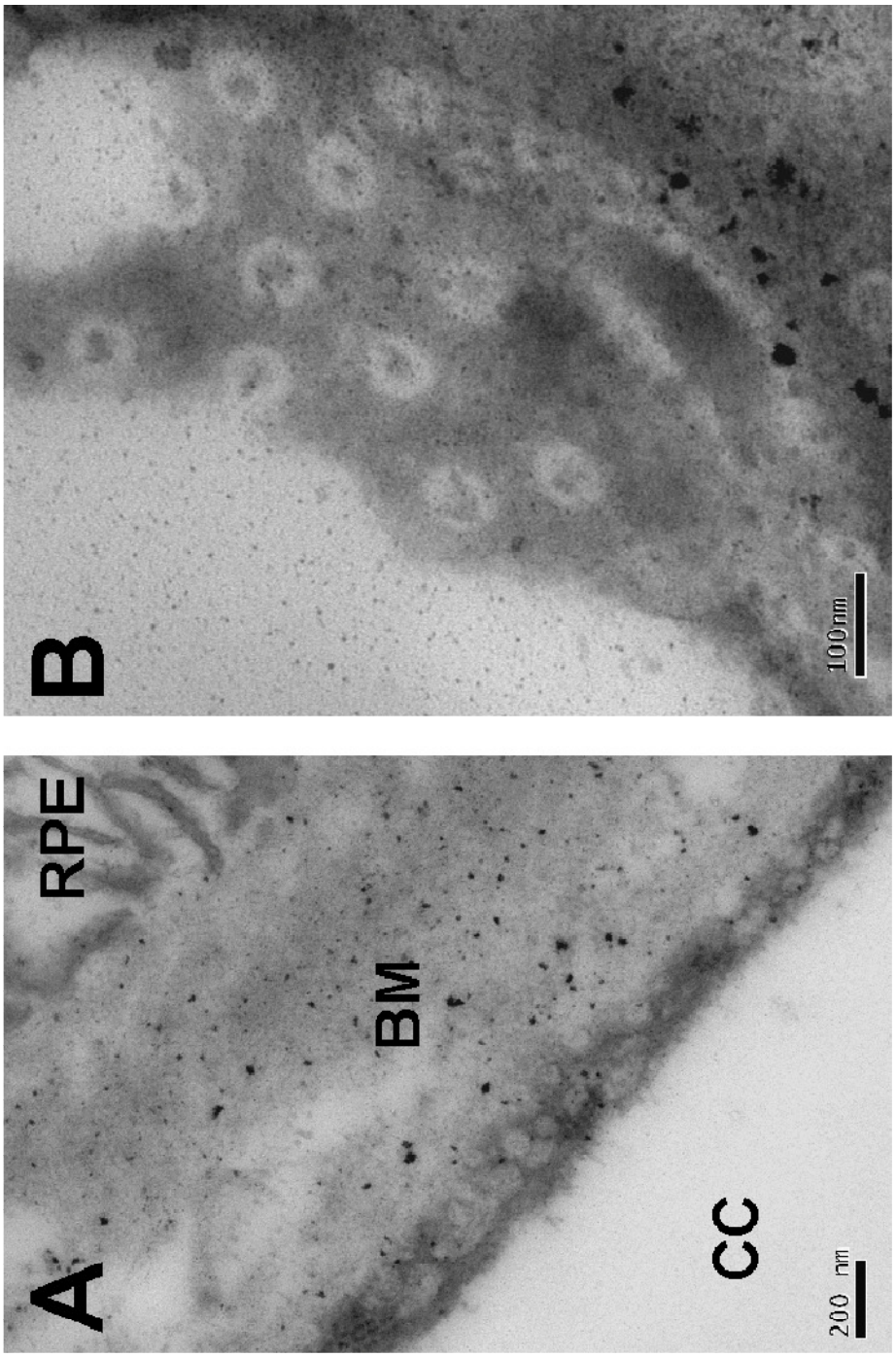

Figure 6-15–Bioavailable zinc in Bruch's membrane

Autometallography on ex vivo human eyes shows the presence of bioavailable zinc in the RPE-Bruch's membrane area (electron dense speckles) (Figure A, B) adjacent to the choriocapillaris (CC). Oblique sections show the presence of fenestrated endothelium (Figure A) between the BM and CC, where the diaphragm of the each fenestra is apparent at higher magnification (Figure B). RPE: Retinal Pigment Epithelium, BM: Bruch's Membrane, CC: Choriocapillaris. Scale bars: Figure A, 200nm, Figure B, 100nm.

6.9. **Further research**

Further experiments will be required to decide whether the model for dual action through both zinc and VEGF does really fit the *in vivo* situation. We will need to explore how fenestrae formation is affected when VEGF and zinc are present in the growth medium, an experiment that is already in the planning. It will also be interesting to see whether *in vivo* zinc deficiency in animals would alter fenestration of the choroidal capillaries and we are collaborating with Professor John Beattie at the Rowette Institute in Scotland to induce controlled zinc deficiency in mice. Zinc deficiency had been associated with loss of endothelial cell permeability (Di Cello et al., 2005). Whether in the choriocapillaristhis translates to loss of fenestrae will be exciting to explore. The generation of zinc deficiency in mice study is about to be finished and we will have the chance to analyse eyes for molecular and morphological changes. We will also need to explore further the molecular networks involved zinc-induced fenestration. Experiments are ongoing to identify the changes in protein phosphorylation in cell homogenates as well as in cells.

6.10. **Conclusion**

In conclusion we propose here that the under normal conditions, optimal zinc and VEGF levels are required to maintain a healthy outer retina-blood barrier including appropriate fenestration of the choriocapillaris. Pathological changes like thickening of Bruch's membrane or development of sub-RPE deposits will prevent VEGF and/or zinc to reach the choroidal microvessels as well as lead to entrapment of zinc in proteinaceous aggregates the impairment of clearance through the loss of fenestration will be seriously compromised. As sub-RPE deposit formation has been strongly associated with the choroidal capillaries (Lengyel et al., 2004, Mullins et al., 2011) the issue of altered zinc availability will probably need to be addressed. In fact, zinc supplementation has a positive effect on progression to end stage disease in AMD as described in the AREDS study no 8 (2001) and zinc supplementation had been shown to directly affect the RPE/choroid interface one of the steps in this positive effect might be through the reopening of fenestrae to provide better clearance of waste products.

7. General Discussion

Zinc is an indispensable and ubiquitous trace element present in many tissues in a wide range of organisms. The overall amount of zinc found in the human body is estimated to be 1.4-2.3 grams (Strauss, 2005). The highest tissue concentration of zinc in man is found in the RPE-choroid complex where the zinc content is 472 µg/g dry weight (Karcioglu, 1982). The high zinc concentration of zinc in the RPE-choroid complex is likely to be required for its function in regulating enzymes involved in the retinal cycle, phagocytic activity of the RPE and combating free radicals present in the RPE-choroid complex.

In 2004, Lengyel *et al* reported that sub-retinal RPE deposits contained a very high>500 ppm of zinc (Lengyel et al., 2007). This observation raises questions about where zinc in the RPE-choroid interface is coming from, and how it reaches the sub-RPE space. Furthermore, it remains unknown whether the bioavailable zinc found in Bruch's membrane (see Figure 6.15) is needed for RPE function, or whether it is involved in pathological processes. It is known that zinc deficiency is associated with age-related macular degeneration (AMD) (Newsome et al., 1988) and clinical trials have reported that zinc supplementation can delay AMD-associated vision loss (Ho et al., 2011a). This has highlighted the need to better understand how zinc is metabolised and transported at the RPE/choroid interface. At the outset of this study, we aimed at obtaining support for this idea by examining three major areas.

We set out to study the largely unexplored zinc transporters at the RPE-choroid by determining the expression for all the 24 known zinc transporters genes at this site. In parallel with our work two other groups published partial characterisation of zinc transporter expression (Leung et al., 2008a, Rezaei et al., 2008a), highlighting potential antioxidative functions of zinc transporter proteins (Rezaei et al., 2008a). Throughout this basic characterisation we identified ZIP12 protein as a potentially important zinc transporter at the RPE-choroid interface based on its gene expression in cadaveric RPE. We acknowledge the major caveat contributed by the cross-contamination present within the cadaveric samples, and thereby suggest improvements in isolating RNA from cadaveric tissues to be carried out to improve the data presented in this thesis and to confirm that ZIP12 is indeed expressed in the

RPE. Other studies have suggested that ZIP12 protein appears to be specific to RPE, as shown by the Bergen group (Booij et al., 2010b). Based on this and the lack of published data on ZIP12, after a careful consideration we carried out a series of experiments to learn more of the function of this protein. ZIP12 turned out to be a zinc importer located at least partly on the plasma membrane. Therefore, it is likely that if ZIP12 is confirmed to be present in the RPE, it is likely to be involved in loading, or reloading zinc into RPE cells. While the association of ZIP12 polymorphisms or mutations with AMD was not examined in this thesis, we have started to analyze results of genome-wide association studies to look at whether polymorphism of SLC39A12, the gene for ZIP12, could be associated with AMD (in collaboration with Professor John Yates). In order to understand the protein's potential function, we started the characterisation of commercially available antibody as well as generating an antibody against ZIP12 to monitor the localisation and potential reorganisation of ZIP12 in tissue sections. The plasma membrane localisation predicted from sequence data was confirmed (Chapter 4) but further characterisation of the antibodies and its distribution in disease is awaited. This part of the project still has to overcome several obstacles as none of the antibodies could unambiguously detect ZIP12.

The high concentration of zinc present in the extracellular matrix between the RPE and the fenestrated choroidal capillaries called Bruch's membrane (Lengyel et al., 2007) gave rise to the speculation that zinc could be directly involved in modulating the RPE and/or the choriocapillaris. To explore one possible action, we exposed both epithelial and fenestrated endothelial cell lines to elevated extracellular zinc and found that both responded to increased zinc. ARPE19 cells changed their transepithelial resistance and RPE specific gene expression profile in response to zinc treatment. However, it is likely that the changes in transepithelial resistance are mediated by the effect of zinc on cell proliferation as assessed through alamarBlue assay. In parallel, using immunocytochemistry and electron microscopy we found that the presence of extracellular zinc by itself can induce fenestrae formation. These show that if bioavailable (free or easily releasable) zinc levels reach ~200-500 nM in Bruch's membrane it could directly affect both of these cell types. It has already been mentioned earlier that this concentration could

potentially be present in Bruch's membrane (Lengyel et al., 2007), and an even higher concentration might be available locally (Nan et al., 2011, Nan et al., 2008).

Based on the information above and data we obtained from literature we developed a model for zinc regulation and deregulation at the RPE-choroid interface (Figure 7.1). This model is based on the assumption that under normal conditions zinc (Figure 7.1 –A), derived from the RPE or the blood, can be maintained at a concentration that is sufficient for the regulation of enzymes like matrix metalloproteinases that play an important role in the maintenance of elasticity and permeability of Bruch's membrane (Hussain et al., 2011). The presence of zinc transporters on the plasma membrane will help to maintain zinc influx into the cells in order to create a "healthy" zinc balance. We speculate that this zinc balance will be important for maintaining the phenotype of the surrounding cells will help to maintain pigmentation and optimal functioning of RPE and will facilitate the maintenance of the fenestration of the choroidal endothelium.

In diseases like AMD this balance could be altered in several ways: As AMD is associated with systemic zinc deficiency, replenishment of zinc in Bruch's membrane from the circulation will be compromised. Possibly, a negative gradient could develop triggering the removal of zinc from Bruch's membrane. Zinc levels in the RPE have also been shown to decrease in AMD (Tate et al., 1995, Tate et al., 1999, Newsome et al., 1988) possibly due to decrease in pigment in parallel with accumulation of lipofuscin (Biesemeier et al., 2010, Schraermeyer et al., 1999) therefore replenishment from this source could also be compromised. A third factor that could contribute to the loss of biologically active zinc in Bruch's membrane is its entrapment in sub-RPE deposits (Lengyel et al., 2007).

Once the bio-available zinc levels dip below functionally required levels the reorganization of Bruch's membrane by metalloproteinases will be altered, potentially contributing to the thickening of Bruch's membrane. Furthermore, the loss of bio available zinc may trigger VEGF production in the RPE by signalling to the RPE that fenestration requires more VEGF. Zinc deficiency in Bruch's membrane could directlylead to elevated VEGF levels through the lack of regulation of VEGF expression by zinc (Golovine et al., 2008, Nardinocchi et al., 2010) in RPE. These eventually could lead to the development of choroidal

neovascularisation (CNV) or so-called wet AMD. Alternatively, through its potential direct effects on the RPE, zinc deregulation could lead to cell atrophy and the development of dry AMD.

Zinc supplementation could therefore have several direct or indirect effects on the RPE-choroid interface. By elevating zinc levels in the circulation (2001) zinc could potentially reverse the zinc deficiency in Bruch's membrane. While we do not know whether this happens, systemic injection of radioactive zinc has been shown to reach the RPE (Newsome et al., 1992). The most likely route for the selective enrichment of zinc in RPE is through the bloodstream/ choroidal capillaries and therefore Bruch's membrane. Elevated zinc might help to bring VEGF levels under control and help the reforming of fenestration to allow better clearance of waste material and the availability of zinc to regulate proteases could help the clearance process. Therefore, it is probably not surprising that zinc was able to slow the progression to blindness in wet AMD (2001)(AREDS report number 8).

In conclusion, we have shown the expression of zinc transporters in the RPE-choroid interface, as well as potential effects of altering extracellular zinc concentration on cellular models of vascular endothelium and retinal pigment epithelium. Based on our results, we have tried to model how zinc can affect the RPE-choroid interface. While the studies require further experimentation, it is hoped that the model and the results presented within this PhD will perhaps help refine our current understanding and treatment strategies for AMD.

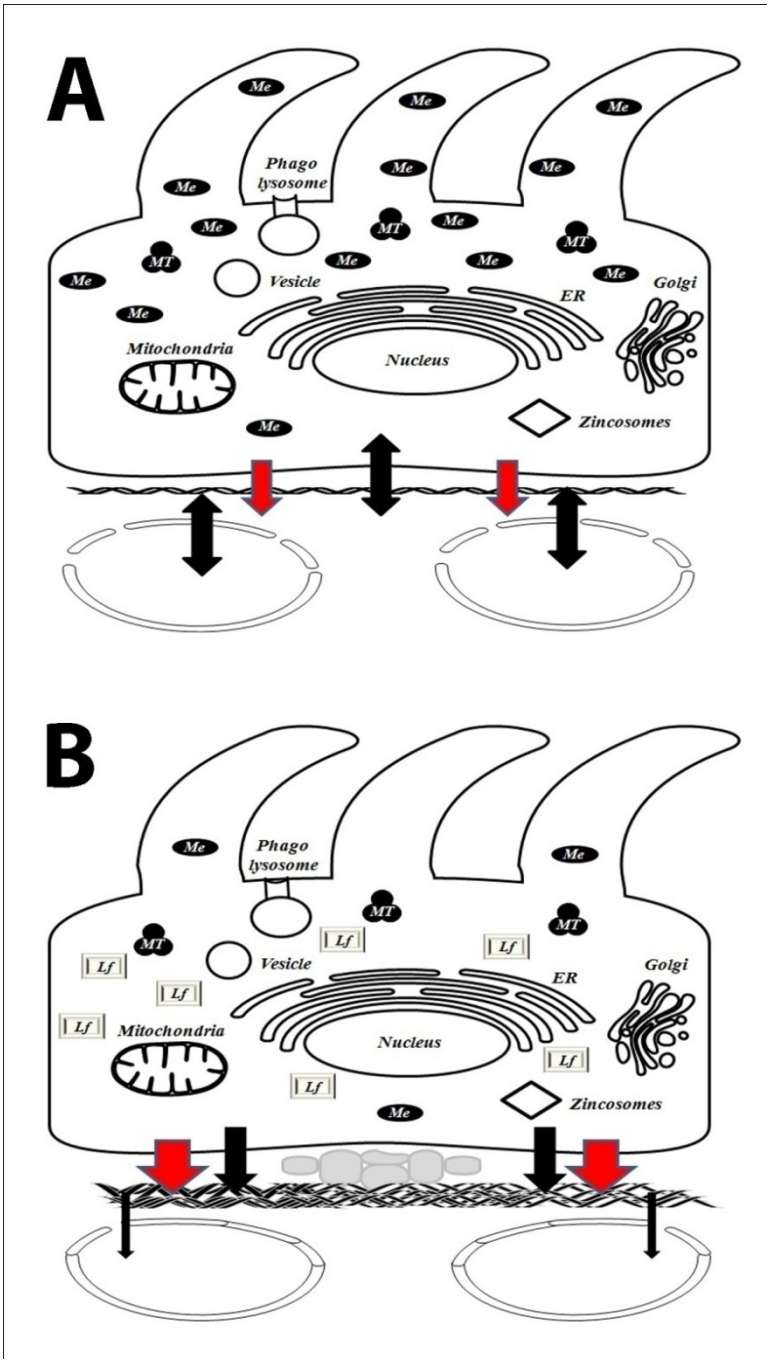

Figure 7-1–Schematic model of normal and diseased RPE

Schematic model of the normal RPE (A) and the diseased (AMD) RPE (B). In the normal RPE (A), melanin, metallothionein (MT) and phagocytic activities of the RPE are optimal. No thickening of Bruch's membrane is observed, and fenestrated capillaries allow material transport to occur. In diseased RPE (B), studies have shown that there is reduced melanin (Me) and metallothionein (MT), accumulation of lipofuscin (Lf) material, and thickening of Bruch's membrane. In AMD, sub-RPE deposits develop between Bruch's membrane and the RPE. The loss of fenestration which has been observed in AMD cases can further obstruct material transport from occurring, leading to a vicious cycle which cumulatively results in RPE atrophy. Figure legends: MT- metallothionein, Me – melanin, Lf – Lipofuscin, ER – endoplasmic reticulum.

8. Appendices

8.1. Appendix 1 – Antibodies

No	Name of Antibody	Reacting Species	Staining	Dilution	Source
1	Alpha-P 63 Isomerase	Rabbit Polyclonal	ER	1:500 ICC	Kind gift from Prof. Karl Matter
2	9.3 Golgi	Rabbit Polyclonal	Golgi	1:500 ICC	Kind gift from Prof. Karl Matter
3	ERGIC53 (Intermediate Compartment of Golgi)	Mouse Monoclonal	Golgi	1:200 ICC	Kind gift from Prof. Karl Matter
4	GI50059	Mouse Monoclonal	Lysosomes	1:50 ICC	Kind gift from Prof. Karl Matter
5	CathepsinD	Rabbit Polyclonal	Lysosomes	1:200 ICC	Kind gift from Dr. Claire Futter
6	TGN46	Sheep Polyclonal	Lysosomes	1:300 ICC	Kind gift from Dr. Claire Futter
7	V5	Mouse Monoclonal	V5 peptide	1:200 ICC 1:10000 WB	Invitrogen
8	ZIP12 ab64463	Rabbit Polyclonal	ZIP12 protein	1:200 ICC 1:1000 WB	Abcam
9	ZIP12 first bleed 5193	Rabbit polyclonal	ZIP12 protein	1:200 ICC 1:7500 WB	BioGene Germany
10	ZIP12 first bleed 5194	Rabbit polyclonal	ZIP12 protein	1:200 ICC 1:7500 WB	BioGene Germany
11	ZIP12 final bleed 5193	Rabbit polyclonal	ZIP12 protein	1:200 ICC 1:7500 WB	BioGene Germany
12	ZIP12 final bleed 5194	Rabbit polyclonal	ZIP12 protein	1:200 ICC 1:7500 WB	BioGene Germany
13	Actin C2	Mouse Monoclonal	Actin	1:500 WB	Santa Cruz Biotechnology
14	PV-1	Rat monoclonal	PV-1 protein	1:400	Kind gift from Prof. David Shima
15	GFP B2	Mouse Monoclonal	GFP protein	1:500 WB	Santa Cruz Biotechnology
16	Horseradish Peroxidase	Goat-anti-Mouse	HRP protein	1:7500 WB	Jackson ImmunoResearch
17	Horseradish Peroxidase	Goat-anti-Rabbit	HRP protein	1:7500 WB	Jackson ImmunoResearch
18	RhodamineP halloidin	-	Actin	1:300 ICC	Invitrogen
19	Phospho-p44/42 MAPK	Rabbit monoclonal	Phospho ERK1/2	1:1000 WB	Cell Signalling
20	p44/42 MAPK	Rabbit monoclonal	ERK1/2	1:1000 WB	Cell Signalling
21	Phospho-Akt (SER473) #9271	Rabbit monoclonal	Phospho AKT	1:1000 WB	Cell Signalling
22	Akt Antibody #9272	Rabbit monoclonal	AKT	1:1000 WB	Cell Signalling

23	Phospho-PI3K p85 (Tyr458) /p55 (Tyr199)	Rabbit monoclonal	Phospho PI3K	1:1000 WB	Cell Signalling
24	p38 MAPK Antibody #9212	Rabbit monoclonal	P38	1:1000 WB	Cell Signalling
25	Phospho-p38 MAPK (Thr180/Tyr182) Antibody #9211	Rabbit monoclonal	Phospho Pp38	1:1000 WB	Cell signalling
26	Src 184Q20	Mouse Monoclonal	Src	1:400 WB	Invitrogen
27	SRC [Py418]	Rabbit Polyclonal	PhosphoSrc	1:1000 WB	Invitrogen
27	ZO-1	Mouse Monoclonal	Primary Antibody	1:400	BD Biosciences
28	FITC	Goat anti Mouse	Secondary Antibody	1:300 ICC	BD Biosciences
29	Alexa 488	Goat anti Rat	Secondary Antibody	1:1000 ICC	Invitrogen
30	Alexa 568	Goat anti Rabbit	Secondary Antibody	1:1000 ICC	Invitrogen

8.2. **Appendix 2: Cell Lines**

No	Name of Cell Line	Type	Media	Supplements	Seeding Density
1	ARPE-19	Human RPE	DMEM/F12	10% FCS 1% Penicillin/Streptomycin	1:3
2	RPE-1	Human RPE	DMEM/F12	10% FCS 1% Penicillin/Streptomycin	1:3
3	BEND5	Murine endothelioma	DMEM 4.5g/L glucose with Glutamine and Pyruvate	5 ml NEAA 100x 10% FCS (v/v) 1% Penicillin/Streptomycin (v/v) 50 µl of 50mM b-mercaptoethanol	1:3
4	HEK293	Human embryonic kidney	DMEM 4.5g/L glucose with Glutamine and Pyruvate	10% FCS 1% Penicillin/Streptomycin	1:15
5	Primary RPE culture	Human RPE	DMEM/F12	10% FCS 1% Penicillin/Streptomycin	1:3
6	MDCK	Madin-Darby canine kidney with epithelial-like appearance	DMEM 4.5g/L glucose with Glutamine and Pyruvate	10% FCS 1% Penicillin/Streptomycin	1:10
7	CHO	Chinese hamster ovary	DMEM/F12	10% FCS10% FCS 1% Penicillin/Streptomycin	1:5

8.3. **Appendix 3 – Primer List**

8.3.1. Cloning Primers

ZIP12-attB CTerminal	FWD	GGGGACAAGTTTGTACAAAAAAGCAGGCTTCACCAT GTGCTTCCGGACAAAGCTCTCAG
	REV	GGGGACCACTTTGTACAAGAAAGCTGGGTGTATTTTA ATATTTTGCTCATATATA
ZIP12-attB NTerminal	FWD	GGGGACAAGTTTGTACAAAAAAGCAGGCTTCACCAT GTGCTTCCGGACAAAGCTCTCAG
	REV	GGGGACCACTTTGTACAAGAAAGCTGGGTGTTATATT TTAATATTTTGCTCATAT

8.3.2. Sequencing Primers

No	Name	Sequence
1	T7 Promoter	TAATACGACTCACTATAGGG
2	V5	ACCGAGGAGAGGGTTAAGGGAT
3	M13 Forward	GTAAAACGACGGCCAG
4	M13 Reverse	CAGGAAACAGCTATGAC
5	ZIP12-FWD1	ATGTGCTTCCGGACAAAGCTC
6	ZIP12-FWD2	CTATTACATTATTCATCAGGA
7	ZIP12-FWD3	CAGTTCCTTGAATCGTACGAA
8	ZIP12-FWD4	CATAGCTGTGAGGAGAACTAC
9	ZIP12-FWD5	CATAGGAGCAGCCTTCTCATC
10	ZIP12-REV1	CCTCCAGCTATTAGTAATAGT
11	ZIP12-REV2	TTATATTTTAATATTTTGCTCATAT

8.4. **QRT-PCR Primer Sequences (Primer Design, Southampton, UK)**

8.4.1. Mouse Primers

		Primer Sequences Mus Musculus		
Gene	Accession Number	Forward	Reverse	BP
SLC30A1	NM_009579	TCTGGGCAGGTTTATGTCATG	CCACTTTTATACATAGAACCCACTTA	107
SLC30A2	NM_001039677	TTAGCCTCTTCGCCCTCTG	GATGGAAAGCACGGACAACA	107
SLC30A3	NM_011773	GTCACTGGCATCCTCCTGTA	CATTAGCAGATTGGCACAGACA	117
SLC30A4	NM_011774	TAAAGTGGGTGTACCTGTAATCTC	CTTCCTCTATGGGTTCTGACAAG	131
SLC30A5	NM_022885	ACACCCAATAACAGACCAACTC	CACTACCACTCCTCCAGACA	88
SLC30A6	NM_144798	AAGTGCTCCTCCAGACAACA	GCCAAATCCAAGGGTCCAAA	125
SLC30A7	NM_023214	CCTGTGCCTGAACCTCTCT	GTGGAAGGAGTCGGAGATCA	88
SLC30A8	NM_172816	CCCTGCTGTCTGTCCTTTG	CCTGCTTGGATCTGGTAATCA	97
SLC30A9	NM_178651	GGGTTCCTTTGGCGTTGAG	TGTGCTTTCGTCCTGTGTTC	132
SLC30A10	NM_001033286	TGAGACAGAAGAGTTGCTTGAG	TGCCCATCAGCCTCCAAAT	119
SLC39A1	NM_13901	AAGTAGTGAGGACCAAAGAGTTC	CGTCTGTAGTAACTTCGCTATCT	134
SLC39A2	NM_001039676	CCTGGGCTTTTTCTTTGTCTTC	CGCTGGATGCTTGTGGAAT	133
SLC39A3	NM_134135	ACAATGGCATTCTCTCCTTTCC	CTGGCACTTGGGATGACTCT	119
SLC39A4	NM_028064	GCTTCTTTTCCTGCTCCACAA	GACAAGGACTGGGATGGGATA	118
SLC39A5	NM_028051	GGTGGCAGTATCGCATGGA	CTGGAGAAGCCGTCTGAGAA	98
SLC39A6	NM_139143	GGAGACGCACCAAAGATGTAA	GGCTCACTCACAGACTCATTG	115
SLC39A7	NM_001077709	CTCCGTTCTTCGTGCTGTTC	GGAAGCAAAACTGAGCAGGAT	89
SLC39A8	NM_026228	CCAGTGTTTGTCAGCAGAAGA	TCGCAGGGATGGAAGTTCA	126
SLC39A9	XM_891220	TTCTCTGCTGGGACATTTCTTTA	GCGTCACACACTTGCTCTT	130
SLC39A10	NM_172653	CTGGTTCCTGAAGATAAGACAAATAT	AAGCAGACTAATGACGGTGATAG	81
SLC39A11	NM_027216	GGATGGATATTGTAGTCTGTGAATG	AATGTGTGATTGAAGCCTTTGAT	106
SLC39A12	NM_001012305	TGCCCTGCTCCATCTCATAC	GCCTCCAAGTAGTCCCAACA	115
SLC39A13	NM_026721	TGAAGCCATAATCCCCAACTATT	CCACATCTCTAACATCCACAGT	111
SLC39A14	NM_144808	AGGCTCCTGCTCTACTTCATAG	CGTAATTGTCCTGAGGGTTGAA	106

8.5. **Appendix 4: PCR and DNA Sequencing Conditions**

8.5.1. Cloning PCR Cycling Conditions

95'C	95'C	60'C	72'C	75'C
2'	15"	30"	41"	2'05"
Denaturation		Annealing	Elongation	Hold
	35 Cycles			

	Name of Primers	Product Size	Optimisation time	MgCl/MgSO4	DMSO
1	ZIP12-attBForward-CTerm ZIP12-attBReverse-CTerm	2000 kb	X =60'C A=41" B=2'05"	2 mM	No
2	ZIP12-attBForward-NTerm ZIP12-attBReverse-NTerm	2000 kb	X =60'C A=41" B=2'05"	2 mM	No

8.5.2. DNA Sequencing Conditions

95'C	96'C	50'C	60'C	10'C
5'	10"	5'	4'	∞
	25 Cycles			

No	**Materials**	**Amount**
1	BigDye 3.1	0.5 µl
2	Sequencing buffer	2.5 µl
3	Sequencing Primer (100 µM)	0.5 µl
4	Plasmid DNA	3.0 µl
5	Deionised nuclease free H2O	16.5 µl
		20 µl

8.6. **Appendix 5: Plasmids Used**

GATEWAY DONOR

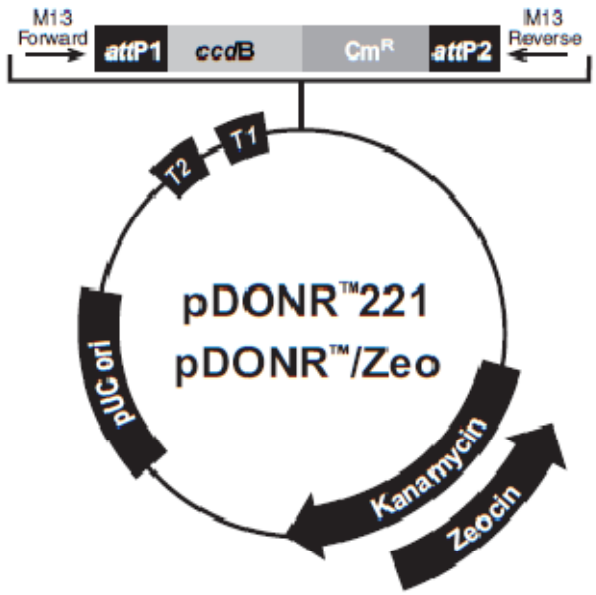

Comments for:	pDONR™221 4762 nucleotides	pDONR™/Zeo 4291 nucleotides
*rrn*B T2 transcription termination sequence (c):	268-295	268-295
rrnB T1 transcription termination sequence (c):	427-470	427-470
M13 Forward (-20) priming site:	537-552	537-552
*att*P1:	570-801	570-801
*ccd*B gene (c):	1197-1502	1197-1502
Chloramphenicol resistance gene (c):	1847-2506	1847-2506
*att*P2 (c):	2754-2985	2754-2985
T7 Promoter/priming site (c):	3000-3019	3003-3022
M13 Reverse priming site:	3027-3043	3027-3043
Kanamycin resistance gene:	3156-3965	---
EM7 promoter (c):	---	3486-3552
Zeocin resistance gene (c):	---	3111-3485
pUC origin:	4086-4759	3615-4288

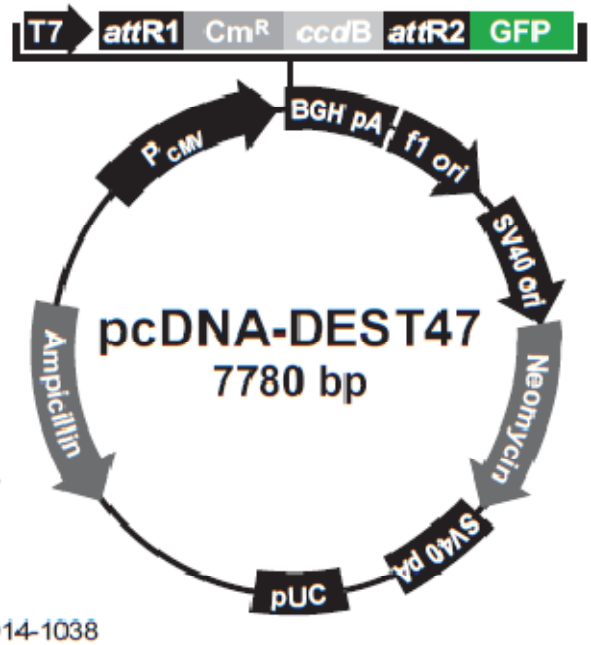

Comments for pcDNA-DEST47
7780 nucleotides

CMV promoter: bases 232-819
T7 promoter: bases 863-882
*att*R1 recombination site: bases 914-1038
Chloramphenicol resistance gene: bases 1147-1827
*ccd*B gene: bases 2147-2452
*att*R2 recombination site: bases 2493-2617
Cycle 3 GFP (C-terminal): bases 2628-3347
BGH polyadenylation region: bases 3372-3599
f1 origin: bases 3645-4073
SV40 early promoter and origin: bases 4100-4408
Neomycin resistance ORF: bases 4483-5277
SV40 early polyadenylation region: bases 5453-5583
pUC origin: bases 5966-6639
Ampicillin resistance ORF (*bla*): bases 6784-7644 (c)
bla promoter: bases 7645-7743 (c)
(c) = complementary strand

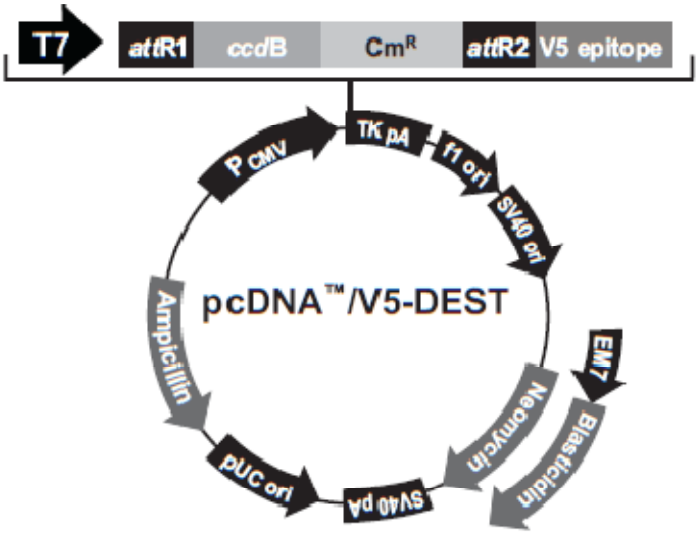

Comments for:	pcDNA™3.2/V5-DEST 7711 nucleotides	pcDNA™6.2/V5-DEST 7341 nucleotides
CMV promoter:	232-819	232-819
T7 promoter/priming site:	863-882	863-882
*att*R1 site:	911-1035	911-1035
*ccd*B gene (c):	1464-1769	1464-1769
Chloramphenicol resistance gene (c):	2111-2770	2111-2770
*att*R2 site:	3051-3175	3051-3175
V5 epitope:	3201-3242	3201-3242
V5 reverse priming site:	3210-3230	3210-3230
TK polyadenylation signal:	3269-3540	3269-3540
f1 origin:	3576-4004	3576-4004
SV40 early promoter and origin:	4031-4339	4031-4339
Neomycin resistance gene:	4414-5208	---
EM7 promoter:	---	4394-4460
Blasticidin resistance gene:	---	4461-4859
SV40 early polyadenylation signal:	5384-5514	5017-5147
pUC origin (c):	5897-6570	5530-6200
Ampicillin (*bla*) resistance gene (c):	6715-7575	6345-7205
bla promoter (c):	7576-7674	7206-7304

(c) = complementary strand

9. References

2001. A randomized, placebo-controlled, clinical trial of high-dose supplementation with vitamins C and E, beta carotene, and zinc for age-related macular degeneration and vision loss: AREDS report no. 8. *Archives of ophthalmology,* 119**,** 1417-36.

ADKINS, J. N., VARNUM, S. M., AUBERRY, K. J., MOORE, R. J., ANGELL, N. H., SMITH, R. D., SPRINGER, D. L. & POUNDS, J. G. 2002. Toward a human blood serum proteome: analysis by multidimensional separation coupled with mass spectrometry. *Molecular & cellular proteomics : MCP,* 1**,** 947-55.

AHMADO, A., CARR, A. J., VUGLER, A. A., SEMO, M., GIAS, C., LAWRENCE, J. M., CHEN, L. L., CHEN, F. K., TUROWSKI, P., DA CRUZ, L. & COFFEY, P. J. 2011a. Induction of differentiation by pyruvate and DMEM in the human retinal pigment epithelium cell line ARPE-19. *Investigative ophthalmology & visual science,* 52**,** 7148-59.

AIRD, W. C. 2007. Phenotypic heterogeneity of the endothelium: I. Structure, function, and mechanisms. *Circulation research,* 100**,** 158-73.

AKAGI, T., KANEDA, M., ISHII, K. & HASHIKAWA, T. 2001. Differential subcellular localization of zinc in the rat retina. *The journal of histochemistry and cytochemistry : official journal of the Histochemistry Society,* 49**,** 87-96.

AMASHEH, S., MEIRI, N., SHONEBERG, T., MANKERTZ, J., SCHULZKE, J.D. & FROMM, M. 2002. Claudin-2 expression induces cation-selective channels in tight junctions of epithelial cells. *Journal of cell science*, 115, 4969-4976.

AMEMIYA, K., HARUTA, M., TAKAHASHI, M., KOSAKA, M. & EGUCHI, G. 2004. Adult human retinal pigment epithelial cells capable of differentiating into neurons. *Biochemical and biophysical research communications,* 316**,** 1-5.

ANAND-APTE, B., PEPPER, M. S., VOEST, E., MONTESANO, R., OLSEN, B., MURPHY, G., APTE, S. S. & ZETTER, B. 1997. Inhibition of angiogenesis

by tissue inhibitor of metalloproteinase-3. *Investigative ophthalmology & visual science,* 38**,** 817-23.

ANDERSON, A. R., KASTL, P. R. & KARCIOGLU, Z. A. 1987. Comparison of aqueous humour and serum zinc levels in humans. *The British journal of ophthalmology,* 71**,** 212-4.

ANDREINI, C., BANCI, L., BERTINI, I. & ROSATO, A. 2006. Counting the zinc-proteins encoded in the human genome. *Journal of proteome research,* 5**,** 196-201.

AYDEMIR, T. B., LIUZZI, J. P., MCCLELLAN, S. & COUSINS, R. J. 2009. Zinc transporter ZIP8 (SLC39A8) and zinc influence IFN-gamma expression in activated human T cells. *Journal of leukocyte biology,* 86**,** 337-48.

AYMERICH, M.S., ALBERDI, E.M., MARTINEZ, A. & BECERRA, S.P. 2001. Evidence for pigment epithelium-derived factor receptors in the neural retina. *Investigative ophthalmology visual science,* 42, 3287-3293.

BALDA, M. S. & MATTER, K. 2008. Tight junctions at a glance. *Journal of cell science,* 121**,** 3677-82.

BALDA, M., WHITNEY, J.A., FLORES, J.A., GONZALEZ, S., CEREIJIDO, M. & MATTER, K. 1996. Functional dissociation of paracellular permeability and transepithelial electrical resistance and disruption of the apical-basolateral intramembrane diffusion barrier by expression of a mutant tight junction membrane protein. *Journal of cell biology*, 134, 1031-1049.

BALKOVETZ, D. 2006. Claudins at the gate: determinants of renal epithelial tight junction. *American journal of physiology and renal physiology*, 290, F572-F579.

BARASH, H., POSTON, H. A. & RUMSEY, G. L. 1982. Differentiation of soluble proteins in cataracts caused by deficiencies of methionine, riboflavin or zinc in diets fed to Atlantic salmon, Salmo salar, rainbow trout, Salmo gairdneri, and lake trout, Salvelinus namaycush. *The Cornell veterinarian,* 72**,** 361-71.

BEATTY, S., BOULTON, M., HENSON, D., KOH, H.H. & MURRAY, I.J. 1999. Macular pigment and age-related macular degeneration. *British journal of ophthalmology*, 83, 867-877.

BEHNDIG, A., SVENSSON, B., MARKLUND, S. L. & KARLSSON, K. 1998. Superoxide dismutase isoenzymes in the human eye. *Investigative ophthalmology & visual science,* 39**,** 471-5.

BELLONI-OLIVI, L., MARSHALL, C., LAAL, B., ANDREWS, G. K. & BRESSLER, J. 2009. Localization of zip1 and zip4 mRNA in the adult rat brain. *Journal of neuroscience research,* 87**,** 3221-30.

BENTLEY, P. J. & GRUBB, B. R. 1991. Effects of a zinc-deficient diet on tissue zinc concentrations in rabbits. *Journal of animal science,* 69**,** 4876-82.

BERMAN, M. B. & MANABE, R. 1973. Corneal collagenases: evidence for zinc metalloenzymes. *Annals of ophthalmology,* 5**,** 1193-5 passim.

BERNSTEIN, M. H. & HOLLENBERG, M. J. 1965. Fine structure of the choriocappillaris and retinal capillaries. *Investigative ophthalmology,* 4**,** 1016-25.

BESECKER, B., BAO, S., BOHACOVA, B., PAPP, A., SADEE, W. & KNOELL, D. L. 2008. The human zinc transporter SLC39A8 (Zip8) is critical in zinc-mediated cytoprotection in lung epithelia. *American journal of physiology. Lung cellular and molecular physiology,* 294**,** L1127-36.

BETTGER, W. J. 1993. Zinc and selenium, site-specific versus general antioxidation. *Canadian journal of physiology and pharmacology,* 71**,** 721-4.

BHOOMA, V., SULOCHANA, K. N., BISWAS, J. & RAMAKRISHNAN, S. 1997. Eales' disease: accumulation of reactive oxygen intermediates and lipid peroxides and decrease of antioxidants causing inflammation, neovascularization and retinal damage. *Current eye research,* 16**,** 91-5.

BHUTTO, I.A., UNO, K., MERGES, C., ZHANG, L., MCLEOD, S. & LUTTY, G.A. 2008. Reduction of endogeneous angiogenesis inhibitors in Bruch's membrane

of the submacular region in eyes with age-related macular degeneration. *Archives ophthalmology,* 126, 670-678.

BIESEMEIER, A., KREPPEL, F., KOCHANEK, S. & SCHRAERMEYER, U. 2010. The classical pathway of melanogenesis is not essential for melanin synthesis in the adult retinal pigment epithelium. *Cell and tissue research,* 339, 551-60.

BINDER, S., STANZEL, B. V., KREBS, I. & GLITTENBERG, C. 2007. Transplantation of the RPE in AMD. *Progress in retinal and eye research,* 26, 516-54.

BLAAUWGEERS, H.G., HOLTKAMP, G.M., RUTTEN, H., WITMER, A.N., KOOLWIJK, P., PARTANEN, T.A., ALITALO, K., KROON, M.E., KIJLSTRA A., VAN HINSBERGH, V.W. & SCHLINGEMANN, R.O. 1999. Polarized vascular endothelial growth factor secretion by human retinal pigment epithelium and localization of vascular endothelial growth factor receptors on the inner choriocapillaris. Evidence for a trophic paracrine relation. *American journal of pathology*, 155, 421-428.

BLY, M. 2006. Examination of the zinc transporter gene, SLC39A12. *Schizophrenia research,* 81, 321-2.

BOBILYA, D. J., GAUTHIER, N. A., KARKI, S., OLLEY, B. J. & THOMAS, W. K. 2008. Longitudinal changes in zinc transport kinetics, metallothionein and zinc transporter expression in a blood-brain barrier model in response to a moderately excessive zinc environment. *The Journal of nutritional biochemistry,* 19**,** 129-37.

BODNAR, A. G., OUELLETTE, M., FROLKIS, M., HOLT, S. E., CHIU, C. P., MORIN, G. B., HARLEY, C. B., SHAY, J. W., LICHTSTEINER, S. & WRIGHT, W. E. 1998. Extension of life-span by introduction of telomerase into normal human cells. *Science,* 279**,** 349-52.

BOK, D. 1993. The retinal pigment epithelium: a versatile partner in vision. *Journal of cell science. Supplement,* 17**,** 189-95.

BOOIJ, J. C., BAAS, D. C., BEISEKEEVA, J., GORGELS, T. G. & BERGEN, A. A. 2010a. The dynamic nature of Bruch's membrane. *Progress in retinal and eye research,* 29**,** 1-18.

BOOIJ, J. C., TEN BRINK, J. B., SWAGEMAKERS, S. M., VERKERK, A. J., ESSING, A. H., VAN DER SPEK, P. J. & BERGEN, A. A. 2010b. A new strategy to identify and annotate human RPE-specific gene expression. *PloS one,* 5**,** e9341.

BOWNESS, J. M., MORTON, R. A., SHAKIR, M. H. & STUBBS, A. L. 1952. Distribution of copper and zinc in mammalian eyes. Occurrence of metals in melanin fractions from eye tissues. *The Biochemical journal,* 51**,** 521-30.

BOZYM, R. A., CHIMIENTI, F., GIBLIN, L. J., GROSS, G. W., KORICHNEVA, I., LI, Y., LIBERT, S., MARET, W., PARVIZ, M., FREDERICKSON, C. J. &THOMPSON, R. B. 2010. Free zinc ions outside a narrow concentration range are toxic to a variety of cells in vitro. *Experimental biology and medicine,* 235**,** 741-50.

BOZYM, R. A., THOMPSON, R. B., STODDARD, A. K. & FIERKE, C. A. 2006. Measuring picomolar intracellular exchangeable zinc in PC-12 cells using a ratiometric fluorescence biosensor. *ACS chemical biology,* 1**,** 103-11.

BRAET, F. & WISSE, E. 2002. Structural and functional aspects of liver sinusoidal endothelial cell fenestrae: a review. *Comparative hepatology,* 1**,** 1.

BRUBAN, J., GLOTIN, A., DINET, V., CHALOUR, N., SENNLAUB, F., JONET, L., AN, N., FAUSSAT, A.M. & MASCARELLI, F. 2009. Amyloid- (1-42) alters structure and function of retinal pigmented epithelial cells. *Aging cell*, 8, 162-177.

BURKE, J.M., KACZARA, P., SKUMATZ, C.M.B., ZAREBA, M., RACITI, M.W. & SARNA, T. 2011. Dynamic analyses reveal cytoprotection by RPE melanosomes against non-photic stress. *Molecular vision*, 17, 2864-2877.

BURKE, J.M., CAO, F., IRVING, P.E. & SKUMATZ, C.M.B. 1999. Expression of E-Cadherin by human retinal pigment epithelium: delayed expression in vitro. *Investigative ophthalmology and visual science*, 40, 12.

BURNS, M. S. & HARTZ, M. J. 1992. The retinal pigment epithelium induces fenestration of endothelial cells in vivo. *Current eye research,* 11**,** 863-73.

BURY, N. R., CHUNG, M. J., STURM, A., WALKER, P. A. & HOGSTRAND, C. 2008. Cortisol stimulates the zinc signaling pathway and expression of metallothioneins and ZnT1 in rainbow trout gill epithelial cells. *American journal of physiology. Regulatory, integrative and comparative physiology,* 294**,** R623-9.

CAI, H. & DEL PRIORE, L. V. 2006. Gene expression profile of cultured adult compared to immortalized human RPE. *Molecular vision,* 12**,** 1-14.

CAMERON, J. D. & MCCLAIN, C. J. 1986. Ocular histopathology of acrodermatitis enteropathica. *The British journal of ophthalmology,* 70**,** 662-7.

CAO, J., BOBO, J. A., LIUZZI, J. P. & COUSINS, R. J. 2001. Effects of intracellular zinc depletion on metallothionein and ZIP2 transporter expression and apoptosis. *Journal of leukocyte biology,* 70**,** 559-66.

CHEN, M., MUCKERSIE, E., ROBERTSON, M., FRACZEK, M., FORRESTER, J. V. & XU, H. 2008. Characterization of a spontaneous mouse retinal pigment epithelial cell line B6-RPE07. *Investigative ophthalmology & visual science,* 49**,** 3699-706.

CHIMIENTI, F., DEVERGNAS, S., PATTOU, F., SCHUIT, F., GARCIA-CUENCA, R., VANDEWALLE, B., KERR-CONTE, J., VAN LOMMEL, L., GRUNWALD, D., FAVIER, A. & SEVE, M. 2006. In vivo expression and functional characterization of the zinc transporter ZnT8 in glucose-induced insulin secretion. *Journal of cell science,* 119**,** 4199-206.

CHIMIENTI, F., FAVIER, A. & SEVE, M. 2005. ZnT-8, a pancreatic beta-cell-specific zinc transporter. *Biometals : an international journal on the role of metal ions in biology, biochemistry, and medicine,* 18**,** 313-7.

CHOWANADISAI, W., KELLEHER, S. L. & LONNERDAL, B. 2005. Zinc deficiency is associated with increased brain zinc import and LIV-1 expression and decreased ZnT-1 expression in neonatal rats. *The Journal of nutrition,* 135**,** 1002-7.

CLEGG, M.S., HANNA, L.A., NILES, B.J., MOMMA, T.Y., & KEEN, C.L. Zinc deficiency-induced cell death. 2005. *IUBMB LIFE*, 57, 661-669.

COLVIN, R. A., HOLMES, W. R., FONTAINE, C. P. & MARET, W. 2010. Cytosolic zinc buffering and muffling: their role in intracellular zinc homeostasis. *Metallomics : integrated biometal science,* 2**,** 306-17.

CONSTABLE, P. A. & LAWRENSON, J. G. 2009. Glial cell factors and the outer blood retinal barrier. *Ophthalmic & physiological optics : the journal of the British College of Ophthalmic Opticians,* 29**,** 557-64.

COUE, M., BRENNER, S. L., SPECTOR, I. & KORN, E. D. 1987. Inhibition of actin polymerization by latrunculin A. *FEBS letters,* 213**,** 316-8.

CRAGG, R. A., PHILLIPS, S. R., PIPER, J. M., VARMA, J. S., CAMPBELL, F. C., MATHERS, J. C. & FORD, D. 2005. Homeostatic regulation of zinc transporters in the human small intestine by dietary zinc supplementation. *Gut,* 54**,** 469-78.

CUNHA-VAZ, J. 1979. The blood-ocular barriers. *Survey of ophthalmology,* 23**,** 279-96.

DANKS, D. M. 1988. Copper deficiency in humans. *Annual review of nutrition,* 8**,** 235-57.

DAVIS, A. A., BERNSTEIN, P. S., BOK, D., TURNER, J., NACHTIGAL, M. & HUNT, R. C. 1995. A human retinal pigment epithelial cell line that retains epithelial characteristics after prolonged culture. *Investigative ophthalmology & visual science,* 36**,** 955-64.

DEVERGNAS, S., CHIMIENTI, F., NAUD, N., PENNEQUIN, A., COQUEREL, Y., CHANTEGREL, J., FAVIER, A. & SEVE, M. 2004. Differential regulation of zinc efflux transporters ZnT-1, ZnT-5 and ZnT-7 gene expression by zinc levels: a real-time RT-PCR study. *Biochemical pharmacology,* 68**,** 699-709.

DEWAN, A., LIU, M., HARTMAN, S., ZHANG, S. S., LIU, D. T., ZHAO, C., TAM, P. O., CHAN, W. M., LAM, D. S., SNYDER, M., BARNSTABLE, C., PANG,

C. P. & HOH, J. 2006. HTRA1 promoter polymorphism in wet age-related macular degeneration. *Science,* 314**,** 989-92.

DI CELLO, F., SIDDHARTHAN, V., PAUL-SATYASEELA, M. & KIM, K. S. 2005. Divergent effects of zinc depletion in brain vs non-brain endothelial cells. *Biochemical and biophysical research communications,* 335**,** 373-6.

DUFNER-BEATTIE, J., WANG, F., KUO, Y. M., GITSCHIER, J., EIDE, D. & ANDREWS, G. K. 2003. The acrodermatitis enteropathica gene ZIP4 encodes a tissue-specific, zinc-regulated zinc transporter in mice. *The Journal of biological chemistry,* 278**,** 33474-81.

DUFNER-BEATTIE, J., WEAVER, B. P., GEISER, J., BILGEN, M., LARSON, M., XU, W. & ANDREWS, G. K. 2007. The mouse acrodermatitis enteropathica gene Slc39a4 (Zip4) is essential for early development and heterozygosity causes hypersensitivity to zinc deficiency. *Hum Mol Genet,* 16**,** 1391-9.

DUNN, K. C., AOTAKI-KEEN, A. E., PUTKEY, F. R. & HJELMELAND, L. M. 1996. ARPE-19, a human retinal pigment epithelial cell line with differentiated properties. *Experimental eye research,* 62**,** 155-69.

DUNN, K. C., MARMORSTEIN, A. D., BONILHA, V. L., RODRIGUEZ-BOULAN, E., GIORDANO, F. & HJELMELAND, L. M. 1998. Use of the ARPE-19 cell line as a model of RPE polarity: basolateral secretion of FGF5. *Investigative ophthalmology & visual science,* 39**,** 2744-9.

ECKHERT, C. D. 1983. Elemental concentrations in ocular tissues of various species. *Experimental eye research,* 37**,** 639-47.

EHSANI, S., HUO, H., SALEHZADEH, A., POCANSCHI, C. L., WATTS, J. C., WILLE, H., WESTAWAY, D., ROGAEVA, E., ST GEORGE-HYSLOP, P. H. & SCHMITT-ULMS, G. 2011. Family reunion--the ZIP/prion gene family. *Progress in neurobiology,* 93**,** 405-20.

EIDE, D. J. 2004. The SLC39 family of metal ion transporters. *Pflugers Archiv : European journal of physiology,* 447**,** 796-800.

EIDE, D.J. 2006. Zinc transporters and the cellular trafficking of zinc. *Biochimica et biophysica acta*, 1763, 711-72.

ERIE, J. C., GOOD, J. A., BUTZ, J. A. & PULIDO, J. S. 2009. Reduced zinc and copper in the retinal pigment epithelium and choroid in age-related macular degeneration. *American journal of ophthalmology,* 147**,** 276-282 e1.

ESPINOSA-HEIDMANN, D. G., SUNER, I. J., CATANUTO, P., HERNANDEZ, E. P., MARIN-CASTANO, M. E. & COUSINS, S. W. 2006. Cigarette smoke-related oxidants and the development of sub-RPE deposits in an experimental animal model of dry AMD. *Investigative ophthalmology & visual science,* 47**,** 729-37.

ESSER, S., WOLBURG, K., WOLBURG, H., BREIER, G., KURZCHALIA, T. & RISAU, W. 1998. Vascular endothelial growth factor induces endothelial fenestrations in vitro. *The Journal of cell biology,* 140**,** 947-59.

ETIENNE-MANVILLE, S. & HALL, A. 2002. Rho-GTPases in cell biology. *Nature*, 420, 629-635.

FABE, J. S., GRAHN, B. H. & PATERSON, P. G. 2000. Zinc concentration of selected ocular tissues in zinc-deficient rats. *Biological trace element research,* 75**,** 43-52.

FALCON-PEREZ, J. M. & DELL'ANGELICA, E. C. 2007. Zinc transporter 2 (SLC30A2) can suppress the vesicular zinc defect of adaptor protein 3-depleted fibroblasts by promoting zinc accumulation in lysosomes. *Experimental cell research,* 313**,** 1473-83.

FINNEMANN, S.C., LEUNG, L.W. & RODRIGUEZ-BOULAN, E. 2002. The lipofuscin component A2E selectively inhibits phagolysosomal degradation of photoreceptor phospholipid by the retinal pigment epithelium. *Proceedings of the National Academy of Sciences*, 99, 3842-3847.

FLOOD, V., SMITH, W., WANG, J. J., MANZI, F., WEBB, K. & MITCHELL, P. 2002. Dietary antioxidant intake and incidence of early age-related maculopathy: the Blue Mountains Eye Study. *Ophthalmology,* 109**,** 2272-8.

FRANCIS, P. J. & KLEIN, M. L. 2011. Update on the role of genetics in the onset of age-related macular degeneration. *Clinical ophthalmology,* 5**,** 1127-33.

FUJII, Y., KACHI, S., ITO, A., KAWASUMI, T., HONDA, H. & TERASAKI, H. 2010. Transfer of gene to human retinal pigment epithelial cells using magnetite cationic liposomes. *The British journal of ophthalmology,* 94**,** 1074-7.

FUJISHIRO, H., OKUGAKI, S., YASUMITSU, S., ENOMOTO, S. & HIMENO, S. 2009. Involvement of DNA hypermethylation in down-regulation of the zinc transporter ZIP8 in cadmium-resistant metallothionein-null cells. *Toxicology and applied pharmacology,* 241**,** 195-201.

FUKADA, T., CIVIC, N., FURUICHI, T., SHIMODA, S., MISHIMA, K., HIGASHIYAMA, H., IDAIRA, Y., ASADA, Y., KITAMURA, H., YAMASAKI, S., HOJYO, S., NAKAYAMA, M., OHARA, O., KOSEKI, H., DOS SANTOS, H. G., BONAFE, L., HA-VINH, R., ZANKL, A., UNGER, S., KRAENZLIN, M. E., BECKMANN, J. S., SAITO, I., RIVOLTA, C., IKEGAWA, S., SUPERTI-FURGA, A. & HIRANO, T. 2008. The zinc transporter SLC39A13/ZIP13 is required for connective tissue development; its involvement in BMP/TGF-beta signaling pathways. *PloS one,* 3**,** e3642.

FURUSE, M., HIRASE, T., ITOH, M., NAGAFUCHI, A., YONEMURA, S., TSUKITA, S & TSUKITA, S. 1993. Occludin: a novel integral membrane protein localizing at tight junctions. *Journal of cell biology*, 123, 1777-1788.

FURUSE, M., HATA, M., FURUSE, K., YOSHIDA, Y., HARATAKE, A., SUGITANI, Y. & TSUKITA, S. 2002. Claudin-based tight junctions are crucial for the mammalian epidermal barrier: a lesson from claudin-1 deficient mice. *Journal of cell biology*, 156, 1099-111.

FURUSE, M., ITOH, M., HIRASE, T., NAGAFUCHI, A., YONEMURA, S., TSUKITA, S. & TSUKITA, S. 1994. Direct association of occluding with ZO-1 and its possible involvement in the localisation of occludin at tight junctions. *Journal of cell biology,* 127, 1617-1626.

GAITHER, L. A. & EIDE, D. J. 2001. Eukaryotic zinc transporters and their regulation. *Biometals : an international journal on the role of metal ions in biology, biochemistry, and medicine,* 14**,** 251-70.

GALIN, M. A., NANO, H. D. & HALL, T. 1962. Ocular zinc concentration. *Investigative ophthalmology,* 1**,** 142-8.

GASMAN, S., CHASSEROT-GOLAZ, S., POPOFF, M.R., AUNIS, D. & BADER, M.F. 1999. Involvement of Rho GTPases in calcium-regulated exocytosis from adrenal chromaffin cells. *Journal of cell science*, 112, 4763-4771.

GATON, D. D., SAGARA, T., LINDSEY, J. D. & WEINREB, R. N. 1999. Matrix metalloproteinase-1 localization in the normal human uveoscleral outflow pathway. *Investigative ophthalmology & visual science,* 40**,** 363-9.

GEISEN, P., MCCOLM, J. R., KING, B. M. & HARTNETT, M. E. 2006. Characterization of barrier properties and inducible VEGF expression of several types of retinal pigment epithelium in medium-term culture. *Current eye research,* 31**,** 739-48.

GERMAN, O. L., BUZZI, E., ROTSTEIN, N. P., RODRIGUEZ-BOULAN, E. & POLITI, L. E. 2008. Retinal pigment epithelial cells promote spatial reorganization and differentiation of retina photoreceptors. *Journal of neuroscience research,* 86**,** 3503-14.

GLEIM, S., STOJANOVIC, A., AREHART, E., BYINGTON, D. & HWA, J. 2009. Conserved rhodopsin intradiscal structural motifs mediate stabilization: effects of zinc. *Biochemistry,* 48**,** 1793-800.

GOLOVINE, K., UZZO, R. G., MAKHOV, P., CRISPEN, P. L., KUNKLE, D. & KOLENKO, V. M. 2008. Depletion of intracellular zinc increases expression of tumorigenic cytokines VEGF, IL-6 and IL-8 in prostate cancer cells via NF-kappaB-dependent pathway. *The Prostate,* 68**,** 1443-9.

GONG, H. & AMEMIYA, T. 2001. Optic nerve changes in zinc-deficient rats. *Experimental eye research,* 72**,** 363-9.

GONG, H., TAKAMI, Y., AMEMIYA, T., TOZU, M. & OHASHI, Y. 2004. Ocular surface in Zn-deficient rats. *Ophthalmic research,* 36**,** 129-38.

GRAHAM, S. M., DALEY, H. M., BANERJEE, A., SALANIPONI, F. M. & HARRIES, A. D. 1998. Ethambutol in tuberculosis: time to reconsider? *Archives of disease in childhood,* 79**,** 274-8.

GRAHN, B. H., PATERSON, P. G., GOTTSCHALL-PASS, K. T. & ZHANG, Z. 2001. Zinc and the eye. *Journal of the American College of Nutrition,* 20**,** 106-18.

GEORGIADIS, A., TSCHERNUTTER, M., BAINBRIDGE, J.W.B, BALAGGAN, K.S., MOWAT, F., WEST, E.L., MUNRO, P.M.G., THRASHER, A.J., MATTER, K., BALDA., M. & ALI, R. 2010. The tight junction associated signalling proteins- ZO-1 and ZONAB regulate retinal pigment epithelium homeostasis in mice. *PLOSone*, 5, e15730.

GRUPE, A., LI, Y., ROWLAND, C., NOWOTNY, P., HINRICHS, A. L., SMEMO, S., KAUWE, J. S., MAXWELL, T. J., CHERNY, S., DOIL, L., TACEY, K., VAN LUCHENE, R., MYERS, A., WAVRANT-DE VRIEZE, F., KALEEM, M., HOLLINGWORTH, P., JEHU, L., FOY, C., ARCHER, N., HAMILTON, G., HOLMANS, P., MORRIS, C. M., CATANESE, J., SNINSKY, J., WHITE, T. J., POWELL, J., HARDY, J., O'DONOVAN, M., LOVESTONE, S., JONES, L., MORRIS, J. C., THAL, L., OWEN, M., WILLIAMS, J. & GOATE, A. 2006. A scan of chromosome 10 identifies a novel locus showing strong association with late-onset Alzheimer disease. *American journal of human genetics,* 78**,** 78-88.

GUERINOT, M. L. 2000. The ZIP family of metal transporters. *Biochimica et biophysica acta,* 1465**,** 190-8.

GUNDERSEN, D., ORLOWSKI, J. & RODRIGUEZ-BOULAN, E. Apical polarity of Na,K-ATPase in retinal pigment epithelium is linked to a reversal of the anykrin-fodrin submembrane cytoskeleton. *The journal of cell biology.* 5, 863-868.

GURUSAMY, K. S., FAROOQUI, N., LOIZIDOU, M., DIJK, S., TAANMAN, J. W., WHITING, S., FARQUHARSON, M. J., FULLER, B. J. & DAVIDSON, B. R. 2011. Influence of zinc and zinc chelator on HT-29 colorectal cell line. *Biometals : an international journal on the role of metal ions in biology, biochemistry, and medicine,* 24**,** 143-51.

HA, K.-N., CHEN, Y., CAI, J. & STERNBERG, P., JR. 2006. Increased Glutathione Synthesis through an ARE-Nrf2-Dependent Pathway by Zinc in the RPE: Implication for Protection against Oxidative Stress. *Invest. Ophthalmol. Vis. Sci.,* 47**,** 2709-2715.

HAO, R., CERUTIS, D. R., BLAXALL, H. S., RODRIGUEZ-SIERRA, J. F., PFEIFFER, R. F. & EBADI, M. 1994. Distribution of zinc metallothionein I mRNA in rat brain using in situ hybridization. *Neurochemical research,* 19**,** 761-7.

HARRIS, W. R. & STENBACK, J. Z. 1988. The bicarbonate-dependence of zinc(II)-transferrin binding. *Journal of inorganic biochemistry,* 33**,** 211-23.

HARTSOCK, A. & NELSON, W.J. 2008. Adherens and tight junctions: structure, function and connections to the actin cytoskeleton. *Biochemical biophysical acta,* 1778, 660-669.

HE, L., GIRIJASHANKER, K., DALTON, T.P., REED, J., LI, H., SOLEIMANI, M., & NEBERT D.W. 2006. ZIP8, member of the solute-carrier-39 (SLC39) metal-transporter family: characterisation of transporter properties. *Molecular Pharmacology*, 70(1), 171-180.

HENNIG, B., MEERARANI, P., TOBOREK, M. & MCCLAIN, C.J. 1999. Antioxidant-like properties of zinc in activated endothelial cells. *Journal of the American College of Nutrition,* 18, 152-158.

HERNANDEZ, J.M, DOMINGUEZ-ROBLES, M.C., PALMER, E., & SABORIO, J.L. 1989. Interaction of cadmium with actin microfilaments in vitro. *Toxicology in vitro*, 4, 277-284.

HIRAYAMA, Y. 1990. Histochemical localization of zinc and copper in rat ocular tissues. *Acta histochemica,* 89**,** 107-11.

HO, L., VAN LEEUWEN, R., WITTEMAN, J. C., VAN DUIJN, C. M., UITTERLINDEN, A. G., HOFMAN, A., DE JONG, P. T., VINGERLING, J. R. & KLAVER, C. C. 2011a. Reducing the Genetic Risk of Age-Related Macular Degeneration With Dietary Antioxidants, Zinc, and {omega}-3 Fatty Acids: The Rotterdam Study. *Archives of ophthalmology,* 129**,** 758-66.

HO, L., VAN LEEUWEN, R., WITTEMAN, J. C., VAN DUIJN, C. M., UITTERLINDEN, A. G., HOFMAN, A., DE JONG, P. T., VINGERLING, J. R. & KLAVER, C. C. 2011b. Reducing the genetic risk of age-related macular degeneration with dietary antioxidants, zinc, and omega-3 fatty acids: the Rotterdam study. *Archives of ophthalmology,* 129**,** 758-66.

HO, J., WITKIN, A.J., LIU, J., CHEN, Y., FUJIMOTO, J.G., SCHUMAN, J.S. & DUKER, J.S. 2011. Documentation of intraretinal retinal pigment epithelium migration via high-speed ultrahigh resolution optical coherence tomography. *Ophthalmology.* 118, 687-693.

HOFMAN, P., HOYNG, P., VANDERWERF, F., VRENSEN, G. F. & SCHLINGEMANN, R. O. 2001. Lack of blood-brain barrier properties in microvessels of the prelaminar optic nerve head. *Investigative ophthalmology & visual science,* 42**,** 895-901.

HOGSTRAND, C., KILLE, P., NICHOLSON, R. I. & TAYLOR, K. M. 2009. Zinc transporters and cancer: a potential role for ZIP7 as a hub for tyrosine kinase activation. *Trends in molecular medicine,* 15**,** 101-11.

HOSIE, A. M., DUNNE, E. L., HARVEY, R. J. & SMART, T. G. 2003. Zinc-mediated inhibition of GABA(A) receptors: discrete binding sites underlie subtype specificity. *Nature neuroscience,* 6**,** 362-9.

HU, J. & BOK, D. 2001. A cell culture medium that supports the differentiation of human retinal pigment epithelium into functionally polarised monolayers. *Molecular vision*, 7, 14-19.

HUANG, L., YU, Y. Y., KIRSCHKE, C. P., GERTZ, E. R. & LLOYD, K. K. 2007. Znt7 (Slc30a7)-deficient mice display reduced body zinc status and body fat accumulation. *The Journal of biological chemistry,* 282**,** 37053-63.

HUANG, Z. L., DUFNER-BEATTIE, J. & ANDREWS, G. K. 2006. Expression and regulation of SLC39A family zinc transporters in the developing mouse intestine. *Developmental biology,* 295**,** 571-9.

HUSSAIN, A. A., LEE, Y., ZHANG, J. J. & MARSHALL, J. 2011. Disturbed matrix metalloproteinase activity of Bruch's membrane in age-related macular degeneration. *Investigative ophthalmology & visual science,* 52**,** 4459-66.

IDA, H., TOBE, T., NAMBU, H., MATSUMURA, M., UYAMA, M. & CAMPOCHIARO, P. A. 2003. RPE cells modulate subretinal neovascularization, but do not cause regression in mice with sustained expression of VEGF. *Investigative ophthalmology & visual science,* 44**,** 5430-7.

IOANNIDOU, S., DEINHARDT, K., MIOTLA, J., BRADLEY, J., CHEUNG, E., SAMUELSSON, S., NG, Y. S. & SHIMA, D. T. 2006. An in vitro assay reveals a role for the diaphragm protein PV-1 in endothelial fenestra morphogenesis. *Proceedings of the National Academy of Sciences of the United States of America,* 103**,** 16770-5.

JACKSON, K. A., HELSTON, R. M., MCKAY, J. A., O'NEILL, E. D., MATHERS, J. C. & FORD, D. 2007. Splice variants of the human zinc transporter ZnT5 (SLC30A5) are differentially localized and regulated by zinc through transcription and mRNA stability. *J Biol Chem,* 282**,** 10423-31.

JAGER, R. D., MIELER, W. F. & MILLER, J. W. 2008. Age-related macular degeneration. *The New England journal of medicine,* 358**,** 2606-17.

JAKOBSDOTTIR, J., CONLEY, Y.P., WEEKS, D.E., MAH, T.S., FERRELL, R.E. & GORIN. 2005. Susceptibility genes for age-related maculopathy on chromosome 10q26. *American journal of human genetics,* 77, 389-407.

JANKOWSKI, M. A., URIU-HARE, J. Y., RUCKER, R. B., ROGERS, J. M. & KEEN, C. L. 1995. Maternal zinc deficiency, but not copper deficiency or diabetes, results in increased embryonic cell death in the rat: implications for mechanisms underlying abnormal development. *Teratology,* 51**,** 85-93.

JUNG, T., BADER, N. & GRUNE, T. 2007. Lipofuscin: Formation, distribution and metabolic consequences. *Annals of the New York academy of sciences*, 1119, 91-111.

KALER, P. & PRASAD, R. 2007. Molecular cloning and functional characterization of novel zinc transporter rZip10 (Slc39a10) involved in zinc uptake across rat renal brush-border membrane. *American journal of physiology. Renal physiology,* 292**,** F217-29.

KAMBE, T., GEISER, J., LAHNER, B., SALT, D. E. & ANDREWS, G. K. 2008. Slc39a1 to 3 (subfamily II) Zip genes in mice have unique cell-specific functions during adaptation to zinc deficiency. *American journal of physiology. Regulatory, integrative and comparative physiology,* 294**,** R1474-81.

KAMBE, T., NARITA, H., YAMAGUCHI-IWAI, Y., HIROSE, J., AMANO, T., SUGIURA, N., SASAKI, R., MORI, K., IWANAGA, T. & NAGAO, M. 2002. Cloning and characterization of a novel mammalian zinc transporter, zinc transporter 5, abundantly expressed in pancreatic beta cells. *J Biol Chem,* 277**,** 19049-55.

KAMBE, T., YAMAGUCHI-IWAI, Y., SASAKI, R. & NAGAO, M. 2004. Overview of mammalian zinc transporters. *Cellular and molecular life sciences : CMLS,* 61**,** 49-68.

KAMEI, M. & HOLLYFIELD, J.G. 1999. TIMP-3 in Bruch's membrane: changes during aging and in age-related macular degeneration. *Investigative ophthalmology visual science,* 40, 2367-2375.

KANDA, A., CHEN, W., OTHMAN, M., BRANHAM, K. E., BROOKS, M., KHANNA, R., HE, S., LYONS, R., ABECASIS, G. R. & SWAROOP, A. 2007. A variant of mitochondrial protein LOC387715/ARMS2, not HTRA1, is strongly associated with age-related macular degeneration. *Proceedings of the National Academy of Sciences of the United States of America,* 104**,** 16227-32.

KANEDA, M., ISHII, K., AKAGI, T., TATSUKAWA, T. & HASHIKAWA, T. 2005. Endogenous zinc can be a modulator of glycinergic signaling pathway in the rat retina. *Journal of molecular histology,* 36**,** 179-85.

KARCIOGLU, Z. A. 1982. Zinc in the eye. *Survey of ophthalmology,* 27**,** 114-22.

KATOH, K., KANO, Y., MASUDA, M., ONISHI, H. & FUJIWARA, K. 1998. Isolation and contraction of the Stress Fiber. *Molecular Biology of the Cell*, 9, 1919-1938.

KELLEHER, S. L. & LOPEZ, V. 2008. Zinc transproter-2 (ZnT2) is associated with mitochondria and functions as a zinc importer in mammary epithelial cells *The FASEB Journal,* 22**,** 692.2.

KETOLA, H. G. 1979. Influence of dietary zinc on cataracts in rainbow trout (Salmo gairdneri). *The Journal of nutrition,* 109**,** 965-9.

KIMURA, E., KOIKE, T. & SHIONOYA, M. 1997. Advances in zinc enzyme models by small, mononuclear zinc (II) complexes. *Metal sites in proteins and models*, 87, 1-28.

KINDERMANN, B., DORING, F., FUCHS, D., PFAFFL, M. W. & DANIEL, H. 2005. Effects of increased cellular zinc levels on gene and protein expression in HT-29 cells. *Biometals : an international journal on the role of metal ions in biology, biochemistry, and medicine,* 18**,** 243-53.

KIRSCHKE, C. P. & HUANG, L. 2003. ZnT7, a novel mammalian zinc transporter, accumulates zinc in the Golgi apparatus. *The Journal of biological chemistry,* 278**,** 4096-102.

KIRSCHKE, C. P. & HUANG, L. 2008. Expression of the ZNT (SLC30) family members in the epithelium of the mouse prostate during sexual maturation. *J Mol Histol,* 39**,** 359-70.

KITAMURA, H., MORIKAWA, H., KAMON, H., IGUCHI, M., HOJYO, S., FUKADA, T., YAMASHITA, S., KAISHO, T., AKIRA, S., MURAKAMI, M. & HIRANO, T. 2006. Toll-like receptor-mediated regulation of zinc homeostasis influences dendritic cell function. *Nature immunology,* 7**,** 971-7.

KLEIN, R. J., ZEISS, C., CHEW, E. Y., TSAI, J. Y., SACKLER, R. S., HAYNES, C., HENNING, A. K., SANGIOVANNI, J. P., MANE, S. M., MAYNE, S. T., BRACKEN, M. B., FERRIS, F. L., OTT, J., BARNSTABLE, C. & HOH, J.

2005. Complement factor H polymorphism in age-related macular degeneration. *Science,* 308**,** 385-9.

KOKKINOU, D., KASPER, H. U., BARTZ-SCHMIDT, K. U. & SCHRAERMEYER, U. 2004. The pigmentation of human iris influences the uptake and storing of zinc. *Pigment cell research / sponsored by the European Society for Pigment Cell Research and the International Pigment Cell Society,* 17**,** 515-8.

KOLLURU, G.K., TAMILARASAN, K.P., GEETHA-PRIYA, S., DURGHA, N.P. & CHATTERJEE, S. 2006. Cadmium induced endothelial dysfunction: consequence of defective migratory pattern of endothelial cells in association with poor nitric oxide availability under cadmium challenge. *Cell biology international*, 30, 427-438.

KONERIRAJAPURAM, N. S., CORAL, K., PUNITHAM, R., SHARMA, T., KASINATHAN, N. & SIVARAMAKRISHNAN, R. 2004. Trace elements iron, copper and zinc in vitreous of patients with various vitreoretinal diseases. *Indian journal of ophthalmology,* 52**,** 145-8.

KOUMANTAKIS, E., ALEXIOU, D., GRIMANIS, A., KASKARELIS, D. & BOUZAS, A. 1983. Zinc, cobalt and selenium concentrations in the premature and full-term newborn eye. *Ophthalmologica. Journal international d'ophtalmologie. International journal of ophthalmology. Zeitschrift fur Augenheilkunde,* 186**,** 41-6.

KUNZELMANN, K., MILENKOVIC, V. M., SPITZNER, M., SORIA, R. B. & SCHREIBER, R. 2007. Calcium-dependent chloride conductance in epithelia: is there a contribution by Bestrophin? *Pflugers Archiv : European journal of physiology,* 454**,** 879-89.

LANGMADE, S. J., RAVINDRA, R., DANIELS, P. J. & ANDREWS, G. K. 2000. The transcription factor MTF-1 mediates metal regulation of the mouse ZnT1 gene. *The Journal of biological chemistry,* 275**,** 34803-9.

LENGYEL, I., FLINN, J. M., PETO, T., LINKOUS, D. H., CANO, K., BIRD, A. C., LANZIROTTI, A., FREDERICKSON, C. J. & VAN KUIJK, F. J. 2007. High

concentration of zinc in sub-retinal pigment epithelial deposits. *Experimental eye research,* 84**,** 772-80.

LENGYEL, I., TUFAIL, A., HOSAINI, H. A., LUTHERT, P., BIRD, A. C. & JEFFERY, G. 2004. Association of drusen deposition with choroidal intercapillary pillars in the aging human eye. *Investigative ophthalmology & visual science,* 45**,** 2886-92.

LESBURG, C.A., AND CHRISTIANSON, D.W. 1995. X-ray crystallographic studies of engineered hydrogen bond networks in a protein-zinc binding site. *The Journal of American Chemistry Society*, 117, 6838-6844.

LEUNG, K. W., LIU, M., XU, X., SEILER, M. J., BARNSTABLE, C. J. & TOMBRAN-TINK, J. 2008. Expression of ZnT and ZIP zinc transporters in the human RPE and their regulation by neurotrophic factors. *Investigative ophthalmology & visual science,* 49**,** 1221-31.

LEURE-DUPREE, A. E. 1986. Vascularization of the rat cornea after prolonged zinc deficiency. *The Anatomical record,* 216**,** 27-32.

LIN, Y.F., LIANG, H.M., YANG, S.Y., BOCH, A., CLEMENS, S., CHEN, C.C., WU, J.F., HUANG, J.L., & YEH, K.C. 2009. Arabidopsis IRT3 is a zinc-regulated and plasma membrane localized zinc/iron transporter. *New Phytologist*, 2, 392-404.

LIU, L.B., XUE, Y.X., LIU, Y.H. & WANG, Y.B. 2008. Bradykinin increases blood-tumor barrier permeability by down-regulating the expression levels of ZO-1, occludin and claudin-5 and rearranging actin cytoskeleton. *Journal of neuroscience research.* 5, 1153-1168.

LIUZZI, J. P., BLANCHARD, R. K. & COUSINS, R. J. 2001a. Differential regulation of zinc transporter 1, 2, and 4 mRNA expression by dietary zinc in rats. *J Nutr,* 131**,** 46-52.

LIUZZI, J. P. & COUSINS, R. J. 2004a. Mammalian zinc transporters. *Annu Rev Nutr,* 24**,** 151-72.

LIUZZI, J. P., LICHTEN, L. A., RIVERA, S., BLANCHARD, R. K., AYDEMIR, T. B., KNUTSON, M. D., GANZ, T. & COUSINS, R. J. 2005. Interleukin-6 regulates the zinc transporter Zip14 in liver and contributes to the hypozincemia of the acute-phase response. *Proceedings of the National Academy of Sciences of the United States of America,* 102**,** 6843-8.

LOOMANS, H. J., HAHN, B. L., LI, Q. Q., PHADNIS, S. H. & SOHNLE, P. G. 1998. Histidine-based zinc-binding sequences and the antimicrobial activity of calprotectin. *The Journal of infectious diseases,* 177**,** 812-4.

LOPEZ, V. & KELLEHER, S. L. 2009. Zinc transporter-2 (ZnT2) variants are localized to distinct subcellular compartments and functionally transport zinc. *The Biochemical journal,* 422**,** 43-52.

LUTTY, G. A., HASEGAWA, T., BABA, T., GREBE, R., BHUTTO, I. & MCLEOD, D. S. 2010. Development of the human choriocapillaris. *Eye,* 24**,** 408-15.

LYUBARTSEVA, G., SMITH, J. L., MARKESBERY, W. R. & LOVELL, M. A. 2010. Alterations of zinc transporter proteins ZnT-1, ZnT-4 and ZnT-6 in preclinical Alzheimer's disease brain. *Brain pathology,* 20**,** 343-50.

MAIER, J.A.M., BERNARDINI, D., RAYSSIGUIER, Y. & MAZUR, A. 2004. High concentrations of magnesium modulate vascular endothelial cell behaviour in vitro. *Biochemical biophysical acta,* 1689, 6-12.

MANCINI, M. A., FRANK, R. N., KEIRN, R. J., KENNEDY, A. & KHOURY, J. K. 1986. Does the retinal pigment epithelium polarize the choriocapillaris? *Investigative ophthalmology & visual science,* 27**,** 336-45.

MARET, W. 2008. Metallothionein redox biology in the cytoprotective and cytotoxic functions of zinc. *Experimental gerontology,* 43**,** 363-9.

MARET, W. & LI, Y. 2009. Coordination dynamics of zinc in proteins. *Chemical reviews,* 109**,** 4682-707.

MARTIN, T.A. & GIANG, W.G. 2009. Loss of tight junction barrier and its role in cancer metastasis. *Biochimica et biophysica acta.* 1788, 872-891.

MATSUURA, W., YAMAZAKI, T., YAMAGUCHI-IWAI, Y., MASUDA, S., NAGAO, M., ANDREWS, G. K. & KAMBE, T. 2009. SLC39A9 (ZIP9) regulates zinc homeostasis in the secretory pathway: characterization of the ZIP subfamily I protein in vertebrate cells. *Bioscience, biotechnology, and biochemistry,* 73**,** 1142-8.

MCBEAN, L. D., DOVE, J. T., HALSTED, J. A. & SMITH, J. C., JR. 1972. Zinc concentration in human tissues. *The American journal of clinical nutrition,* 25**,** 672-6.

MCCLAIN, C. J., ANTONOW, D. R., COHEN, D. A. & SHEDLOFSKY, S. I. 1986. Zinc metabolism in alcoholic liver disease. *Alcoholism, clinical and experimental research,* 10**,** 582-9.

MCLEOD, D. S., GREBE, R., BHUTTO, I., MERGES, C., BABA, T. & LUTTY, G. A. 2009. Relationship between RPE and choriocapillaris in age-related macular degeneration. *Investigative ophthalmology & visual science,* 50**,** 4982-91.

MICELI, M. V., TATE, D. J., JR., ALCOCK, N. W. & NEWSOME, D. A. 1999. Zinc deficiency and oxidative stress in the retina of pigmented rats. *Investigative ophthalmology & visual science,* 40**,** 1238-44.

MILON, B., DHERMY, D., POUNTNEY, D., BOURGEOIS, M. & BEAUMONT, C. 2001. Differential subcellular localization of hZip1 in adherent and non-adherent cells. *FEBS letters,* 507**,** 241-6.

MITCHELL, P., SMITH, W., ATTEBO, K. & WANG, J. J. 1995. Prevalence of age-related maculopathy in Australia. The Blue Mountains Eye Study. *Ophthalmology,* 102**,** 1450-60.

MOISEYEV, G., TAKAHASHI, Y., CHEN, Y., GENTLEMAN, S., REDMOND, T. M., CROUCH, R. K. & MA, J. X. 2006. RPE65 is an iron(II)-dependent isomerohydrolase in the retinoid visual cycle. *The Journal of biological chemistry,* 281**,** 2835-40.

MORI, K., DUH, E., GEHLBACH, P., ANDO, A., TAKAHASHI, K., PEARLMAN, J., YANG, H. S., ZACK, D. J., ETTYREDDY, D., BROUGH, D. E., WEI, L. L. & CAMPOCHIARO, P. A. 2001. Pigment epithelium-derived factor inhibits

retinal and choroidal neovascularization. *Journal of cellular physiology,* 188**,** 253-63.

MORIARTY-CRAIGE, S. E., HA, K. N., STERNBERG, P., JR., LYNN, M., BRESSLER, S., GENSLER, G. & JONES, D. P. 2007. Effects of long-term zinc supplementation on plasma thiol metabolites and redox status in patients with age-related macular degeneration. *American journal of ophthalmology,* 143**,** 206-211.

MUGA, S. J. & GRIDER, A. 1999. Partial characterization of a human zinc-deficiency syndrome by differential display. *Biological trace element research,* 68**,** 1-12.

MULLINS, R. F., JOHNSON, M. N., FAIDLEY, E. A., SKEIE, J. M. & HUANG, J. 2011. Choriocapillaris vascular dropout related to density of drusen in human eyes with early age-related macular degeneration. *Investigative ophthalmology & visual science,* 52**,** 1606-12.

MURAKAMI, M. & HIRANO, T. 2008. Intracellular zinc homeostasis and zinc signaling. *Cancer science,* 99**,** 1515-22.

MURGIA, C., VESPIGNANI, I., CERASE, J., NOBILI, F. & PEROZZI, G. 1999. Cloning, expression, and vesicular localization of zinc transporter Dri 27/ZnT4 in intestinal tissue and cells. *The American journal of physiology,* 277**,** G1231-9.

MURGIA, C., VESPIGNANI, I., RAMI, R. & PEROZZI, G. 2006. The Znt4 mutation inlethal milk mice affects intestinal zinc homeostasis through the expression of other Zn transporters. *Genes & nutrition,* 1**,** 61-70.

NABI, I. R., MATHEWS, A. P., COHEN-GOULD, L., GUNDERSEN, D. & RODRIGUEZ-BOULAN, E. 1993. Immortalization of polarized rat retinal pigment epithelium. *Journal of cell science,* 104 (Pt 1)**,** 37-49.

NAN, R., FARABELLA, I., SCHUMACHER, F. F., MILLER, A., GOR, J., MARTIN, A. C., JONES, D. T., LENGYEL, I. & PERKINS, S. J. 2011. Zinc binding to the Tyr402 and His402 allotypes of complement factor H: possible

implications for age-related macular degeneration. *Journal of molecular biology,* 408**,** 714-35.

NAN, R., GOR, J., LENGYEL, I. & PERKINS, S. J. 2008. Uncontrolled zinc- and copper-induced oligomerisation of the human complement regulator factor H and its possible implications for function and disease. *Journal of molecular biology,* 384**,** 1341-52.

NARDINOCCHI, L., PANTISANO, V., PUCA, R., PORRU, M., AIELLO, A., GRASSELLI, A., LEONETTI, C., SAFRAN, M., RECHAVI, G., GIVOL, D., FARSETTI, A. & D'ORAZI, G. 2010. Zinc downregulates HIF-1alpha and inhibits its activity in tumor cells in vitro and in vivo. *PloS one,* 5**,** e15048.

NEWSOME, D. A., OLIVER, P. D., DEUPREE, D. M., MICELI, M. V. & DIAMOND, J. G. 1992. Zinc uptake by primate retinal pigment epithelium and choroid. *Current eye research,* 11**,** 213-7.

NEWSOME, D. A., SWARTZ, M., LEONE, N. C., ELSTON, R. C. & MILLER, E. 1988. Oral zinc in macular degeneration. *Archives of ophthalmology,* 106**,** 192-8.

NIESSEN, C.M. 2007. Tight junctions/ adherens junctions: basic structure and function. *Journal of investigative dermatology.* 127, 2525-2532.

NISHIMURA, M. & NAITO, S. 2008. Tissue-specific mRNA expression profiles of human solute carrier transporter superfamilies. *Drug metabolism and pharmacokinetics,* 23**,** 22-44.

NOBES, C.D. & HALL, A. 1995. Rho, rac, and cdc42 GTPases regulate the assembly of multimolecular focal complexes associated with actin stress fibers, lamellipodia and filopodia. *Cell*, 81, 53-62

NOURMOHAMMADI, I., MODARRESS, M. & PAKDEL, F. 2006. Assessment of aqueous humor zinc status in human age-related cataract. *Annals of nutrition & metabolism,* 50**,** 51-3.

NOWAK, J.Z. 2006. Age-related macular degeneration (AMD): Pathogenesis and Therapy. *Pharmacological reports*. 58, 353-363.

OGATA, N., WADA, M., OTSUJI, T., JO, N., TOMBRAN-TINK, J. & MATSUMURA, M. 1999. Expression of pigment epithelium-derived factor in normal adult rat eye and experimental choroidal neovascularisation. *Investigative ophthalmology visual science*, 43, 1168-1175.

PALMITER, R. D., COLE, T. B., QUAIFE, C. J. & FINDLEY, S. D. 1996. ZnT-3, a putative transporter of zinc into synaptic vesicles. *Proc Natl Acad Sci U S A,* 93**,** 14934-9.

PALMITER, R. D. & FINDLEY, S. D. 1995. Cloning and functional characterization of a mammalian zinc transporter that confers resistance to zinc. *The EMBO journal,* 14**,** 639-49.

PALMITER, R. D. & HUANG, L. 2004. Efflux and compartmentalization of zinc by members of the SLC30 family of solute carriers. *Pflugers Archiv : European journal of physiology,* 447**,** 744-51.

PARK, K., JIN, J., HU, Y., ZHOU, K. & MA, J. X. 2011. Overexpression of pigment epithelium-derived factor inhibits retinal inflammation and neovascularization. *The American journal of pathology,* 178**,** 688-98.

PEDELACQ, J. D., CABANTOUS, S., TRAN, T., TERWILLIGER, T. C. & WALDO, G. S. 2006. Engineering and characterization of a superfolder green fluorescent protein. *Nature biotechnology,* 24**,** 79-88.

PRASAD, A. S. 1998. Zinc and immunity. *Mol Cell Biochem,* 188**,** 63-9.

PRASAD, A. S. 2008. Zinc in human health: effect of zinc on immune cells. *Molecular medicine,* 14**,** 353-7.

PRASAD, A. S., MIALE, A., JR., FARID, Z., SANDSTEAD, H. H. & SCHULERT, A. R. 1963. Zinc metabolism in patients with the syndrome of iron deficiency anemia, hepatosplenomegaly, dwarfism, and hypognadism. *The Journal of laboratory and clinical medicine,* 61**,** 537-49.

PREBEN-MORTH, PEDERSEN, B.P., TOUSTRUP-JENSEN, M.S., SORENSEN, T.L.M., PETERSEN, J., ANDERSEN, J.P., VILSEN, B. & NISSEN, P. 2007. Crystal structure of the sodium-potassium pump. *Nature*, 450, 1043-1049.

PREDESCU, D., HORVAT, R., PREDESCU, S. & PALADE, G. E. 1994. Transcytosis in the continuous endothelium of the myocardial microvasculature is inhibited by N-ethylmaleimide. *Proceedings of the National Academy of Sciences of the United States of America,* 91**,** 3014-8.

RACZ, P., KOVACS, B., VARGA, L., UJLAKI, E., ZOMBAI, E. & KARBUCZKY, S. 1979. Bilateral cataract in acrodermatitis enteropathica. *Journal of pediatric ophthalmology and strabismus,* 16**,** 180-2.

RAJASEKARAN, S.A., HU, J., GOPAL, J., GALLEMORE, R., RYAZANTSEV, S., BOK, D. & RAJASEKARAN, A.K. 2003. Na,K-ATPase inhibition alters tight junction structure and permeability in human retinal pigment epithelial cells. *The American journal of physiology and cell physiology.* 284, C1497-C1507.

RAJASEKARAN, S.A., PALMER, L.G., MOON, S.Y., SOLER, A.P., HARPER, J.F., ZHENG, Y. & APODACA, G.L. 2001. Na,K-ATPase Activity Is Required for Formation of Tight Junctions, Desmosomes, and Induction of Polarity in Epithelial Cells. *Molecular biology of the cell*, 12, 3717-3732.

RATTNER, A. & NATHANS, J. 2006. Macular degeneration: recent advances and therapeutic opportunities. *Nature reviews. Neuroscience,* 7**,** 860-72.

REAUME, A. G., ELLIOTT, J. L., HOFFMAN, E. K., KOWALL, N. W., FERRANTE, R. J., SIWEK, D. F., WILCOX, H. M., FLOOD, D. G., BEAL, M. F., BROWN, R. H., JR., SCOTT, R. W. & SNIDER, W. D. 1996. Motor neurons in Cu/Zn superoxide dismutase-deficient mice develop normally but exhibit enhanced cell death after axonal injury. *Nature genetics,* 13**,** 43-7.

REDENTI, S. & CHAPPELL, R. L. 2003. Zinc chelation enhances the sensitivity of the ERG b-wave in dark-adapted skate retina. *The Biological bulletin,* 205**,** 213-4.

REDENTI, S. & CHAPPELL, R. L. 2004a. Localization of zinc transporter-3 (ZnT-3) in mouse retina. *Vision Res,* 44**,** 3317-21.

REDENTI, S. & CHAPPELL, R. L. 2005. Neuroimaging of zinc released by depolarization of rat retinal cells. *Vision research,* 45**,** 3520-5.

REMINGTON, Lee Ann. Clinical Anatomy of the Visual System. Newton, Massachusetts: Butterworth-Heinemann, 1998.

REYES, J. G. 1996. Zinc transport in mammalian cells. *The American journal of physiology,* 270**,** C401-10.

REZAEI, K. A., CHEN, Y., CAI, J. & STERNBERG, P. 2008a. Modulation of Nrf2-dependent antioxidant functions in the RPE by Zip2, a zinc transporter protein. *Investigative ophthalmology & visual science,* 49**,** 1665-70.

RICHARD, M. J., GUIRAUD, P., LECCIA, M. T., BEANI, J. C. & FAVIER, A. 1993. Effect of zinc supplementation on resistance of cultured human skin fibroblasts toward oxidant stress. *Biological trace element research,* 37**,** 187-99.

RICHARDSON, N. L., HIGGS, D. A., BEAMES, R. M. & MCBRIDE, J. R. 1985. Influence of dietary calcium, phosphorus, zinc and sodium phytate level on cataract incidence, growth and histopathology in juvenile chinook salmon (Oncorhynchus tshawytscha). *The Journal of nutrition,* 115**,** 553-67.

RINK, LOTHAR. Zinc in Human Health. Amsterdam, Netherlands: IOS Press, 2011.

ROBERTS, W. G. & PALADE, G. E. 1995. Increased microvascular permeability and endothelial fenestration induced by vascular endothelial growth factor. *Journal of cell science,* 108 (Pt 6)**,** 2369-79.

ROBINSON, N.J. 2007. A more discerning zinc exporter. *Nature chemical biology*, 3, 692-693.

ROGERS, J. M. & HURLEY, L. S. 1987. Effects of zinc deficiency on morphogenesis of the fetal rat eye. *Development,* 99**,** 231-8.

ROHRER, B., GOLETZ, P., ZNOIKO, S., ABLONCZY, Z., MA, J. X., REDMOND, T. M. & CROUCH, R. K. 2003. Correlation of regenerable opsin with rod ERG signal in Rpe65-/- mice during development and aging. *Investigative ophthalmology & visual science,* 44**,** 310-5.

ROSENSTEIN, F. J. & CHAPPELL, R. L. 2003. Endogenous zinc as a retinal neuromodulator: evidence from the skate (Raja erinacea). *Neuroscience letters,* 345**,** 81-4.

ROWE, D. J. & BOBILYA, D. J. 2000. Albumin facilitates zinc acquisition by endothelial cells. *Proceedings of the Society for Experimental Biology and Medicine. Society for Experimental Biology and Medicine,* 224**,** 178-86.

SAINT-GENIEZ, M., KURIHARA, T. & D'AMORE, P. A. 2009a. Role of cell and matrix-bound VEGF isoforms in lens development. *Investigative ophthalmology & visual science,* 50**,** 311-21.

SAINT-GENIEZ, M., KURIHARA, T., SEKIYAMA, E., MALDONADO, A. E. & D'AMORE, P. A. 2009b. An essential role for RPE-derived soluble VEGF in the maintenance of the choriocapillaris. *Proceedings of the National Academy of Sciences of the United States of America,* 106**,** 18751-6.

SATCHELL, S. C. & BRAET, F. 2009. Glomerular endothelial cell fenestrations: an integral component of the glomerular filtration barrier. *American journal of physiology. Renal physiology,* 296**,** F947-56.

SCHMITTGEN, T. D. & LIVAK, K. J. 2008. Analyzing real-time PCR data by the comparative C(T) method. *Nature protocols,* 3**,** 1101-8.

SCHNITZER, J. E. 1992. gp60 is an albumin-binding glycoprotein expressed by continuous endothelium involved in albumin transcytosis. *The American journal of physiology,* 262**,** H246-54.

SCHRAERMEYER, U., PETERS, S., THUMANN, G., KOCIOK, N. & HEIMANN, K. 1999. Melanin granules of retinal pigment epithelium are connected with the lysosomal degradation pathway. *Experimental eye research,* 68**,** 237-45.

SCHUPP, C., OLANO-MARTIN, E., GERTH, C., MORRISSEY, B.M., CROSS, C.E.& WERNE, J.S. 2004. Lutein, zeaxanthin, macular pigment, and visual function in adult cystic fibrosis patients. *American journal of clinical nutrition*, 79, 1045-1052.

SEDDON, J. M. 2007. Multivitamin-multimineral supplements and eye disease: age-related macular degeneration and cataract. *The American journal of clinical nutrition,* 85**,** 304S-307S.

SEKLER, I., SENSI, S. L., HERSHFINKEL, M. & SILVERMAN, W. F. 2007. Mechanism and regulation of cellular zinc transport. *Molecular medicine,* 13**,** 337-43.

SENSI, S. L., YIN, H. Z. & WEISS, J. H. 2000. AMPA/kainate receptor-triggered Zn2+ entry into cortical neurons induces mitochondrial Zn2+ uptake and persistent mitochondrial dysfunction. *The European journal of neuroscience,* 12**,** 3813-8.

SEVE, M., CHIMIENTI, F., DEVERGNAS, S. & FAVIER, A. 2004. In silico identification and expression of SLC30 family genes: an expressed sequence tag data mining strategy for the characterization of zinc transporters' tissue expression. *BMC genomics,* 5**,** 32.

SHUE, E. H., CARSON-WALTER, E. B., LIU, Y., WINANS, B. N., ALI, Z. S., CHEN, J. & WALTER, K. A. 2008. Plasmalemmal vesicle associated protein-1 (PV-1) is a marker of blood-brain barrier disruption in rodent models. *BMC neuroscience,* 9**,** 29.

SIM, D. L. & CHOW, V. T. 1999. The novel human HUEL (C4orf1) gene maps to chromosome 4p12-p13 and encodes a nuclear protein containing the nuclear receptor interaction motif. *Genomics,* 59**,** 224-33.

SIM, D. L., YEO, W. M. & CHOW, V. T. 2002. The novel human HUEL (C4orf1) protein shares homology with the DNA-binding domain of the XPA DNA repair protein and displays nuclear translocation in a cell cycle-dependent manner. *The international journal of biochemistry & cell biology,* 34**,** 487-504.

SONDERGAARD, L. G., BROCK, B., STOLTENBERG, M., FLYVBJERG, A., SCHMITZ, O., SMIDT, K., DANSCHER, G. & RUNGBY, J. 2005. Zinc fluxes during acute and chronic exposure of INS-1E cells to increasing glucose levels. *Hormone and metabolic research = Hormon- und Stoffwechselforschung = Hormones et metabolisme,* 37**,** 133-9.

SONODA, S., SREEKUMAR, P.G., KASE, S., SPEE, C., RYAN, S.J, KANNAN, R. & HINTON D.R. 2010. Attainment of polarity promotes growth factor secretion by retinal pigment epithelial cells: Relevance to age-related macular degeneration. 2003. *The journal of cell biology.* 3, 423-432.

SONODA, S., SPEE, C., BARRON, E., RYAN, S. J., KANNAN, R. & HINTON, D. R. 2009. A protocol for the culture and differentiation of highly polarized human retinal pigment epithelial cells. *Nature protocols,* 4**,** 662-73.

SOTIRIOU, C., WIRAPATI, P., LOI, S., HARRIS, A., FOX, S., SMEDS, J., NORDGREN, H., FARMER, P., PRAZ, V., HAIBE-KAINS, B., DESMEDT, C., LARSIMONT, D., CARDOSO, F., PETERSE, H., NUYTEN, D., BUYSE, M., VAN DE VIJVER, M. J., BERGH, J., PICCART, M. & DELORENZI, M. 2006. Gene expression profiling in breast cancer: understanding the molecular basis of histologic grade to improve prognosis. *Journal of the National Cancer Institute,* 98**,** 262-72.

SPARROW, J.R., BEN-SHABAT, S., VOLLMER, H., ITAGAKI, Y. & NAKANISHI, K. 2002. Involvement of oxidative mechanisms in blue-light induced damage to AE2-laden RPE. *Investigative ophthalmology visual science*, 43, 1222-1227.

STAN, R. V. 2004. Multiple PV1 dimers reside in the same stomatal or fenestral diaphragm. *American journal of physiology. Heart and circulatory physiology,* 286**,** H1347-53.

STAN, R. V. 2007. Endothelial stomatal and fenestral diaphragms in normal vessels and angiogenesis. *Journal of cellular and molecular medicine,* 11**,** 621-43.

STAN, R. V., ARDEN, K. C. & PALADE, G. E. 2001. cDNA and protein sequence, genomic organization, and analysis of cis regulatory elements of mouse and human PLVAP genes. *Genomics,* 72**,** 304-13.

STAN, R. V., KUBITZA, M. & PALADE, G. E. 1999. PV-1 is a component of the fenestral and stomatal diaphragms in fenestrated endothelia. *Proceedings of the National Academy of Sciences of the United States of America,* 96**,** 13203-7.

STONE, E. M. 2007. Macular degeneration. *Annual review of medicine,* 58**,** 477-90.

STRAUSS, O. 2005. The retinal pigment epithelium in visual function. *Physiological reviews,* 85**,** 845-81.

STRICKLAND, L. A., JUBB, A. M., HONGO, J. A., ZHONG, F., BURWICK, J., FU, L., FRANTZ, G. D. & KOEPPEN, H. 2005. Plasmalemmal vesicle-associated protein (PLVAP) is expressed by tumour endothelium and is upregulated by vascular endothelial growth factor-A (VEGF). *The Journal of pathology,* 206**,** 466-75.

STRZELECKA-GOLASZEWSKA, H., PROCHNIEWICZ, E. & DRABIKOWSKI, W. 1978. Interaction of actin with divalent cations. 2. Characterization of protein-metal complexes. *European journal of biochemistry / FEBS,* 88**,** 229-37.

SUMITA, R. 1961. The fine structure of Bruch's Membrane of the Human Choroid as Revealed by Electron Microscopy. *The Journal of Electron Microscopy (Tokyo)*, 10(2), 111-118.

SWAROOP, A., CHEW, E.Y. & ABECASIS, A. 2009. Unraveling a multifactorial late onset disease: From genetic susceptibility to disease mechanisms for age-related macular degeneration. *Annual Reviews Genomics: Human Genetics*, 10, 19-43.

TAKAHASHI, H., AKIBA, K., NOGUCHI, T., OHMURA, T., TAKAHASHI, R., EZURE, Y., OHARA, K. & ZIESKE, J. D. 2000. Matrix metalloproteinase activity is enhanced during corneal wound repair in high glucose condition. *Current eye research,* 21**,** 608-15.

TAM, S. W., WILBER, K. E. & WAGNER, F. W. 1976. Light sensitive zinc content of protein fractions from bovine rod outer segments. *Biochemical and biophysical research communications,* 72**,** 302-9.

TAMIYA, S., LIU, L.H. & KAPLAN, H.J. 2009. Epithelial-mesenchymal transition and proliferation of retinal pigment epithelial cells initiated upon loss of cell-cell contact. *Investigative ophthalmology visual science*. 51, 52755-52763.

TATE, D. J., JR., MICELI, M. V. & NEWSOME, D. A. 1997. Zinc induces catalase expression in cultured fetal human retinal pigment epithelial cells. *Current eye research,* 16**,** 1017-23.

TATE, D. J., JR., MICELI, M. V. & NEWSOME, D. A. 1999. Zinc protects against oxidative damage in cultured human retinal pigment epithelial cells. *Free radical biology & medicine,* 26**,** 704-13.

TATE, D. J., MICELI, M. V., NEWSOME, D. A., ALCOCK, N. W. & OLIVER, P. D. 1995. Influence of zinc on selected cellular functions of cultured human retinal pigment epithelium. *Current eye research,* 14**,** 897-903.

TAYLOR, K. M. 2000. LIV-1 breast cancer protein belongs to new family of histidine-rich membrane proteins with potential to control intracellular Zn2+ homeostasis. *IUBMB life,* 49**,** 249-53.

TAYLOR, K. M., MORGAN, H. E., JOHNSON, A., HADLEY, L. J. & NICHOLSON, R. I. 2003. Structure-function analysis of LIV-1, the breast cancer-associated protein that belongs to a new subfamily of zinc transporters. *The Biochemical journal,* 375**,** 51-9.

TAYLOR, K. M., MORGAN, H. E., SMART, K., ZAHARI, N. M., PUMFORD, S., ELLIS, I. O., ROBERTSON, J. F. & NICHOLSON, R. I. 2007. The emerging role of the LIV-1 subfamily of zinc transporters in breast cancer. *Molecular medicine,* 13**,** 396-406.

TAYLOR, K. M. & NICHOLSON, R. I. 2003. The LZT proteins; the LIV-1 subfamily of zinc transporters. *Biochimica et biophysica acta,* 1611**,** 16-30.

TAYLOR, K. M., VICHOVA, P., JORDAN, N., HISCOX, S., HENDLEY, R. & NICHOLSON, R. I. 2008. ZIP7-mediated intracellular zinc transport contributes to aberrant growth factor signaling in antihormone-resistant breast cancer Cells. *Endocrinology,* 149**,** 4912-20.

THOMPSON, D. A., GYURUS, P., FLEISCHER, L. L., BINGHAM, E. L., MCHENRY, C. L., APFELSTEDT-SYLLA, E., ZRENNER, E., LORENZ, B., RICHARDS, J. E., JACOBSON, S. G., SIEVING, P. A. & GAL, A. 2000.

Genetics and phenotypes of RPE65 mutations in inherited retinal degeneration. *Investigative ophthalmology & visual science,* 41**,** 4293-9.

THORNTON, J. K., TAYLOR, K. M., FORD, D. & VALENTINE, R. A. 2011. Differential subcellular localization of the splice variants of the zinc transporter ZnT5 is dictated by the different C-terminal regions. *PloS one,* 6**,** e23878.

TOMAT, A. L., WEISSTAUB, A. R., JAUREGUI, A., PINEIRO, A., BALASZCZUK, A. M., COSTA, M. A. & ARRANZ, C. T. 2005. Moderate zinc deficiency influences arterial blood pressure and vascular nitric oxide pathway in growing rats. *Pediatric research,* 58**,** 672-6.

TOMBRAN-TINK, J., CHADER, G.G. & JOHNSON, L.V. 1991. PEDF: a pigment epithelium-derived factor with potent neuronal differentiative capacity. *Experimental eye research,* 53, 411-414.

TOMBRAN-TINK, J. & BARNSTABLE, C.J. 2002. PEDF: a multifaceted neurotrophic factor. *Nature reviews neuroscience*, 4, 628-636.

TSUDA, M., IMAIZUMI, K., KATAYAMA, T., KITAGAWA, K., WANAKA, A., TOHYAMA, M. & TAKAGI, T. 1997. Expression of zinc transporter gene, ZnT-1, is induced after transient forebrain ischemia in the gerbil. *The Journal of neuroscience : the official journal of the Society for Neuroscience,* 17**,** 6678-84.

TUROWSKI, P., ADAMSON, P., SATHIA, J., ZHANG, J. J., MOSS, S. E., AYLWARD, G. W., HAYES, M. J., KANUGA, N. & GREENWOOD, J. 2004. Basement membrane-dependent modification of phenotype and gene expression in human retinal pigment epithelial ARPE-19 cells. *Investigative ophthalmology & visual science,* 45**,** 2786-94.

UENO, S., TSUKAMOTO, M., HIRANO, T., KIKUCHI, K., YAMADA, M. K., NISHIYAMA, N., NAGANO, T., MATSUKI, N. & IKEGAYA, Y. 2002. Mossy fiber Zn2+ spillover modulates heterosynaptic N-methyl-D-aspartate receptor activity in hippocampal CA3 circuits. *The Journal of cell biology,* 158**,** 215-20.

UGARTE, M. & OSBORNE, N. N. 2001. Zinc in the retina. *Progress in neurobiology,* 64**,** 219-49.

ULSHAFER, R. J. 1989. Zinc content in melanosomes of degenerating RPE as measured by X-ray mapping. *Progress in clinical and biological research,* 314**,** 131-9.

ULSHAFER, R. J., ALLEN, C. B. & RUBIN, M. L. 1990. Distributions of elements in the human retinal pigment epithelium. *Archives of ophthalmology,* 108**,** 113-7.

UZZO, R.G., CRISPEN, P.L., GOLOVINE, K., MAKHOV, P., HORWITZ, E.M. & KOLENKO, V.M. 2006. Diverse effects of zinc on NF-κB and AP-1 transcription factors: implications for prostate cancer progression. *Carcinogenesis*, 27, 1980-1990.

VALENTINE, R. A., JACKSON, K. A., CHRISTIE, G. R., MATHERS, J. C., TAYLOR, P. M. & FORD, D. 2007. ZnT5 variant B is a bidirectional zinc transporter and mediates zinc uptake in human intestinal Caco-2 cells. *J Biol Chem,* 282**,** 14389-93.

VALLEE, B. L. & FALCHUK, K. H. 1993. The biochemical basis of zinc physiology. *Physiological reviews,* 73**,** 79-118.

VUGLER, A., CARR, A. J., LAWRENCE, J., CHEN, L. L., BURRELL, K., WRIGHT, A., LUNDH, P., SEMO, M., AHMADO, A., GIAS, C., DA CRUZ, L., MOORE, H., ANDREWS, P., WALSH, J. & COFFEY, P. 2008. Elucidating the phenomenon of HESC-derived RPE: anatomy of cell genesis, expansion and retinal transplantation. *Experimental neurology,* 214**,** 347-61.

WALKUP, G. K., BURDETTE, S. C., LIPPARD, S. J. & TSIEN, R. Y. 2000. A new cell-permeable fluorescent probe for Zn2+. *Journal of the American Chemical Society,* 122**,** 5644-5645.

WANG, B. Y., JU, X. H., FU, B. Y., ZHANG, J. & CAO, Y. X. 2005. Effects of ethanol on liver sinusoidal endothelial cells-fenestrae of rats. *Hepatobiliary & pancreatic diseases international : HBPD INT,* 4**,** 422-6.

WANG, F., DUFNER-BEATTIE, J., KIM, B. E., PETRIS, M. J., ANDREWS, G. & EIDE, D. J. 2004a. Zinc-stimulated endocytosis controls activity of the mouse ZIP1 and ZIP3 zinc uptake transporters. *The Journal of biological chemistry,* 279**,** 24631-9.

WANG, X., WANG, Z. Y., GAO, H. L., DANSCHER, G. & HUANG, L. 2006. Localization of ZnT7 and zinc ions in mouse retina--immunohistochemistry and selenium autometallography. *Brain research bulletin,* 71**,** 91-6.

WANG, X., WU, Y. & ZHOU, B. 2009a. Dietary zinc absorption is mediated by ZnT1 in Drosophila melanogaster. *FASEB J,* 23**,** 2650-61.

WANG, Z. Y., STOLTENBERG, M., JO, S. M., HUANG, L., LARSEN, A., DAHLSTROM, A. & DANSCHER, G. 2004b. Dynamic zinc pools in mouse choroid plexus. *Neuroreport,* 15**,** 1801-4.

WEAVER, B. P., DUFNER-BEATTIE, J., KAMBE, T. & ANDREWS, G. K. 2007. Novel zinc-responsive post-transcriptional mechanisms reciprocally regulate expression of the mouse Slc39a4 and Slc39a5 zinc transporters (Zip4 and Zip5). *Biological chemistry,* 388**,** 1301-12.

WENZLAU, J.M., JUHL, K., YU, L., MOUA, O., SARKAR, S.A., GOTTLIEB, P., REWERS, M., EISENBARTH, G.S., JENSEN, J., DAVIDSON, H.W., & HUTTON J.C. 2007. The cation efflux transporter ZnT8 (SLC30A8) is a major autoantigen in human type1 diabetes. *Proceedings of the National Academy of Sciences*, 43, 17040-17045.

WESTENKOW, P., PICCOLO, S. & FUHRMANN, S. 2009. Beta-catenin controls differentiation of the retinal pigment epithelium in the mouse optic cup by regulating Mitf and Otx2 expression. *Development*, 136, 2505-2510.

WILLS, N. K., KALARIYA, N., SADAGOPA RAMANUJAM, V. M., LEWIS, J. R., HAJI ABDOLLAHI, S., HUSAIN, A. & VAN KUIJK, F. J. 2009. Human retinal cadmium accumulation as a factor in the etiology of age-related macular degeneration. *Experimental eye research,* 89**,** 79-87.

WILLS, N. K., RAMANUJAM, V. M., KALARIYA, N., LEWIS, J. R. & VAN KUIJK, F. J. 2008. Copper and zinc distribution in the human retina:

relationship to cadmium accumulation, age, and gender. *Experimental eye research,* 87**,** 80-8.

WOJCIAK-STOTHARD, B., POTEMPA, S., EICHHOLTZ, T & RIDLEY, A.J. 2001. 9Rgr and Rac but not Cdc43 regulate endothelial cell permeability. *Journal of cell science*, 114, 1343-1355.

WOOD, J. P. & OSBORNE, N. N. 2003. Zinc and energy requirements in induction of oxidative stress to retinal pigmented epithelial cells. *Neurochemical research,* 28**,** 1525-33.

WRIGHT, P. L., SMITH, K. F., DAY, W. A. & FRASER, R. 1983. Small liver fenestrae may explain the susceptibility of rabbits to atherosclerosis. *Arteriosclerosis,* 3**,** 344-8.

WU, S. M., QIAO, X., NOEBELS, J. L. & YANG, X. L. 1993. Localization and modulatory actions of zinc in vertebrate retina. *Vision research,* 33**,** 2611-6.

WYSZYNSKI, R. E., BRUNER, W. E., CANO, D. B., MORGAN, K. M., DAVIS, C. B. & STERNBERG, P. 1989. A donor-age-dependent change in the activity of alpha-mannosidase in human cultured RPE cells. *Investigative ophthalmology & visual science,* 30**,** 2341-7.

XU, T. F., WANG, X. L., YANG, J. Z., HU, X. Y., WU, W. F., GUO, L., KANG, L. D. & ZHANG, L. Y. 2009. Overexpression of Zip-2 mRNA in the leukocytes of asthmatic infants. *Pediatric pulmonology,* 44**,** 763-7.

YAN, A., Xu, G. & YANG, Z.B. 2009. Calcium participates in feedback regulation of the oscillating ROP1 Rho GTPase in pollen tubes. *Proceedings of the National Academy of Sciences*, 51, 22002-22007.

YANG, L., GONG, H., WANG, Y., YIN, H., CHEN, P. & ZHANG, H. 2010. Nicotine alters morphology and function of retinal pigment epithelial cells in mice. *Toxicologic pathology,* 38**,** 560-7.

YOLTON, D. P. 1981. Nutritional effects of zinc on ocular and systemic physiology. *Journal of the American Optometric Association,* 52**,** 409-14.

YU, Y. Y., KIRSCHKE, C. P. & HUANG, L. 2007. Immunohistochemical analysis of ZnT1, 4, 5, 6, and 7 in the mouse gastrointestinal tract. *The journal of histochemistry and cytochemistry : official journal of the Histochemistry Society,* 55**,** 223-34.

ZHANG, B., ZHANG, Y., WANG, Z.X. & ZHENG, Y. 2000. The Role of Mg^{2+} Cofactor in the Guanine Nucleotide Exchange and GTP Hydrolysis Reactions of Rho Family GTP-binding Proteins. *The journal of biological chemistry*, 275, 25299-25307.

ZHANG, L. H., WANG, X., STOLTENBERG, M., DANSCHER, G., HUANG, L. & WANG, Z. Y. 2008. Abundant expression of zinc transporters in the amyloid plaques of Alzheimer's disease brain. *Brain research bulletin,* 77**,** 55-60.